SEISMIC PERFORMANCE EVALUATION OF PROTOTYPE UN-BONDED FIBRE REINFORCED ELASTOMERIC ISOLATORS

Thesis Submitted in Partial Fulfilment of the Requirements

for the Degree of

DOCTOR OF PHILOSOPHY

By

NGO VAN THUYET

DEPARTMENT OF CIVIL ENGINEERING

INDIAN INSTITUTE OF TECHNOLOGY GUWAHATI

GUWAHATI-781039, ASSAM, INDIA

APRIL 2017

DEDICATION

To

My father Ngo-Quang-Thiem,

My mother Vu-Thi-Hoa

and my girlfriend Pham-Thu-Tra

For

Their unconditional love, encouragement and support.

CANDIDATE'S DECLARATION

I hereby declare that the work presented in the thesis entitled "**Seismic Performance Evaluation of Prototype Un-bonded Fibre Reinforced Elastomeric Isolators**" in partial fulfilment of the requirement for the award of the degree of Doctor of Philosophy is an authentic record of my own work carried out in Department of Civil Engineering of the Institute. The work has been carried out under guidance of Prof. Sajal Kanti Deb and Prof. Anjan Dutta.

The content presented in this thesis has not been submitted by me for the award of any other degree of this or any other Institute.

NGO VAN THUYET

This is to clarify that the above statement made by the candidate is correct to the best of our knowledge.

Dr. Sajal Kanti Deb
Professor
Department of Civil Engineering
Indian Institute of Technology Guwahati
Guwahati-781039
India

Dr. Anjan Dutta
Professor
Department of Civil Engineering
Indian Institute of Technology Guwahati
Guwahati-781039
India

ACKNOWLEDGEMENT

This thesis is the outcome of experimental and numerical studies carried out in the Department of Civil Engineering at Indian Institute of Technology (IIT) Guwahati, Assam, India. At the outset, I would like to express my deepest gratitude and respect to my supervisors Prof. Sajal Kanti Deb and Prof. Anjan Dutta for their guidance and unconditional support throughout my doctoral programme in India. The professional knowledge and research methodology that I learned from them would be useful to pursue my career goal.

The experimental studies conducted for this research work would not have been possible without the support of technical staff of the Department of Civil Engineering, IIT Guwahati. I express my gratitude to Dr. Arun Chandra Borsaikia and Mr. Biswajit Debnath for their earnest effort during experimentation and data acquisition.

I am very much grateful to Dr. Animesh Das, a former research scholar in IIT Guwahati, who helped me in finite element simulation.

I would like to thank my doctoral committee members, Dr. Kaustubh Dasgupta, Dr. Sandip Das and Prof. Debabrata Chakraborty for their remarks and valuable suggestions during the entire course of my research. I would like to acknowledge the contribution of METCO Pvt. Ltd., Kolkata, India for manufacturing fibre-reinforced elastomeric isolator.

I would like to thank the Indian Council for Cultural Relations (ICCR) for the scholarship granted to me. The financial support only provided me the opportunity to carry out the research at IIT Guwahati.

I am grateful to my Indian friends and my foreign PhD students in IIT Guwahati for their friendship and support.

Finally, the great motivation that helped me to overcome obstacles during the course of my research was the endless encouragement and support from my parents and my girlfriend. I would like to thank them deeply for their invaluable love and support. I would like to dedicate this thesis to my father Ngo-Quang-Thiem, my mother Vu-Thi-Hoa, and my girlfriend Pham-Thu-Tra.

Ngo Van Thuyet

TABLE OF CONTENTS

भारतीय प्रौद्योगिकी संस्थान गुवाहाटी
Indian Institute of Technology Guwahati

ABSTRACT

Base isolation system is a class of passive control system which can reduce the seismic vulnerability of a structure located in high seismic regions. Generally, base isolators are installed at the interface of substructure and superstructure to reduce transmission of earthquake energy to the structure by lengthening the fundamental horizontal period of the structural system.

Conventionally, a laminated elastomeric isolators consisting of elastomer / rubber layers interleaved with thin steel reinforcing plates and commonly known as steel-reinforced elastomeric isolator (SREI) are used. This class of isolators is very stiff in the vertical direction, but is highly flexible in horizontal direction to deflect the earthquake energy associated with strong ground motion. However, SREI has some disadvantages, limiting its use in low cost low-rise buildings. The limitations are mainly due to their heavy weight as well as cost and thus restricting their applications primarily in important and expensive buildings. Development of light weight, less expensive isolators has made implementation of the seismic isolation technology feasible in seismically vulnerable low-rise masonry building in general.

Seismic isolators designed using layers of elastomer / rubber vulcanized with thin layers of bi-directional fibre fabric as reinforcement are known as fibre reinforced elastomeric isolators (FREI). Both weight and height of isolators can be reduced by replacing steel with fibre fabric as reinforcement material. Traditionally SREIs are installed in any structure by connecting the top end plate of the isolator with the bottom surface of superstructure and bottom end plate with the top of foundation, and hence SREIs are also called as bonded isolator. Study on un-bonded fibre reinforced elastomeric isolator (U-FREI) is a significant step towards enhancement of ease of installation of isolators in buildings. Heavy steel-end-plates are not provided in U-FREIs and these devices are

installed at the interface of foundation and superstructure without any connection. Thus, elastomer layers at top and bottom of U-FREIs will be in frictional contact with superstructure and foundation respectively. Reduced weight and ease of installation would thus facilitate implementation of U-FREIs for control of seismic response of low-rise vulnerable lifeline buildings in developing countries. In the present study, seismic performance evaluation of prototype square U-FREIs are investigated.

From review of literature, most of experimental studies are limited to scaled sizes of FREI specimens with low shape factors. Shear modulus of elastomer has significant influence on the force-displacement relationship. In order to understand the horizontal behaviour of prototype U-FREIs and effect of shear modulus of elastomer on it, experimental investigations are carried out. Testing of prototype carbon fibre reinforced specimens with two different dimensions in plan and different values of shear moduli are carried out under the simultaneous action of design vertical load and cyclic horizontal displacement. Results obtained from experiment show that effective horizontal stiffness of prototype U-FREI decreases with increasing horizontal displacement. The isolators exhibit stable rollover deformation with the increase in amplitude of applied horizontal displacement. Further, since the angle of incidence of earthquake to a structure may be from any directions, experimental evaluation for the effect of different loading directions (0^o, 15^o, 30^o and 45^o) on horizontal response of prototype square U-FREI is also carried out. It can be observed that as the loading direction is varied from 0^o to 45^o, the effective horizontal stiffness of square U-FREI increases at any displacement.

Analysis of FREIs using numerical technique like FE method is carried out using ANSYS (v.14.0). This is done to address both bonded and un-bonded FREIs and for a displacement range much beyond the limitations encountered during experimental

study. The force-displacement hysteresis loops and deformed shapes of U-FREIs obtained from the FE analysis are compared with those obtained from experimental investigations to validate the FE model of U-FREIs. Comparison of horizontal behaviour of bonded and un-bonded U-FREIs shows that horizontal stiffness of U-FREI is significantly lesser than that of B-FREI at higher displacement. It is also observed that a considerably lower compressive stress demand in elastomer layers as well as significantly lower peeling stress demand on the bond between elastomer and fibre reinforcement layers in U-FREI. Effect of shear modulus and shape factor on horizontal response of the isolator is also evaluated. Influence of loading direction on horizontal load-displacement behaviour of square B-FREI and U-FREI is also studied. Generally, as loading direction changes from 0^o to 45^o, the effective horizontal stiffness of U-FREI increases while that of B-FREI remains more or less unchanged.

As observed from review of literature, a few analytical methods were suggested by researchers to evaluate the secant horizontal stiffness of U-FREI. However, the agreement between the results obtained from these analytical methods and experimental data was not in close agreement. The present study proposes an analytical method for the evaluation of secant horizontal stiffness of both bonded and un-bonded FREIs. The method incorporating the effect of both nonlinearity of shear modulus and effective shear area is proposed as a basic analysis tool for predicting the secant horizontal stiffness of U-FREIs. Results obtained from the proposed analytical method are compared with experimental as well as numerical results and very good agreement is observed.

Stability of elastomeric isolators is an important requirement for acceptable design of seismic isolation system. However, most of the suggested models for predicting stability of elastomeric isolators in literature were used for conventional isolators in bonded

application. The stability of U-FREI is investigated adopting an existing strategy wherein the isolators are subjected to various vertical loads and varying amplitudes of cyclic horizontal displacement to determine the critical load carrying capacity. It is observed that the critical buckling load of the isolator decreases with the increase in horizontal displacement amplitude. Critical load carrying capacity of the prototype U-FREI is significantly higher than the design vertical load. Effect of vertical load on the horizontal response of the U-FREI is also evaluated.

U-FREI is an improved system for seismic mitigation of low-rise buildings. However, no studies were found in the literature on the vulnerability assessment of low-rise masonry buildings seismically isolated by U-FREIs. In the present study, seismic vulnerability of a two-storey stone masonry building supported on in-house designed U-FREIs is evaluated by analytical fragility curves. U-FREIs supported prototype low-rise masonry building, located at Tawang, India, is the first such building constructed anywhere in the world. Significant reductions in probability of exceedance at all the considered damage states of the base-isolated building are observed as compared to those of fixed-base building. Further, dynamic responses of the base-isolated building subjected to different intensities of input earthquakes are compared to those of fixed-base building. Significant reduction in floor accelerations and inter-storey drifts of the base-isolated building are also clear indicative of the effectiveness of U-FREIs in enhancing the seismic performance.

Base isolation technology for low-rise buildings supported on U-FREIs is relatively new in the world. Development of step-by-step design procedure of U-FREIs for seismic isolation systems is thus introduced following the design provisions of ASCE/SEI 7-10. Detailed design calculations are also shown for the prototype isolators considered in the present study.

LIST OF FIGURES

LIST OF TABLES

NOTATIONS

Symbol		Meaning
a	=	Width of square isolator
A	=	Full cross-sectional area of isolator
A_{eff}	=	Effective plan area in contact with support surfaces of isolator
α	=	Geometrical parameter
b	=	Width of rectangular isolator
β	=	Equivalent viscous damping of isolator (damping factor)
β_D	=	Damping coefficient
β_{DS}	=	Standard deviation of damage state
c	=	cohesion
$c_b(t)$	=	Damping coefficient
d	=	Projected length of curved part of rollover region
D_D	=	Design displacement
E	=	Elastic modulus of carbon fibre laminate
E_c	=	Compression modulus of isolator
E_m	=	Young's modulus of masonry
ε_{13}, ε_{23}	=	Shear strain
F	=	Horizontal force on isolator
F_{max}	=	Maximum shear force of isolator
F_{min}	=	Minimum horizontal force of isolator
F_y	=	Yield strength
f	=	Frequency of actuator
f_b	=	Compressive strength of brick (stone)

$f_{db}(t)$	=	Corresponding force due to damping
f_j	=	Compressive strength of mortar
f'_m	=	Compressive of masonry
$f_{sb}(t)$	=	Stiffness force
f_t	=	Tensile strength of masonry
g	=	Acceleration due to gravity
G	=	Shear modulus of elastomer
G_{eff}	=	Effective shear modulus
G_m	=	Shear modulus of masonry
h	=	Total height of isolator
K_1	=	Initial stiffness
K_2	=	Post yield stiffness
K_2/K_1	=	Post yield to pre-yield stiffness ratio
K_b	=	Horizontal stiffness of bonded isolator
$k_b(v_b(t))$	=	Horizontal secant stiffness
K_{eff}^{h}	=	Effective horizontal stiffness of isolator
K_t	=	Transverse stiffness
$k_{tb}(v_b(t))$	=	Tangential stiffness
K_{ub}	=	Horizontal stiffness of unbonded isolator
K_v	=	Vertical stiffness of isolator
l	=	Length of rectangular isolator
μ	=	Poisson's ration of carbon fibre laminate
N	=	Number of isolator
n_e	=	Number of elastomer layer
n_f	=	Number of fibre layer

p	=	Vertical pressure of isolator
P	=	Vertical force on isolator
P_{cr}	=	Critical load
r	=	Radius of gyration
R	=	Radius of bearing
ρ	=	Aspect ratio
S	=	Shape factor
S_1	=	Spectral acceleration at a period of 1 second
S_{11}, S_{33}	=	Normal stress
S_{11}/p, S_{33}/p	=	Normalized stress
S_a	=	Spectral acceleration
S_d	=	Spectral displacement
$S_{d,DS}$	=	Median value of spectral displacement of a damage state
T_D	=	Desired period
t_e	=	Thickness of single elastomer layer
t_f	=	Thickness of single fibre layer
t_r	=	Total height of elastomer
u	=	Horizontal displacement
u_{max}	=	Maximum horizontal displacement of isolator
u_{min}	=	Minimum horizontal displacement of isolator
$v_b(t)$	=	Horizontal displacement
W_d	=	Energy dissipated in each cycle of hysteresis loop
Δ	=	Average of the positive and negative maximum displacements

भारतीय प्रौद्योगिकी संस्थान गुवाहाटी
Indian Institute of Technology Guwahati

Chapter 1

Introduction

1.1. Background

Base isolation is an efficient and viable method to reduce the seismic vulnerability of structures in seismic prone zones. Base isolators are installed in between substructure and superstructure to reduce transmission of earthquake energy to the superstructure by lengthening the fundamental horizontal period of the structure.

Idea of base isolation technology for seismic protection of buildings was conceptualized during early part of twentieth century but it has been used as one of the most effective anti-seismic devices for last three decades. Development of multi-layered elastomeric isolators has increased the popularity of this technology. Generally, these isolators are made by vulcanization of sheets of elastomer / rubber to thin steel reinforcing plates. They are very stiff in the vertical direction to enable them to safely carry the vertical load of the building, but are very flexible in horizontal direction to allow the building to move horizontally under strong ground motion of earthquakes. Thus, base isolation system introduces an element with low horizontal stiffness between the foundation and superstructure to lengthen the fundamental period of isolated building system without compromising vertical stability. Both inter-storey drifts and floor accelerations can be reduced simultaneously by using base isolators. The base isolation concept is widely accepted across the world for protecting important structures, heritage buildings from the damaging motion of earthquakes.

Low-rise building, especially masonry building, is one of the most commonly adopted structural types even in earthquake prone regions in developing countries. The building can be built rapidly and economically using locally available materials like stone, clay

brick or adobe. These buildings can sustain gravity loads very easily due to high compressive strength of masonry, but are highly susceptible to ground shaking due to their low tensile as well as shear strength making them often susceptible to damage. Therefore, development of less expensive and light weight laminated elastomeric isolators, which are easy to install, would play an important role in reduction of seismic vulnerability of low-rise masonry buildings.

Various types of structural control systems used for reduction of structural response during earthquakes are briefly described in following section.

1.2. Overview of Structural Control Systems

Structural control is a rapidly expanding field. Family of control systems, also known as earthquake protective systems, now embraces passive, active, semi-active and hybrid control systems. A schematic classification of structural control system is shown in Fig 1.1.

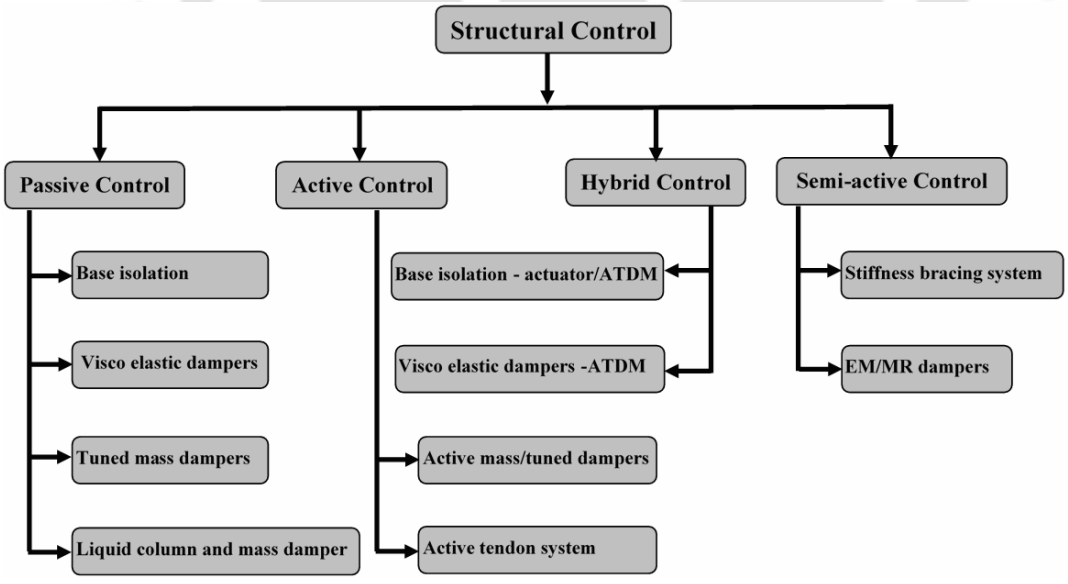

Fig. 1.1 Classification of structural control system

1.2.1. Passive control system

Passive control systems are installed into the structural system permanently and generally these require no attention. No power supply is required for the functioning of these systems. This class of structural control systems are relatively simple and very effective for mitigation of earthquake damage. Schematic diagram of few types of passive control systems employed in civil structures are shown in Fig. 1.2.

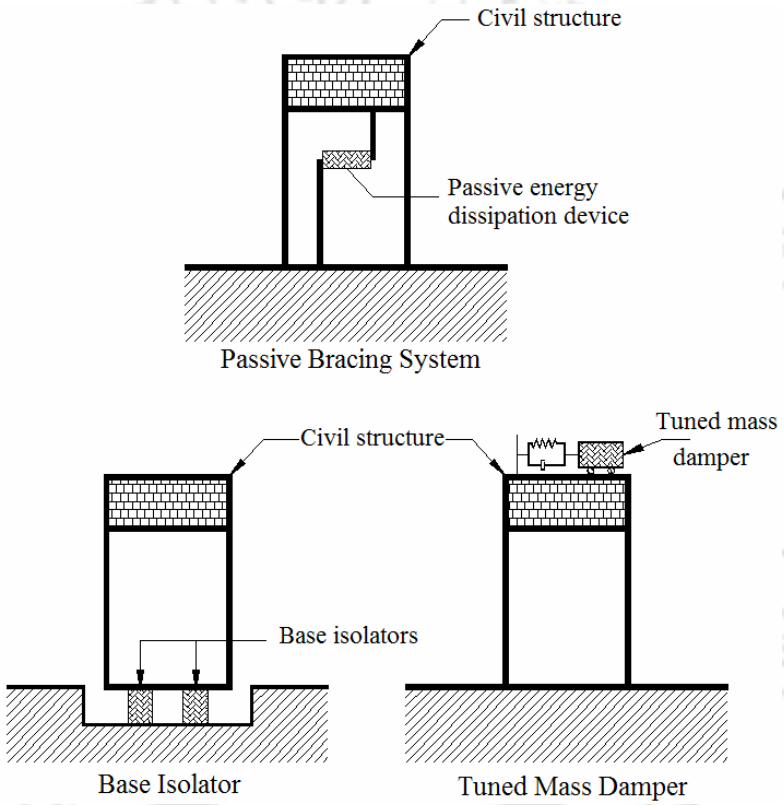

Fig. 1.2 Schematic diagram of passive control systems in civil structure (Datta, 2003)

1.2.2. Active control system

Active control systems are installed in the structural system after completion of construction of structures. In active control, earthquake input and response histories are measured by sensors and response of the building is controlled by adding a force using external energy source. These require continuous power supply for functioning of the system.

1.2.3. Hybrid control system

Hybrid control systems are combination of passive and active control systems. The forces from the active system are employed to increase the efficiency of passive control systems. The energy and forces required to operate a hybrid system is far less than active control systems.

1.2.4. Semi-active control system

Semi-active control systems are active control systems, which require very less power to operate. These systems do not directly add or remove energy to the structural system, but can control the parameter of structures such as spring stiffness or coefficient of viscous damping. Performances of appropriately designed semi-active system are better than passive control system.

1.3. Base Isolation

Base isolation system is a class of passive control system based on simple concept. The system decouples the building from the horizontal components of earthquake ground motion by interposing structural elements with low horizontal stiffness between the foundation and superstructure. Thus, it results in reduction in the magnitude of fundamental frequency of the base-isolated structure to a much lower value than both its fixed-base frequency and the predominant frequency range of the ground motion, reducing acceleration response as illustrated in Fig. 1.3.

Generally, the spectral acceleration experienced by buildings during an earthquake is at its highest between the periods of 0.1 to 0.5 seconds. Low-rise buildings with fundamental periods in this range amplify these accelerations. This leads to increase inter-storey drifts, which results in structural damage. In order to avoid structural

damage, it is advantageous to lengthen the fundamental period of the structural system. This can be accomplished by introducing an element with low horizontal stiffness at the interface of foundation and superstructure. The first dynamic mode of the isolated structure involves deformations only in the isolated system, the structure above acts as rigid body system.

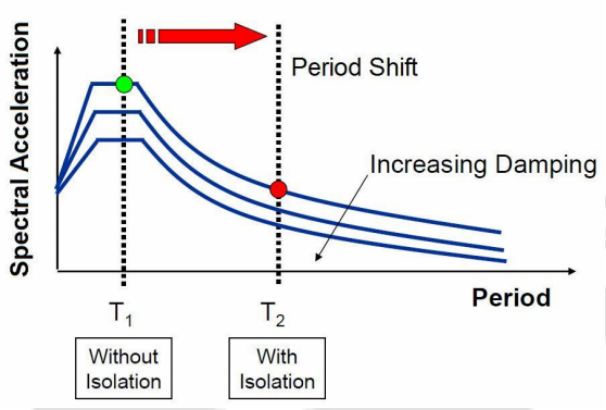

Fig. 1.3 Idealized acceleration response spectra showing the decrease in response acceleration caused by a base isolation system (Symans, 2003)

Idealized bilinear force-displacement behaviour of a typical isolator is illustrated in Fig. 1.4. Generally, the initial horizontal stiffness of isolation bearing (K_1) is relatively high, and it is reduced with increasing horizontal displacement. High initial stiffness would prevent wind induced oscillation. Further, larger area of force-displacement hysteresis loop would provide higher hysteretic damping.

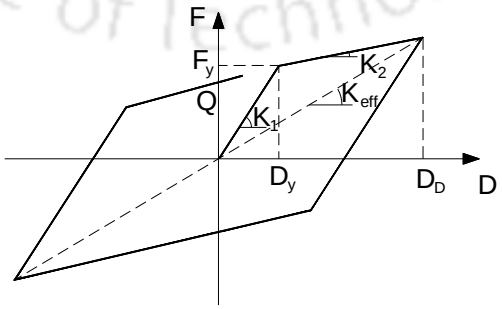

Fig. 1.4 Idealized force-displacement behaviour of a typical isolator

1.3.1. Basic Concept and Advantages of Base Isolation System

Conventional structures (buildings and bridges) are constructed directly on top of a foundation that transfers the loads from the structure to the ground. In the case of strong ground motion from earthquakes, the foundation can be viewed as an avenue for loads to be transferred to the superstructure, causing the structure to experience large floor accelerations or high inter-storey drifts and related inertial forces.

The aim of earthquake resistant design for a building is to reduce both inter-storey drifts and floor accelerations. Large inter-storey drifts of flexible structure cause damage to non-structural components and to sensitive internal equipment housed in the building. Stiffening the structure can reduce inter-storey drift but lead to amplification of the floor accelerations. Minimization of both the floor level accelerations and inter-storey drifts simultaneously is achieved by using base isolators at the interface of substructure and superstructure. These isolators provide the flexibility to the structural system, with the displacement concentrated at the isolator level.

Commonly, a base isolation system is installed in between substructure and superstructure. Isolated building undergoes almost rigid body motion and isolators undergo large deformation and absorb the seismic energy through hysteresis. Typical deflected pattern of fixed-base and base-isolated buildings are shown in Fig. 1.5.

The basic features of a base isolated system consist of the horizontal flexibility and energy absorption capacity. The horizontal flexibility of base isolators can increase the natural period of the isolated structure so as to avoid the frequency range in which earthquake energy is dominant. However, due to the horizontal flexibility, the horizontal displacement of the isolated structure increases. On the other hands, the energy absorption capacity and damping of base isolation counteract the excessive deformation of the structures. Owning to this characteristic of base isolated system, they

can attenuate the harmful horizontal acceleration transmitted to the superstructure and reduce the member forces of the superstructure.

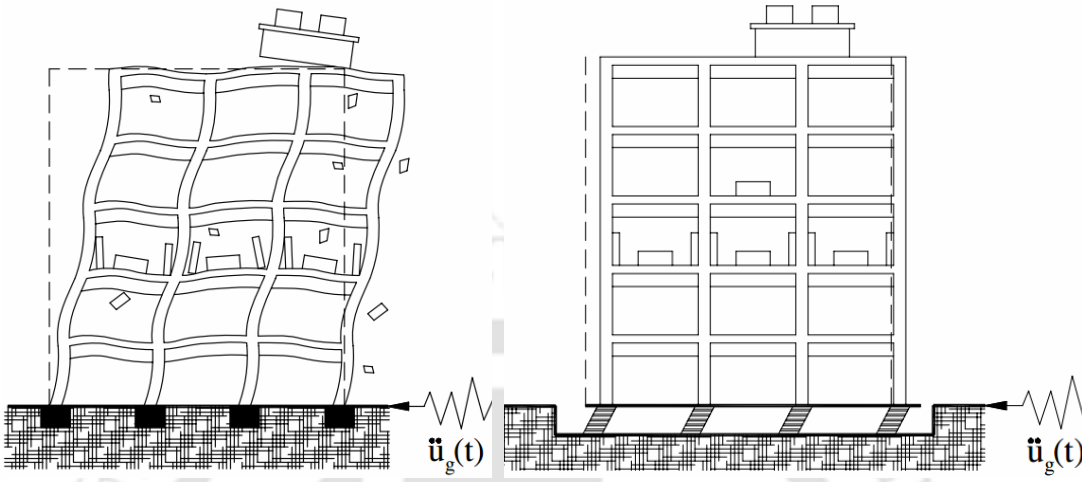

(a) Conventional structure (b) Base-isolated structure

Fig. 1.5 Displaced configuration of fixed-base and base-isolated structures

1.3.2. Classification of Base Isolation

There are primarily two types of isolation systems currently in use: the most common type involves laminated elastomeric isolators, and other is a low-friction sliding system. In the first type, a multilayer elastomeric isolator consists of alternating layers of rubber and reinforcement sheets, and two thick steel end plates at top and bottom. Generally, type of rubber in use is damped natural gum rubber or neoprene with the soft material properties and near incompressibility. Thin steel plates are the typical choice of reinforcement for multilayer elastomeric isolators. The second type of base isolation involves the use of a sliding system. A number of sliding systems have been developed and installed around the world. A characteristic property of this type is slip between two or more surfaces with a low coefficient of friction. Some examples of sliding systems include the Resilient Friction Base Isolator (R-FBI) system, the Électricité de France (EDF) system, and Friction Pendulum Bearing (FPB) system. Both systems provide an

interface with low horizontal stiffness between the foundation and superstructure of the building. This study deals with the multilayer elastomeric isolators. Various types of multilayer elastomeric isolators are briefly described.

Steel Reinforced Elastomeric Isolator (SREI) is the most common type of multilayer reinforced elastomeric isolators. It is made by vulcanization of sheets of rubber to thin steel reinforcing plates, and two thick steel end plates at top and bottom. There are many types of multilayer elastomeric isolators, e.g., Natural Rubber Bearing (NRB), High-Damping Rubber Bearing (HDRB), and Lead Rubber Bearing (LRB). Typical elastomeric seismic isolators are shown in Fig. 1.6.

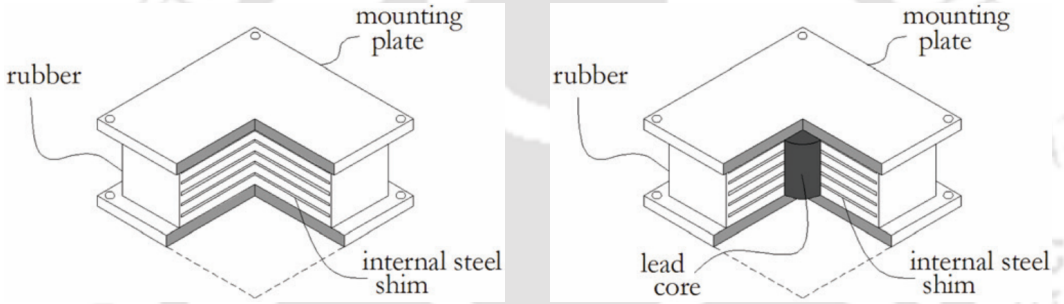

(a) NRB / HDRB (b) LRB

Fig. 1.6 Types of steel reinforced elastomeric isolator

Horizontal stiffness and damping of these isolators are dependent on the rubber materials used. Low damping elastomeric isolators of NRB are easy to manufacture and model. However, isolation systems with low damping require supplementary damping systems (e.g. steel U-shaped dampers or lead dampers) (Naeim and Kelly, 1999). Supplementary damping systems would require additional costs, which can be avoided when sufficient damping can be developed by the isolators themselves. Additional damping can be achieved by either adding a hole and lead-plug to the isolator (LRB) or by using a high damping natural rubber (HDRB). A lead-plug core can be added to a steel reinforced bearing by simply placing a cylindrical lead-plug to the centre of the

bearing. Lead is chosen because of its energy dissipating capabilities. Both LRB and HDRB are widely accepted mechanism for adding damping to multilayer elastomeric isolators.

Conventional SREIs are currently the most widely used multilayer elastomeric isolators for base isolation purposes worldwide. However, these isolators are having disadvantages due to their heavy weight and high installation cost. The manufacturing process of SREI, which is complicated and expensive, requires steel plates to be cut into proper sizes, sand blasted, acid cleaned and then coated with bonding compound. The layers of elastomer and steel plates are placed into the mould and heated under pressure for several hours to complete the manufacturing process. The weight of the isolator is heavy mainly due to the weight of these steel plates and two thick steel end plates at top and bottom. The cost and weight of SREIs have been perceived to act as barriers to its widespread application. Thus, for these reasons they often are applied for large and important buildings, but not widely used for low-rise masonry buildings in developing countries, which are vulnerable under seismic action. Development of less expensive isolators is thus necessary for implementation of the seismic isolation technology to such low-rise buildings vulnerable to seismic ground motions.

Fibre Reinforced Elastomeric Isolator (FREI) is a result of the effort for reducing the weight and cost of isolator, which is expected to be utilized in low-rise buildings. The components of FREI are similar to that of the SREI, in which steel plates are replaced by multilayer of fibre fabric as reinforcement. The fibre reinforcement is substantially lighter than steel reinforcement. Generally, fibre fabric has high stiffness in extension, but lacks flexural rigidity.

Un-bonded Fibre Reinforced Elastomeric Isolator (U-FREI) further improves the ease of installation as well as seismic performance as two thick steel end plates are

removed. It is installed directly between the foundation and superstructure without any connection at the interfaces. Reduced weight and ease of installation will facilitate implementation of U-FREIs for seismic response control of low-rise lifeline buildings in developing countries. The comparison of deformed shapes of bonded and un-bonded isolators is presented in Fig. 1.7. Rollover deformation portrays a unique behaviour of U-FREIs, having no bonding between the contact surfaces and the supports at top and bottom. Low flexural rigidity of adopted carbon fibre fabric is responsible for rollover deformation. As a result of un-bonded boundary conditions, FREIs "rollover" under horizontal displacement. Rollover occurs as initial horizontal surfaces of the isolator rotate and lose contact with the supports as illustrated in Fig 1.7(b). Rollover will continue until the original vertical faces of the isolator become horizontal and touch the supports. This condition is referred as full rollover. Rollover is the special characteristic feature of U-FREIs.

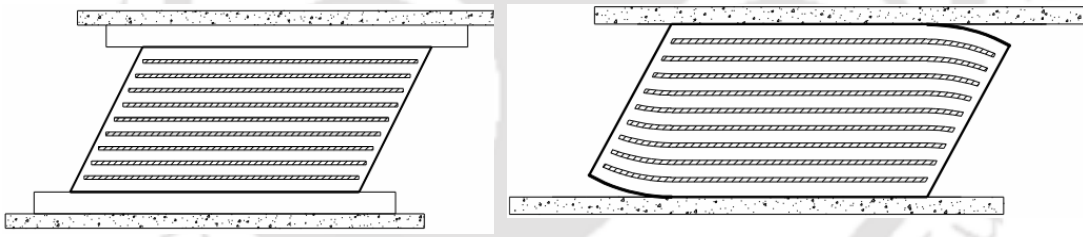

(a) Bonded Isolator (b) Un-bonded Isolator

Fig. 1.7 Deformation of isolator in different boundary conditions

1.4. Application of Base Isolation

Multilayer elastomeric isolators are widely used in civil, mechanical and automotive engineering. They have been used as seismic isolation devices for protection of buildings in highly seismically active regions. However, base isolation technology is utilized predominantly for large or important buildings with historical significance and

structures housing expensive equipment or essential services in developed countries like United States, Japan, New Zealand, Italy, etc. The reason for the limited use of the technology is primarily due to the cost of manufacturing and installation of these devices.

Base isolation technique has been used for several buildings and bridges in the United States, both in new and retrofitted constructions. There are several base isolation projects for new construction, for example, The Foothill Communities Law and Justice Center (Rancho Cucamonga, California) using isolation bearings made from HDRB, Flight Simulator Manufacturing Facility (Salt Lake City, Utah) using LRB and Emergency Operation Center (Los Angeles, California) using HDRB. Similarly, some of the prominent structures retrofitted using base isolation systems in United States are The Oakland City Hall, The Los Angeles City Hall, and The San Francisco City Hall (Naeim and Kelly, 1999). Figure 1.8 shows the University of Southern California (USC) hospital building in the United States, where isolation bearing used in the building is of LRB type.

(a) USC hospital building (b) LRB for USC hospital building

Fig. 1.8 LRB base isolation system in USC hospital building

Application of base isolation technology has been very limited so far in developing countries like India. After the disastrous earthquake of Killari, Maharashtra in 1993, one

school building and a shopping complex were built with rubber base isolator. Similarly, a new Bhuj General Hospital building at Gujrat, India was supported on base isolators (Fig. 1.9) after the Bhuj earthquake (2001).

Fig. 1.9 Base isolation system of New General Hospital Bhuj building

Research activities have been undertaken in India to develop and manufacture base isolation systems and construct base isolated building. Indian Institute of Technology (IIT) Guwahati is one of the pioneering institutes to start the research activities in this field and constructed a base isolated building (Funded by Department of Atomic Energy (DAE), Govt. of India) in 2006 to study the performances of base isolated building. Figure 1.10 shows the base isolated building supported on HDRB in the campus of the institute, which is located in the most severe seismic zone (Zone V) as per IS 1893 (Part 1): 2002.

Thus, it is seen that most of these examples are high value structures such as government buildings and medical centres, where SREIs were used as base isolation systems. However, for low-rise masonry buildings in less developed parts of the world, like residential structures or school buildings, it is not economically feasible to use a base isolation system for seismic protection. In order to expand the application of isolation system in common structures in developing countries, it is necessary to reduce both cost and ease of installation. FREIs, especially un-bonded category, are expected to

provide cost effective solution in implementation of base-isolated technology in low-rise buildings. Some studies have been carried out to understand the behaviour of U-FREIs in recent time. However, effort to employ these isolators in prototype low-rise buildings are not reported in literature.

Fig. 1.10 Base isolated (HDRB) building at IIT Guwahati

1.5. Vulnerability Assessment of Low-rise Masonry Buildings under the action of Earthquakes

Low-rise building, especially masonry buildings, which include residential quarters, schools, government offices, markets, etc, are one of the most commonly adopted structural types in developing countries like India, Bangladesh, Nepal, Myanmar, etc. Vast majority of these buildings are also located in high seismicity regions. The building can be built rapidly and economically by adopting traditional technology and using locally available materials like stone, clay brick or adobe. These buildings can sustain gravity loads very easily due to high compressive strength of masonry, but are

highly susceptible to ground shaking due to their low tensile as well as shear strength making them often susceptible to damage. As example, typical failure pattern of masonry buildings after Nepal earthquake (2015) with the magnitude of 7.9 in Richter scale is shown in Fig. 1.11. Therefore, assessment of seismic vulnerability of low-rise buildings located in seismic prone regions is an essential step in the seismic risk mitigation of these buildings.

Fig. 1.11 Typical failure pattern of masonry buildings under Nepal earthquake, 2015

In order to carry out rational estimation of seismic losses in buildings, the seismic performance level should be quantitatively measured through vulnerability assessment of such structures. Fragility curves provide a powerful solution tool for vulnerability assessment of such structures. Developing fragility curves for a specific type of building is a probabilistic method to estimate the probability that the building will exceed a specific state of damage for a definite value of the seismic intensity parameter (Bakhshi and Karimi, 2008), which includes peak ground acceleration (*PGA*), spectral acceleration (S_a), spectral displacement (S_d), etc. A lognormal distribution function is usually used to develop a fragility curve. The uncertainty related with capacity of the structure under earthquake and damage level are taken into account in this curve. Fragility curves are commonly developed by three approaches: empirical, expert-

opinion (or judgement-based) and analytical methods. Empirical fragility curves are developed based on observations of actual damage from post-earthquake surveys. However, main constraint for implementation of this approach is the availability of quality data. In expert-opinion method, fragility curves are directly estimated by the experts on the basis of their knowledge and experience. Some of the fragility curves proposed in HAZUS [1999] as per Applied Technology Council ATC-13 (1985), ATC-40 (1996) are developed using this method. However, the results rely solely on the experience and knowledge of consulting experts. The potential bias in the curves can be reduced by extending the number of experts and by assigning some weight to their estimations, based on their expertise level. When actual damage and ground motion data are not available, analytical fragility curves must be used to assess the vulnerability of structures. In this method, response of a structure is simulated using finite element (FE) method. The damage distribution over the members is obtained with the help of computed structural response. Some methodologies such as elastic spectral response, nonlinear static analysis and nonlinear time history analysis are used to develop analytical fragility curves. Analytical method reduces bias and increases reliability as compared to other approaches, and thus it is generally adopted for development fragility curve in the recent past.

Mitigation of seismic vulnerability of low-rise buildings is an important area of research in recent time. Development of less expensive, light weight laminated elastomeric isolators, which are easy to install e.g. U-FREIs, is expected to be effective in reducing the seismic vulnerability of low-rise buildings. However, little effort has been made for assessment of seismic vulnerability of low-rise masonry buildings isolated by U-FREIs.

1.6. Problem Identification

A two-storey stone masonry building located at Tawang, India is selected for seismic base isolation using square U-FREIs in this study. This type of masonry building is considered since similar structures are built as low-rise building units in some areas of north-eastern region of India, which happens to be in the highest seismic zone of the country.

Seismic isolation systems of base-isolated building decouple the superstructure from foundation and thereby deflects the seismic energy associated with ground motion. Consequently, floor accelerations as well as inter-storey drifts experienced by the base isolated building would get reduced. However, there is no cost effective light weight and easy to install prototype isolation system which can be used for seismic protection of low-rise buildings. Therefore, there is a need for development of efficient, less expensive and light weight prototype isolators for implementation in low-rise masonry buildings vulnerable to seismic ground motions.

In the present study, prototype U-FREI is considered for seismic protection of low-rise masonry building because of less expensive, light weight and ease of installation. Performance of prototype U-FREIs would be evaluated in seismic response control of low-rise building. Mechanical properties of prototype U-FREI would be investigated by laboratory tests before installing these devices in the actual building. Performance of U-FREI as compared to that of conventional B-FREI would be evaluated. Stability of the prototype U-FREI would be further evaluated as compared to the vertical design load in columns of the actual building. Reduction in seismic vulnerability of the base-isolated building supported on prototype U-FREIs under earthquakes induced vibrations would also be performed.

1.7. Research Objectives

The objective of this study is to develop and demonstrate the feasibility of prototype FREIs as a viable alternative to the conventional SREIs. The development of light weight, less expensive isolator is crucial if this technology for seismic protection is to be implemented to low-rise buildings, such as residential, school and hospital buildings etc. in urban as well as rural earthquake-prone zones. Numerical method for computation of response of prototype U-FREIs would be validated through experimental investigations. Such validated numerical model may provide an effective tool for initial design of the isolators which are relatively light weight and less expensive. The major objectives of the present study are as follows:

I. To develop light weight, less expensive prototype U-FREIs for seismic response control of low-rise masonry buildings in seismic zones.
II. To carry out experimental investigations for the evaluation of horizontal force-displacement behaviour of prototype U-FREIs.
III. To carry out numerical simulation of both bonded and un-bonded FREIs for the evaluation of their horizontal force-displacement behaviour.
IV. To validate FE model of U-FREIs by comparing the horizontal force-displacement behaviour obtained from numerical analysis with that obtained from experiment.
V. To observe the effect of shear modulus and shape factor on the behaviour of prototype U-FREIs.
VI. To develop an analytical method for predicting the horizontal stiffness of FREIs.

VII. To carry out experimental and numerical studies for the evaluation of the effect of different directions of horizontal loading on the behaviour of square U-FREIs.

VIII. To carry out numerical study for predicting stability of a prototype U-FREI.

IX. To compare seismic vulnerability of base-isolated masonry building with that of fixed-base building.

X. To develop step-by-step procedure for the design of prototype U-FREIs for seismic isolation of low-rise buildings.

1.8. Scope of Study

The major scope of study in the present research comprises of both experimental and numerical investigations of prototype square carbon fibre reinforced elastomeric isolator to be used for seismic isolation of low-rise masonry buildings. Further, an analytical approach for predicting the horizontal stiffness of FREI is also proposed. A step-by-step design procedure is also suggested for U-FREIs. The detailed scopes for experimental and numerical studies are given as follows:

1.8.1. Experimental Study

I. To carry out experiments in laboratory to determine the horizontal force-displacement relationships, mechanical characteristics of prototype U-FREIs of two different dimensions in plan under design vertical loads and cyclic horizontal displacement. Variability in geometry and material (elastomer) is studied considering two different values of shape factor and shear modulus of elastomer.

II. To carry out experiments in laboratory for the evaluation of the effect of

different horizontal loading directions (0^o, 15^o, 30^o and 45^o) on the behaviour of square U-FREIs.

1.8.2. Numerical Study

I. To carry out FE modelling and analysis of bonded and un-bonded square FREIs under design vertical load and cyclic horizontal displacement using commercial software ANSYS (v.14.0). Force-displacement hysteretic behaviour for the evaluation of mechanical characteristics and detailed stress, strain in elastomer and fibre reinforcement layers of these isolators are evaluated. Numerically evaluated mechanical characteristics of prototype square U-FREIs are validated by comparing with those obtained from laboratory tests.

II. To carry out FE modelling and analysis of bonded and un-bonded square FREIs loaded in different directions (0^o, 15^o, 30^o and 45^o). To evaluate force-displacement behaviour for the evaluation of mechanical characteristics and detailed stress, strain in elastomer and fibre reinforcement layers of the isolator subjected to horizontal displacement in different directions.

III. To predict stability of prototype U-FREI under various combinations of vertical loads and cyclic horizontal displacements based on FE analysis. Stability of an U-FREI is ascertained by a method of fitting a polynomial to shear force-displacement hysteresis data.

IV. To analyse base-isolated masonry building supported on prototype U-FREIs using commercial software SAP2000 (v.15.2.1). Vulnerability assessment of both fixed-base and base-isolated two-storey masonry buildings is evaluated by analytical fragility curves. Reduction in vulnerability, floor accelerations

and inter-storey drifts of base-isolated building as compared to those of fixed-base building is investigated.

1.9. Outline of the Thesis

In this thesis, detailed experimental investigations of prototype U-FREIs and numerical studies of these isolators (both bonded and un-bonded) are conducted. Vulnerability assessment of a low-rise masonry building supported on these isolators is also performed by using the response of the base isolated structural system from FE analysis.

In Chapter 1, general description of isolated systems, summary of the scopes and objectives of the study are presented.

Chapter 2 provides the brief review of the existing literature on laminated elastomeric isolators developed in different parts of the world. Experimental and analytical behaviour of FREI, stability of laminated elastomeric isolators as reported in different literature are presented in details. Study report on FE analysis of the isolators made with rubber like material is also reviewed. Literature on vulnerability assessment of base-isolated structures and low-rise masonry buildings is included in this chapter.

Chapter 3 describes the experimental investigations of prototype U-FREIs with two sizes and different shear moduli of elastomer. Tests are carried out for the evaluation of horizontal force-displacement behaviour of the isolators under simultaneous action of cyclic horizontal displacement and a constant design vertical load. Effect of shear modulus and loading direction (0^o, 15^o, 30^o and 45^o) on horizontal response of the isolators is also reported.

Chapter 4 presents FE simulation of the prototype FREIs (both bonded and un-bonded) using commercially available software ANSYS (v.14.0). Results of numerically obtained horizontal response of U-FREIs are compared to experimental results for

validation of FE model. Effect of shear modulus, shape factor and horizontal loading directions on the horizontal response of the FREIs are also reported.

Chapter 5 describes some analytical approaches for evaluation of the horizontal stiffness of multilayer elastomeric isolators in the existing literature. Proposed analytical method for predicting the horizontal stiffness of FREIs (both bonded and un-bonded) is presented.

Chapter 6 presents method of predicting stability of a prototype U-FREI. A method of fitting a polynomial to hysteresis loop is used to predict stability of the isolator. The effect of vertical load in horizontal response of U-FREI is also reported.

Chapter 7 describes the vulnerability assessment of the low-rise masonry building supported on prototype U-FREIs. The base isolated building is analysed by FE method using SAP2000 (v.15.2.1).

Chapter 8 provides the development of step-by-step procedure for the design of prototype U-FREIs to be adopted in seismic isolation of structural system.

Chapter 9 presents the summary and conclusion of research work undertaken. Major finding during the work and scopes of future work have also been listed in this chapter.

भारतीय प्रौद्योगिकी संस्थान गुवाहाटी
Indian Institute of Technology Guwahati

Chapter 2

Literature Review

2.1. Introduction

Base isolation technology had been proposed for mitigation of seismic induced effects on structures about a century back; but it found worldwide application only in the recent past. Generally, conventional SREIs, which are made by vulcanization bonding of sheets of elastomer / rubber to thin steel reinforcing plates, are used in large or important buildings, such as building housing sensitive equipment, hospitals, emergency operation centres, etc. These isolations are very heavy, expensive and hence their implementations are limited to very special applications. To spread the use of seismic base isolation technology for mitigation of seismic effect on vulnerable low-rise buildings, it is necessary to reduce the weight as well as cost of the isolator and enhance ease of installation. Idea of reducing the weight and cost of the isolator by using material like fibre-reinforced polymer in place of steel plates has been recently undertaken by researchers. Development of light weight and less expensive isolator as FREI would facilitate implementation of base isolation technology in low-rise masonry buildings, which are otherwise vulnerable to seismic ground motions. Low-rise building, especially masonry building, is one of the most commonly adopted structural types in developing countries. A vast majority of them are found in high seismicity regions, and are susceptible to earthquake induced damage, either partial or total collapse, as observed in various past earthquakes. In this chapter, a brief review of base isolation bearings, experimental investigation, FE modelling, stability of laminated elastomeric isolators and seismic vulnerability assessment of both conventional and base-isolated structures, especially low-rise masonry buildings, are presented.

2.2. Base Isolation Bearing

Base isolation technology for seismic isolation of structures has been used from last three decades. Development of multi-layered elastomeric isolators has increased the popularity of this technology. Conventional SREIs are very stiff in the vertical direction to enable them to safely carry the vertical load of the structure, but are very flexible in horizontal direction to allow the structure to move horizontally under strong ground motion. These isolators are costly and heavy due to the interleaved steel reinforcing plates and two thick steel end plates at top and bottom. The weight and cost of SREIs can be reduced by introducing fibre fabric as reinforcement and removing two end steel plates. A good numbers of studies of SREIs in literature have been performed during last few decades, but very few studies are reported on FREIs. A brief review on the origin and development of laminated elastomeric isolators in general are presented in the following section.

Roeder and Stanton [1983] gave brief description of the state of art of knowledge of elastomeric bearing available throughout the world. This paper helps structural engineer to understand the material and large strain behaviour of elastomeric bearing. It summarized the material behaviour of elastomer, theoretical and experimental research on bearings. Various modes of failure of elastomeric bearings were also presented. Design methods of four major specifications like American Association of State Highway and Transportation Official (AASHTO), German procedure, British specification and International railway specification were compared by the researchers.

Kelly [1986] summarised the bibliography of all literature on theoretical aspect of seismic isolation as published from 1900 to 1984. In the early years, it was tried to achieve base isolation by using sliding concept to decouple the structure from the ground. The first use of un-reinforced rubber block as earthquake protection was in an

elementary school in Skopje, Yugoslavia. The base isolated building underwent rigid body motion during the first mode of vibration with all the deformation mainly at the isolator level. For higher mode, seismic load was treated as an equivalent lateral load which was proportional to the rigid body mode. This is the property of a linear vibrating system with all higher modes being mutually orthogonal to each other. Energy associated with higher frequency of earthquake ground motion can not be transmitted to the structures. Thus working principle of base isolation system is to deflect energy rather than to absorb energy.

Kelly [1999] presented method of evaluation of the mechanical characteristics of fibre-reinforced elastomeric isolator in which steel plates of conventional elastomeric isolators were replaced by fibre reinforcements. Fibre fabric has high stiffness in extension, but lacks flexural rigidity. The influence of fibre flexibility on the mechanical properties of FREI, such as vertical and horizontal stiffness were studied. Some specific advantages of FREI as light weight and ease of manufacturing were also presented in this study.

Ibrahim [2008] carried out a comprehensive assessment of recent developments of non-linear isolators like ultra-low-frequency isolators. Base isolation of buildings, bridges, and liquid storage tanks subjected to earthquake ground motion were described. Nonlinear visco-elastic and composite material springs, and smart material elements were described in terms of mechanical characteristics of the material.

Kelly [2009] presented the origin and development of base isolation system in various parts of the world. Two basic types of isolation system and their working principle using elastomeric bearings and sliding systems were described. A review of the base isolated structures using rubber isolators in different countries like Unites States, Japan were presented in this paper. Stability, rollover behaviour and failure issues of isolators

were addressed. Manufacture of bearing with high vertical load carrying capacity and size up to 1.5m in diameter were reported.

Review of origin, development of base isolation bearing in different parts of the world and their working principles were presented in this sub-section. This will thus help in enhancing the understanding of the state-of-the-art of base isolation systems and their applicability to protect structure against earthquake motion.

2.3. Experimental Study of Isolators

Experimental studies of both SREI and FREI were performed by many researchers to determine their mechanical characteristics. The effectiveness of base-isolated structures as compared to fixed-base structures was reported in literature based on shake table tests. Reviews of some of the literature relevant to present study are summarized in the subsequent paragraphs.

Kelly and Takhirov [2001] carried out theoretical and experimental analyses for the evaluation of mechanical characteristics of FREIs. Compression stiffness of isolator with flexible reinforcement was derived. Four 305 mm diameter isolators were tested in shear in pairs under a vertical load equivalent to a pressure of 6.90 MPa. Isolators were tested in cyclic shear, with three fully reversed cycles at three maximum strain levels of 50%, 100% and 150%. The test result showed that it was possible to use un-bonded isolators for seismic isolation of structures. Although a considerable amount of edge uplift occurs, the force-displacement curve always had positive stiffness, indicating that the bearing was still stable at 150% shear deformation even though it appears to be undergoing roll over deformation.

Moon *et al.* [2002] designed and manufactured some specimens of fibre-reinforced multilayer elastomeric isolator using different kinds of fibre such as carbon, glass, nylon

and polyester. Experiments were carried out to evaluate and compare the performances of fibre reinforcement with performance of steel reinforcement, and the differences in performance among different kinds of fibre reinforcement. Experiments showed that performance of the carbon FREI was even superior to that of SREI in view of vertical stiffness and effective damping. Vertical stiffness of carbon fibre reinforcement was higher than that of glass fibre reinforcement. Vertical stiffness of the carbon FREI was three times higher than that of SREI. Further, the bulging of carbon FREI was lesser than that of SREI.

Experimental study of strip isolator was carried out by Kelly and Takhirov [2002]. Using long strips of rectangular isolators had many advantages over conventional isolators, especially in case of buildings where walls provide lateral resistance. Generally, at base level of base isolated buildings, wall beams are provided between isolators to carry the load of walls. This base level wall beams can be avoided by using long strip isolators on continuous wall footing of the building. The test result showed that the concept of a strip isolator reinforced with carbon fibre was viable. The isolator could be made in long rectangular strip and cut to the required width for use as a strip below wall of the building. Manufacturing cost of large size rectangular strip isolator will be less as compared to the manufacturing of individual circular or rectangular isolator.

The effect of hole and lead plug on the FREI were studied by Kang *et al.* [2003]. Experiments were carried out to evaluate and compare the performances of fibre reinforcement with steel reinforcement. The hole and lead plug effect on effective stiffness and effective damping of carbon FREI were also studied. From the experiments, the performance of the FREI was observed to be superior to that of the SREI in respect of horizontal stiffness and vertical stiffness of the isolator. It was shown

that hole and lead plug did not make much difference with FREI without hole and lead plug.

Moon *et al.* [2004] provided the results of theoretical and experimental study of FREIs. Several samples of strip isolator were designed, manufactured and tested to prove its effectiveness in base isolation of building subjected to earthquake motion. The experiments on several specimens of isolators were carried out to determine the vertical stiffness and horizontal stiffness under a constant vertical load. Experimental results showed that horizontal stiffness of strip fibre reinforced isolator in 0^o and 45^o direction were found to be superior to conventional rigid reinforced isolator. Further, the study suggested that the time period of building could be adjusted by staking strip isolator one above another.

Warn *et al.* [2007] presented experimental study to investigate the influence of horizontal displacement on the vertical stiffness of elastomeric and lead-rubber bearings. Low-damping rubber bearings and lead-rubber bearings were subjected to a series of tests with varying levels of combined horizontal displacement and axial loading. Experimental results showed that the vertical stiffness of bearings decreased with increasing horizontal displacement. The vertical stiffness data obtained from experiments were used to evaluate four formulations for estimation of vertical stiffness. These formulations were based on Koh and Kelly (1988) two-spring model and a piecewise linear model. Good agreement was observed between results obtained from experimental data and these formulations over a wide range of horizontal displacements considered in this study.

Ashkezari *et al.* [2008] designed, manufactured and tested FREI. Dynamic and mechanical characteristics were studied by performing vertical and cyclic horizontal tests. To manufacture the fibre reinforced isolator, initially the woven fibres were

completely impregnated by adhesive. The raw rubber compounds which were filled with carbon black, was also formed as sheets of desired thickness. The fibre layer and raw rubber sheets were then cut to desired dimensions and set in the mould. For comparison of mechanical properties of FREI, a similar type of SREI was also tested and test results showed that behaviour of the manufactured FREI was similar to that of SREI. Therefore, the FREI was named as "steel like FREI". It was observed that the effective shear modulus decreased, when the horizontal test was repeated at different shear strains. In contrary to this, damping values of isolator increased for the above sequence of test.

Nezhad *et al.* [2008a] provided a brief literature review on the experimental investigation carried out on FREI. FREIs were manufactured by using soft compound of natural gum rubber as elastomer and bi-directional carbon fibre fabric as the reinforcement. Bearings were fabricated without using mould. Vertical compression test, rate sensitivity test and cyclic lateral load test of bearings were conducted to evaluate the performance of FREI. Effect of first and second shape factors were reported in the study.

Nezhad *et al.* [2008b] studied the lateral response characteristics of square U-FREI. Isolators were manufactured by using unfilled soft neoprene compound as elastomer and bidirectional carbon fibre fabric as the reinforcement. Lateral cyclic testing was conducted on $1/4^{th}$ scaled carbon FREI bearings. As the fibre reinforcement had no appreciable flexural rigidity, the un-bonded application resulted in a stable rollover deformation in the bearings when they were laterally deformed. Experimental results showed that effective lateral stiffness and damping increased with an increase in the rate of lateral displacements.

Nezhad *et al.* [2009a] carried out parametric studies of U-FREI to investigate their

vertical and lateral behaviour. Influence of amplitudes histories on lateral displacement and variations in vertical loads on isolators was evaluated. Two types of sinusoidal lateral displacement time histories were considered for the study. The first type was ascending lateral displacement pattern and second type was descending lateral displacement pattern. Significant stiffening behaviour was observed at the ends of hysteresis for the test with ascending types of lateral displacement. However, this response was not observed for the test with descending types of lateral displacement. Generally for 0^o and 90^o orientations, bearing exhibit higher effective stiffness and lower damping ratio as compared to 45^o orientation. Damping ratios of tested bearings were higher than that of elastomer layers and it was postulated that additional damping was attributed by the relative volume of fibre to elastomer. Vertical cyclic loading test result showed that effective stiffness and damping ratio increased with the increased vertical pressure. From the test result with different loading cycle and variation of pressure, it was concluded that the full scale FREI could be used to mitigate the seismic response of structures located in moderate to high seismic regions.

Nezhad *et al.* [2009b] conducted a shake table study on a two-storey structure having well defined elastic response characteristics supported on U-FREIs. Detailed dynamic response result of shake table study of base-isolated steel structure and corresponding fixed-base structures were compared. The initial fundamental frequency and equivalent viscous damping of the structures were determine by performing free vibration tests on the structures using Fourier amplitudes spectra of measured roof accelerations. Experimental results showed that the peak values of accelerations at roof level were 24-32% lesser in base-isolated structure as compared to fixed-base structure. Similarly, base shear, base moment and total drift of the base-isolated structure were 30-45%, 23-33% and 28-42% lesser respectively as compared to fixed-base structure. There was no

damage to the bearings after the completion of entire test program. From the testing it was concluded that the U-FREI has significant potential of reducing the seismic response of structures in high seismic regions.

Nezhad *et al.* [2009c] presented two simplified analytical models to predict the seismic response of low-rise building isolated using U-FREI. Both of these models were constructed from the load-displacement hysteresis loops of bearing testing results. In the first model, the parametric constants were evaluated from the lateral load-displacement hysteresis loops of cyclic shear test by using least square methods. In the second model, bilinear idealization of load displacement hysteresis loop was considered for prediction of response. Simplified equation with some parameters were derived for prediction of response of building supported FREI. These parameters were evaluated from the load-displacement hysteresis loops of the bearings. Iterative procedure was used for the evaluation of solution of equation to determine the responses of the building. Accuracy of both the models in predicting the responses of isolated structures were dependent on the input earthquake and discrepancy up to 24% and 23% were observed between the models in predicting the drift and base shear respectively.

Russo and Pauletta [2013a] carried out investigation for the evaluation of influence on friction behaviour of different parameter such as compressive stress, shear strain, concrete roughness, aging etc. of U-FREI. Elastomeric compound influenced the sliding behaviour of U-FREI. Isolator made with non-seismic compound like poly-chloroprene required almost 50% more compressive stress to limit the sliding as compared to the isolator made with natural rubber. Lower limit of minimum compressive stress of aged isolator should be assumed 50% than un-aged isolator to avoid sliding instability. Higher loading rate increased the stiffness and maximum force of isolator as compared to lower loading rate and quasi-static test results provided conservative strength values

with respect to those actually occurring. The limiting value of compressive stress recommended to avoid sliding instability was based on the particular geometry and shape factor of isolator, which might not hold good for isolators with different geometry, shape factor and aspect ratio.

Russo *et al.* [2013b] proposed a simplified analytical model to calculate the horizontal stiffness of U-FREI by modifying the formula used to calculate horizontal stiffness of SREI. Experimental result of vertical and horizontal stiffness of different specimens of isolators made with low and high damping neoprene reinforced with bidirectional and quadric-directional fabric were presented. Effect of aging on stiffness and damping were also summarized. It was concluded that the process of aging leads to an increase in average horizontal stiffness and reduction in damping ratio. Isolator with quadric-directional fibre reinforcement exhibited higher horizontal stiffness than isolator with bidirectional fabric. The proposed formula for calculating the horizontal stiffness was based on the simplified geometrical configuration of the displaced isolator. Shear modulus was considered as constant and this value was assumed to be independent of shear strain applied in the elastomer.

Dezfuli and Alam [2014] presented experimental studies of U-FREIs to evaluate the effect of number and thickness of elastomer and fibre-reinforced layers on their vertical and horizontal response. All carbon FREIs were produced in scaled size with same dimensions in plan; but with different numbers and thickness of elastomer and fibre-reinforced layers using a simple and fast manufacturing process. Experimental results showed that the vertical stiffness increased with increasing the fibre-reinforced layer thickness and with decreasing the elastomer layer thickness. The flexibility in the horizontal direction increases by increasing the total thickness of rubber layers, while the energy dissipation capacity enhances with increasing the thickness of both fibre-

reinforced and elastomer layers. The paper indicated that reduction in the horizontal stiffness of U-FREIs with increasing horizontal displacement amplitude was mostly due to the decrease in shear modulus of elastomer and the rollover deformation.

Naghshineh *et al.* [2014] carried out experimental studies to compare the fundamental properties of fibre meshed reinforced elastomeric with the conventional SREI. Influences of lead in both types of isolators were also investigated. SREIs had higher horizontal stiffness as compared to fibre mesh reinforced bearing. However, damping values were comparable for the bearing without lead core. Presence of lead plug increased the horizontal stiffness of fibre mesh reinforced bearing up to 52% and conventional bearing up to 89% at 100% strain level of the tested bearings. Experimental results of vertical stiffness were compared with the theoretical results from existing literature and observed that for low shape factor bearing, the experimental results were comparable with the theoretical result. However, for high shape factor bearing, the effect of material incompressibility played a vital role. Presence of lead plug reduced the difference of vertical stiffness between the fibre mesh reinforced isolator and conventional isolators.

Spizzuoco *et al.* [2014] carried out the experimental study on the un-bonded square recycled rubber-fibre (carbon) reinforced bearings (RR-FRB) to investigate their lateral and vertical behaviour under seismic loading. These low-cost rubber bearings are innovative elastomeric bearings that employed recycled rubber (RR) and fibre as reinforcement material. The seismic performance of the bearings was investigated by means of both experimental tests and FE analysis. Experimental results showed that the effective lateral stiffness of the bearings decreased significantly due to rollover deformation, while the equivalent viscous damping ratios increased with the increasing amplitude of lateral displacement. The paper introduced RR-FRB as an innovative

seismic isolator device with higher dissipation capacity, lower manufacturing cost and light weight.

Engelen *et al*. [2014] investigated the compressive behaviour of un-bonded modified rectangular fibre-reinforced elastomeric isolators (MR-FREIs). The geometric modifications such as the reducing plan area for improving the design of the isolation system were introduced. Experimental data from vertical tests of four rectangular-FREIs with and without geometric modifications were used to evaluate a three-dimensional finite element model. A parametric study was conducted on interior and exterior geometric modifications. The results showed that both the vertical stiffness and compression modulus were highly sensitive to interior modifications and, to a lesser extent, exterior modifications. The peak shear stress was also greater in isolators with interior modifications and the peak shear stress usually occurred in the vicinity of the modification. The paper concluded that the lateral stiffness of MR-FREIs decreased and energy dissipation increased with increasing lateral displacement.

Strauss *et al.* [2014] carried out the experimental study to determine the effective shear modulus and damping coefficient of multilayer elastomeric bearings with various reinforcing materials (fibre and steel) and under various loading and support conditions (bonded or un-bonded). Cyclic loading tests for 27 specimens, which were divided in nine specimens of three different groups in term of dimension (thickness and number of elastomer layers) and reinforcement material, were carried out. Effect of vertical pressure, horizontal displacement, bearing height, number of elastomer and reinforcement layers, reinforcement material, and support type of bearings on the effective shear modulus and damping coefficient were examined. The experimental results showed that unlike prescribed clause of European standards, the effective shear modulus decreased with increasing shear train. Further, an analytical approach for

predicting the horizontal stiffness of bonded and un-bonded isolators were proposed. Comparison between experimental and analytical results were presented.

Engelen *et al.* [2015a] proposed a new FREI, namely, partially bonded FREI (PB-FREI), which was partially bonding the U-FREIs to the upper and lower supports. Validation of FE model of un-bonded and partially bonded FREIs under vertical compression were carried out by comparison of results obtained from experiment and FE analysis. Results of FE analysis and experiment indicated that portions of a FREI could be bonded without substantially altering the rollover characteristics of the isolator within the range of average vertical compressive and tensile stresses considered. PB-FREIs could retain the beneficial characteristics of U-FREIs while addressing concerns over tensile forces and slip.

Kumar *et al.* [2015] carried out a series of experiments to characterize the behaviour of elastomeric bearings. Sixteen low-damping rubber bearings from two manufacturers with similar geometric properties but different shear moduli, were tested under various loading conditions to determine factors that affect cavitation in an elastomeric bearing. The effect of cavitation on the shear and axial properties of elastomeric bearings were investigated by performing post-cavitation tests. The experimental results showed that the pre-cavitation tensile stiffness of a bearing decreased with an increasing number of loading cycles, and an increase in co-existing shear strain. Cavitation strength decreased with co-existing shear strain. No significant reduction in the buckling load of a bearing was however observed due to prior cavitation.

Das *et al.* [2016a] studied the feasibility of U-FREI as an alternative to SREI for seismic isolation of un-reinforced brick masonry buildings by shake table test. A base-isolated two-storey building model subjected to four excitations to ascertain its effectiveness in controlling seismic response. To compare the performance of U-FREI,

the same building was placed directly on the shake table without isolator and subjected to the same excitations. Dynamic response characteristic of base-isolated building was then compared with that of fixed-base building. Experimental results showed that floor accelerations, inertia forces, shear forces and moment of base-isolated building supported on U-FREIs were substantially lesser than those of the fixed-base building. The improved seismic performance of un-reinforced masonry building model supported on U-FREIs under different ground motions was demonstrated in the paper.

Das *et al.* [2016b] studied the comparison of numerically and experimentally obtained seismic response of un-reinforced brick masonry building supported on in-house designed U-FREIs. Experimental studies were carried out on a shake table with elaborate instrumentations for measurement of acceleration and displacements at different floor levels. Numerical study of the model building supported on U-FREIs using SAP2000 software was carried out to compare the numerical results with those obtained from experimental investigation. Multi-linear pivot hysteretic plasticity model was used to simulate the behavior of U-FREIs, while plate elements were used for brick-masonry walls. Comparison of numerical and experimental results showed that the seismic response of the building supported on U-FREIs could be numerically evaluated with quite reasonable accuracy.

Engelen *et al.* [2016] altered the full rollover displacement of stable U-FREIs by introducing a geometric modification of the upper and lower supports applied to tailor the hysteresis loops of the isolator. Experimental results were used to calibrate a numerical model of a base-isolated structure. Full rollover and geometric modification was observed to be advantageous to maintain horizontal stability and to provide control over the stiffening of stable U-FREIs.

In this sub-section, the experimental investigations for determining the mechanical properties of laminated elastomeric bearings (both SREI and FREI) are reviewed. Kelly (1999) proposed the mechanic of fibre-reinforced light weight laminated elastomeric bearings for the first time, incorporating the influence of flexibility of reinforcement to analyse FREI bearings. Researchers in different parts of the world carried out substantial studies for development of FREIs. Different types of rubber material such as natural rubber, elastomer, recycled rubber and different fibre fabrics were used along with different types of boundary conditions (e.g. bonded, un-bonded, partially bonded and modified support geometry). Many parametric studies, based on both experimental and numerical model were carried out by different investigators using scaled model of FREIs. However, experimental study for the assessment of behaviour of large and prototype FREIs is very limited in literature.

2.4. Finite Element Analysis of Isolators

Finite elements modelling and analysis of multilayer elastomeric isolator is a challenge due to the hyper-elastic and visco-elastic behaviour of rubber-like material. Brief review of relevant previous researches on modelling and analysis of rubber-like material and elastomeric isolators are summarized below.

Sussman and Bathe [1987] provided a displacement-pressure (*u/p*) based on FE methods for compressible and nearly incompressible solids having material and geometrical nonlinearities to overcome the difficulties of displacement based analysis. In this formulation the pressure computed from the displacement field was explicitly replaced by a separately interpolated pressure using a general procedure. Material model description such as isotropic linear elasticity, anisotropic linear elasticity, von Mises elasto-plasticity, Mooney-Rivilin nonlinear elasticity and Ogden nonlinear elasticity

were implemented in the formulation. Some examples were solved using the *u/p* formulation, including the contact analysis of rubber material to demonstrate the robustness of the process.

Chang [1988] investigated three commercially available software ABAQUS, B-RUBBER, and MARC for FE analysis of rubber material. Basic mechanics, element technology, numerical solution schemes, contact elements and slip/friction features adopted in the three codes were compared. After comparison of analysis capability, ABAQUS was used for modelling the load displacement behaviour of a rubber seal used in automobile industry.

Herrmann *et al.* [1989] conducted parametric study using nonlinear FE analysis for wide range of elastomeric bearing. Computer codes were developed for the FE analysis for plain strain (2D) conditions and for general 3D conditions. Results were presented in non-dimensional form in order to extend the use of these results to a wide range of bearing designs. Various parametric study result presented for different shape factors included the effect of elastomeric parameter on compressive response, effect of reinforcement stiffness on compression response, effect of bulking on compressive response, effect of eccentrically loading on compressive stiffness, effect of shear response on compressed bearings, beading effect on compressed bearings and combination of bending, shear on compression. Modified shape factor definition was provided for different 3D elastomeric bearings.

Kulak and Wang [1991] presented the methodology for performing 3D FE analysis of individual rubber bearings and for simulating the response of 3D systems of isolated reactor structures including the surrounding soil under earthquake excitation. The NEPTUNE computer program was used to perform the 3D analysis of bearing. An eight node hexahedral element was used to model the elastomer with Mooney-Rivilin

material. A four-node quadrilateral plate element was used to model the interleaved steel plates. To model the global response of isolator and isolated structure with surrounding soil, a preliminary computer program was developed. Two sample problems of strip and cylindrical bearings were analysed using the code. Response and performances of structures with and without elastomeric bearings were compared.

The continuum formulation of finite strain visco-elasticity and its numerical simulation with FE method were studied by Holzapfel [1996]. For sufficiently slow processes, the material responded in rubbery elastic manner which was modelled with an Ogden type material model. Ogden model, with only three pairs of coefficients known from empirical rubber elasticity, excellently replicated the finite extensibility domain of polymer chains and represented the best-known approximation to real behaviour.

Peng and Chang [1997] presented a finite element analysis procedure for rubber-like materials based on a compressible strain energy function. The function was developed by adding a bulk term to the Ogden-Tschoegl model. A method for finite element implementation of a strain energy function in terms of principal stretches was proposed. Two finite element formulations, including the total Lagrangian (TL) and the updated Lagrangian (UL), were presented explicitly for the proposed strain energy function. Finite element codes for plane stress, plane strain, axisymmetric and three-dimensional problems were developed based on the proposed algorithm. Results showed the effectiveness of the proposed procedure for the analyses of rubber-like materials.

Jerrams *et al.* [2001] considered the physical properties of rubber elastomeric isolators by finite elements analysis. The uni-axial compressive test data were subjected to regression analysis to determine parameter of Neo- Hookean and Ogden physical model properties for describing rubber material in FE program. Physical properties of rubber material were influenced by the technique used for manufacturing. Cross linked density

influence the force in elastomer, since high cross linking material were less prone to swelling. Force displacement behaviour of elastomeric bearing subjected to combined axial and shear loading were compared by using FE analysis, test and theoretical analysis. The force-displacement relationship as obtained from FE analysis using Ogden material model differed slightly with the test result. However, the Neo-Hookean model under-predicted the force by around 22.5% at 2mm displacement.

Mordini and Strauss [2008] carried out numerical investigation and parametric study of high damping rubber bearings strengthened with glass fibre to find out its mechanical behaviour under both static and dynamic loads. Parametric study was performed numerically by using commercial FE code ABAQUS and modelling technique was also described. The hyper-elastic behaviour of rubber material was defined by Ogden model. For static analysis, vertical load was applied in several steps and horizontal displacement was applied keeping the vertical load constant. In dynamic analysis, the mass was applied to the top surface and acceleration time history was applied to the bottom surface. An alternative solution methodology was proposed in the study to include the bearings in full-scale 3D model analysis. Comparison of vertical and shear displacement for analytical and numerical solution showed close agreement but in contrast, horizontal stiffness provided different result as the shear displacement increases. FE analysis of liquid storage tank was performed for both isolated and fixed based conditions. All the analyses showed substantial reduction in dynamic responses using bearings and validity of design was also established.

Hyper-elastic behaviours of rubber-like materials were mostly model by Mooney-Rivlin and Ogden model. In both of these material model, at least uni-axial and bi-axial stretching test results were required to fit the material model. Sasso *et al.* [2008] carried out uni-axial and equi-biaxial test coupled with optical devices to measure the real time

values of stress and elongation level of specimen. Test data were used to calibrate the constitutive model and FE analysis results were compared with the test result. They concluded that the use of second order Mooney-Rivlin model and Ogden model in FE analysis produced the most accurate result among the various models available.

Nezhad *et al.* [2011] investigated the lateral responses of both bonded and U-FREI under a constant vertical load and increasing lateral displacement by FE analysis. Plain strain FE analyses of strip FREI with bonded and un-bonded conditions were carried out. Different states of stress within the isolator were also evaluated. It was shown that tension in the stable U-FREI was limited to outer rubber layer at the regions where the bearing had rolled of support. Further, tensile stress in the U-FREI was shown to be much lesser as compared to B-FREI. U-FREI exhibited stable rollover deformation on application of horizontal load. Due to high geometrical nonlinearity in lateral direction, horizontal stiffness varied with isolator lateral deformation. No closed form analytical solutions were available for ascertaining the horizontal stiffness of this type of complex U-FREI. Further, closed form solution of even B-FREI served for the preliminary design. The dependency of rubber material properties on the amplitude of the shear strain, rate and history of the lateral displacement on the lateral response of isolator were not addressed in the closed form solution. Hence, FE solution flowed by experimental load testing of FREI should be carried out before eventual installation in any structure.

Kelly and Calabrese [2012] presented the study report of the mechanical behaviour of U-FREI. The rollover deformation of bearing eliminated the tensile stresses in the bearing and thereby reducing the stringent bonding requirement of fibre and elastomer. A comparison between the approximate linear elastic theory and the FE analysis result of strip, circular and square isolators was presented. For FE analysis 2D models under

plain strain assumption for strip bearings and 3D models for circular and square bearings were considered. The contact between isolator and support was modelled by Coulomb friction in MSC.Marc 2005 software. The stress at peak horizontal force and with constant vertical load was twice the stress due to compressive load. Shape factor had only effects on the distribution of stresses in the bearings, but the magnitude of stress was same. FE analyses of circular and square bearings were carried out only for compressive load and comparisons of results with pressure solution were shown.

Osgooei *et al.* [2014a] carried out 3D parametric numerical FE analysis on sixteen circular FREI bearings. All the bearing were of same overall dimensions, while the thickness of elastomer layers and the axial stiffness of reinforcement were the parameters that were varied. FE analysis results were compared with the predicted values obtained using the pressure solution and the pressure approach methods. FE analysis showed a good agreement with the result obtained from analytical solution. It was concluded that the end boundary conditions affect the vertical response of FREI.

Osgooei *et al.* [2014b] carried out three-dimensional FE analysis to investigate the lateral response of square FREIs having different aspect ratios and loaded in different horizontal directions. The FE analysis results were validated using experimental test results. The result showed that effective horizontal stiffness of the bearing increased as the loading direction changes from 0^o to 45^o. Further, as the aspect ratio was decreased, the sensitivity of the lateral response to the loading directions also increased.

Das *et al.* [2014] carried out studies to evaluate performance of square FREI subjected to a constant vertical load and cyclic lateral displacement by 3D finite element analysis using ANSYS, a general purpose finite element software. Ogden (three-term) material model and Lagrange multiplier-based mixed *u-P* element was used to simulate deformation of fully incompressible hyper-elastic materials. These bearings were made

by vulcanization of sheets of elastomer to bi-directional carbon fibre fabric. Analysis of all bearings were carried out for both bonded and un-bonded boundary conditions and two lateral loading directions, namely, $0/90^{o}$ and 45^{o}. Numerical results showed that the lateral stiffness of U-FREI was lesser than B-FREI at higher lateral displacement, and hence efficacy for seismic isolation would be higher. Lateral stiffness of U-FREI corresponding to 45^{o} loading direction was higher than that in 0^{o} loading direction. An experimental validation of numerical results was carried out and very good agreement was observed in terms of mechanical properties and deformed configuration of U-FREIs.

Al-Anany and Tait [2015] presented a method of computing response of both bonded and un-bonded FREIs under combined vertical and rotational deformations. Five FREIs having the same material properties and same shape factor but having different geometrical properties were analyzed under various levels of vertical pressures from 1 to 10 MPa and different angles of rotation. FE analysis results and the values obtained from available closed-form analytical solution were found to be in excellent agreement. FE analysis results also showed that lower normal stresses and shear strains in elastomer and lower strains in the fibre reinforcement of U-FREI as compared to those in B-FREI.

Osgooei *et al.* [2016a] carried out numerical analysis to compute seismic response of a 2-storey reinforced concrete shear wall structure seismically isolated using rectangular U-FREIs. Time history analyses were conducted for both fixed-base (FB) and base-isolated (BI) structures subjected to 10 earthquake ground motions compatible to the design response spectrum. The mechanical properties of the isolators were obtained from lateral cyclic test carried out on scaled model FREIs. Numerical results showed that the peak response values of the BI structure were significantly reduced as compared to that of the FB structure. It was concluded that rectangular U-FREIs could be

effectively designed and used to seismically isolate masonry or reinforced concrete shear wall structures.

Osgooei *et al.* [2016b] investigated the variation in vertical stiffness of bonded and un-bonded strip-shaped FREIs under different lateral displacement amplitudes by FE analysis. The vertical stiffness of the isolators under pure compression obtained from FE analysis was in good agreement with the predictions of two available closed-form solutions: the pressure solution proposed by Kelly and Calabrese (2012), and the pressure approach proposed by Tsai (2004). As the lateral displacement increases, the vertical stiffness of B-FREI decreases monotonically, whereas that of U-FREI decreases with increase in displacement till 175% shear deformation, thereafter an increase in vertical stiffness was observed.

From literature review, it is observed that main challenge in FE analysis of rubber based isolators can be mainly attributed to material modelling of rubber and development of efficient computer code considering the hyper-elastic and visco-elastic material behaviour of rubber. Previous studies suggested that Ogden (three-term) material model provide reasonably accurate estimation of force-displacement behaviour of rubber-like material. Lagrange multiplier-based mixed *u-P* element is essentially used to simulate deformation of fully incompressible hyper-elastic materials. Some recent studies involving both 2D and 3D analysis of FREI were carried out to determine the mechanical properties, stresses and strains at different levels of elastomer and fibre. FE analysis for rubber material though quite involve is observed to be highly useful in assessing the distribution of stresses across layers of FREI and would thus help in more accurate estimation of design requirement.

2.5. Analysis of Isolators using Analytical Solution

Many analytical studies of both SREI and FREI were carried out to develop governing equation or formula for evaluation the mechanical properties of the bearing. Reviews of some of the literature relevant to present study are summarised below.

Chalhoub and Kelly [1991] developed the governing equation for hydrostatic pressure in the elastomer including bulk compressibility. The solution of equations of pressure under pure compression and pure moments were provided for long rectangular strip elastomeric isolator. Effect of shape factor on pressure distribution of isolator was derived. Compression modulus was overestimated for large shape factor bearing if the material was assumed incompressible. They recommended the use of bulk compressibility effect in the design of bonded rubber isolator and bulk compressibility could be ignored for very low shape factored bearings.

Nagarajaiah *et al.* [1991] developed an analytical model and solution algorithm for nonlinear dynamic analysis of three dimensional base-isolated structures supported on elastomeric or sliding isolation bearings. Three-dimensional analysis was carried out for the base-isolated system considering nonlinear behaviour of isolator and elastic behaviour of superstructure. The solution algorithm developed especially for analysis of base-isolated structures with elastomeric and sliding isolation systems to overcome the deficiency of existing programs, which were not capable of modelling sliding isolation systems accurately. Stick-slip behaviour of sliding bearing was represented by using hysteretic model. Shake table analysis results of previous experiments were compared with the result from the program developed by the researchers. Various dynamic responses of a six-storey reinforced concrete structure obtained using the developed algorithms were also verified with the results of ETABS and DRAIN-2D.

Tsai and Lee [1998] derived a closed form solution for the compression stiffness of circular, strip and square shapes elastomeric layer bonded between rigid plates. The approximate pressure solution proposed by earlier researcher was only valid for high shape factor elastomeric layer with Poisson's ration of material between 0.49 and 0.50. Exact equilibrium equation and solution were presented by satisfying the boundary conditions, without using any approximation for normal stress component. The compressive stiffness calculated from proposed equations was compared with the FE result for validation for all values of Poisson's ratios.

Imbimbo and Kelly [1998] presented an analytical method to capture the behaviour of strain induced crystallization of elastomer at large range of shear strain. This strain induced crystallization at large shear strain enhanced horizontal stiffness of elastomeric bearing bolted to their endplates as compared to bearing doweled to their endplates. A method based on the linear elastic theories presented by Koh and Kelly (1986) was proposed to determine the buckling load carrying capacity of elastomeric bearing by replacing shear modulus by shear modulus-shear strain relationship. The analytical model adequately represented the stiffening behaviour of elastomeric bearing and result showed a good agreement with experimental result.

Naeim and Kelly [1999] wrote a book on the design of seismic isolation bearing and its theory in details. They compiled all the existing theories and equations available on this subject for complete design and analysis of elastomeric bearing used in seismic base isolation. Theoretical basis of seismic isolation, code provisions, mechanical characteristics including buckling and stability phenomena of elastomeric isolator were presented. Design examples and computer aided analysis by using different software such as N-PAD, 3D-BASIS, ETABS AND SAP2000 were also included.

Tsai and Kelly [2001] carried out theoretical analysis of single layered elastomer

bonded to flexible reinforcement to study the influence of reinforcement on the mechanical properties of FREI. Analyses were carried out for infinite long strip isolators, rectangular isolators and circular isolators subjected to compression loading and pure bending. Flexibility of reinforcement was included in the Pressure solution approach developed by Kelly to evaluate the stiffness of FREI. It was shown that shape factor and flexibility of reinforcement affect the compression and bending stiffness of FREI, evaluated from pressure solution. Stiffness of circular reinforced isolator varied with the Poisson's ratio of reinforcement and this influence became insignificant as the reinforcement become more rigid. Approximate boundary conditions were applied for the solution of stiffness of rectangular isolator and the solution became independent of Poisson's ratio.

Koh and Lim [2001] presented the analytical formulation of compression stiffness of bonded rectangular layer of elastomer. Using two kinematic assumptions and applying the principle of variable transformation, governing equations for compression stiffness of bonded rectangular elastomeric were derived and solved. The limitation of incompressibility of material which led to overestimate the bulking load and resonant frequency was also overcome by the theory. The square and strip layers of elastomer were special cases of their theory and compression modulus calculated by this theory was identical with the results of previous research. Parametric studies carried out by them showed that compression modulus decreased with the elongation for a given value of shape factor and Poisson's ratio.

Tsai and Kelly [2002a] carried out theoretical approaches for analysing the compressive stiffness and bending stiffness of rectangular FREIs. Influence of fibre flexibility on the stiffness of isolators was studied. In addition to theoretical stiffness solution which was expressed in series form, simplified stiffness formulae based on the solutions of an

infinitely long strip pad were also presented.

Tsai and Kelly [2002b] presented a theoretical approach to analyse the bending stiffness of circular FREIs. The elastomer was assumed to be incompressible and pressure dominant. The stiffness formula was derived. The influences of fibre flexibility on the mechanical properties of the FREI subjected to pure bending moment were studied. Mechanical properties such as the pressure in elastomer, the stress in reinforcement and the bonding shear stress between elastomer and reinforcement affected by the bending moment were presented.

Tsai [2003] carried out flexure analysis and developed governing equations for horizontal displacements function of circular elastomer layer bonded between rigid plates subjected to pure bending. The horizontal displacement functions were solved by satisfying the stress boundary condition of the bonded elastomer layer. Horizontal displacement in the middle plane of the layer and effective bending modulus calculated from the theoretical solutions were shown to be very close to the FE analysis result. The bonding shear stress in radial direction as obtained from theoretical solution was very close to FE analysis result except at the edges of circular layer. The bonding shear stress in tangential direction obtained from theoretical solution and FE analysis result showed large variation apparently due to numerical error in FE analysis.

Kelly [2003] derived the tension buckling load for elastomeric bearings. The tension buckling load would not be achievable in practice in most bearings since it would generally be much larger than the load that would induce cavitation in the elastomer. This could occur when extreme seismic loading on an isolated building would induce global overturning. Isolator at the periphery of the building could be in a state of combined tension and shear.

Tsai [2004] derived a closed-form solution for evaluation of compression stiffness for

laminated elastomeric bearing of infinite-strip shape considering flexibility of reinforcement sheet. Three types of the elastic layers bonded to flexible reinforcements were studied. The first type simulated the interior elastic layers of the bearings with shear-free ends. The second type simulated the exterior elastic layers of the free-end bearings. The third type simulated the elastic layers in the bearings where ends were bonded to rigid plates. In bearing with rigid reinforcements, each bonded elastic layer had the same compression stiffness because of rigid reinforcement. However, this might not be applicable to the bearings with flexible reinforcement, where the compression stiffness of bonded elastic layers varies with the deformation of flexible reinforcements. Moreover, the boundary condition at the ends of the fibre-reinforced bearings could also affect the compression stiffness. When performing the compression analysis of the bearing subjected to vertical loading only, two types of boundary conditions could be imposed at the ends of the bearings, which were referred to as "free end" and "rigid end". "Free end" means the end of the bearing did not have any horizontal constraint so that it was free from any shear force. "Rigid end" means the end of the bearing was bonded to rigid plate so that it did not have any horizontal deformation. The theoretical solutions to the compression stiffness of the bearings were really close to the result obtained by the FE method.

Tsai [2005] developed closed form solution having faster convergence by extending the pressure solution approach to solve the compression stiffness of rectangular elastomer layer bonded between rigid plates. The assumption of incompressibility of rubber material generally overestimates the compression stiffness and tilting stiffness of rubber layer bonded between rigid plates. The results of the closed form solution developed by using approximate shear boundary conditions were in good agreement with the results of FE solution and previous research result of square and strip rubber layers. The aspect

ratio significantly affected the compression modulus when Poisson's ratio was closed to 0.5. The effect of relaxing the exact shear boundary condition was negligible on the compressive stiffness of rectangular layers but this relaxation would cause some error in calculation of horizontal displacement and bonding stress near the edges of rectangular layers.

The assumption of Haringx theory that plane section remains plane after the deformation of elastomeric bearing limits the study of influence of flexibility of reinforcement layer on buckling of isolators. Tsai and Kelly [2005a] developed a theory that extends the Haringx theory by allowing the cross section to deform into a non-planner surface. The effect of warping and shear on the stiffness and buckling load of a beam carrying axial compression load and shear force at one end was derived. The numerical solution of buckling load of homogeneous rectangular and circular beam showed that buckling load increased with the increasing ratio of flexural rigidity to shear rigidity and cross section warping had also effect on buckling load.

Analysis was carried out by Tsai and Kelly [2005b] for the evaluation of buckling load of multilayer elastomeric isolators considering the effect of flexibility of reinforcement layer. The analysis treated the isolator as short elastic column in which shear deformation and warping of the cross-section were included. A cubic equation for the buckling load of the isolator was derived. The buckling load of the isolator was a function of the ratio of elastic modulus between the elastomer layer and the reinforcement, the shape factor of the elastomer layer, the width-thickness ratio of the reinforcement and the width-height ratio of the isolator. The buckling load decreased with reduction in reinforcement thickness.

Tsai [2006] derived closed form solution for the compression stiffness of circular bearing consisting of elastomer layers interleaved with flexible reinforcement. The

closed form solution was proposed incorporating the effect of bulk compressibility of reinforcement layer and boundary condition at the ends of bearing. Two types of boundary conditions were considered while performing the compression analysis with only vertical load. In the first type, ends of the bearing were not restraint against lateral displacement and it was free from any shear force. In the second type, ends of the bearing were bonded to the rigid plates so that its ends were restraint against lateral displacement. The theoretical and FE results showed that the end boundary conditions and flexibility of reinforcement affected the compression stiffness of elastomeric bearing.

Fibre reinforcement in elastomeric isolator provides in-plane rigidity when it is stretched, but loses rigidity when it is compressed. Tsai [2008] developed the solution to include this "tension-only" nonlinearity in the deformation analysis of FREI. The procedure including this type of behaviour in deformation analysis of FREIs was developed. To validate the developed procedure, FE analysis of isolator was carried out and it showed a good agreement with FE result. The result showed that thickness reduction of elastomer layers and tilting angle was proportional to the variation of compression force and bending moment. The lateral force variation affected the vertical buckling load carrying capacity of elastomeric bearing with "tension-only" reinforcement and it was smaller than the buckling load of bearing with linear reinforcement.

Kelly and Konstantinidis [2011] presented detailed information on the mechanics of rubber bearings for seismic and vibration isolation. Development of multilayer rubber bearings, mechanics of the bearings, behaviour of multilayer rubber bearings under compression and bending, buckling of multilayer rubber bearings, influence of plate flexibility on the buckling load of multilayer rubber bearings, frictional restraint on un-

bonded rubber pads, and effect of friction on un-bonded rubber bearings were furnished in this book.

Nezhad [2014] proposed two simplified analytical models to evaluate horizontal stiffness of U-FREI. These two models were derived based on the geometry. The net contact area and free area of the bearing under horizontal displacement were used to derive the horizontal stiffness of bearing. Results of analytical solution for horizontal stiffness showed a close agreement with FE analysis results with maximum error up to 13%. These formulae can be used for preliminary design of FREI. However 3D effects were neglected and influence of vertical load and stress-softening of elastomer were not addressed in the developed simplified model. Limitation of these models were identified by the author.

Engelen *et al.* [2015b] developed an analytical model to predict the horizontal response of U-FREIs. The force-displacement relationship was modelled by dividing the isolator into three sections: a central section and two rollover sections. The displacements of rollover section were used to establish the curved deformed profile and predict full rollover. The model was evaluated with experimental data from four types of U-FREIs. A good agreement was found between the results obtained from the proposed model and the experimental results.

In this sub-section, analytical methods for determining the mechanical properties of elastomeric bearings are reviewed. Analytical procedures for estimation of secant horizontal stiffness of isolators were reported in literature on the basis of approximate deformed cross-section of the isolator. Further, effect of the area in contact with support surfaces due to rollover deformation of U-FREI on horizontal stiffness of the isolator was also observed. However, in such evaluation, shear modulus of the isolator subjected to a constant vertical load and increasing horizontal displacement was kept constant.

Change in shear modulus of the isolators subjected to large shear strain was not accounted for in these solutions. Thus, there are scopes of improvement in analytical evaluation procedure of horizontal stiffness of both bonded and un-bonded FREIs.

2.6. Stability Analysis of Isolators

Stability of laminated elastomeric isolators is an important requirement for design of seismic isolation systems. Elastomeric isolators used for base isolation of structure are required to resist large displacement imposed by strong ground motion of earthquakes along with vertical load. Study on stability of elastomeric isolators refers to the determination of critical load carrying capacity, while undergoing large lateral displacement. Some experimental studies for evaluation the critical load carrying capacity and analytical studies for predicting stability of the isolators are available in literature. Brief review on the stability of laminated elastomeric isolators are presented below.

The earliest theoretical approach for evaluation of the stability of rubber rod was presented by Haringx [1948, 1949], which was based on an extension of Euler buckling load theory. The rubber rods were studied considering linear behaviour and small displacement. The theory was a modification of the linear theory of an elastic column with axial load and shear deformation.

Buckle and Kelly [1986] carried out experimental studies to evaluate stability of SREIs under quasi-static loading and dynamic loading on a scaled model of bridge deck using shaking table test. Stable rollover of isolators could be observed in this study. These studies were however conducted under small imposed displacement.

Koh and Kelly [1988] proposed a two-spring mechanical model as shown in Fig. 2.1 based on extension of Haringx's theory to evaluate stability of elastomeric isolation

bearings. Stability of the isolator was highly influenced by large horizontal displacement experienced during earthquakes. The correlation between results obtained from analytical model and experimental results were discussed.

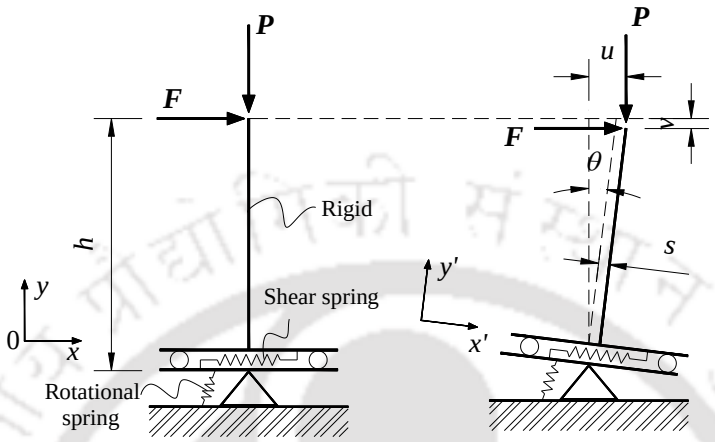

Fig. 2.1 A linear two-spring model (Koh and Kelly, 1988)

Stanton *et al.* [1990] studied the stability of SREI bearings using a modified linear model based on Haringx's theory to account for nonlinearity. An elastomeric bearing was simultaneously subjected to vertical load and increasing lateral displacement and the shear force on bearing was observed to have passed through a maximum value. This point was identified as location of zero tangential stiffness, which was considered as the stability limit. Two different SREI bearings were selected for experimental study. Buckling load, bending stiffness and compressive stiffness obtained from experimental study were compared with the analytical results.

Buckle and Liu [1993] experimentally studied the critical buckling behavior of SREIs at high shear strains using quasi-static testing. It was observed that the critical load carrying capacity of the bearings got reduced with increasing horizontal displacement. A simple reduced-area method based on overlapping area, as shown in Fig. 2.2, was proposed to estimate the critical load of bearings. The formulation was used in several subsequent studies.

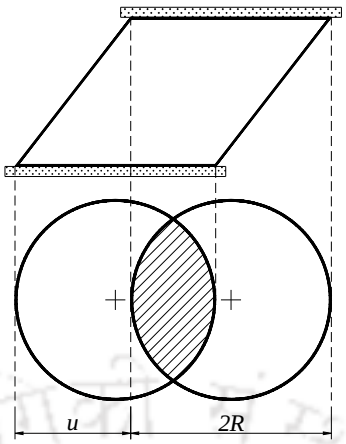

Fig. 2.2 Illustration of overlapping area method (Buckle and Liu, 1993)

A nonlinear analytical model consisting of two-spring systems as shown in Fig. 2.3 was proposed by Nagarajaiah and Ferrell [1999] in an effort to more accurately predict the critical load capacity of SREIs of different sizes and shape factors. The model was developed using two-spring model of Koh and Kelly (1988), including large displacements, large rotations and nonlinearity of rubber. It was shown that the critical load carrying capacity got reduced with increasing lateral displacement.

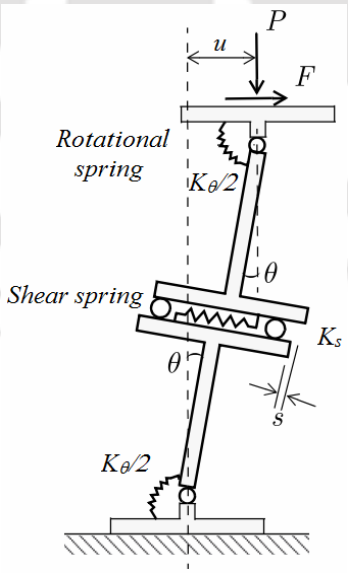

Fig. 2.3 A nonlinear analytical model (Nagarajaiah and Ferrell, 1999)

Iizuka [2000] proposed a nonlinear macroscopic model based on the two-spring model proposed by Koh and Kelly (1988), where the linear springs were replaced by nonlinear springs, for predicting the stability of laminated rubber bearings at large deformations and under different vertical loads. The nonlinear parameters of the shear and rotational springs were determined from basic load test.

Buckle *et al.* [2002] validated the nonlinear analytical model proposed by Nagarajaiah and Ferrell (1999) and determined the effect of lateral displacement on critical load by experimental study using a series of elastomeric bearings with low-shape-factor.

A study related to the prediction of stability of scaled model of U-FREI under cyclic loading was carried out experimentally by Raaf *et al.* [2011]. A method based on fitting a polynomial to experimental force-displacement hysteresis data to predict the critical load capacity of the isolator was proposed. This method was used to determine the fitted backbone curve, horizontal tangential stiffness and transverse stiffness. Critical bulking load of the isolator was observed to decrease with the increase in excitation amplitude. Effect of vertical load on the horizontal response of the isolator was also investigated.

Detailed nonlinear finite element analysis and an improved analytical formulation for predicting the reduced load-carrying capacity of bearings based on overlapping area method were presented by Weisman and Warn [2012]. Results established that the critical load carrying capacity of low-damping rubber and lead-rubber bearings reduced with increasing lateral displacement, and the lead core had a negligible effect on critical load over a range of lateral displacements corresponding to 150-280% shear strain. The overlapping area method was found to be conservative in estimation of the critical load capacity of this bearing as compared to the experimental results.

Sanchez *et al.* [2013] carried out comprehensive experimental studies on bonded SREIs to determine their stability. Three tests, including two quasi-static and one dynamic

loading tests, were conducted to predict the stability limits of bearings. Critical load obtained from experimental tests was also compared with that obtained from the reduced-area method proposed by Buckle and Liu (1993).

Han *et al.* [2013] proposed a modified analytical model based on the sensitivity analysis using Iizuka's model for the prediction of critical load capacity of bearings. Results of the sensitivity analysis showed that the prediction was sensitive to the properties that control the nonlinear behavior of the rotational spring for lateral displacement greater than approximately 0.6 times bearing diameter/width.

Verumu *et al.* [2014] presented a nonlinear analytical model capable of modelling the dynamic response of bearings more accurately at all displacement ranges, especially beyond the stability limit. The results obtained from this analytical model was verified with experimental data from an earlier experimental study. It was observed from the results of dynamic experiments that the bearings have a far larger capability to sustain horizontal loads at displacements exceeding their stability limit than predicted by earlier models and more importantly the bearings re-centred themselves after these large displacement excursions.

Pauletta *et al.* [2015] proposed a model for prediction of roll-out instability of small size U-FREI. When the un-bonded isolators were subjected to lateral displacements, the top and bottom surfaces of the isolator exhibited rollover deformation. Generally, rollover deformation is stable if the stabilizing moment due to vertical loads is higher than the overturning moment due to horizontal loads. However, if this condition is not satisfied, rollout instability of isolator will occur. The proposed model was developed considering that the isolator contact area varied with the applied displacement, and consequently the compressive stresses vary. Experimental tests for the evaluation of rollout instability of U-FREIs with different aspect ratios and under different compression levels were also

investigated. Comparison of the measured displacement at rollout obtained from experiments and the results obtained from the proposed model proved that the model could accurately and reliably predict rollout displacement of FREIs subjected to horizontal and vertical forces.

In this sub-section, existing research works related to assessment of critical load carrying capacity of laminated elastomeric isolators based on experimental as well as analytical methods are reported. However, most these works were related to bonded conventional SREIs. Fibre reinforcement is more flexible in bending as compared to steel reinforcement. Therefore, assessment of stability of FREIs is more complex. Study on evaluation of stability of FREIs, especially prototype U-FREIs, is not observed in literature. Stability analysis of only scaled model U-FREIs was observed. It is thus necessary to carry out studies for predicting the stability of prototype U-FREI, before these isolators are used in actual applications.

2.7. Vulnerability Assessment of Structures

Low-rise building, especially masonry building, is one of the most commonly adopted structural types in developing countries. Vast majority of these buildings are located in high seismicity regions. These buildings are thus generally susceptible to damage due to earthquake induced motion and may suffer partial or total collapse. Assessment of seismic vulnerability of low-rise masonry buildings located in seismic prone regions is thus an essential step in the seismic risk mitigation of this class of buildings. Fragility curve is a powerful tool for vulnerability assessment of such structures. A brief review on assessment of seismic vulnerability of both conventional and base-isolated structures, especially low-rise masonry buildings by fragility curves are reported in the following section.

Many studies were carried out on development of analytical fragility curves to evaluate the seismic vulnerability of reinforced concrete structures. Hwang *et al.* [2000] developed fragility curves for assessment of risk of highway bridges. Karim and Yamazaki [2001] presented an analytical approach using non-linear dynamic analysis to construct fragility curves for some specific highway bridge piers. Kim and Feng [2003] carried out the fragility analysis of highway bridges under ground motion with spatial variation. Nielson and DesRoches [2007] developed analytical fragility curves for nine classes of bridges by nonlinear time-history analyses using 3D numerically simulated models. Padgett and DesRoches [2008, 2009] developed fragility curves for retrofitted bridges. Lagomarsino and Giovinazzi [2006] proposed two models (marco-seismic and mechanical models) to develop analytical fragility curves for vulnerability assessment of European towns and regions. Barbat *et al.* [2008] presented the vulnerability assessment for reinforced concrete buildings and un-reinforced masonry buildings. Most of these studies were focused on the vulnerability assessment of reinforced concrete structures in high seismic regions.

Recently, a few studies on the seismic fragility analyses of masonry buildings were reported. Most of these studies were focused on the development of analytical fragility curves of the masonry buildings and the results were compared with other methods (empirical and expert-opinion methods), if available. Brief review of relevant previous studies for vulnerability assessment of masonry buildings are presented.

Bakhshi and Karimi [2008] evaluated the performance of masonry buildings by analytical fragility curves. Two types of masonry buildings having different number of stories were considered. The probable damage of these types of masonry buildings under different earthquake intensities was evaluated. The study also indicated that soil type did not significantly influence the fragility curves of masonry buildings.

Park *et al.* [2009] performed the seismic fragility analysis of a low-rise masonry building in United States (US). The masonry building was modelled using a simplified nonlinear spring model. Analytical fragility curves were developed for different damage states of the building under strong ground motions. Analytical fragility curves were then compared with available fragility curves based on expert-opinion method of HAZUS.

Rota *et al.* [2010] proposed a new analytical approach using Monte Carlo solutions for the derivation of fragility curves for different classes of masonry buildings. Nonlinear macro-element model was used to simulate the masonry building using the program TREMURI. The probability density functions of selected damage thresholds were determined based on pushover analyses and then convolved with the probability distribution of displacement demand obtained from nonlinear time history analyses.

Abo-El-Ezz *et al*. [2013] proposed an analytical method to develop fragility curves for risk assessment of stone masonry buildings relevant in Eastern, Canada. Comparison of analytical fragility curves developed from proposed method with the fragility curves obtained from HAZUS (FEMA, 2003) and earthquake loss estimation routine (ELER) were also presented. HAZUS showed the highest probability of the occurrence of nil to slight damage, whereas the highest probability of extensive and complete damage was predicted with ELER.

Base isolation is an effective technique to reduce the seismic vulnerability of a structure. However, it has been used mostly in large and important structures. Some researchers evaluated the efficiency of base isolation system by analytical fragility curves. A brief review on vulnerability assessment of base-isolated structures by fragility curves are summarized.

Zhang and Huo [2009] developed the fragility function to determine optimum design parameters of isolation devices to maximize effectiveness of seismically-isolated

bridges. Fragility functions were derived using nonlinear time history analyses of typical highway bridges (conventionally designed or base-isolated) subjected to a suite of 250 earthquake motions. Both Probabilistic Seismic Demand Analysis (PSDA) and Incremental Dynamic Analysis (IDA) methods were used to generate fragility curves of the highway bridges. The study showed that the mechanical properties of isolation devices had a significant influence on the damage probability of isolated bridges.

Tavares *et al.* [2012] presented the seismic vulnerability assessment of typical bridge classes supported on elastomeric bearings in Canada. Approach based on analytical fragility curves using 3D nonlinear FE models was developed for each bridge class in eastern Canada. Bridge-system fragility curves were developed considering the vulnerability of critical components to assess the probability of bridge damage for a given ground motion intensity measure (peak ground acceleration). It was observed that the fragility curves of bridge system changed depending on bridges class. The fragility curves could be used in determining the potential losses resulting from earthquakes and prioritization of retrofitting.

Jara *et al.* [2013] presented the influence of two earthquake sources with different fault characteristics to assess the seismic vulnerability of an isolated bridge in Mexico. Numerical models were developed to assess the demand and capacity of the structure. A bilinear hysteretic behaviour of the isolation system was modelled utilizing the elastic stiffness, yield strength and post-yielding strength. Results showed that the effect of the fault type on the seismic vulnerability of the bridge was significant.

Siqueira *et al.* [2014] presented the seismic vulnerability assessment of a class of bridge retrofitted with seismic-isolation devices in Canada. Analytical fragility curve, based on nonlinear time-history analysis considering 3D detailed models, was developed for typical configurations of highway bridges. Experimental results of square elastomeric

bearings with different sizes and shape factors were used to account for uncertainties related to the mechanical properties of seismic-isolators. Tests for evaluation of critical loads were conducted on slender seismic isolation bearings. Finite element model was calibrated with the test results to define the seismic-isolator limit states. It was observed that seismic isolation was effective in reducing the probability of damage of bridge piers.

In this sub-section, studies on development of analytical fragility curves for evaluation of seismic vulnerability of reinforced concrete structures, masonry buildings and base-isolated structures were reviewed. Post-earthquake damage surveys established that masonry buildings are susceptible to earthquake damage. Therefore, mitigation of seismic vulnerability of masonry building is an important area of research. Cost-effective base isolation system could play an important role to reduce the seismic vulnerability of such structure. Most of the studies reported seismic vulnerability assessment using analytical fragility curves for reinforced concrete buildings and highway bridges with and without conventional SREIs. U-FREI is an improved device for seismic mitigation of low-rise buildings. However, no studies are found in the literature on the vulnerability assessment of low-rise masonry buildings isolated using U-FREI.

2.8. Concluding Remarks

Literature on development and feasibility of use of FREI as a viable alternative to the conventional SREI are reviewed in details. The distinct advantages of FREIs over SREIs, namely, light weight, low cost and ease of installation, were reported in many literatures. Numerical studies were conducted in the past to assess the effectiveness of scaled models of FREIs, and thereafter these results were also validated by experimental

investigations. However, very limited numbers of both numerical and experimental studies were carried out to determine the mechanical properties of prototype FREIs. Unlike bonded isolator, horizontal response of square U-FREI is affected by the loading direction due to change in effective area of the isolator in contact with the support surfaces. However, no experimental study on the effect of horizontal loading direction of prototype square U-FREIs was published in literature. Further, fibre fabric has high stiffness in extension, but lacks flexural rigidity. Evaluation of horizontal response of FREI with both bonded and un-bonded boundary conditions is complex due to flexibility of rubber and fibre reinforcement. Reduction in shear modulus actually occurs with increase in horizontal displacement amplitude. Effect of change in shear modulus on horizontal stiffness of FREIs under large horizontal displacement was not accounted for in most of the previous studies. Furthermore, stability of laminated elastomeric isolators is an important issue for their effectiveness in controlling seismic response. However, most of the studies on literature on evaluation of the critical loads of isolators were carried out on scaled models of bonded conventional isolators. Studies on the stability of prototype U-FREIs are very limited. Moreover, no study on the vulnerability assessment of prototype seismically vulnerable low-rise masonry buildings isolated using U-FREIs is reported in literature, although potential of large scale application of this class of isolator in seismic response control is very high.

भारतीय प्रौद्योगिकी संस्थान गुवाहाटी
Indian Institute of Technology Guwahati

Chapter 3

Experimental Study on Horizontal Force-Displacement Behaviour of prototype U-FREIs

3.1. Introduction

Detailed discussion on use of passive control system like base isolators are done in Chapters 1 and 2. It is also observed that both weight and cost of isolators can be reduced by replacing steel in SREI with fibre fabric as reinforcement material in FREI. Further, existing research work on scaled specimens of U-FREIs are observed to have more seismic isolation efficacy than B-FREIs. Thus, detailed tests are conducted for better understanding of the behaviour of prototype U-FREIs under the simultaneous action of design vertical load and cyclic horizontal displacement.

Shape factor (*S*), which is defined as the ratio of the loaded area to load free area of a rubber layer, is likely to have influence on the force-displacement behaviour of FREIs. Since, most of the existing studies are limited to low shape factors for scaled specimens, the experimental investigations are also carried out for specimens with higher shape factors. Shear modulus of elastomer has significant influence on the force-displacement relationship. Thus, specimens with two different shear moduli are also considered for the experiments. Since the angle of incidence of earthquake to a structure may be from any directions, experimental evaluation for the effect of different loading directions on horizontal response of U-FREI is also carried out.

A large number of tests are conducted with all the above-mentioned combinations and important seismic performance related parameters like deformed shape, force-displacement relationship, stiffness and damping are examined.

3.2. Details of prototype FREIs

Prototype FREIs considered in the present study are designed for seismic isolation of a two-storey stone masonry building under-construction at Tawang, India. These isolators are manufactured by vulcanizing elastomer layers and bi-directional ($0^o/90^o$) carbon fibre fabric with the support of METCO Pvt. Ltd., Kolkata, India. Two long strips of laminated pads with two different values of shear modulus are made from eighteen elastomer layers interleaved with seventeen carbon fibre fabric layers. Strip with shear modulus, *G* as 0.78 MPa is designated as type A, while similar such strip with value of *G* as 0.90 MPa is designated as type B. The thickness of each elastomer layer is 5 mm, while that of each fibre layer is 0.55 mm and total height of each bearing is 100 mm. Specimens of designed sizes are obtained from these manufactured sheets. Two numbers of bearings of required size as 250x250x100 mm are obtained from sheet type A and the bearings are named as $A1_{(a,b)}$. Similarly, four numbers of bearings of size 250x250x100 mm are obtained from sheet type B and the bearings are named as $B1_{(a,b,c,d)}$. Further, two numbers of bearings of size 310x310x100 mm are also cut from sheet type B and the bearings are named as $B2_{(a,b)}$. Thus, eight bearings with two different values of shear modulus and two different sizes in plan are considered in this study. A typical view of a prototype isolator with layer details is shown in Fig. 3.1. The shape factor of these isolators are S = 12.5 for type A1 and B1, while S = 15.5 for isolator type B2, which is significantly higher than those of model FREIs used in most of the previous investigations. Aspect ratio of the isolator, which defined as the ratio of length to total height of the isolator, is equal to 2.50 for types A1 and B1 and 3.10 for type B2. The geometrical details and material properties of the isolators are shown in Table 3.1.

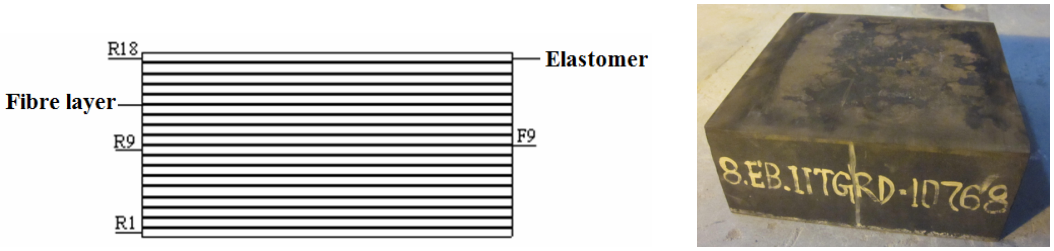

(a) Elastomer and fibre layers in U-FREI (b) 3D view of a typical U-FREI

Fig. 3.1 Prototype U-FREI

Table 3.1 Geometrical details and material properties of square isolators

Description	Isolator A1	Isolator B1	Isolator B2
Size of specimen, mm	250x250x100	250x250x100	310x310x100
Number of isolators, N	2 - $A1_{(a,b)}$	4 - $B1_{(a,b,c,d)}$	2 - $B2_{(a,b)}$
Number of elastomer layer, n_e	18	18	18
Thickness of single elastomer layer, t_e	5 mm	5 mm	5 mm
Total height of elastomer, t_r	90 mm	90 mm	90 mm
Number of fibre layer, n_f	17	17	17
Thickness of single fibre layer, t_f	0.55 mm	0.55 mm	0.55 mm
Shape factor, S	12.5	12.5	15.5
Aspect ratio	2.50	2.50	3.10
Shear modulus of elastomer, G	0.78 MPa	0.90 MPa	0.90 MPa
Elastic modulus of carbon fibre laminate	40 GPa	40 GPa	40 GPa
Poisson's ratio of carbon fibre laminate	0.20	0.20	0.20

3.3. Test for Evaluation of Horizontal Force-Displacement Behaviour of prototype U-FREIs

This section presents experimental investigations of prototype U-FREIs subjected to simultaneous action of constant design vertical pressure and cyclic horizontal displacement in order to evaluate horizontal force-displacement behaviour of these

isolators. All isolators are tested for un-bonded end conditions. These tests are conducted in the Structural Engineering Laboratory of IIT Guwahati, Assam, India.

3.3.1. Experimental Set-up

All the specimens are tested under simultaneous action of horizontal varying cyclic displacement and a constant vertical load. The experimental setup is shown in Fig. 3.2. Two same-size specimens are put one above the other and separated by a steel spacer block. The bearing specimens are in contact with the upper and lower surfaces of the steel block. However, these bearings are without any physical connection to the surfaces of the steel block and hence mimic the un-bonded condition. A horizontally placed servo-hydraulic actuator (make: MTS USA) is connected to the steel block for the application of cyclic displacements to the assembly. A constant design vertical load is applied using hydraulic jack from a compression testing machine, where the assemblage of bearings and steel block is housed. The magnitudes of vertical loads correspond to factored column loads and the values are obtained from the analysis of the actual building. The considered values are 350 and 550 kN for specimen sizes of 250x250x100 and 310x310x100 mm respectively, where a vertical pressure of about 5.6 MPa is maintained in both the cases.

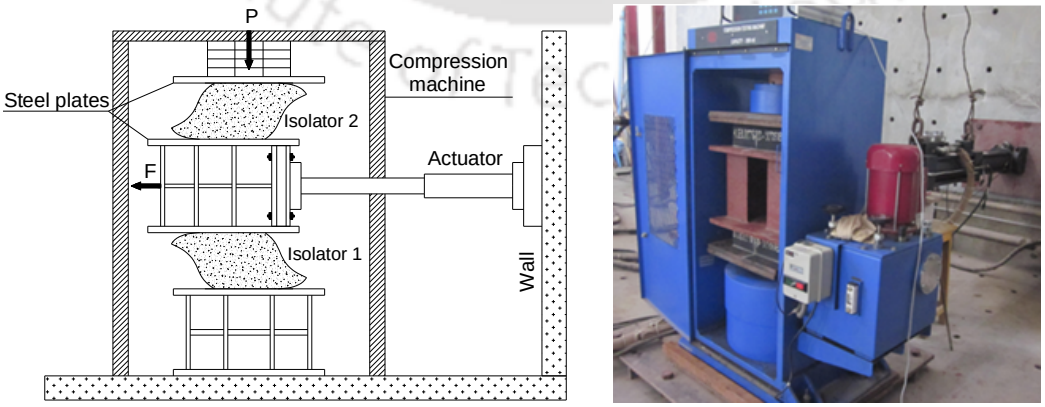

Fig. 3.2 Schematic representation and actual experimental setup

3.3.2. Details of Input Displacement History

The experimental investigations are carried out by subjecting the isolator under cyclic horizontal displacement, while maintaining a constant vertical pressure of 5.6 MPa on the isolator. Three cycles of sinusoidal displacement of frequency f = 0.025 Hz are applied continuously for four levels of displacement amplitudes as 20 mm ($0.22t_r$), 40 mm ($0.44t_r$), 60 mm ($0.67t_r$) and 80 mm ($0.89t_r$) as shown in Fig. 3.3. Horizontal displacement and corresponding lateral forces are measured using in-built linear variable differential transformer (LVDT) and load cell of the actuator.

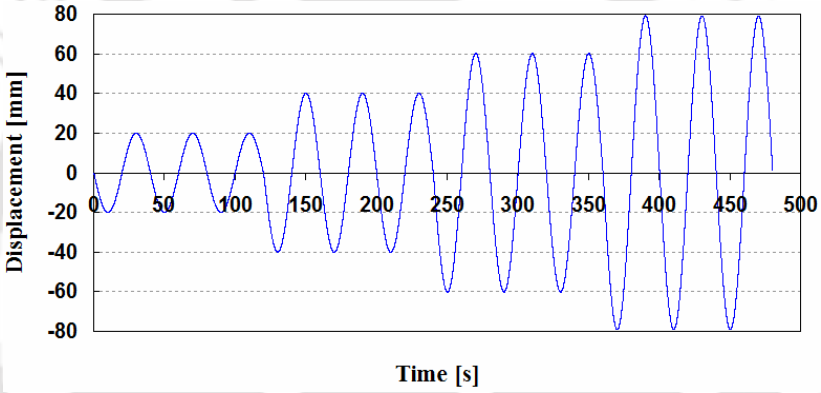

Fig. 3.3 Applied horizontal displacement history

3.3.3. Experimental Results and Discussion

3.3.3.1. Deformed shape

Deformed shape of typical specimen as obtained from experimental tests at 80 mm amplitude of horizontal displacement is shown in Fig. 3.4. The top and bottom surfaces of U-FREI exhibit stable roll off the contact surfaces without any damage. The reduction in contact area due to rollover deformation leads to the reduction in effective horizontal stiffness of isolators and results nonlinear behaviour of elastomer at large displacement. Unlike the steel shims used in a conventional SREI, fibre layers have very low flexural rigidity, and as a result, they can undergo large displacements.

Fig. 3.4 Experimentally observed deformed shape of a typical U-FREI at applied horizontal displacement of 80 mm

3.3.3.2. Hysteresis loops

The nonlinear behaviour of any isolator is generally reflected in hysteresis loop. The hysteresis loop of an isolator represents the relationship between shear forces and cyclic horizontal displacements. The horizontal displacements and shear forces experienced by the U-FREIs are measured by LVDT and load cells respectively, which are built-in the servo-hydraulic actuator. Further, the recorded shear forces actually represent the applied forces on two specimens tested simultaneously and hence, the hysteresis plot is obtained by dividing these measured forces by two to evaluate the shear forces on one specimen in average sense. Fig. 3.5 shows such hysteresis loops of different tested specimens considered in this study.

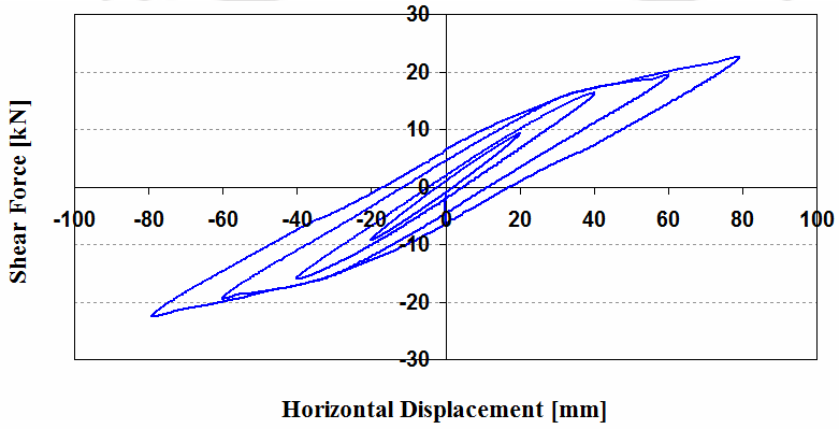

(a) $A1_{(a, b)}$

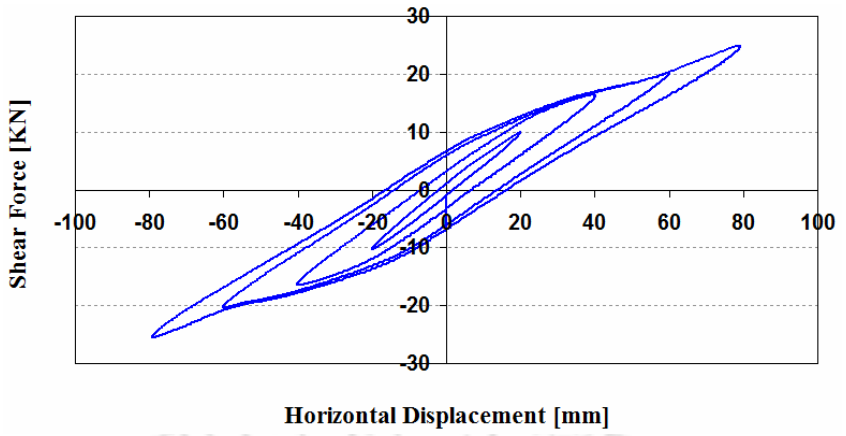

(b) $B1_{(a, b)}$

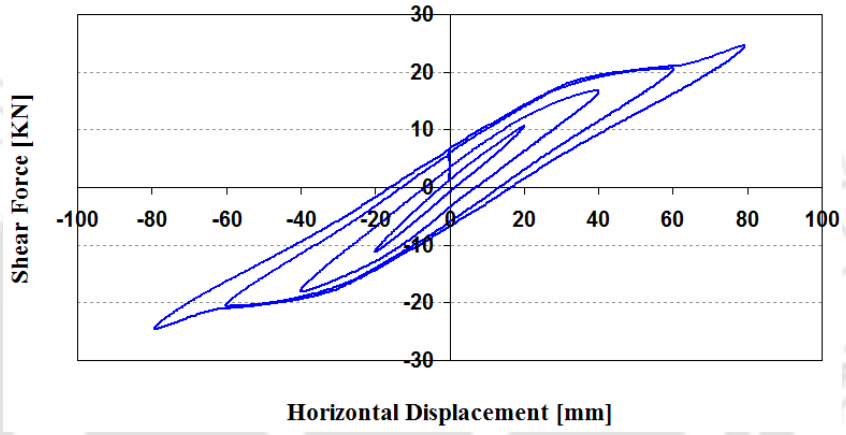

(c) $B1_{(c, d)}$

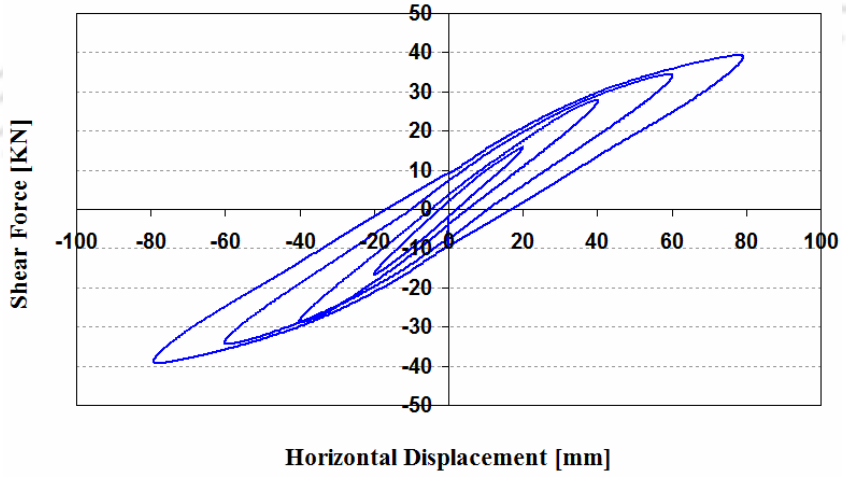

(d) $B2_{(a, b)}$

Fig. 3.5 Experimental hysteresis loops for U-FREI specimens

3.3.3.3. Characteristic properties of the U-FREIs

Two important parameters such as effective horizontal stiffness and equivalent viscous damping (or effective damping factor) are obtained from the hysteresis loops. The effective horizontal stiffness of an isolator at any amplitude of horizontal displacement is defined as Kelly and Takhirov [2001]

$$K_{eff}^{h} = \frac{F_{\max} - F_{\min}}{u_{\max} - u_{\min}} \tag{3.1}$$

where F_{max}, F_{min} are maximum and minimum values of the shear force,

u_{max}, u_{min} are maximum and minimum values of the horizontal displacement.

The equivalent viscous damping of isolator (β) is computed by measuring the energy dissipated in each cycle (W_d), which is the area enclosed by the hysteresis loop. The magnitude of β is computed as

$$\beta = \frac{W_d}{2\pi K_{eff}^{h} \Delta_{\max}^{2}} \tag{3.2}$$

where Δ_{max} is the average of the positive and negative maximum displacements.

Effective horizontal stiffness and equivalent viscous damping of these isolators at different horizontal displacement amplitudes are furnished in Table 3.2. These results are obtained by considering the average values over three cycles of each horizontal displacement amplitude.

Table 3.2 Experimentally evaluated properties of U-FREIs

Amplitude (mm)	u/t_r	$A1_{(a, b)}$		$B1_{(a, b)}$		$B1_{(c, d)}$		$B2_{(a, b)}$	
		K_{eff}^{h} (kN/m)	β (%)	K_{eff}^{h} (kN/m)	β (%)	K_{eff}^{h} (kN/m)	β (%)	K_{eff}^{h} (kN/m)	β (%)
20	0.22	464.26	5.18	507.26	5.00	547.00	4.79	814.54	5.82
40	0.44	403.41	6.94	410.21	9.67	436.10	9.57	708.04	6.89
60	0.67	324.22	11.15	339.01	12.02	343.86	13.12	573.36	10.14
80	0.89	282.60	11.83	318.68	10.02	310.52	11.51	497.48	11.84

It can be seen from Table 3.2 that the effective horizontal stiffness of an U-FREI decreases, while the equivalent viscous damping increases with the increase in horizontal displacement. The decreases in effective horizontal stiffness corresponding to increase in amplitude of horizontal displacement from 20 to 80 mm are found to be 39.1%, 37.2%, 43.2% and 38.9% for specimen $A1_{(a,b)}$, $B1_{(a,b)}$, $B1_{(c,d)}$ and $B2_{(a,b)}$ respectively. These reductions are due to rollover deformation, which will result in an increase in time period of the base-isolated structure leading to increase in their seismic response control efficacy.

3.4. Effect of Shear Modulus on Horizontal Response of U-FREIs

As discussed earlier, isolator A1 and B1 are made with same component layers and have same size of 250x250x100 mm. These two U-FREIs are subjected to same vertical load of 350 kN and cyclic horizontal displacement. However, these isolators are having different shear moduli, where G = 0.78 MPa for isolator A1 and G = 0.90 MPa for isolator B1. The response and characteristics of these isolators are compared to infer on the influence of shear modulus on isolators.

Reduction in effective horizontal stiffness with increasing horizontal displacement of U-FREIs having different values of shear modulus is shown in Fig. 3.6. Due to rollover deformation, the area of these specimens in contact with the support surfaces decrease with the increase in horizontal displacement, thus resulting in the reduction in effective horizontal stiffness.

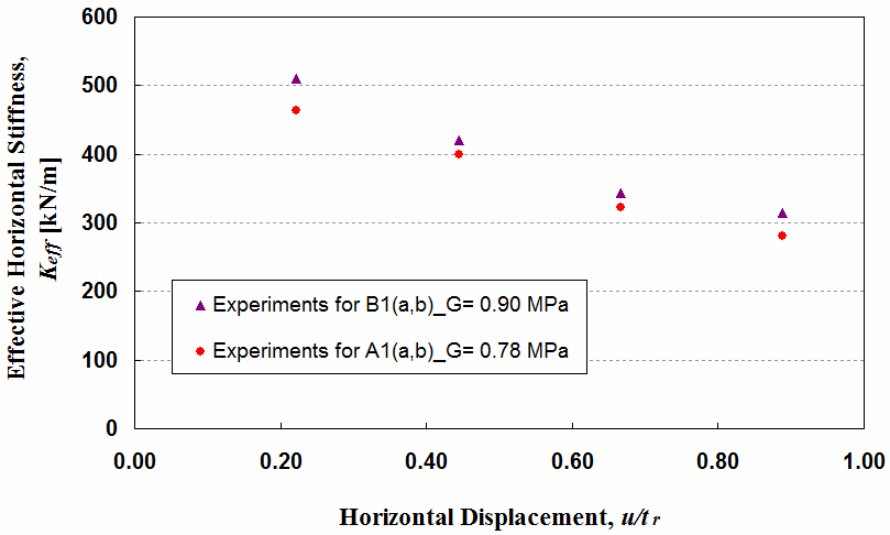

Fig. 3.6 Effective horizontal stiffness versus horizontal displacement of U-FREIs types A1 and B1

It can be observed from Fig. 3.6 that at any given horizontal displacement amplitude, where the U-FREI types A1 and B1 are likely to have same area in contact with the supports, the effective horizontal stiffness decreases with decreasing shear modulus. Thus, reduction in effective horizontal stiffness of U-FREIs with increasing horizontal displacement is not only due to rollover deformation, but also due to reduction in shear modulus of elastomer. It is presented in more details in the subsequent chapters.

3.5. Test for Evaluation of Effect of Loading Direction on Horizontal Response of square U-FREIs

In order to ascertain the influence of any arbitrary direction of incidence of an earthquake to a structure, experimental investigation of square U-FREIs (type A1) under cyclic horizontal displacement at different angles (0^o, 15^o, 30^o and 45^o) with the major axes of the isolator along with a constant vertical load are carried out. The study shows the influence of direction of loading quite clearly on the seismic performance of an isolator as the level of imposed displacement is increased.

3.5.1. Experimental Set-up and Input Loads

The experimental set-up for evaluation the effect of loading direction on horizontal response of square U-FREI type A1 is similar to the test set-up in Fig. 3.2. The arrangements for the application of horizontal displacement to the isolators in four different loading directions (0^o, 15^o, 30^o and 45^o) are as shown in Fig. 3.7. Experimental investigations in different directions are carried out under the same cyclic horizontal displacement history as shown in Fig. 3.3 and same vertical load of 350 kN (vertical pressure of 5.6 MPa).

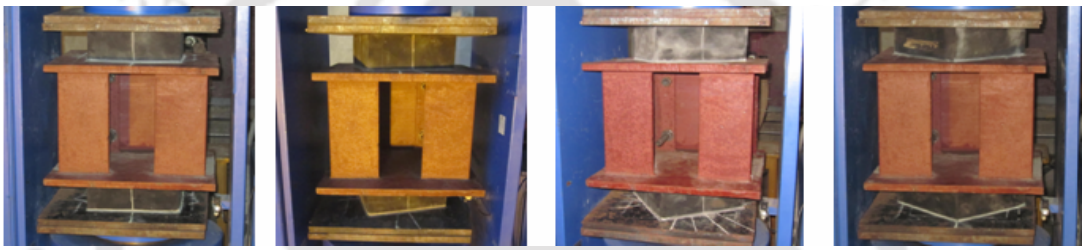

Fig. 3.7 Specimens undergoing test under horizontal displacement in different directions (0^o, 15^o, 30^o and 45^o)

3.5.2. Experimental Results and Discussion

3.5.2.1. Deformed shapes

Deformed shapes of the specimens under different loading directions at 80mm amplitude of horizontal displacement are shown in Fig. 3.8. Similar to the Section 3.3.3.1, the top and bottom surfaces of the specimens exhibit stable roll off the contact surfaces without any damage.

Further, a comparison among the deformed shapes of the specimens in four directions at any displacement amplitude reveals that as the loading direction changes from 0^o to 45^o, the area of the isolator in contact with the support surfaces increases. It also indicates

that the region of isolator that experiences rollover decreases. This results in an increase in effective shear area, which in turn increases effective horizontal stiffness.

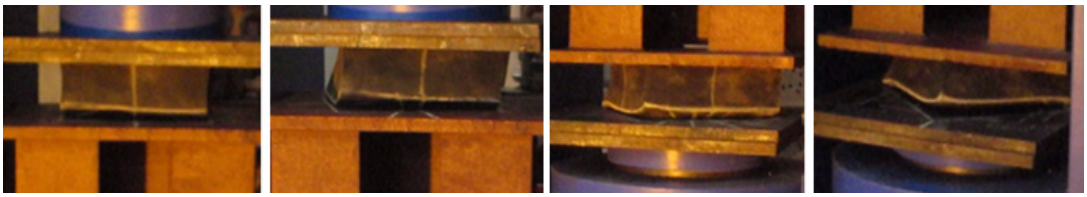

Fig. 3.8 Deformed shapes of U-FREI type A1 corresponding to 0^o, 15^o, 30^o and 45^o loading directions at 80mm amplitude of horizontal displacement obtained from experimental tests

3.5.2.2. Hysteresis loops

Fig. 3.9 shows the hysteresis loops of an isolator type A1 in different loading directions.

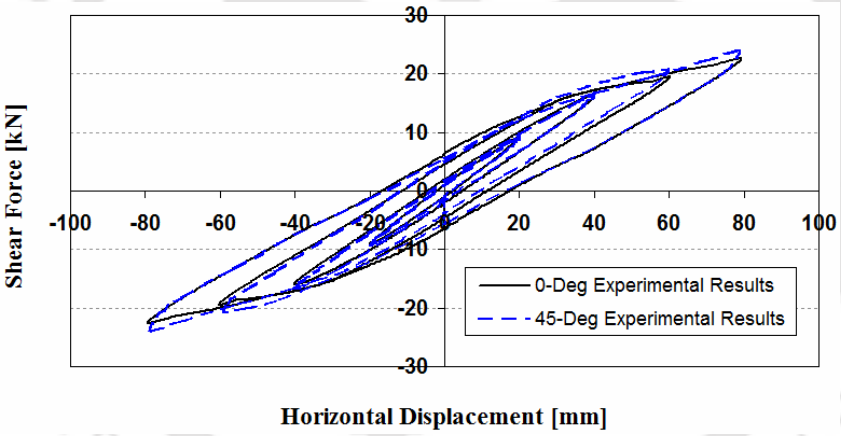

Fig. 3.9 Hysteresis loops of U-FREI type A1 under horizontal displacement in different directions obtained from experimental tests

3.5.2.3. Mechanical properties of U-FREI under different loading directions

Effective horizontal stiffness and equivalent viscous damping of the isolators type A1 under four loading directions at different horizontal displacement amplitudes are furnished in Table 3.3. These results are obtained by considering the average values

over three cycles at each horizontal displacement amplitude and are calculated by Eqs. (3.1) and (3.2).

Table 3.3 Experimentally evaluated properties of U-FREI in different loading directions

Amplitude	0^o Direction		15^o Direction		30^o Direction		45^o Direction	
	K_{eff}^h	β	K_{eff}^h	β	K_{eff}^h	β	K_{eff}^h	β
(mm)	(kN/m)	(%)	(kN/m)	(%)	(kN/m)	(%)	(kN/m)	(%)
20.0	464.26	5.18	467.07	5.16	469.82	5.03	471.95	4.89
40.0	403.41	6.94	408.09	6.70	409.82	6.47	413.04	6.29
60.0	324.22	11.15	329.65	10.86	339.59	10.32	345.42	10.08
80.0	282.60	11.83	289.03	11.58	298.52	11.14	303.25	10.85

It can be seen from Table 3.3 that the effective horizontal stiffness of the specimen in each loading direction decreases, while the equivalent viscous damping increases with the increase in horizontal displacement. The decreases in effective stiffness between amplitude of horizontal displacement of 20 and 80 mm are found to be 39.1% and 35.7% in 0^o and 45^o loading directions respectively. Further, as the loading direction changes from 0^o to 45^o, the effective horizontal stiffness of the specimen increases and the damping factor decreases at a given displacement amplitude. Thus, it is understood that U-FREIs will exhibit more displacement, if the angle of attack is along the fibre direction (either 0^o or 90^o) and least when the same is at 45^o to any of fibre directions. Any structure to be supported on such isolators will require two design considerations, namely, maximum allowable displacement and transmissibility. Maximum displacement should be calculated based on stiffness corresponding to applied horizontal displacement along the fibre direction, while the seismic efficacy should be assessed based on stiffness for applied horizontal displacement along 45^o to any of the fibre directions. Such consideration will provide limiting values to the design requirements.

3.6. Concluding Remarks

In this chapter, experimental investigations are carried out to evaluate the horizontal force-displacement behaviour of prototype U-FREIs. Eight prototype bearings with similar component layers, same total height; but with different values of shear modulus of elastomer and dimensions in plan are manufactured. Experimental studies are done under a constant vertical pressure of 5.6 MPa and cyclic horizontal displacement limit up to $0.89t_r$ (80 mm), considered from the view point of safety of the test set-up. Further, four different loading directions are considered for ascertaining its influence on the horizontal force-displacement behaviour of prototype square U-FREI. It is observed from experimental investigations that the top and bottom surfaces of U-FREIs exhibit stable roll off the contact surfaces without any damage. The following conclusions are made on the basis of the present study:

- Effective horizontal stiffness of U-FREI decreases and equivalent viscous damping increases with increase in horizontal displacement due to rollover deformation.
- Reduction in horizontal stiffness of U-FREI with increasing horizontal displacement is due to both rollover deformation and shear modulus of isolator.
- Generally, as the loading direction is varied from 0^o to 45^o, the effective horizontal stiffness of square U-FREI increases at any given horizontal displacement due to an increase in area of the isolator in contact with the support surfaces.
- U-FREI can be used for seismic isolation of low-rise buildings as they are light weight and less expensive. The weight and cost of the isolator are reduced due to the removal of two thick steel-end-plates present in conventional isolators and replacement of steel shims by fibre fabric reinforcement.

Chapter 4

Finite Element Analysis of FREIs

4.1. Introduction

Experimental findings presented in Chapter 3 show that prototype U-FREIs experience significant reduction in horizontal stiffness with increase in horizontal displacement. However, experimental investigations are limited to U-FREIs only. Further, the experimental study is done up to applied horizontal displacements of $0.89t_r$, considering the overall safety of test set-up. Thus, analysis of FREIs using numerical technique like FE method is carried out to encompass both bonded and un-bonded FREIs and for a displacement range much beyond the limitations encountered during experimental study.

Detailed discussion in Chapter 2 clearly revealed that very limited studies of FREIs are conducted so far using FE analysis. Advantage of FE analysis is well understood as this type of analysis can very easily depict the detailed stress / strain scenario and help a designer to understand important issues like possibility of buckling, peeling etc., which is otherwise quite involved in experimental study. However, the challenge of accurate estimation of response and stress / strain in FE analysis of isolators is always very high. Thus, care is taken to select finite element as well as material model such that the FE analysis is reliable and the force-displacement responses are as close as possible to the experimentally evaluated values.

All the cases of U-FREIs, which are studied experimentally are also simulated in the numerical platform. The range of displacement is considered much beyond $0.89t_r$ and same set of studies are repeated for B-FREIs as well.

4.2. Finite Element Modelling

In the present study, FREIs are modelled using ANSYS v.14.0, a general purpose finite-element software. FE modelling of FREI is a challenging task as it involves large strain, incompressibility of the material and nonlinear solution convergence. Incompressible material behaviour may lead to some difficulties in numerical simulation, such as volumetric locking, inaccuracy of solution, checkerboard pattern of stress distributions, or occasionally, divergence. Three-term Ogden model is considered to represent the behaviour of elastomer as hyper-elastic material. Selected finite element representing elastomer is designed to model material behaviour with high incompressibility. Lagrange multiplier-based mixed *u-P* element is used to simulate deformation of fully incompressible hyper-elastic materials. Lagrange multipliers extend the internal virtual work so that the volume constraint is included explicitly. The FE analyses have been done for multiple cases and no serious convergence issues are encountered.

The square isolators are modelled and analysed for both bonded and un-bonded boundary conditions. As the traditional isolators are bonded, the comparison of bonded and un-bonded isolators would provide information about the advantages, which fibre reinforced un-bonded isolators are likely to possess.

4.2.1. Element Type for Finite Element Model

In FE analysis, the major task is to choose the correct types of elements for representation of realistic behaviour of the physical model. The main components of FREIs are elastomer and multi-layered fibre reinforcement layers. B-FREIs are modelled with rigid end plates connected to top and bottom elastomer surfaces as the superstructure and substructure are directly connected to the isolator. However, in case of U-FREI, the top and bottom plates loose contact on application of horizontal

displacement. To address the issues of large strain, contact conditions and near incompressible behaviour of isolator, suitable elements with appropriate material model are chosen for modelling of isolator.

4.2.1.1. Element Type of Elastomer layer

The elastomer / rubber exhibits nonlinear behaviour under large displacement. It is modelled using SOLID185, which is an eight-node structural solid element having three degrees of freedom at each node: translations in the nodal *x*, *y*, and *z* directions. This element has the capabilities to model plasticity, hyper-elasticity, stress stiffening, creep, large deflection and large strain behaviour of material. It also has Lagrange multiplier-based mixed *u-P* formulation capability for simulating deformations of nearly incompressible elasto-plastic materials, and fully incompressible hyper-elastic materials.

4.2.1.2. Element Type of Fibre reinforcement layer

The fibre reinforcement is modelled using SOLID46, which is an eight-node layered structural solid designed to model layered thick shells or solids. Fibre-reinforcements are provided in the form of bi-directional ($0^o/90^o$) layers interleaved and bonded between elastomer layers. The element has three degrees of freedom at each node: translations in the nodal *x*, *y*, and *z* directions. Arrangement of fibre layers ($0^o/90^o$) used as reinforcement in isolators is shown in Fig. 4.1.

4.2.1.3. Contact and Target Elements

In the numerical simulation, two rigid horizontal plates are considered at the top and bottom of the isolator to represent the superstructure and substructure. Vertical load and

horizontal displacement are applied at the top plate, which is allowed to move both in the vertical and horizontal directions, while all degrees of freedom of bottom plate are restrained.

In order to study U-FREI, surface-to-surface contact elements are used. Contact element CONTA173 is used to define the top most and bottom most elastomer surfaces and target element TARGE170 is used to define the interior surface of top and bottom rigid plates. The contact element supports the Coulomb friction model to transfer the shear forces at the interface of contact and target surface. The FE model of B-FREI is same as the model of U-FREI with contact and target elements being removed. The rigid end plates are directly connected to the top and bottom elastomer surfaces as the superstructure and substructure are directly connected to the isolator.

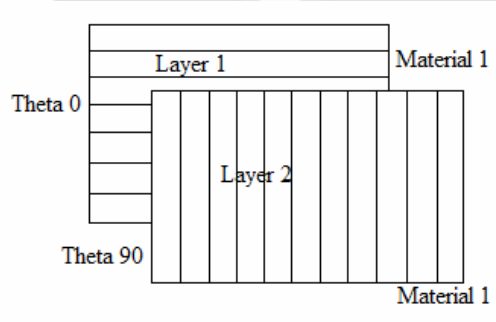

Fig. 4.1 Layer stacking of the fibre-reinforcement in isolator

4.2.2. Material Model

Material properties of components of FREI as shown in Table 3.1 in Chapter 3 are used in FE model. Elastomer is modelled with hyper-elastic and visco-elastic parameters. Hyper-elasticity refers to materials which can experience large elastic strain that is recoverable. Rubber-like and many other polymer materials fall in the category. The constitutive behaviours of hyper-elastic materials are usually derived from the strain energy potentials. Hyper-elastic materials have a stiffness that varies with the stress level.

Ogden 3-terms model has been adopted to model the hyper-elastic behaviour of the elastomer and the visco-elastic behaviour is modelled by Prony Viscoelastic Shear Response parameters. The material parameters used are considered from Ogden [1972] and Holzapfel [1996].

Ogden (3-terms): $\mu_1 = 1.89 \times 10^6$ (N/m^2); $\mu_2 = 3600$ (N/m^2); $\mu_3 = -30000$ (N/m^2);

$\alpha_1 = 1.3$; $\alpha_2 = 5$; $\alpha_3 = -2$;

Prony Shear Response: $a_1 = 0.3333$; $t_1 = 0.04$; $a_2 = 0.3333$; $t_2 = 100$;

Fig. 4.2 shows the nominal stress-stretch plot of the Ogden (three-term) material model for simple tension, simple compression and pure shear following Ogden [1972]. In the present study, experimental observations are obtained up to principal stretch of about 1.3. The deformation pattern follows very closely to what is shown in Fig. 4.2.

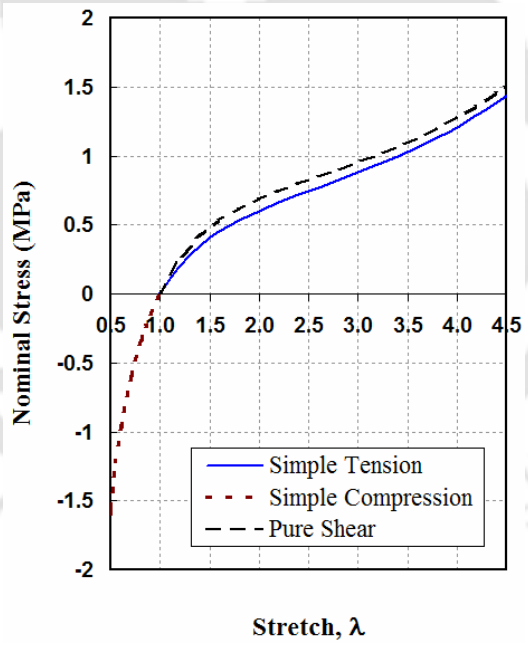

Fig. 4.2 Nominal stress versus stretch plot of Ogden (thee-term) material model

4.2.3. Details of Input Loads

Similar to experimental investigations, horizontal response of different isolator types A1, B1 and B2 are obtained from FE analysis. Analyses of FREIs in both bonded and

un-bonded applications are carried out under cyclic horizontal displacement, while maintaining a constant vertical pressure of p = 5.6 MPa (350 kN for isolator types A1, B1 and 550 kN for isolator type B2) distributed on the top rigid plate of the simulated models. Three fully sinusoidal cycles with increasing displacement amplitudes up to $1.50t_r$ (135 mm) for evaluation of horizontal force-displacement behaviour of the isolators, or up to $2.00t_r$ (180 mm) for evaluation of effect of loading direction on horizontal response of the isolators are applied on the top rigid plate (similar to Fig. 3.3 in Chapter 3). The applied displacement range in FE analysis is much higher than that considered in experimental investigations.

4.2.4. Solution Method

The full transient dynamic analysis is carried out to determining the time-varying responses of the isolator. The full method uses the full system matrices to calculate the transient responses. It is the most general method of analysis used in ANSYS. This method allows calculation of all types of nonlinearities, loads, displacements and stresses in a single pass and there is no mass matrix approximations involved. Full method is used in analysing the isolators because of the material nonlinearity and nonlinearity of the contact element. Displacement-based convergence criterion is used for the analysis under combined action of vertical load and horizontal displacements.

4.2.5. Effect of Mesh Size on FE Analysis Result

The model is meshed with hexagonal volume sweep. The volume sweep fills existing unmeshed volume with elements by sweeping the mesh from an adjacent area through the volume. If the area is not already meshed, volume sweep meshes the area and then extrudes it. In case of nonlinear and large displacement FE analysis, size of mesh plays

an important role. Generally, a refined mesh gives more accurate solution in FE analysis. However, very fine mesh obviously requires large storage space as well as more computational time. Thus, a mesh sensitivity analysis is first carried out to arrive at an acceptable refined mesh by studying the solution convergence with mesh refinement, which is subsequently considered for the detailed analysis.

Fig. 4.3 shows three FE models of FREI type B1 with different discretization named as coarse, fine and very fine mesh size. The *X*-axis matches with fibres oriented along 0°, while *Y*-axis matches with fibres along 90°. Distribution of normalized stress S_{33}/p (p is the vertical pressure due to applied vertical load at the top of isolator, axis-*3* is parallel to *Z*-axis) plotted along the width of the 9^{th} elastomer layer located adjacent to the mid-height and of the 9^{th} fibre layer located at mid-height of U-FREI, type B1 at horizontal displacement of 135 mm are shown in Figs. 4.4 & 4.5 respectively. All the three types of FE meshes as shown in Fig.4.3 are considered for the study. It can be seen from Fig. 4.4 that the stress distribution pattern, peak values of compressive tress in the mid elastomer layer corresponding to the coarse and fine mesh are very close to the results obtained from very fine mesh. However, it may be observed from Fig. 4.5 that the stress distribution corresponding to very fine mesh is much smoother as compared to other two mesh cases, though the peak compressive values are almost in the same range. In view of this, all the subsequent analyses for all the considered isolators are carried out utilizing the very fine mesh as shown in Fig. 4.3 (c).

In this present study, both B-FREI and U-FREI are analysed using the same mesh size like in Fig. 4.3(c). The connections of rigid supports with the top and bottom surfaces of the isolators are appropriately addressed for the simulation of bonded and un-bonded cases. The detailed results from the analyses are presented for proper understanding of the behaviour of these isolators.

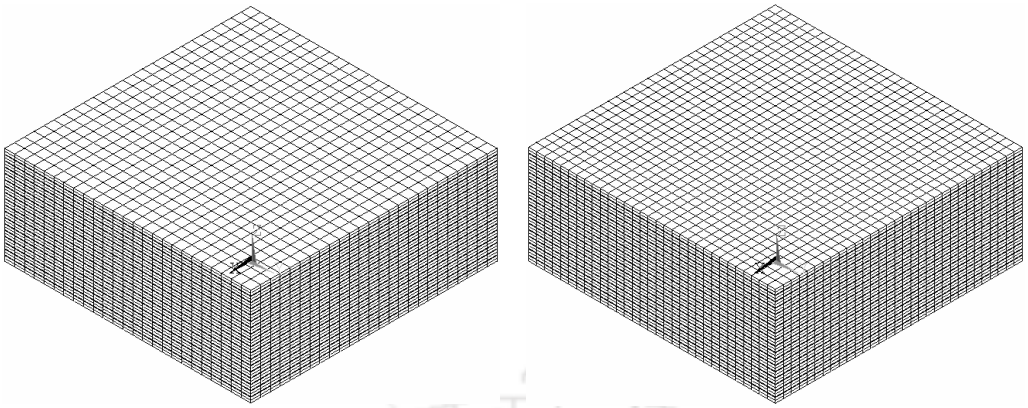

(a) Coarse mesh (b) Fine mesh

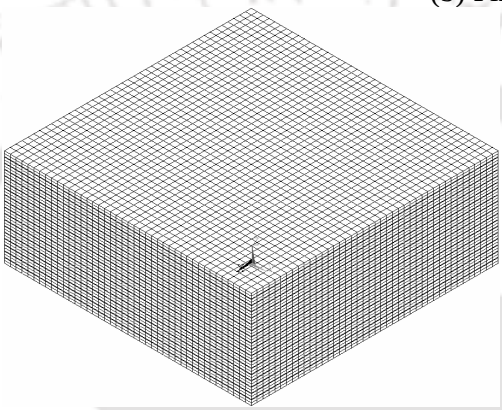

(c) Very fine mesh

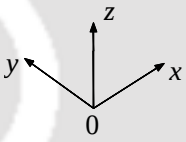

Fig. 4.3 FE model of FREI with different discretization

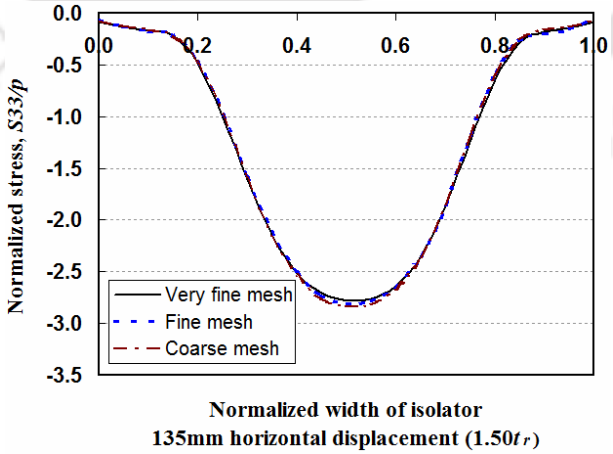

Fig. 4.4 Distribution of normalized stress S_{33}/p plotted along the width in the elastomer layer at mid-height of U-FREI, type B1 at displacement of 135 mm with different meshes

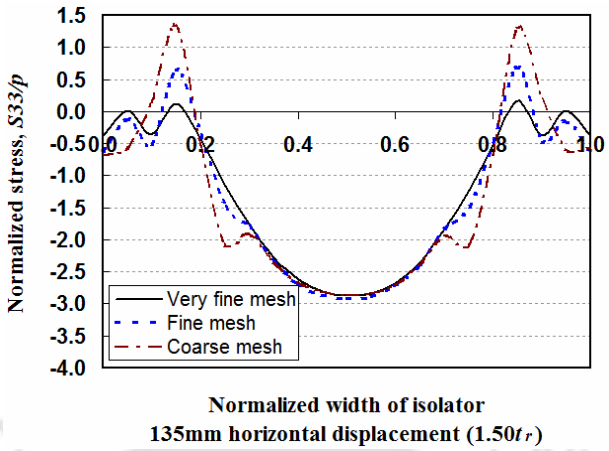

Fig. 4.5 Distribution of normalized stress S_{33}/p plotted along the width in the fibre layer at mid-height of U-FREI, type B1 at displacement of 135 mm with different meshes

4.3. Performance of prototype FREI under Cyclic Horizontal Displacement

Both B-FREI and U-FREI types A1, B1 and B2 are analysed under the same vertical pressure of 5.6 MPa and cyclic horizontal displacement up to $1.50t_r$ (135 mm). Horizontal force-displacement relationship, hysteresis loop, horizontal stiffness, equivalent viscous damping, stresses and strains in elastomer and fibre reinforcement layers of these isolators are investigated. Validation of adopted FE model is performed by comparing mechanical properties of U-FREIs as obtained from FE analysis with those from experiments. A comparison of horizontal responses of B-FREI and U-FREI is also presented to assess the seismic performance of U-FREI.

4.3.1. Validation of Finite Element Model of U-FREI

Deformed shapes, hysteresis loops and horizontal load-displacement relationships of prototype U-FREIs as obtained from FE analyses are compared to those from experimental investigations. The comparison is done for increasing displacement up to

$0.89t_r$. Agreement of experimental and finite element based results would be a testimony to the accurate numerical modelling with appropriate material model for simulating the behaviour of elastomer up to displacement of $0.89t_r$, when the load displacement relationship is no more linear.

4.3.1.1. Deformed shapes

Deformed shape of typical U-FREI as obtained from FE analysis at the horizontal displacement amplitude of 80 mm is shown in Fig. 4.6. Similar to deformed shape of typical U-FREI obtained from experimental investigations as shown in Fig. 3.4 Chapter 3, the upper and lower faces of the U-FREI roll off the contact supports. It results in a nonlinear horizontal load-displacement behaviour of the isolator.

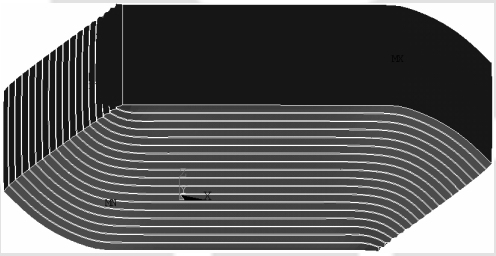

Fig. 4.6 Deformed shape of typical U-FREI at 80 mm horizontal displacement amplitude obtained from FE analysis

4.3.1.2. Hysteresis Loops

The total forces in the loading direction at all the nodes of the top surface of isolator obtained from FE analysis are summed to get the total shear force. Shear forces are then plotted against applied horizontal displacement to get the hysteresis loop for each isolator. Fig. 4.7 shows the hysteresis plots for data obtained from both FE analysis and laboratory tests for displacement up to $0.89t_r$ (80 mm). Comparison of the hysteresis loops of U-FREIs as obtained from experiments and FE analysis for each type show the discrepancy to be quite less.

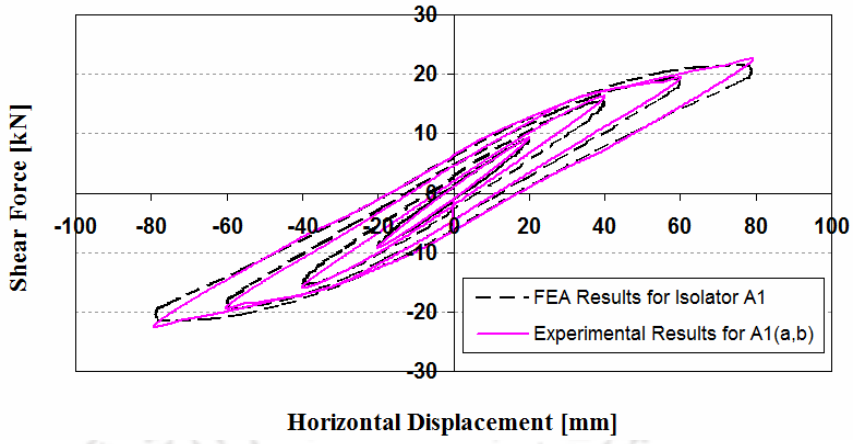

(a) Isolator A1

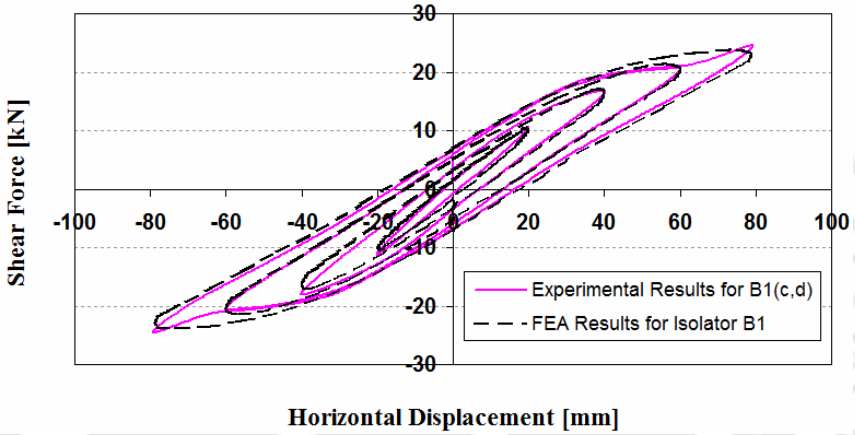

(b) Isolator B1

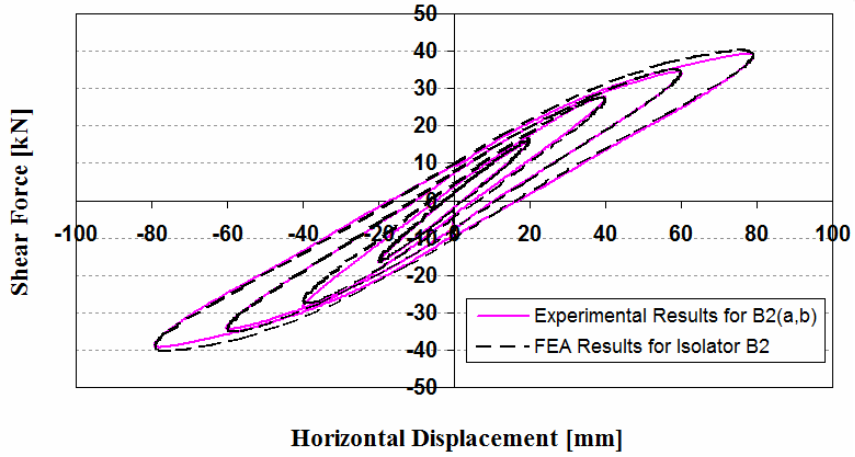

(c) Isolator B2

Fig. 4.7 Comparison of hysteresis loops of different types of U-FREI obtained from FE analysis and experimental results

4.3.1.3. Horizontal Load-Displacement Relationships

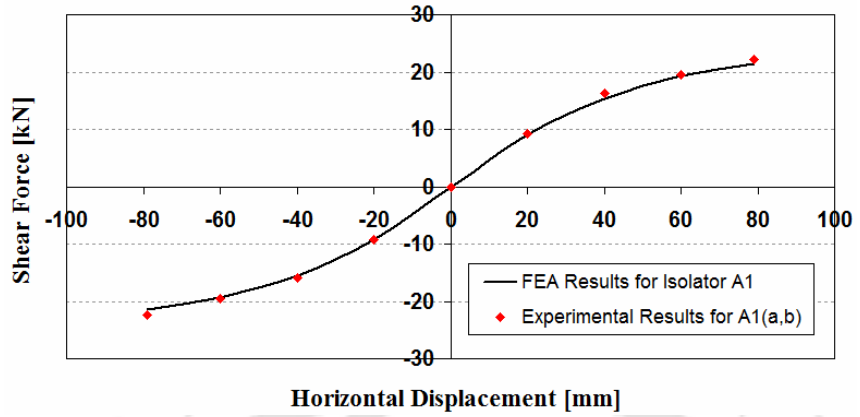

(a) Isolator A1

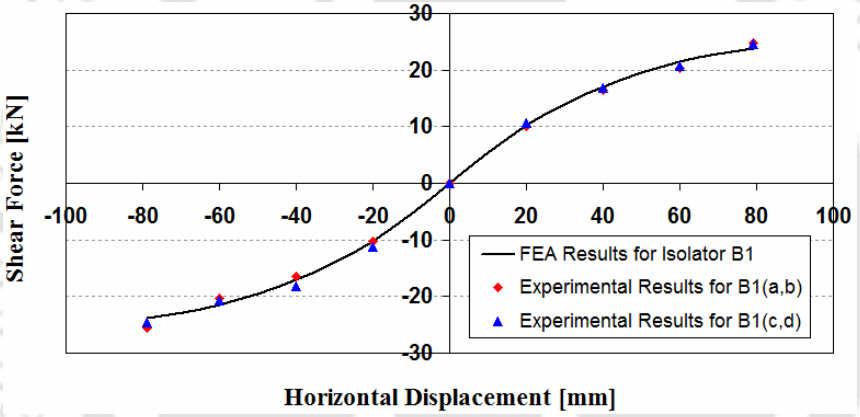

(b) Isolator B1

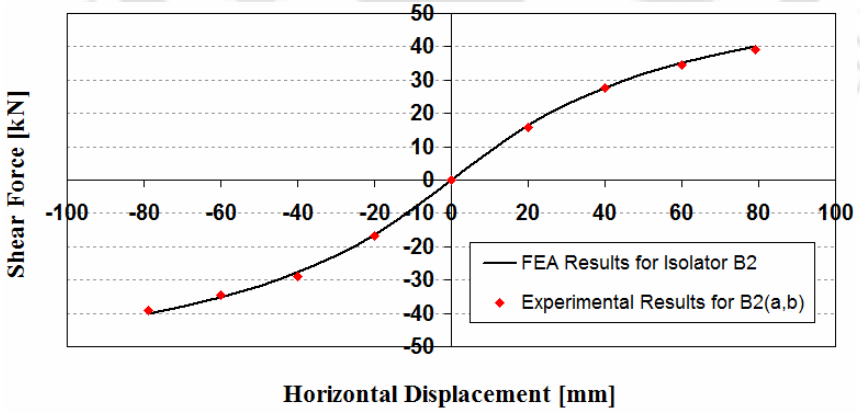

(c) Isolator B2

Fig. 4.8 Comparison of horizontal load-displacement relationships of different types of U-FREI obtained from FE analysis and experimental results

A comparison of horizontal load-displacement relationships (backbone curves) of these U-FREIs with increasing horizontal displacement up to $0.89t_r$ as obtained from load-displacement hysteresis loops recorded during experimental investigations and FE analyses is shown in Fig. 4.8. As may be seen from Figs. 4.7 & 4.8, very good agreement is observed between the experimental and FE results for all these isolators at displacements ranging from 20 mm to 80 mm. Hence, the results obtained by FE analysis for U-FREIs at even larger displacement (from 80 to 135 mm) will be considered as accurate. The accuracy of the FE analysis results are established for the considered problem.

4.3.2. Deformed Shapes of Bonded and Un-bonded FREI

The free body diagram of bonded and un-bonded isolators (Nezhad, *et al.*, 2011) is shown in Fig 4.9. In case of B-FREI, the top and bottom surfaces of isolator always remain in contact with the supports and load application point does not change with the increase of lateral displacement. Equilibrium of isolator is established by the balancing moment generated at top and bottom surfaces of isolator. As a result of this moment, tensile stresses normal to the surface are generated in regions outside the central compression core.

On the contrary, the point of application of vertical load resultant at external top and bottom surfaces of deformed U-FREI shift towards the pressed end. The offset of the resultant compressive loads produces a couple which balances the overturning moment caused by the shear developed in the top and bottom surfaces of isolator as shown in Fig. 4.9(b). Due to this, no tensile stresses are transferred at the contact support of un-bonded isolators.

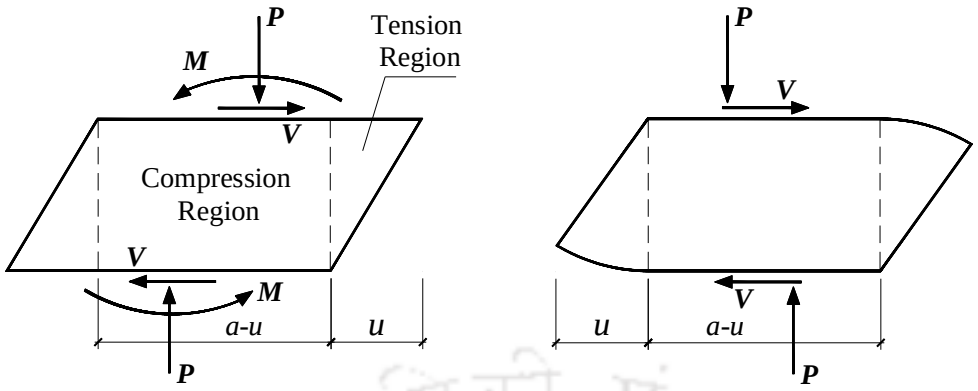

(a) B-FREI (b) U-FREI

Fig. 4.9 Free body diagram of horizontally deformed FREI with different boundary conditions

Deformed shapes of bonded and un-bonded isolator type B1 (similar for isolator types A1, B2) as obtained from FE analyses corresponding to the horizontal displacement amplitude of 90 mm ($1.0t_r$) are shown in Fig. 4.10. It can be seen from the figure that as the isolator is horizontally displaced, the upper and lower faces of B-FREI remain fully in contact with the support surfaces, while the upper and lower faces of U-FREI roll off the contact surfaces and hence result in development of very low tensile stresses in that regions. The rollover deformation of U-FREI results in non-linear load-displacement behaviour of the isolator.

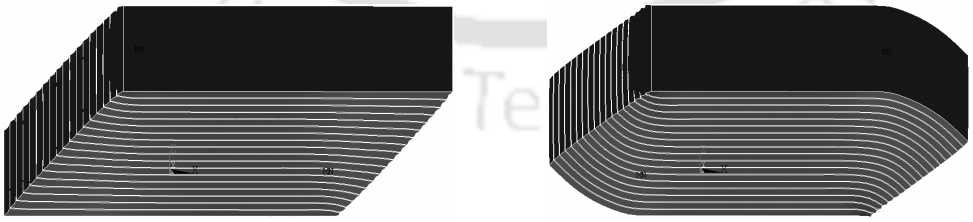

(a) B-FREI (b) U-FREI

Fig. 4.10 Deformed shapes of isolator B1 obtained from FE analyses at 90 mm ($1.00t_r$) of horizontal displacement amplitude

4.3.3. Mechanical Properties of FREI

Similar to Chapter 3, two important parameters such as effective horizontal stiffness and equivalent viscous damping of all isolators are calculated from Eqs. (3.1), (3.2) and are presented in Tables 4.1-4.3. It may be observed from hysteresis loops that the isolators exhibit large amount of change in stiffness as these are subjected to horizontal displacement from small to very large up to $1.50t_r$ (135 mm).

Table 4.1 Mechanical properties of U-FREI and B-FREI type A1

Amplitude (mm)	u/t_r	Experimental results		FE analysis results			
		$A1_{(a,b)}$		Un-bonded		Bonded	
		K_{eff}^{h}	β	K_{eff}^{h}	β	K_{eff}^{h}	β
		(kN/m)	(%)	(kN/m)	(%)	(kN/m)	(%)
20.0	0.22	464.26	5.18	457.72	7.16	468.19	7.15
40.0	0.44	403.41	6.94	385.10	9.30	428.07	8.71
60.0	0.67	324.22	11.15	321.99	11.71	397.23	10.28
80.0	0.89	282.60	11.83	272.20	13.22	373.65	10.73
90.0	1.00	-	-	251.09	13.78	362.60	10.99
112.5	1.25	-	-	219.02	14.19	345.00	11.43
135.0	1.50	-	-	195.75	14.94	333.94	11.68

Table 4.2 Mechanical properties of U-FREI and B-FREI type B1

Amplitude (mm)	Experimental results				FE analysis results			
	$B1_{(a,b)}$		$B1_{(c,d)}$		Un-bonded		Bonded	
	K_{eff}^{h}	β	K_{eff}^{h}	β	K_{eff}^{h}	β	K_{eff}^{h}	β
	(kN/m)	(%)	(kN/m)	(%)	(kN/m)	(%)	(kN/m)	(%)
20.0	507.26	5.00	547.00	4.79	515.87	7.58	528.12	7.51
40.0	410.21	9.67	436.10	9.57	426.93	9.60	486.13	9.03
60.0	339.01	12.02	343.86	13.12	357.01	12.05	452.65	10.52
80.0	318.68	10.02	310.52	11.51	301.67	13.46	425.54	11.10
90.0	-	-	-	-	281.34	14.11	414.90	11.42
112.5	-	-	-	-	247.09	14.58	393.10	11.91
135.0	-	-	-	-	222.03	15.42	379.09	12.27

Table 4.3 Mechanical properties of U-FREI and B-FREI type B2

Amplitude (mm)	u/t_r	Experimental results		FE analysis results			
		$B2_{(a,b)}$		Un-bonded		Bonded	
		K_{eff}^{h}	β	K_{eff}^{h}	β	K_{eff}^{h}	β
		(kN/m)	(%)	(kN/m)	(%)	(kN/m)	(%)
20.0	0.22	814.54	5.82	814.23	6.86	829.81	6.80
40.0	0.44	708.04	6.89	688.00	8.52	760.60	7.77
60.0	0.67	573.36	10.14	586.30	10.35	707.36	9.08
80.0	0.89	497.48	11.84	508.60	12.16	665.01	9.71
90.0	1.00	-	-	480.09	12.57	646.09	10.31
112.5	1.25	-	-	433.13	13.08	615.24	10.86
135.0	1.50	-	-	401.33	13.68	595.62	11.44

It can be observed from Tables 4.1-4.3 that the effective horizontal stiffness of B-FREI and U-FREI obtained from FE analysis decrease with the increase in horizontal displacement. However, the decreases in stiffness of U-FREIs are faster than those of corresponding B-FREIs. Specifically, the decreases in stiffness of type A1, B1, B2 U-FREIs are found to be 57.2%, 57.0% and 50.7%, while the same for B-FREIs are 28.7%, 28.2% and 28.2% respectively in the displacement range of 20 to 135 mm. Similarly, higher rate of increase in damping factors are observed in U-FREIs in comparison to B-FREIs with the increase in applied horizontal displacement. Further, the effective stiffness and damping values of all three types of U-FREIs as obtained from FE analysis as well as experimental investigations are also presented in Tables 4.1-4.3. The values of effective stiffness from experiment and FE analyses (Tables 4.1-4.3) are in good agreement, while some differences are observed in damping.

4.3.4. Horizontal Load-Displacement Relationship of B-FREI and U-FREI

Fig. 4.11 shows the horizontal load-displacement relationships of B-FREIs and U-FREIs obtained from load-displacement hysteresis loops recorded during experimental investigations and FE analyses. It can be observed from Fig. 4.11 that the horizontal load-displacement relationships are nearly linear in the range of small displacement for both the bonded and un-bonded isolators. Slope of these lines are the secant horizontal stiffness of isolators. When the applied displacement increases, the response of B-FREI is almost linear, while the response of U-FREI becomes nonlinear due to the rollover deformation. Consequently, the horizontal secant stiffness of U-FREI decreases at faster rate with increasing horizontal displacement. Thus, fundamental time period of U-FREI supported structure increases with the decrease in stiffness at high imposed displacement, which results in increasing seismic mitigation capacity. Therefore, stable U-FREIs have superior seismic isolation capacity as compared to B-FREIs.

In a base isolated system, the horizontal shear load resisted by the isolators is transmitted to the superstructure. It can be observed from Fig. 4.11 that in the range of small displacement up to 20 mm, the forces that would be transmitted by B-FREI and U-FREI are almost same. However, beyond 20 mm, the forces transmitted by U-FREIs are significantly lower as compared to B-FREIs. Specifically, at the amplitude of displacement of 135 mm ($1.50t_r$), the horizontal forces transmitted by types A1, B1, B2 B-FREIs are 71.1%, 70.5% and 48.4% higher than the corresponding U-FREIs. Consequently, it can be concluded that for a given size of isolator, the performances of un-bonded isolators is far superior to corresponding bonded isolators.

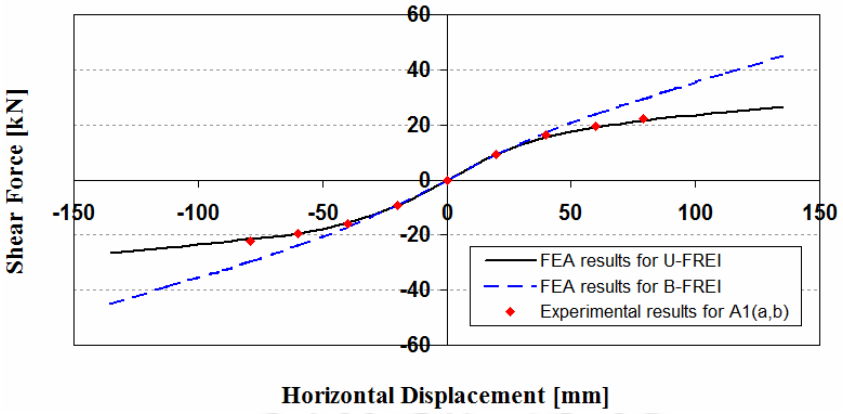

(a) Isolator A1

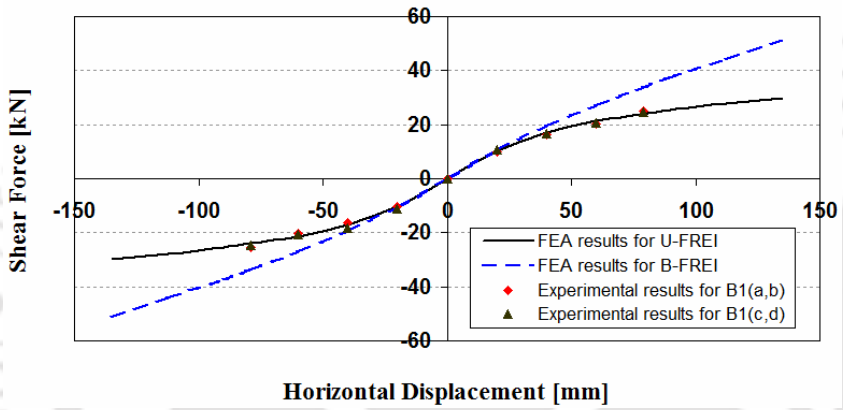

(b) Isolator B1

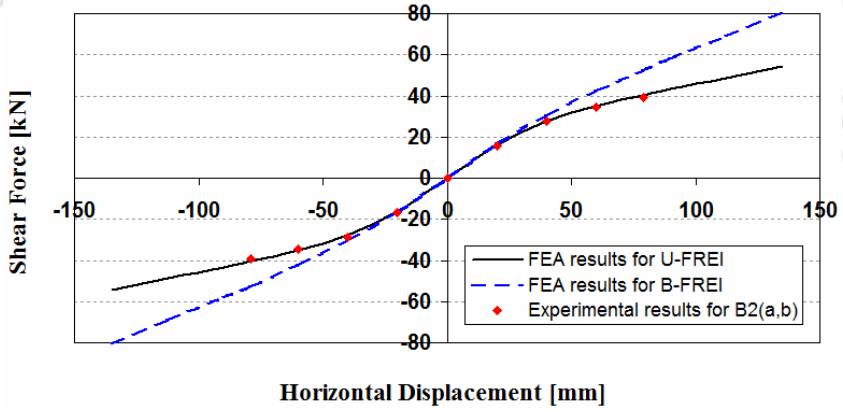

(c) Isolator B2

Fig. 4.11 Horizontal load versus displacement of FREIs obtained from experiments and FE analysis

4.3.5. Stress and Strain in Elastomer Layer

With the increase in the amplitude of applied displacement, U-FREIs experience rollover deformation. Isolators are analyzed under the action of cyclic displacement applied along *X*-axis. For denoting stress, the local axes are designated as axis-*1*, axis-*2* and axis-*3*, which are parallel to the *X*, *Y* and *Z*-axis, respectively. FE analysis results showed similar values for S_{11} and S_{22} stresses, and as a result only S_{11} and S_{33} stresses are plotted.

Contours of normal stress S_{11} in elastomer layers of a half B-FREI and U-FREI corresponding to maximum applied displacement of 135 mm ($u = 1.50t_r$) are shown in Fig. 4.12. These contours are plotted over one half of the isolator for better representation. It may be mentioned that the stress contour in elastomer layers of isolator type A1 is almost identical to that of isolator type B1 and hence details of stress contour for A1 is not shown separately.

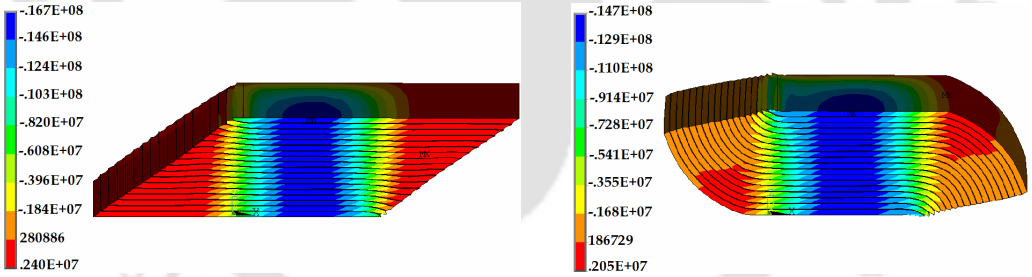

B-FREI U-FREI

(a) Isolator B1

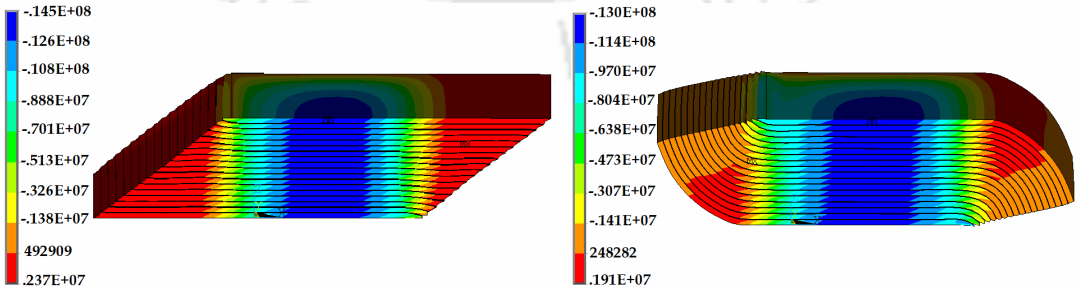

B-FREI U-FREI

(b) Isolator B2

Fig. 4.12 Contour of normal stress S_{11} (N/m^2) in elastomer layers of a half isolator at horizontal displacement of 135 mm (positive value indicates tension)

It can be observed from FE analysis results, as the horizontal displacement increases, area of compression region in elastomer layer of both B-FREI and U-FREI decreases, while the peak values of compressive stress S_{11} increase. In case of B-FREI, the compression in the central core is almost constant throughout the overlapping region between the top and bottom surfaces, and the unbalanced moment is carried by tensile stresses in the regions outside the overlap. For U-FREI, a compression region is observed along the edge of the top and bottom elastomer layers, as the isolator is displaced horizontally. In comparison of B-FREI and U-FREI, the peak values of compressive stress of U-FREI are lesser than B-FREI. Further, when U-FREI is deformed horizontally, near end of the loading direction leaves the contact and moves upward causing tension in fibre-reinforcement. Similarly, the opposite end of the U-FREI moves downward and loses contact with the support. Thus, tension of U-FREI is developed in the region of no contact while other regions remain under compression. It may however be noted that the developed tensile stress in the elastomer and fibre reinforcement layers in the rollover portion of U-FREI is low and hence presents lower peeling stress demand on the bond between layers. However, due to rollover deformation, no tensile stress is transferred to the isolator's contact support. The unbalanced moments are resisted by the vertical load through offset of the force resultants on the top and bottom surfaces.

Fig. 4.13 represents the distribution of the normalized stress S_{11}/p plotted along the width of the 9th elastomer layer located adjacent to the mid-height of both B-FREI and U-FREI at different horizontal displacements, where p is the vertical pressure due to vertical load applied to the top of isolators ($p \approx 5.6$ MPa). It can be observed from Fig. 4.13 that as the horizontal displacement increases, the peak values of compressive stress in the mid elastomer layer of both B-FREI and U-FREI increase. The increase in peak

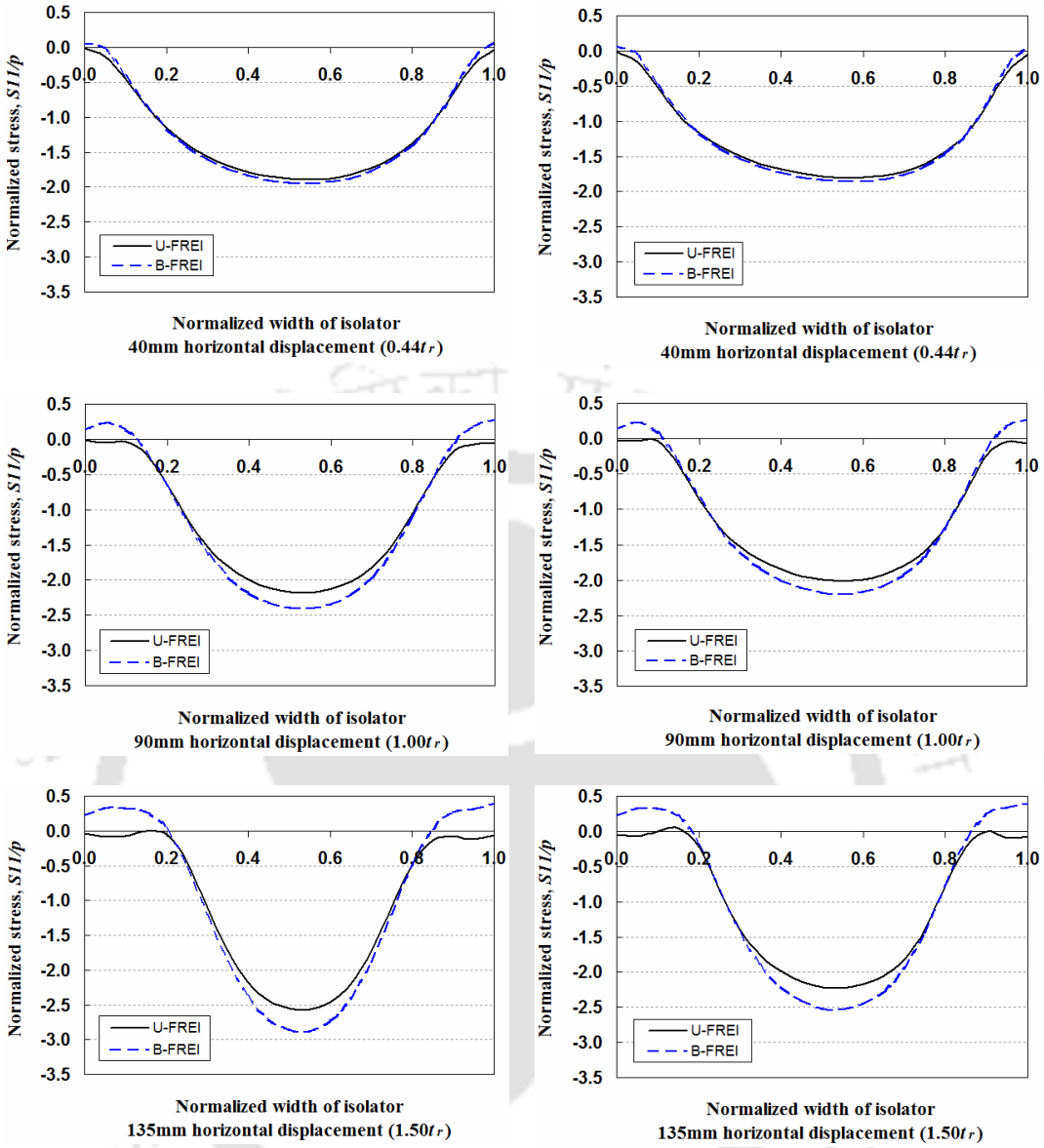

(a) Isolator B1 (b) Isolator B2

Fig. 4.13 Distribution of normalized stress S_{11}/p plotted along the width in the elastomer layer at mid-height of isolator at different horizontal displacements

value of compressive stress in B-FREI is observed to be higher than that in U-FREI at a given horizontal displacement. Specifically, at u = 1.50t_r, the peak values of compressive stress of B-FREIs types B1 and B2 are approximately 12.5% and 13.5% higher than those of corresponding U-FREIs. Hence, the likelihoods of Euler buckling

in U-FREIs are significantly lower than those in B-FREIs. In addition, the peak values of tensile stress of B-FREIs increase with the increase in horizontal displacement, while no tension or a tension region with very low values (at $u > 1.00t_r$) develops in the elastomeric material of U-FREIs. Development of considerable tensile stress is observed in B-FREIs along with the presence of warping effect.

Contours of normal stress S_{11} in the 9th elastomer layer (adjacent to mid-height of the isolator) of both B-FREI and U-FREI corresponding to the maximum applied horizontal displacement of 135 mm are shown in Fig. 4.14. Significant parts of the elastomer layer at mid-height of U-FREI is under compression. However, B-FREI has around 40% area of elastomer layer at mid-height under tension.

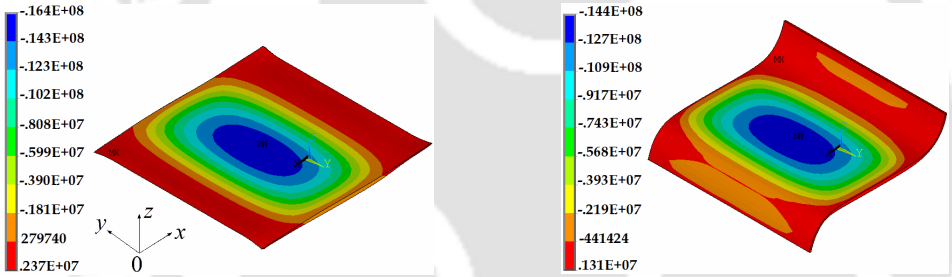

B-FREI U-FREI

(a) Isolator B1

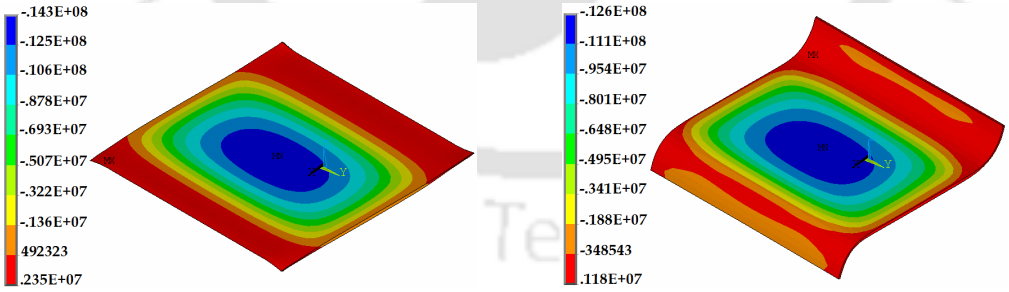

B-FREI U-FREI

(b) Isolator B2

Fig. 4.14 Contour of normal stress S_{11} (N/m^2) in the elastomer layer at mid-height of isolator at displacement of 135 mm (positive value indicates tension)

Contours of normal stress S_{33} in elastomer layers of a half B-FREI and U-FREI at horizontal displacement of 135 mm ($1.50t_r$) are shown in Fig. 4.15. It can be seen from Figs. 4.12 and 4.15 that the overlapping region between the top and bottom faces of B-FREIs is under biaxial compression, while the regions outside the overlapping zone is under biaxial tension. Similar to B-FREIs, the central-core region of U-FREIs also resists biaxial compression. The peak compressive and tensile stress values in U-FREIs are significantly lower than B-FREIs.

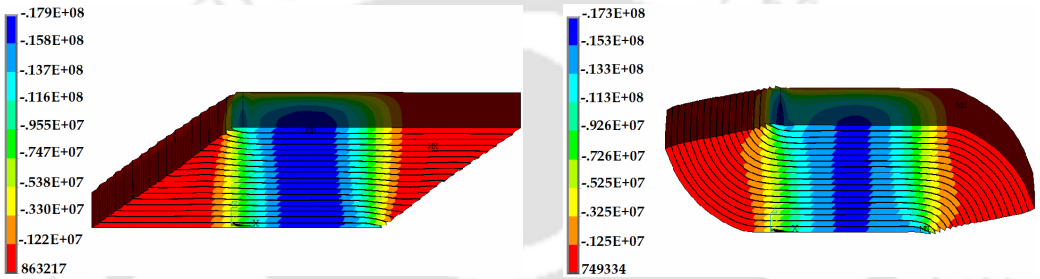

B-FREI U-FREI

(a) Isolator B1

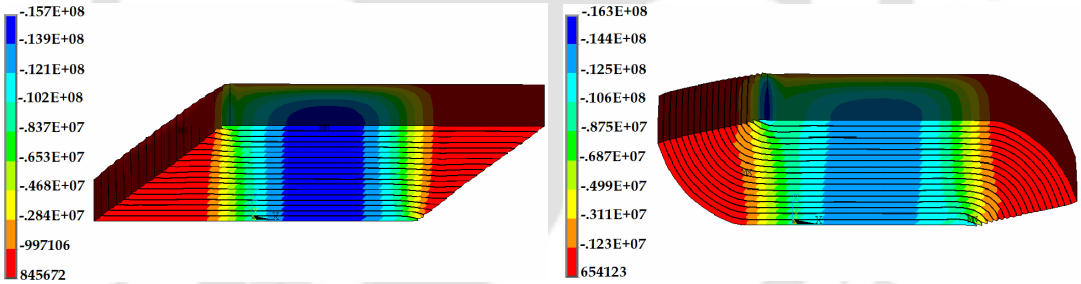

B-FREI U-FREI

(b) Isolator B2

Fig. 4.15 Contour of normal stress S_{33} (N/m^2) in elastomer layers of a half isolator at horizontal displacement of 135 mm (positive value indicates tension)

Distribution of normalized stress S_{33}/p plotted along the width of the 9th elastomer layer located adjacent to the mid-height of isolators types B1, B2 at different displacements are shown in Fig. 4.16. It can be seen in Fig. 4.16, peak values of compressive stress in mid elastomer layer of U-FREIs are lower than those of corresponding B-FREIs. Similar to Fig. 4.13, as the horizontal displacement increases, the peak values of

compressive tress of both B-FREI and U-FREI increase, while the length of compression region decreases. Development of significant tensile stress in B-FREIs along with the existence of warping effect is observed, but no tensile stress is developed in the elastomeric material of U-FREIs for the considered range of horizontal displacement.

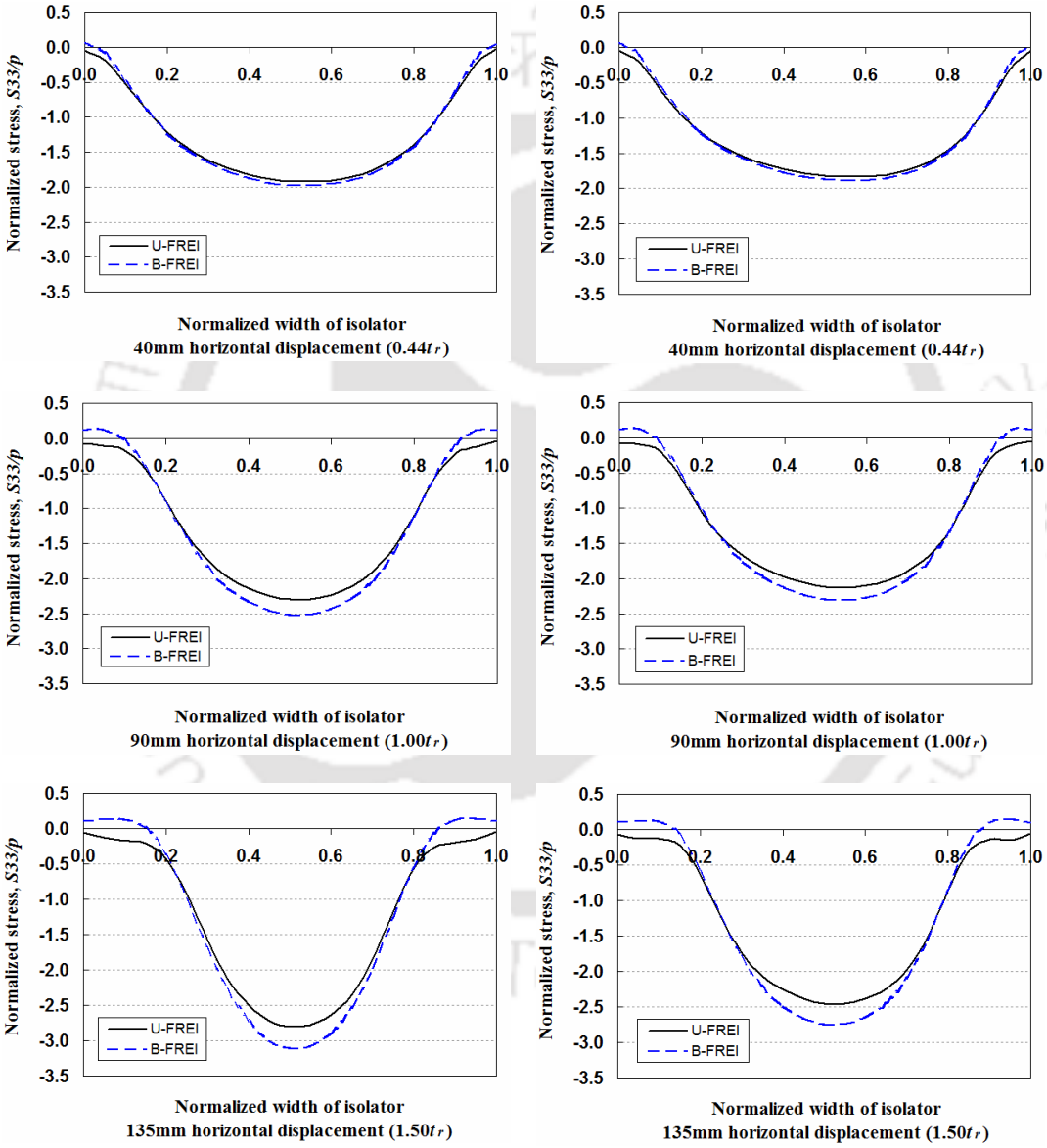

(a) Isolator B1 (b) Isolator B2

Fig. 4.16 Distribution of normalized stress S_{33}/p plotted along the width in the elastomer layer at mid-height of isolator at different horizontal displacements

Fig. 4.17 shows the contours of normal stress S_{33} in the 9th elastomer layer of both B-FREI and U-FREI corresponding to the maximum applied horizontal displacement of 135 mm. The entire mid elastomer layer at mid-height of U-FREI is under compression. Central core of this layer is highly compressed and high stress is shared by larger area along *Y* direction as compared to *X* direction of the isolator. However, the mid elastomer layer at mid-height of B-FREI outside overlapping region is under tension. Like U-FREI, the spread of compression along *Y* direction of B-FREI is more as compared to *X* direction.

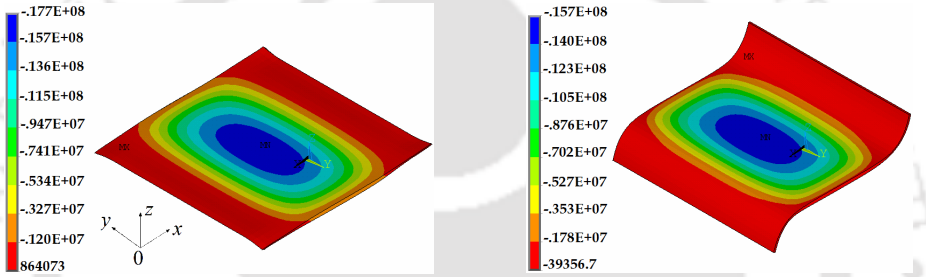

B-FREI U-FREI

(a) Isolator B1

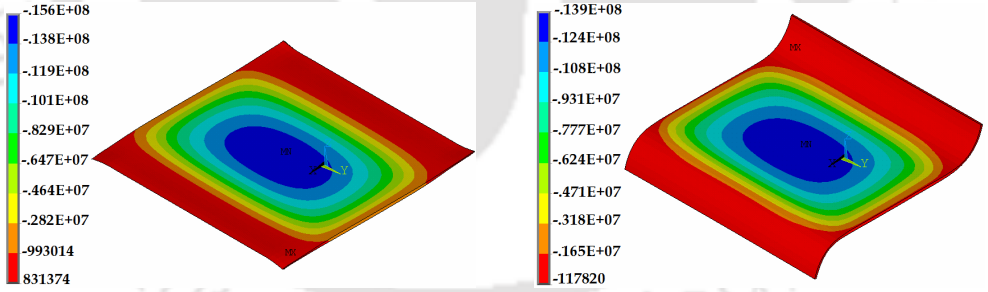

B-FREI U-FREI

(b) Isolator B2

Fig. 4.17 Contour of normal stress S_{33} (N/m^2) in the elastomer layer at mid-height of isolator at displacement of 135 mm (positive value indicates tension)

Shear strain in elastomeric material must be large for efficient operation of an elastomeric isolator. Fig. 4.18 shows the contours of shear strain in elastomer layer of a

half B-FREI and U-FREI corresponding to horizontal displacement of 135 mm. Distribution of shear strain plotted along the width of the 9th elastomer layer located adjacent to the mid-height of both B-FREI and U-FREI at different displacements are shown in Fig. 4.19. It can be seen from Fig. 4.19 that as the horizontal displacement increases, peak values of shear strain of both B-FREI and U-FREI increase. Peak values of shear strain of both B-FREI and U-FREI are quite comparable at any given displacement. U-FREI shows uniform shear strain only in the region in contact with top and bottom supports, while almost constant shear strain is observed across the width of B-FREI. Shear strain in U-FREI is observed to decrease from peak to almost zero where the isolator is not in contact with the supports. Further, at u = 135 mm (1.50t_r), the shear strain in the isolator can be approximated as (135 mm/100 mm) = 1.35. This value is in reasonable agreement with the result shown in Figs. 4.18 and 4.19.

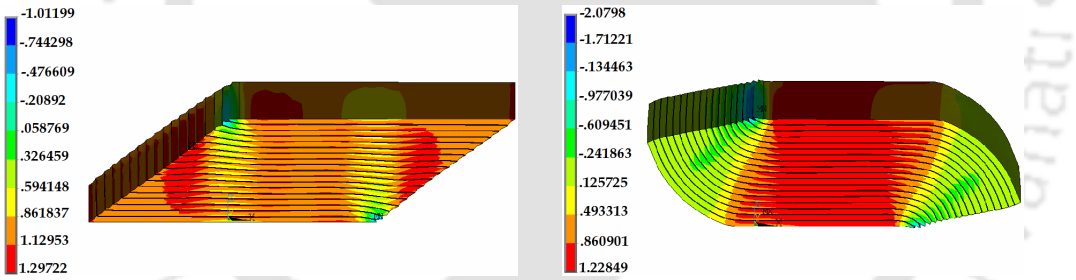

B-FREI U-FREI

(a) Isolator B1

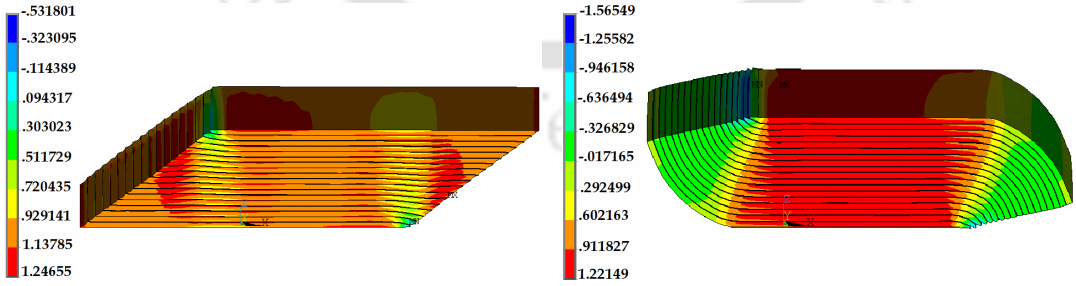

B-FREI U-FREI

(b) Isolator B2

Fig. 4.18 Contour of shear strain in elastomer layers of a half isolator at horizontal displacement of 135 mm

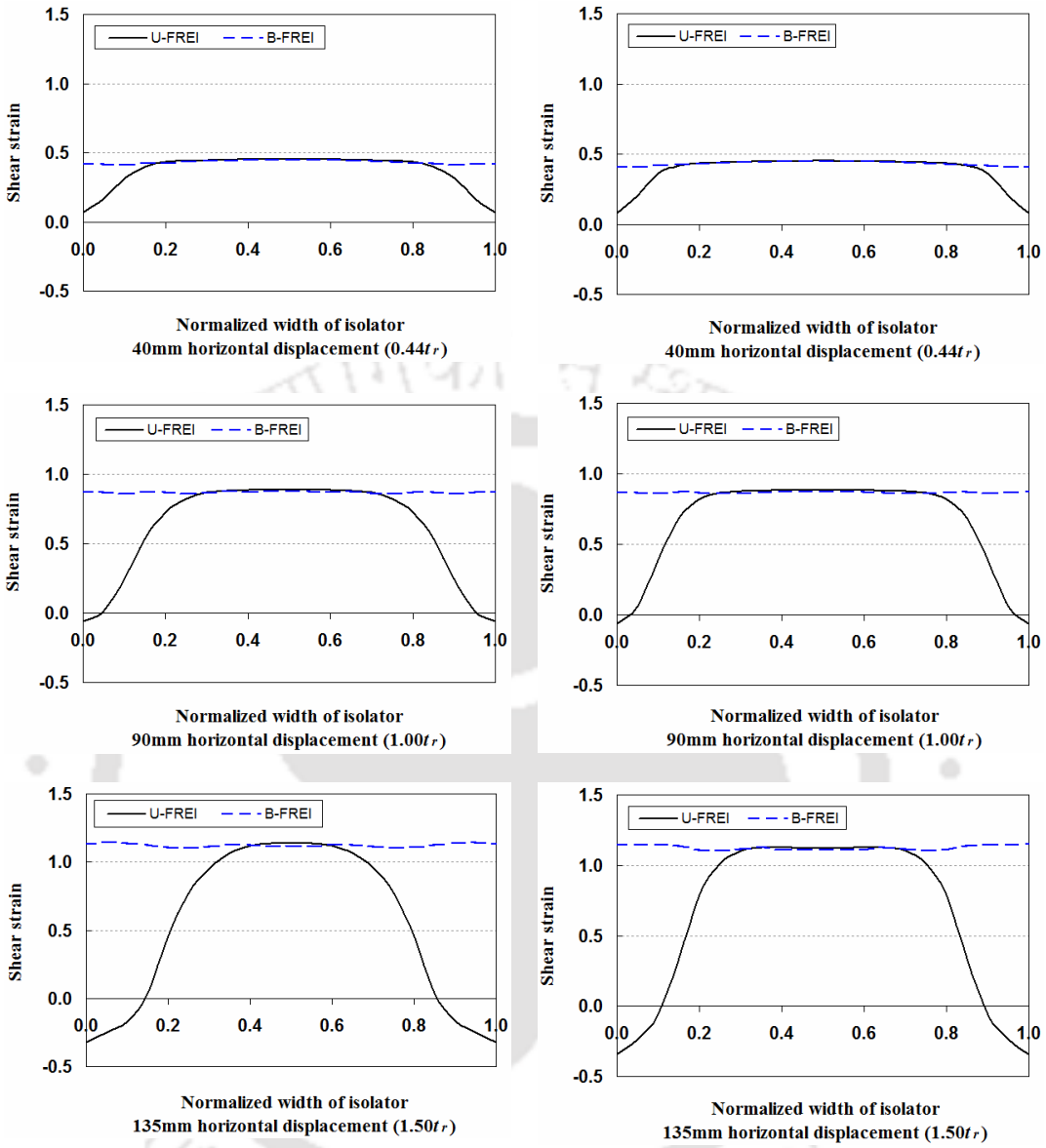

(a) Isolator B1 (b) Isolator B2

Fig. 4.19 Shear strain plotted along the width in the elastomer layer at mid-height of isolator at different horizontal displacements

4.3.6. Stress in Fibre Reinforcement Layer

Normalized stresses S_{11}/p and S_{22}/p plotted along the width of the 9th fibre reinforcement layer located at the mid-height of both B-FREI and U-FREI at different horizontal displacements are shown in Figs. 4.20 and 4.21. It can be seen from these figures that peak values of tensile stress in both B-FREI and U-FREI increase with increasing

horizontal displacement. Comparison of the peak values of tensile stress in B-FREI and U-FREI at any given horizontal displacement show that lower normalized tensile stress demand on the fibre reinforcement layers of U-FREI is observed. Specifically, at u = 1.50t_r the peak values of normalized tensile stress S_{11}/p of B-FREIs types B1, B2 are approximately 4.6%, 6.6% higher than those of corresponding U-FREIs.

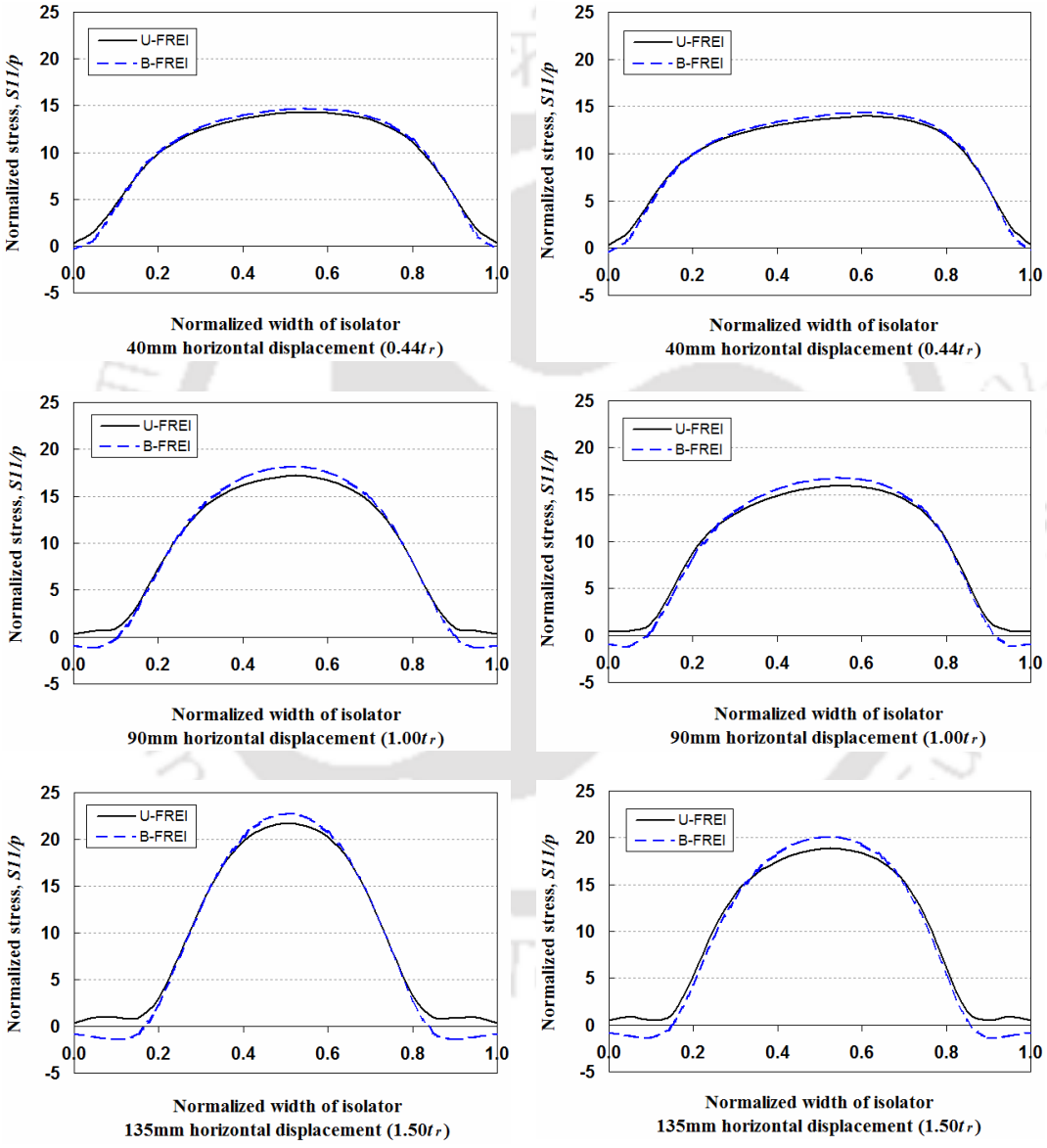

(a) Isolator B1 (b) Isolator B2

Fig. 4.20 Distribution of normalized stress S_{11}/p plotted along the width in the fibre layer at mid-height of isolator at different horizontal displacements

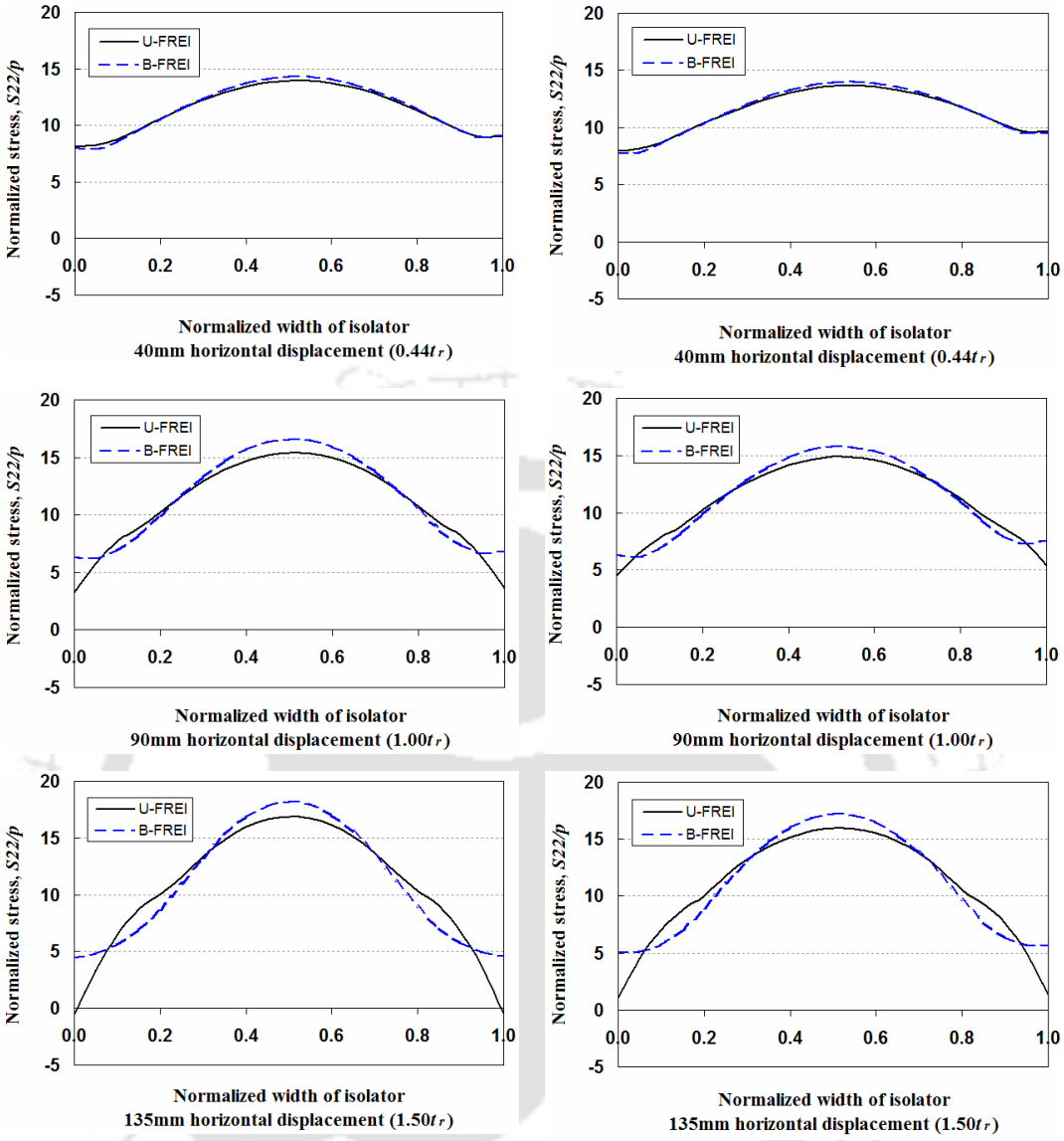

(a) Isolator B1 (b) Isolator B2

Fig. 4.21 Distribution of normalized stress S_{22}/p plotted along the width in the fibre layer at mid-height of isolator at different horizontal displacements

4.4. Effect of Shear Modulus on Horizontal Response of FREI

Effect of shear modulus on horizontal response of both B-FREI and U-FREI is presented in this section. Similar to Section 3.4 in Chapter 3, horizontal responses of isolator types A1 and B1 with the same component layers and size; but with different

values of shear modulus, subjected to same vertical load of 350 kN and cyclic horizontal displacement up to $1.50t_r$ are compared to infer the influence of shear modulus of elastomer.

4.4.1. Specimen type B-FREI

It can be seen from Tables 4.1-4.2 that the effective horizontal stiffness of B-FREI obtained from FE analysis decrease with the increase in horizontal displacement. Reduction in effective horizontal stiffness of B-FREI types A1 and B1 with increasing horizontal displacement is also shown in Fig. 4.22. It can be seen from Fig. 4.22 that the

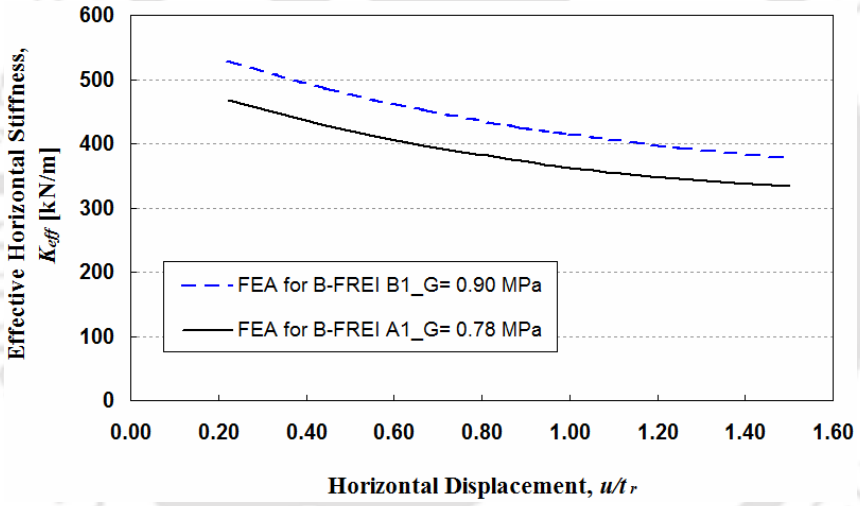

Fig. 4.22 Effective horizontal stiffness *vs* displacement of B-FREI types A1 and B1

rate of decrease in effective stiffness of B-FREI is however not constant with increasing displacements. The effective stiffness decreases faster at low displacement range from $0.22t_r$ to $1.00t_r$, and much slower at horizontal displacement beyond $1.00t_r$. The rate of decrease is observed as 22.6% and 7.9% for isolator A1 for the ranges as mentioned above, while the same is 21.4% and 8.6% for isolator B1. Further, comparison of effective stiffness of B-FREI types A1 and B1 shows that the effective stiffness of B-FREI is dependent on the shear modulus of elastomer. The effective stiffness of B-FREI

type B1 with higher shear modulus is always higher than that of B-FREI type A1 with lower shear modulus at any given horizontal displacement. These observation has immense significance for design and production of isolators.

4.4.2. Specimen type U-FREI

Reduction in effective horizontal stiffness of U-FREI types A1 and B1 with increasing horizontal displacement as obtained from both experiments and FE analyses is shown in Fig. 4.23. It can be seen from Fig. 4.23 that at a given displacement, whereas the U-FREI types A1 and B1 are likely to have same area in contact with the supports, the horizontal stiffness of U-FREI decreases with the decrease in shear modulus. Thus, the decrease in horizontal stiffness of U-FREI with increasing horizontal displacement is not only due to rollover deformation through the decrease in area in contact with the supports, but also due shear modulus of isolator. This understanding is utilized for the development of an analytical approach for predicting the horizontal stiffness of U-FREIs, which is presented in the subsequent chapter.

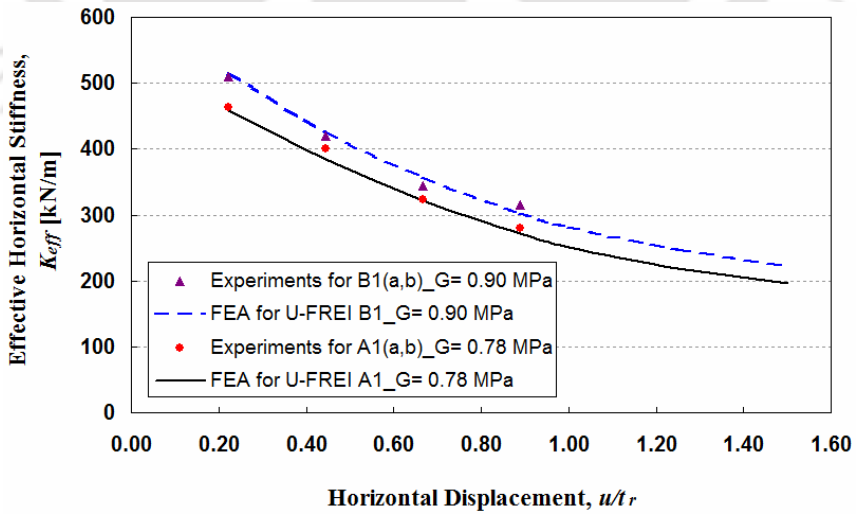

Fig. 4.23 Effective horizontal stiffness *vs* displacement of U-FREI types A1 and B1

4.5. Effect of Shape Factor on Horizontal Response of U-FREI

U-FREI types B1 and B2 have same component layers and total height of 100 mm, same shear modulus of elastomer of 0.90 MPa. They are subjected to same vertical pressure of 5.6 MPa and cyclic horizontal displacement up to $1.50t_r$. However, they are only different in size of plan area or shape factor, *S*. The values of shape factor are 12.5 for isolator B1 and 15.5 for isolator B2. Effective horizontal stiffness, stress in elastomer and fibre reinforcement layers of U-FREI types B1 and B2 are compared to appreciate the influence of shape factor.

4.5.1. Effective Horizontal Stiffness

Reduction in effective horizontal stiffness of U-FREI types B1 and B2 with increasing displacement as obtained from both experiments and FE analyses is shown in Fig. 4.24.

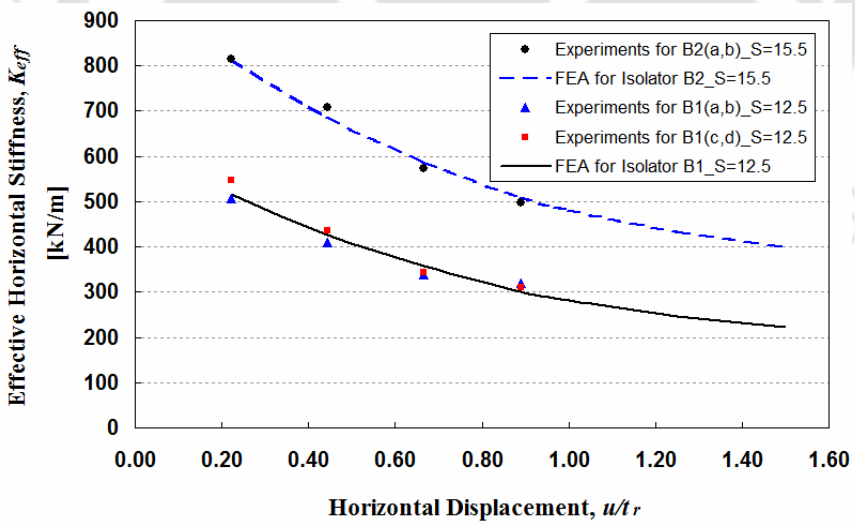

Fig. 4.24 Effective horizontal stiffness *vs* displacement of U-FREI types B1 and B2

It may be observed from FE analysis results that the rates of decrease in horizontal stiffness of isolator B1 (S = 12.5) and isolator B2 (S = 15.5) are found to be 57.0%,

50.7% respectively as the applied displacement varies from 20 mm ($0.22t_r$) to 135 mm ($1.50t_r$).

4.5.2. Stress in Elastomer Layer

Fig. 4.25 represents the comparison of the normalized stress S_{11}/p and S_{33}/p plotted along the width of the 9th elastomer layer located adjacent to the mid-height of U-FREI types B1 and B2 at different horizontal displacements. It can be seen from Fig. 4.25 that peak values of compressive stress of U-FREI type B1 (S = 12.5) is higher than that of U-FREI type B2 (S = 15.5) at any given displacement, while the length of compression region of isolator B1 is smaller than that of isolator B2. Specifically, at $u = 1.50t_r$, the peak values of normalized compressive stress S_{11}/p and S_{33}/p of U-FREI type B1 are found to be 15.1% and 14.5% higher than corresponding values of U-FREI type B2.

Comparison of shear strain plotted along the width of the 9th elastomer layer located adjacent to the mid-height of U-FREI types B1 and B2 at different horizontal displacements is shown in Fig. 4.26. According to Fig. 4.26, the peak values of shear strain of U-FREI types B1, B2 at any given displacement are quite comparable, while the uniform region of shear strain of isolator B2 (S = 15.5) is larger than that of isolator B1 (S = 12.5) due to the larger length of the region in contact with the top and bottom supports.

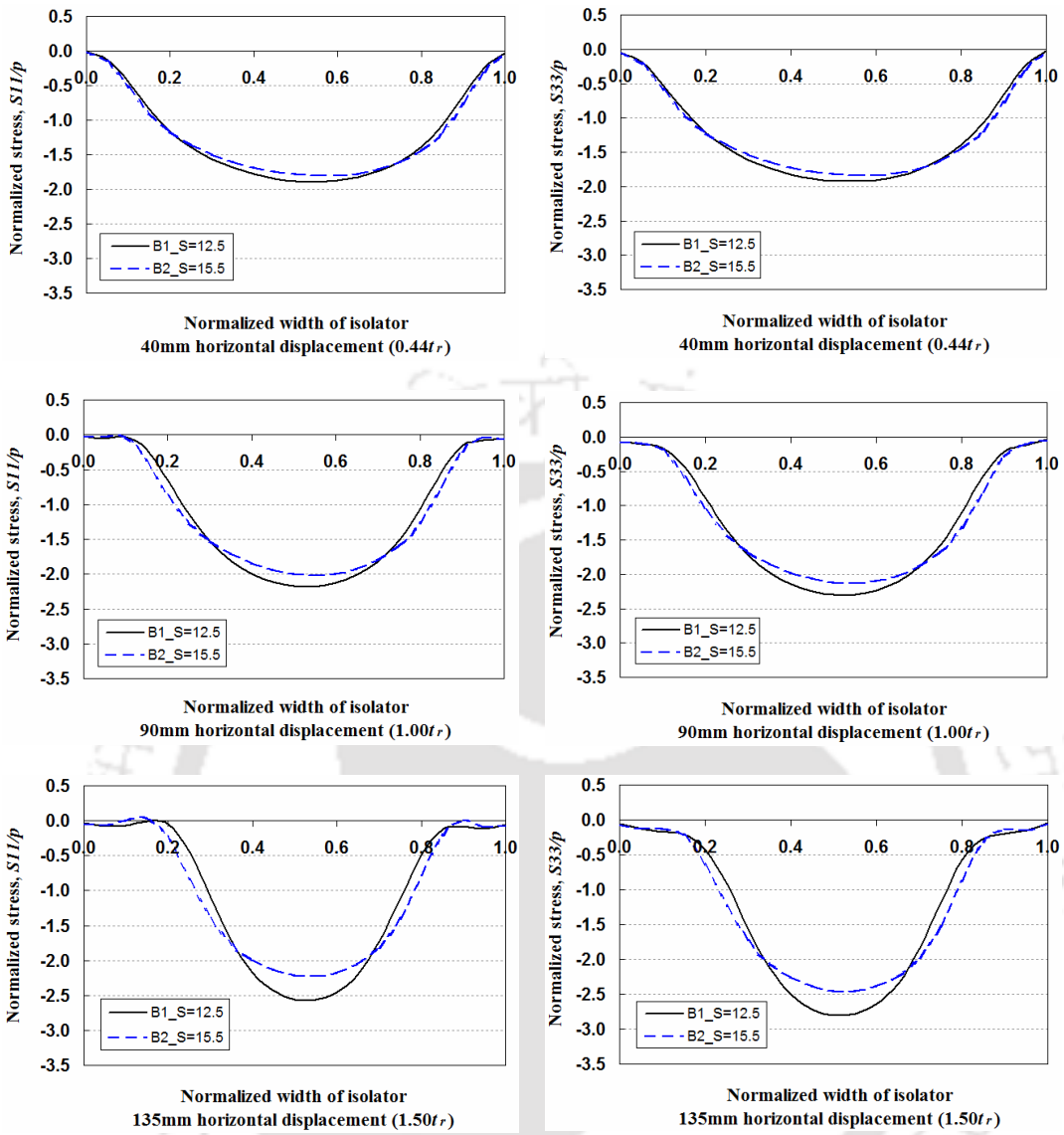

(a) Normalized stress S_{11}/p (b) Normalized stress S_{33}/p

Fig. 4.25 Comparison of normalized stress S_{11}/p and S_{33}/p plotted along the width in the elastomer layer at mid-height of U-FREI types B1 and B2 at different displacements

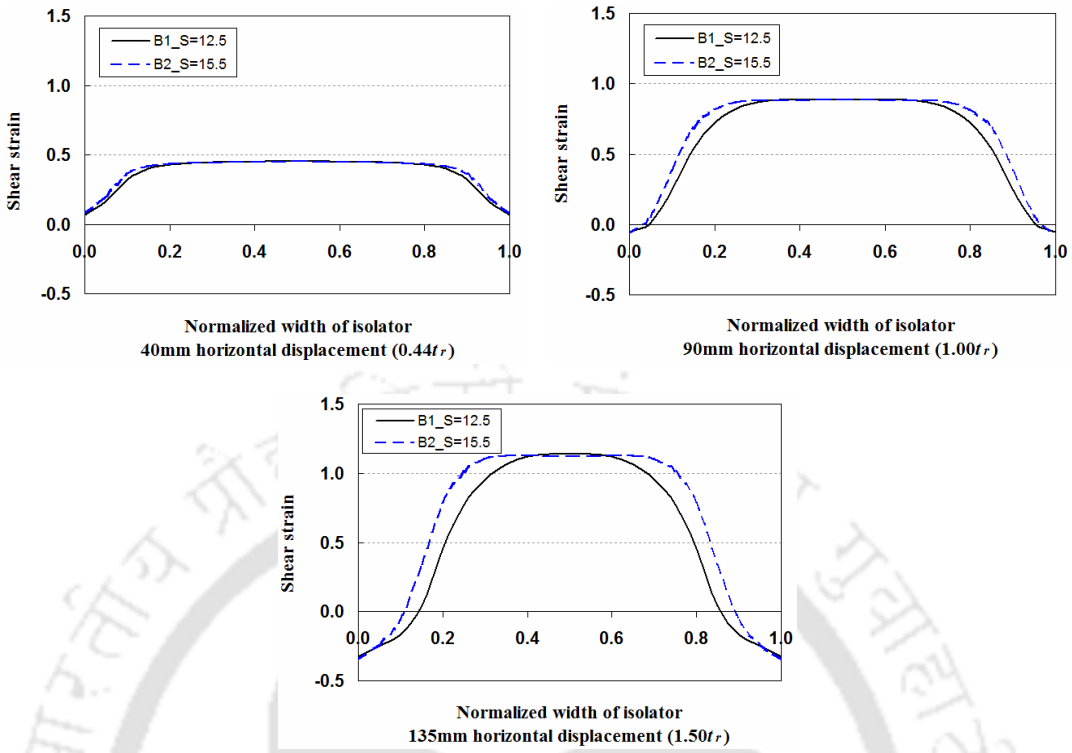

Fig. 4.26 Comparison of shear strain plotted along the width in the elastomer layer at mid-height of U-FREI types B1 and B2 at different horizontal displacements

4.5.3. Stress in Fibre Reinforcement Layer

Comparison of normalized stresses S_{11}/p and S_{22}/p plotted along the width of the 9th fibre reinforcement layer located to the mid-height of U-FREI types B1 and B2 at different horizontal displacements is shown in Fig. 4.27. Similar to the comparison of compressive stress in mid elastomer layer of U-FREI in Fig. 4.25, the peak values of normalized tensile stresses S_{11}/p and S_{22}/p of isolator B1 (S = 12.5) are higher than those of isolator B2 (S = 15.5) at a given displacement. Specifically, at u = 1.50t_r the peak values of tensile stresses S_{11} and S_{22} of U-FREI type B1 are found to be 15.4% and 5.8% higher than those of U-FREI type B2.

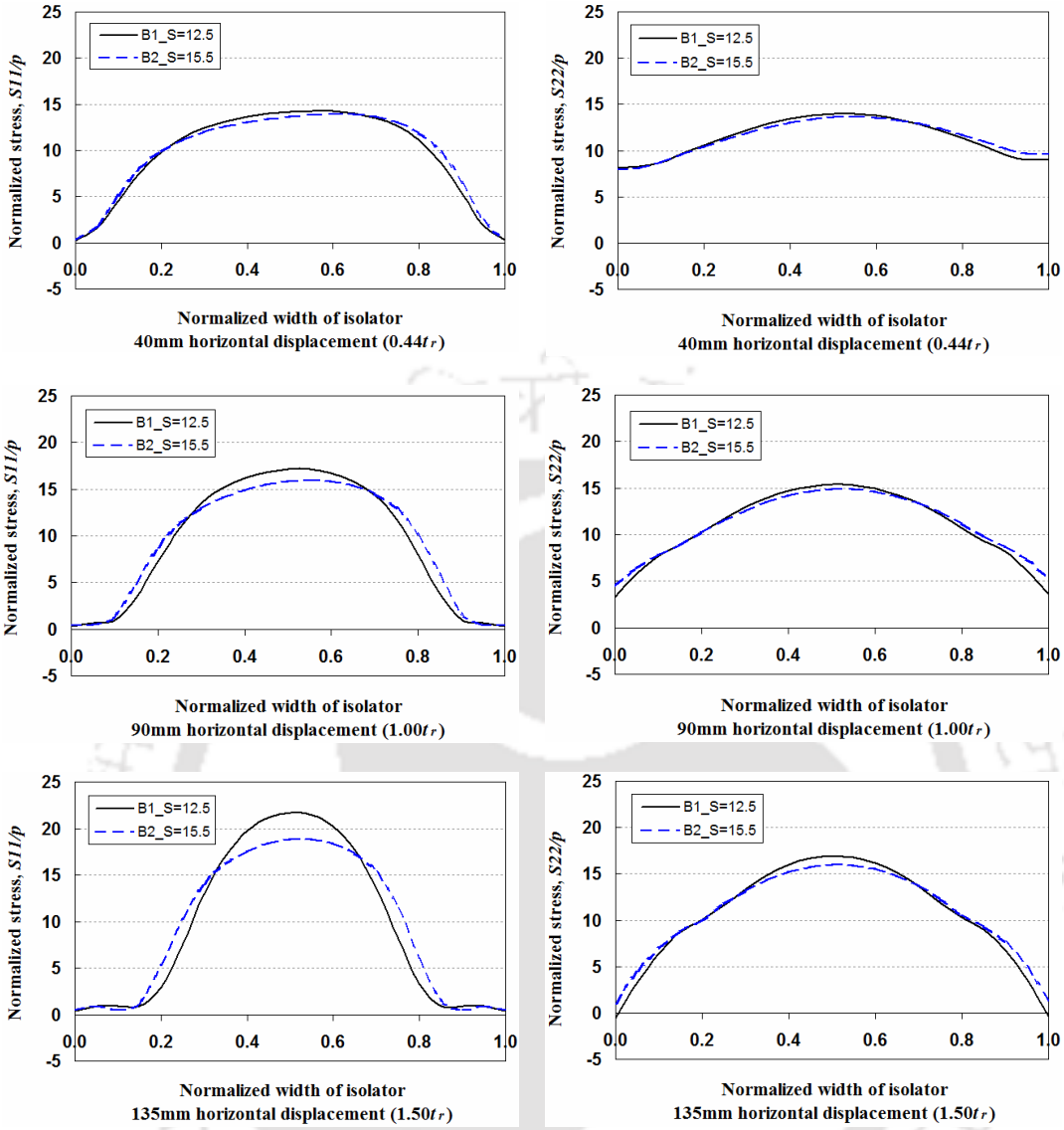

(a) Normalized stress S_{11}/p (b) Normalized stress S_{22}/p

Fig. 4.27 Comparison of normalized stress S_{11}/p and S_{22}/p plotted along the width in the fibre layer at mid-height of U-FREI types B1 and B2 at different displacements

4.6. Effect of Loading Direction on Horizontal Load-Displacement Behaviour of square FREI

This section presents effect of loading direction on the horizontal load-displacement behaviour of square B-FREI and U-FREI type A1 by FE analysis. Both B-FREI and U-FREI are analysed under the same vertical load of 350 kN and cyclic horizontal

displacement up to 2.00t_r (180 mm) applied at four different angles (0^o, 15^o, 30^o and 45^o) with the major axes of the isolator as shown in Fig. 4.28. Effect of loading direction on various response related features such as deformed shape, horizontal load-displacement relationship, hysteresis loop, effective horizontal stiffness, equivalent viscous damping, stresses and strains in elastomer and fibre reinforcement layers are studied. Numerical results of U-FREI loaded in different directions are validated with experimental findings for cyclic horizontal displacement up to 0.89t_r.

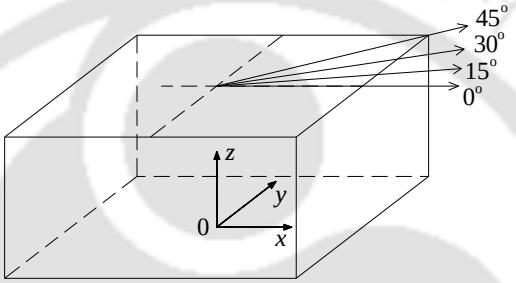

Fig. 4.28 Directions of applied horizontal cyclic displacement to FREI

4.6.1. Specimen type U-FREI

4.6.1.1. Validation of FE Model of U-FREI loaded in different directions

U-FREI type A1 is analysed using FE method, while the specimen is subjected to the simultaneous action of constant vertical load and cyclic horizontal displacement acting along four different directions. Deformed shape, horizontal load-displacement relationship, hysteresis loop obtained from FE analyses are compared with those from experimental investigations up to displacement of 0.89t_r for validation of the FE model.

Deformed shapes:

Deformed shapes of U-FREI under horizontal displacement amplitude of 80 mm in four loading directions as obtained from FE analysis are shown in Fig. 4.29. The upper and lower faces of the U-FREI roll off the contact supports. This results in a non-linear

horizontal load-displacement relationship of the U-FREI. The pattern of deformed configuration of U-FREI in different directions as observed during actual tests (Fig. 3.8 in Chapter 3) agrees very well with Fig. 4.29 obtained from FE analysis.

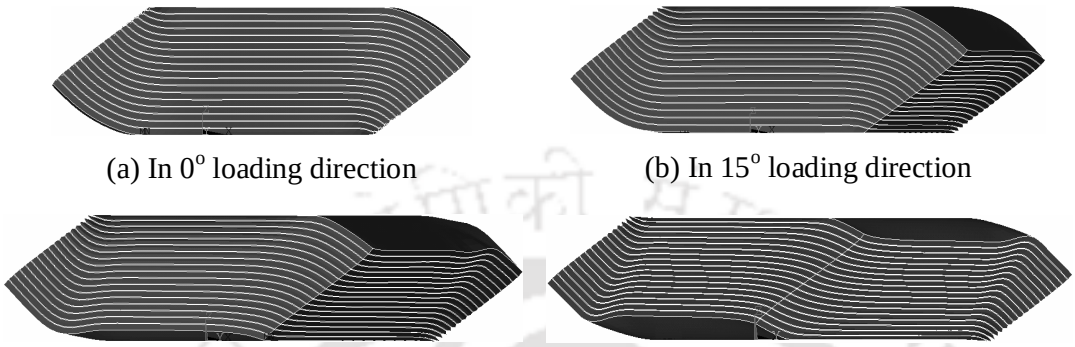

(a) In 0^o loading direction (b) In 15^o loading direction

(c) In 30^o loading direction (d) In 45^o loading direction

Fig. 4.29 Numerically observed deformed shapes of U-FREI type A1 under horizontal displacement amplitude of 80 mm in different directions

Hysteresis loops:

Comparison of hysteresis loops of the U-FREI loaded in 0^o and 45^o directions with increasing horizontal displacement up to $0.89t_r$ (80 mm) obtained from experiment and FE analysis are presented in Fig. 4.30, which shows the discrepancy to be quite less.

Horizontal load-displacement relationships:

Horizontal load-displacement relationships (backbone curves) of the U-FREI loaded in different directions with displacement up to $0.89t_r$ (80 mm) is shown in Fig. 4.31. This is obtained from load-displacement hysteresis loops recorded during experimental investigations and FE analyses. The horizontal load-displacement relation is nearly linear in the range of small displacement. When the applied displacement increases, the response of the U-FREI becomes nonlinear due to the rollover deformation. Further, as the loading direction changes from 0^o to 45^o, the horizontal load carrying capacity is observed to increase. This is primarily due to the increase in effective contact area,

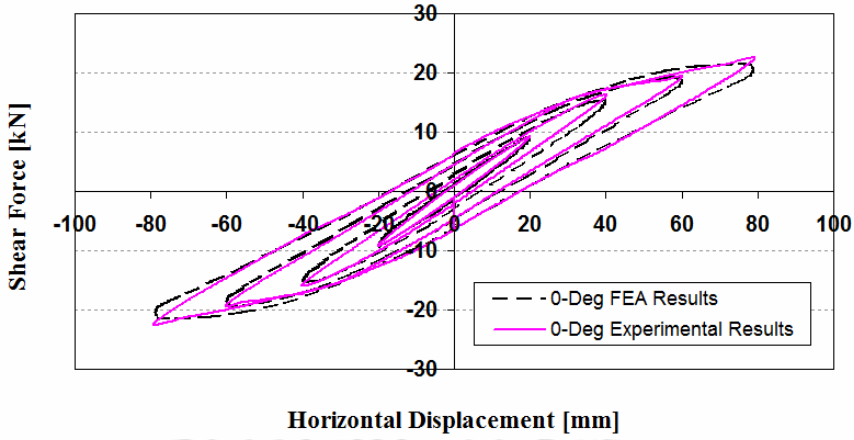

(a) In 0^o loading direction

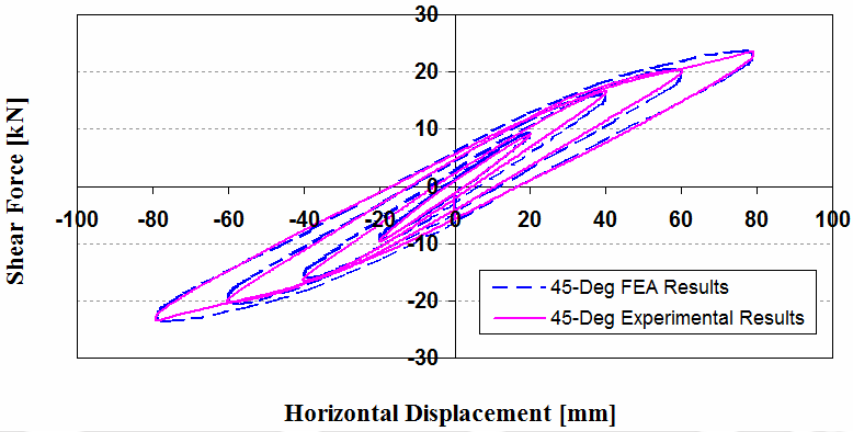

(b) In 45^o loading direction

Fig. 4.30 Comparison of hysteresis loops of U-FREI under horizontal displacement in different directions obtained from FE analysis and experimental results

which results in increase in the horizontal stiffness. The plots corresponding to other two considered angles (e.g. 15^o and 30^o) of experimental results are not shown in Fig. 4.31 as the readability becomes poor due to not so large differences in shear force values. However, very good agreement is observed between the horizontal load-displacement relationships obtained from experiment and FE analysis for all the cases of loading directions. The close agreement of experimental and finite element hysteresis loops is a testimony to the accurate numerical modelling with appropriate material

model for simulating the behaviour of elastomer up to displacement of $0.89t_r$, when the load displacement relationship is no more linear. Hence, results obtained by FE analysis for U-FREIs at even larger displacement will be considered as accurate.

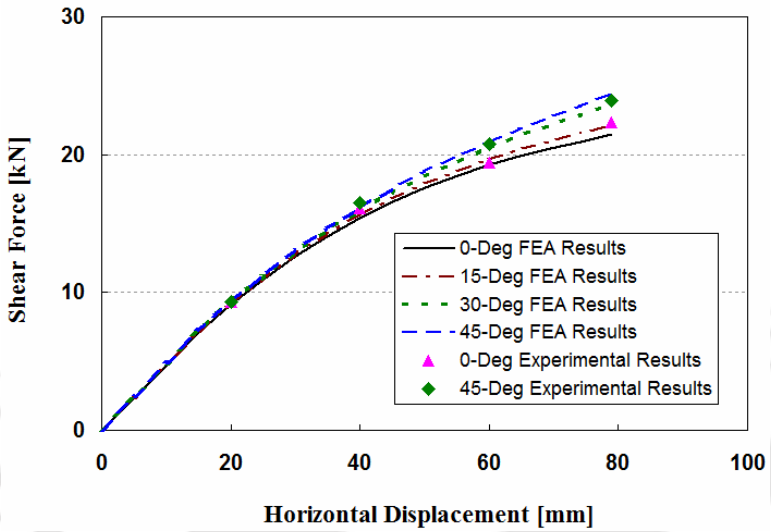

Fig. 4.31 Comparison of horizontal load-displacement relationships of U-FREI type A1 loaded in different directions as obtained from FE analysis and experimental results

4.6.1.2. Deformed Shapes

Deformed shapes of U-FREI loaded in different directions are compared first. Fig. 4.32 shows the deformed shapes of U-FREI obtained from FE analysis in 0^o and 45^o loading directions at horizontal displacement amplitude of $1.00t_r$ and $2.00t_r$. Contact area of the isolator with the support surfaces increases as the loading direction changes from 0^o to 45^o. Similar behaviour is also observed during experimental study. This resulting increase in effective shear area leads to the increase in effective horizontal stiffness of U-FREIs.

At a large horizontal displacement, some parts of originally vertical faces of the U-FREI are in contact with the support surfaces (called as rollover portion), which results in an increase in effective horizontal stiffness.

$u = 1.00t_r$ $u = 2.00t_r$

(a) In 0^o loading direction

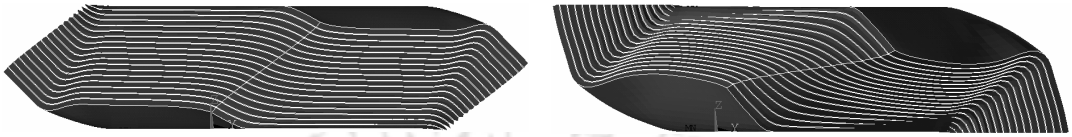

$u = 1.00t_r$ $u = 2.00t_r$

(b) In 45^o loading direction

Fig. 4.32 Deformed shapes of U-FREI type A1 under horizontal displacement in different directions obtained from FE analysis

4.6.1.3. Horizontal Load-Displacement Relationship

Horizontal load-displacement curves of U-FREI loaded in four directions obtained from FE analysis are shown in Fig. 4.33. It can be seen that the horizontal load-displacement relations are nearly linear in the range of small displacement. When the applied displacement increases, the upper and lower contact surfaces of the isolator roll off the supports, and hence the response of the U-FREI becomes nonlinear due to the rollover deformation. Consequently, the horizontal stiffness of U-FREI decreases with increasing horizontal displacement. However, at very large horizontal displacement beyond $1.70t_r$, some parts of originally vertical faces of the U-FREI are in contact with the support surfaces. This results in an increase in the effective horizontal stiffness of the isolator.

Horizontal response of U-FREI under different loading directions with increasing horizontal displacement up to $2.00t_r$, as shown in Fig. 4.33, can be divided into three stages. In the first stage, the horizontal load carrying capacity of U-FREI is approximately comparable as loading direction is varied from 0^o to 45^o in the range of

small displacement ($u \leq 0.22t_r$). In the second stage, as loading direction changes from 0^o to 45^o, the horizontal load carrying capacity of U-FREI increases, indicating higher horizontal stiffness at any given displacement up to $1.70t_r$. The difference in horizontal load carrying capacity with change in loading direction from 0^o to 45^o however increases with increase in horizontal displacement. Specifically, the difference of horizontal load carrying capacity is found to be 2.2% at $u = 0.22t_r$, 16.5% at $u = 1.00t_r$, 27.1% at $u = 1.50t_r$. In the third stage ($u \geq 1.70t_r$), increase in effective horizontal stiffness of U-FREI due to contact between vertical faces of isolator with the support surfaces exceeds the reduction in the horizontal stiffness due to rollover deformation. This results in reversal of the trend in variation of horizontal load carrying capacity with loading directions.

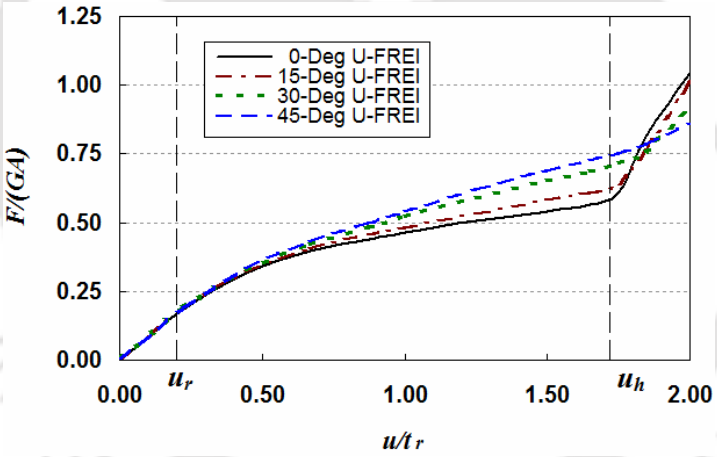

Fig. 4.33 Horizontal load-displacement curves of U-FREI type A1 loaded in different directions as obtained from FE analysis

The horizontal displacement at which the increase in effective horizontal stiffness due to contact between vertical faces of isolator and support surfaces starts to exceed the decrease in the stiffness due to rollover deformation is denoted by u_h and the phenomenon is termed as hardening behaviour. It can be observed from Fig. 4.33 that the hardening behaviour of U-FREI occurs in the third stage at $u_h \geq 1.70t_r$. It is further

observed that u_h = 1.70t_r in 0° loading direction, u_h = 1.75t_r in 15° loading direction, while u_h = 1.82t_r in 30° loading direction. Thus, the displacement limit corresponding to hardening behaviour is observed to increase as the loading direction changes from 0° to 45°.

4.6.1.4. Mechanical Properties

Effective horizontal stiffness and equivalent viscous damping of U-FREI, with increasing displacement up to 2.00t_r, under four different loading directions are presented in Table 4.4. Variation of these parameters with horizontal displacement is shown in Figs. 4.34 & 4.35.

Table 4.4 Numerically mechanical properties of U-FREI in different directions

Amplitude (mm)	u/t_r	0° Direction		15° Direction		30° Direction		45° Direction	
		K_{eff}^h	β	K_{eff}^h	β	K_{eff}^h	β	K_{eff}^h	β
		(kN/m)	(%)	(kN/m)	(%)	(kN/m)	(%)	(kN/m)	(%)
20.0	0.22	457.72	7.16	460.94	7.06	463.85	6.96	467.97	6.87
40.0	0.44	385.10	9.30	390.21	9.16	400.27	8.87	404.98	8.68
60.0	0.67	321.99	11.71	330.70	11.44	342.07	11.15	349.11	10.85
80.0	0.89	272.20	13.22	280.75	12.85	299.90	12.36	308.62	11.88
90.0	1.00	251.09	13.78	261.49	13.43	282.57	12.83	292.54	12.38
112.5	1.25	219.02	14.19	231.13	13.85	256.44	13.24	268.78	12.81
135.0	1.50	195.75	14.94	210.42	14.46	237.08	13.73	250.22	13.31
157.5	1.75	190.16	-	198.95	-	221.71	-	232.83	-
180.0	2.00	282.56	-	273.61	-	248.89	-	233.44	-

It is observed from Table 4.4 and Figs. 4.34 & 4.35 that the effective horizontal stiffness of U-FREI increases and damping factor decreases at any given displacement up to u = 1.70t_r as the loading direction is varied from 0° to 45°. Moreover, comparison of the mechanical properties of U-FREI tested under horizontal displacement in different directions obtained from experiments (Table 3.3 in Chapter 3) and FE analysis (Table

4.4) shows that the values of effective stiffness from experiment and FE analysis are in good agreement, while some differences are observed in damping. The values of damping have not been evaluated for displacement range beyond hardening point.

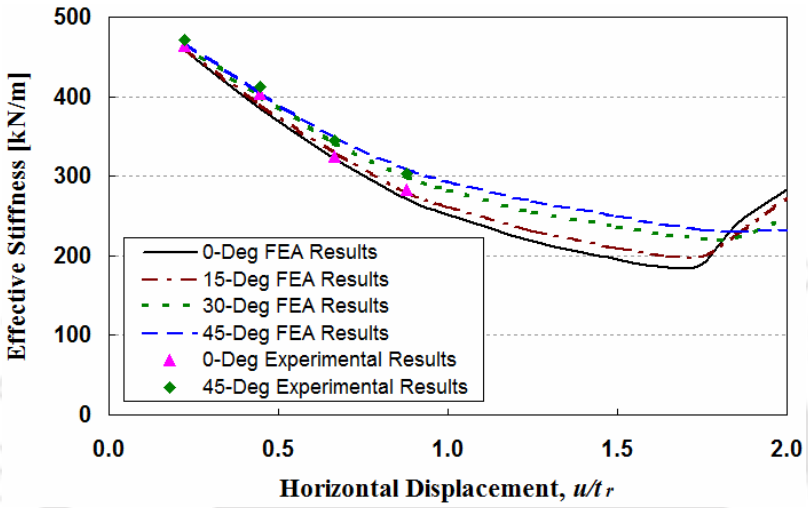

Fig. 4.34 Variation of effective horizontal stiffness with horizontal displacement in different directions

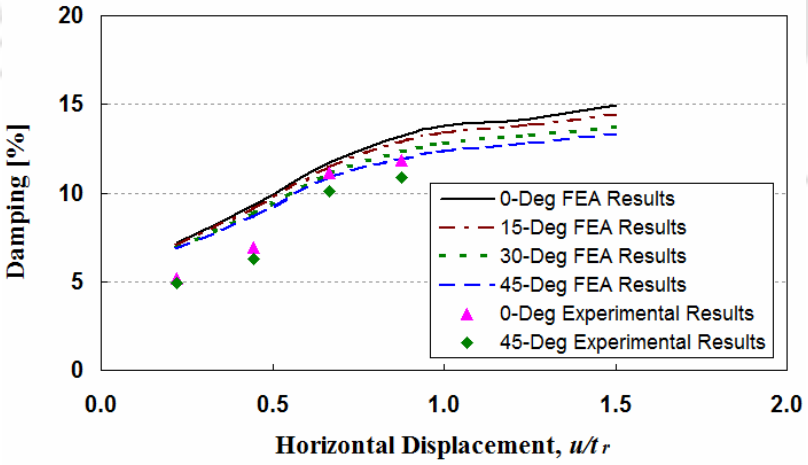

Fig. 4.35 Variation of computed equivalent viscous damping with horizontal displacement in different directions

4.6.1.5. Stress and Strain in Elastomer Layer

Isolators are analysed under the action of cyclic displacement applied along different specified directions with respect to *X*-axis. For denoting stress, the local axes are designated as axis 1, axis 2 and axis 3, which are parallel to the *X*, *Y* and *Z*-axis, respectively.

Contours of normal stress S_{11} in elastomer layers of a half U-FREI in 0^o and 45^o loading directions with increasing horizontal displacement amplitude are shown in Fig. 4.36. It is observed that peak values of compressive and tensile stresses increase, while area of compression region in the top and bottom elastomer layers decreases with increase in the horizontal displacement. Further, as the loading direction changes from 0^o to 45^o,

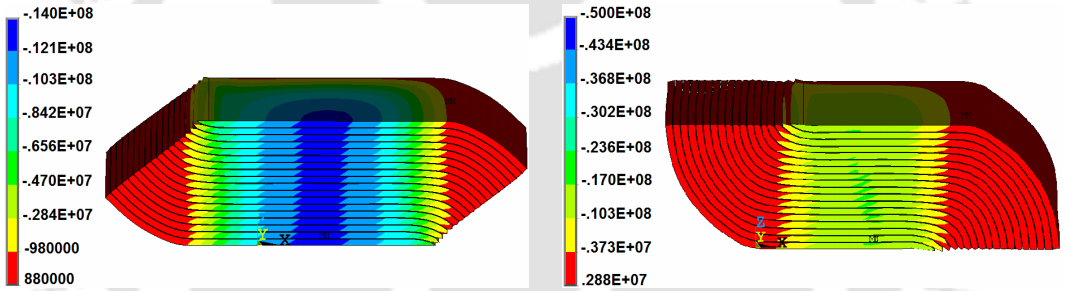

$u = 1.00t_r$ $u = 2.00t_r$

(a) In 0^o loading direction

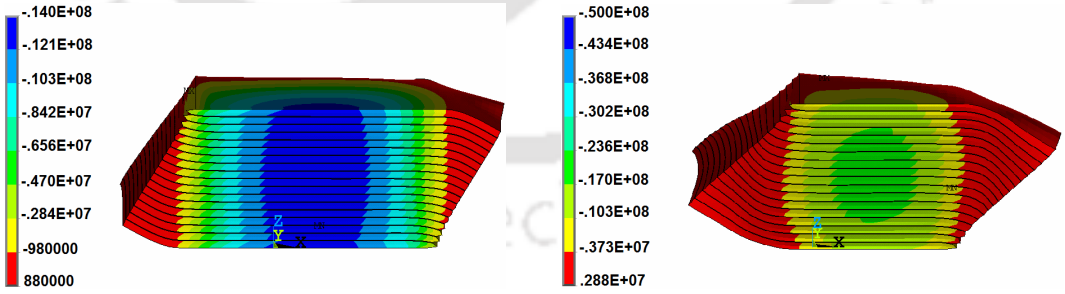

$u = 1.00t_r$ $u = 2.00t_r$

(b) In 45^o loading direction

Fig. 4.36 Contour of normal stress S_{11} (N/m^2) in elastomer layers of a half U-FREI loaded in 0^o and 45^o directions (positive value indicates tension)

the peak value of compressive stress in the central elastomer layers increases, while the compressive stresses in the top and bottom elastomer layers decrease at a given horizontal displacement.

Normalized stress profiles S_{11}/p and S_{33}/p plotted along the width of the 9th elastomer layer located adjacent to the mid-height of U-FREI under different loading directions at $u = 1.00t_r$ and $2.00t_r$ are shown in Fig. 4.37. It can be seen from Fig. 4.37 that the peak

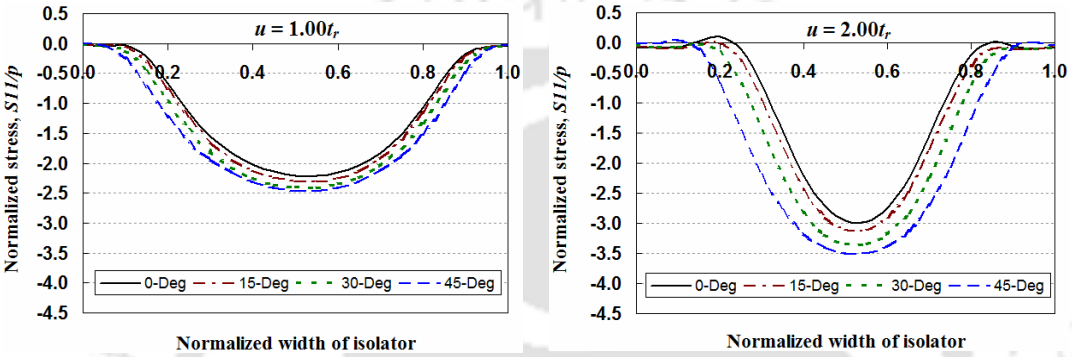

(a) Normalized stress S_{11}/p

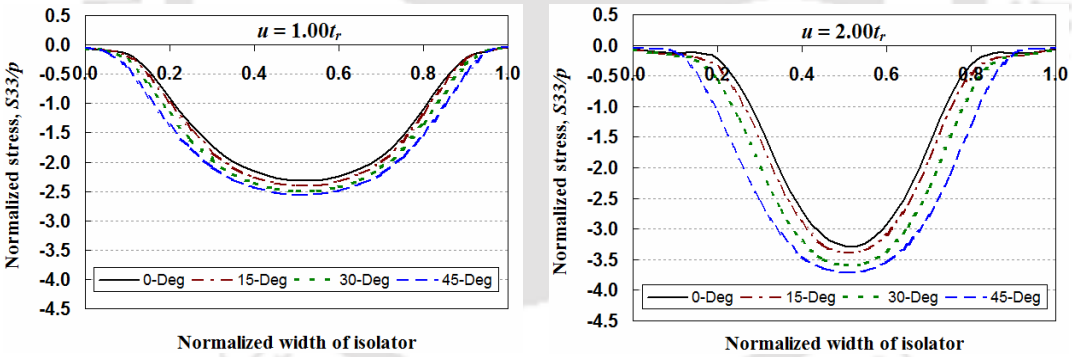

(b) Normalized stress S_{33}/p

Fig. 4.37 Variation of normalized stress profiles plotted along the width in the elastomer layer at mid-height of U-FREI type A1 loaded in different directions

value of normalized compressive stress increases and the length of compression region decreases as the horizontal displacement of U-FREI increases. Moreover, peak value of compressive stress in elastomer layers of U-FREI increases when the loading direction is varied from 0^o to 45^o for any given horizontal displacement.

Contours of shear strain ε_{13} in elastomer layers in one half of U-FREI for 0^o and 45^o loading directions at horizontal displacement amplitude of $u = 1.00t_r$ and $2.00t_r$ are presented in Fig. 4.38. It is observed from this figure that as the horizontal displacement increases, the peak value of shear strains ε_{13} in elastomer layers of U-FREI increases. The peak positive value of shear strains ε_{13} is reduced when the loading direction is varied from 0^o to 45^o. It should be noted that in the 45^o loading direction, the U-FREI is deformed along the global X and Y directions. Thus, unlike in the 0^o loading direction, shear strains ε_{23} have non-zero magnitudes.

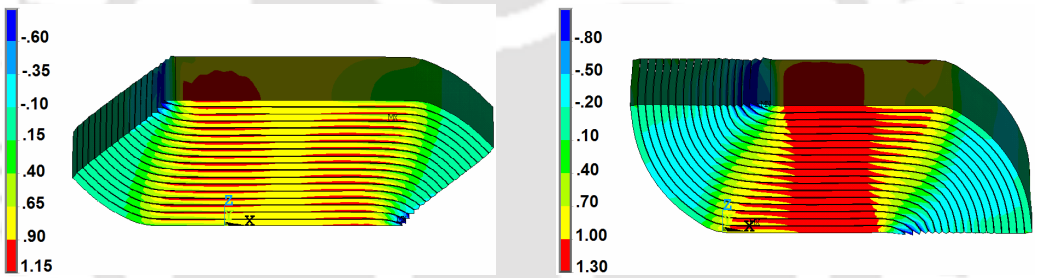

$u = 1.00t_r$ $u = 2.00t_r$

(a) In 0^o loading direction

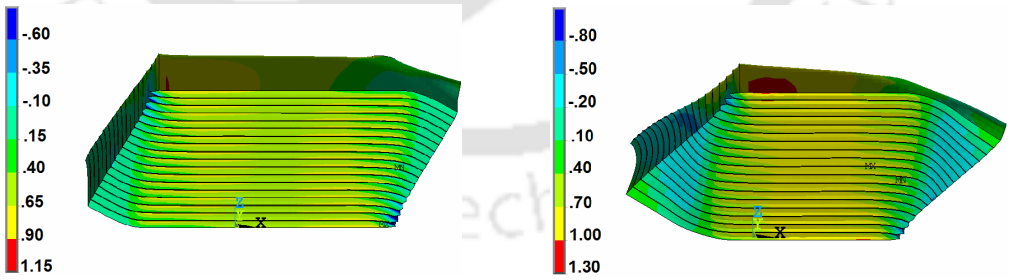

$u = 1.00t_r$ $u = 2.00t_r$

(b) In 45^o loading direction

Fig. 4.38 Contours of shear strain ε_{13} in elastomer layers of a half U-FREI type A1 loaded in 0^o and 45^o directions

4.6.2. Specimen type B-FREI

Effect of loading direction on horizontal load-displacement relationships, deformed shapes, stresses and strains in elastomer and fibre reinforcement layers of B-FREI as obtained from FE analysis is presented in this section. Further, comparison of the horizontal response of B-FREI and U-FREI loaded in different directions is also carried out.

4.6.2.1. Horizontal Load-Displacement Relationship

Horizontal load-displacement curves of both B-FREI and U-FREI corresponding to different loading directions as obtained from FE analysis are shown in Fig. 4.39. Horiz-

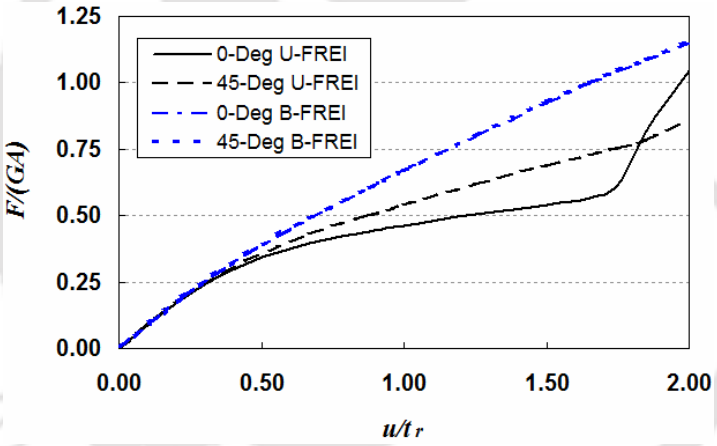

Fig. 4.39 Horizontal load-displacement curves of B-FREI and U-FREI type A1 loaded in 0^o and 45^o directions

-ontal response of B-FREI is almost linear as the horizontal displacement is increased from zero to $2.00t_r$. However, the horizontal load-displacement curve of U-FREI are significantly different corresponding to 0^o and 45^o loading directions. Unlike U-FREI, the horizontal load-displacement relation of B-FREI is not affected by the loading directions varying from 0^o to 45^o. As the isolator is horizontally displaced, the upper and lower faces of B-FREI remain fully in contact with the support surfaces, and hence

the area in contact with support surfaces of B-FREI remains constant even when the loading direction changes from 0^o to 45^o. Thus, the horizontal response of B-FREI under any loading directions is almost same.

4.6.2.2. Stress and Strain in Elastomer Layer

Deformed shapes and contours of normal stress S_{11} in elastomer layers of a half B-FREI type A1 loaded in 0^o direction at $u = 1.00t_r$ and $2.00t_r$ are shown in Fig. 4.40. Similar to U-FREI, peak value of compressive stress in elastomer layers of B-FREI increases, while area of compression region decreases when the horizontal displacement is increased. It can be noted that the peak values of tensile and compressive stresses in elastomer layers of B-FREI are higher than those of U-FREI (as shown in Fig. 4.36(a)).

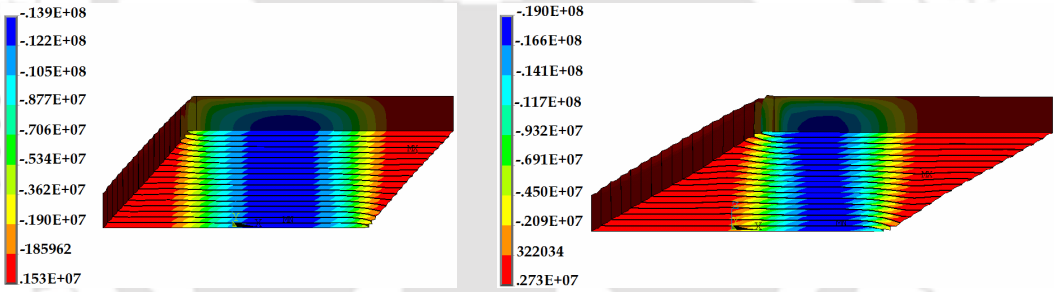

$u = 1.00t_r$ $u = 2.00t_r$

Fig. 4.40 Contours of normal stress S_{11} (N/m^2) in elastomer layers of a half B-FREI type A1 loaded in 0^o direction (positive value indicates tension)

Normalized stress profiles S_{11}/p and S_{33}/p plotted along the width of 9th elastomer layer located adjacent to the mid-height of both B-FREI and U-FREI under different loading directions and corresponding to $u = 1.00t_r$ and $2.00t_r$ are compared in Fig. 4.41. It can be observed from Fig. 4.41 that as the horizontal displacement increases, the peak values of compressive and tensile stresses of B-FREI increase and area of the compression region decreases. Similar to the behaviour of U-FREI, the peak value of

compressive stress in elastomer layers of B-FREI increases at any given horizontal displacement as the loading direction changes from 0^o to 45^o.

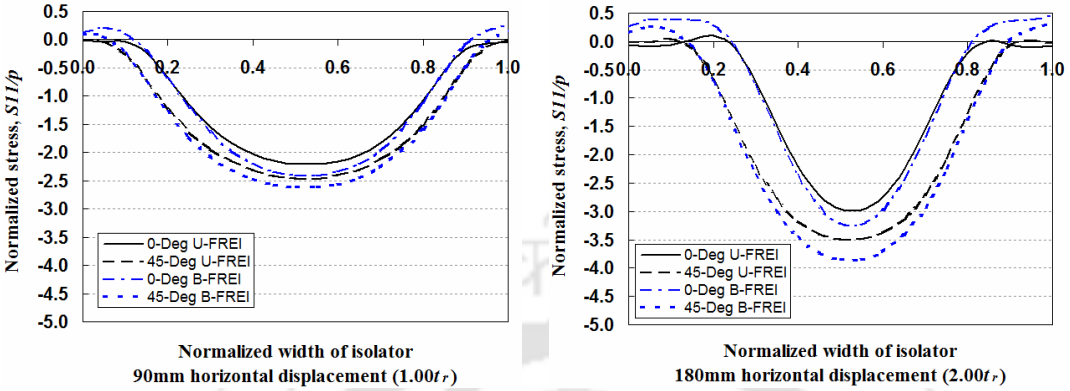

(a) Normalized stress S_{11}/p

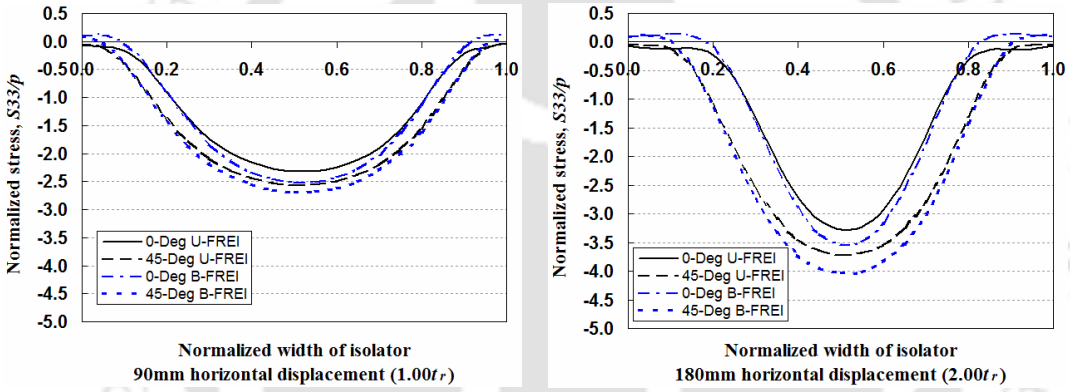

(b) Normalized stress S_{33}/p

Fig. 4.41 Variation of normalized stress profiles plotted along the width in the elastomer layer at mid-height of B-FREI and U-FREI type A1 loaded in different directions

4.7. Concluding Remarks

In this chapter, horizontal load-displacement behaviour of all the prototype FREI specimens that are discussed in Chapter 3 are evaluated by FE analyses. Similar loading and boundary conditions are maintained as in experimental evaluation. The FE based results are compared with those from experiments and very good agreements are observed. The numerical studies are further repeated for bonded end conditions of these

FREIs. The applied displacement range in FE analysis is however much higher than that considered in experimental investigations. Evaluation of stresses and strains in elastomer and fibre reinforcement layers are also performed. The improved seismic performance of U-FREI is perceived by comparing important aspects like load-displacement behaviour, damping characteristics, stress / strain in different layers with those of B-FREI. From experimental and FE analysis results, the influence of shear modulus, shape factor and horizontal loading direction on the horizontal response of the FREIs are studied. On the basis of results obtained from detailed numerical analysis, the following conclusions are drawn.

- Effective horizontal stiffness decreases and equivalent viscous damping increases with increasing horizontal displacement of U-FREI due to rollover deformation.
- Good agreement is observed between the findings from experimental and FE analysis. FE analysis for FREI can be considered to be an effective tool for computation of response of U-FREI, particularly for very large applied displacement, which may be otherwise difficult in experimental study.
- Horizontal stiffness of U-FREI is significantly lesser than that of B-FREI at higher displacement and hence possesses significantly higher seismic isolation efficiency.
- A comparison of stress pattern at large displacement between B-FREI and U-FREI shows a considerably lower compressive stress demand in elastomer layers as well as significantly lower peeling stress demand on the bond between elastomer and fibre reinforcement layers in U-FREI.
- Decrease in horizontal stiffness of B-FREI with increasing horizontal displacement is dependent on the shear modulus, while that of U-FREI is due to both shear modulus and the contact area of the isolator with support surfaces.

- Peak values of compressive stress in elastomer layers and tensile stress in fibre reinforcement layers of U-FREI with smaller shape factor are higher than those of U-FREI with larger shape factor, while peak values of shear strain in elastomer layers of these U-FREIs are quite comparable at any given applied displacement.
- Generally, as the loading direction changes from 0^o to 45^o, the effective horizontal stiffness of square U-FREI increases at a given horizontal displacement ($u < 1.70t_r$), while that of B-FREI remains more or less unchanged.
- Effective horizontal stiffness of U-FREI starts to increase at large horizontal displacement in the range $1.70t_r$ to $2.00t_r$. Further, hardening behaviour in load-displacement relationship of square U-FREI becomes more pronounced when the loading direction changes from 0^o to 45^o.
- As the loading direction is varied from 0^o to 45^o, the peak values of compressive stress in the central elastomer layers of both B-FREI and U-FREI increase, while the peak values of compressive stress in the top and bottom elastomer layers decrease at a given horizontal displacement.

Chapter 5

Analytical Approach for Predicting the Horizontal Stiffness of FREIs

5.1. Introduction

As observed from detailed literature survey in Chapter 2 that some theoretical as well as experimental works were done in recent time for better understanding of the behaviour of U-FREIs. These studies indicate that the horizontal response of U-FREI is affected by some parameters such as material properties, sizes and shape of isolator, loadings and directions of loading, friction between U-FREI and support surfaces, etc. It is also observed that the deformed configuration of U-FREI under large displacement is far more complex than that of B-FREI and hence predicting their behaviour using closed form solution is far more complicated. An analytical approach to calculate the effective horizontal stiffness of U-FREI was proposed by Nezhad [2014]. The author considered the influence of rollover deformation and introduced effective shear area for the evaluation of effective horizontal stiffness, while shear modulus was considered constant. In European Standard Code EN-1337-3, the shear modulus of reinforced elastomeric isolators is also assumed constant and its value is dependent only on the elastomeric material and the ambient temperature. However, experimental observations from Strauss, *et al.* [2014], Dezfuli and Alam [2014] indicated that the shear modulus of isolator decreases with the increasing horizontal displacements. When an unfilled or carbon black-reinforced rubber is subjected to cyclic loading in simple tension, compression or shear from its initial configuration, stress softening is observed. The

stress differences in successive loading cycles are observed to be largest during the initial cycles and becomes negligible after about 6-10 cycles. The extent of softening depends on the amount of filler as well as on the extent of maximum deformation. This phenomenon is described as Mullins effect [1969] and is a result of internal changes in the elastomeric materials. The stress softening associated with the Mullins effect are not accounted for when the mechanical properties are represented in terms of a strain-energy function, i.e. if the material is modelled as hyper-elastic. Dorfmann and Ogden [2004] used the theory of pseudo-elasticity to model the softening characteristics of reinforced rubber. An analytical approach was suggested by Gerhaher, *et al.* [2011] for the evaluation of horizontal behaviour of un-bonded isolators by incorporating changes in shear modulus of isolator. In their approach, the reduction of shear modulus was considered as dependent on parameters such as vertical pressure, horizontal displacement, shape factor, while the shear area of isolator was kept constant. However, the agreement with experimental data was not good. Thus, further effort is necessary to improve the analytical approach for predicting the behaviour of U-FREIs. This will have huge significance in design and production of prototype isolators for field application.

This chapter presents a proposed method for the evaluation of secant horizontal stiffness of FREI in both bonded and un-bonded applications. An analytical approach incorporating the effect of both nonlinearity of shear modulus and effective shear area with increase in displacement is proposed as a basic analysis tool for predicting the secant horizontal stiffness of U-FREIs. Results obtained from the proposed analytical method are compared to experimental and numerical results in Chapters 3 and 4, and very good agreement is observed.

5.2. Proposed Analytical Approach for Determination of Secant Horizontal Stiffness of FREI

Conventional SREIs are made by vulcanization of sheets of elastomer to thin steel reinforcing plates and with two end-steel-plates at top and bottom. These isolators are very rigid in both extension and flexure. The secant horizontal stiffness of bonded SREIs can be computed using the well known expression given by Naeim and Kelly [1999].

$$K = \frac{GA}{t_r} \tag{5.1}$$

where, G is the initial shear modulus, A is the full cross-sectional area of the isolator.

B-FREI is a result of the effort for reducing the weight and cost of isolator. The components of B-FREI are similar to SREI, where steel shims are replaced by multi-layers of fibre fabric. B-FREI is relatively more flexible than bonded SREI for movements in the horizontal direction. This is due to the lack of flexural rigidity of fibre reinforcement sheets in B-FREI. Unlike the steel reinforcing plates, which remain nearly rigid in a horizontally deformed SREI, fibre reinforcement sheets in B-FREI exhibit warping deformations at their ends.

Experimental results from Gerhaher, *et al.* [2011] show that the assumption of constant shear modulus leads to inaccurate estimation of its behaviour. The stiffness of the isolator is influenced by the actual applied shear deformation as well as the previously applied maximum deflection. Some previous experimental results from Ashkezari, *et al.* [2008], Strauss, *et al.* [2014], Naghshinesh, *et al.* [2014] indicated that the secant horizontal stiffness of B-FREI decreased significantly with the increase in horizontal displacements. Thus, the decrease in secant horizontal stiffness of B-FREI is primarily

due to the decrease in shear modulus, G. Therefore, the secant horizontal stiffness of a B-FREI, K_b, can be written as

$$K_b = \frac{G_{eff} A}{t_r} \tag{5.2}$$

where G_{eff} is the effective shear modulus of isolator.

Gerhaher [2010] suggested for the evaluation of horizontal stiffness of B-FREI considering vertical pressure to account for the internal material friction, the horizontal displacement amplitude, shape factor and the stability as

$$K_b = \frac{GA}{t_r}\left[1-\left(\frac{p_z}{p_{crit,0}\left(1-\left(\frac{u}{a}\right)^2\right)}\right)^2\right] \tag{5.3}$$

where, $p_{crit,0}$ is the critical stress state according to Kelly [2003] and is given by

$$p_{crit,0} = \frac{P_{crit}}{a^2} \text{ with } P_{crit} = \frac{\sqrt{2}\pi GASr}{t_r} \text{ and } r = \frac{a}{2\sqrt{3}} \tag{5.4}$$

a is the length of square isolator, u is horizontal displacement and r is the radius of gyration.

From Eqs. (5.2) and (5.3), the effective shear modulus is computed as

$$G_{eff}^{b} = G\left[1-\left(\frac{p_z}{p_{crit,0}\left(1-\left(\frac{u}{a}\right)^2\right)}\right)^2\right] \tag{5.5}$$

U-FREI is a further seismically improved version of FREI, where end connecting plates are removed. Gerhaher, *et al.* [2011] suggested for the evaluation of horizontal stiffness of U-FREI using an analytical expression as

$$K_{ub} = \frac{GA}{t_r}\left[1-\left(\frac{p_z}{p_{crit,0}\left(1-\left(\frac{u}{a}\right)^2\right)}\right)^2\right]\left(1-\frac{u}{a}\right) \tag{5.6}$$

$$G_{eff}^{ub} = G\left[1-\left(\frac{p_z}{p_{crit,0}\left(1-\left(\frac{u}{a}\right)^2\right)}\right)^2\right]\left(1-\frac{u}{a}\right) \tag{5.7}$$

Strauss, *et al.* [2014] found that horizontal stiffness of B-FREI obtained using Eq. (5.3) showed a significant deviation from the experimental results. However, horizontal stiffness using Eq. (5.6) agreed well with experimental results for B-FREI. The calculated values of horizontal stiffness of U-FREIs using Eq. (5.6) also showed somewhat good agreement with experimental results.

From the experimental studies conducted by Ashkezari, *et al.* [2008], Strauss, *et al.* [2014], it was observed that the rate of decrease of effective shear modulus of B-FREI and U-FREI with the increase in horizontal displacements was not a constant. The magnitude of effective shear modulus decreased quickly at the range of low horizontal displacement, after which it remained either constant or even increased at very large horizontal displacements. In the present study, Eq. (5.7) is utilized to calculate the effective shear modulus, G_{eff} of both B-FREI and U-FREI for horizontal displacement up to $u \leq 1.00t_r$ and G_{eff} is considered constant for $u > 1.00t_r$, where the value of G_{eff} at $u = 1.00t_r$ is adopted. Proposed strategy is elaborated in the subsequent section.

U-FREIs are installed directly between the foundation and superstructure without any connection to these elements. When the isolator is deformed horizontally, its top and bottom faces roll off the contact supports as a result of its un-bonded boundary conditions, called as rollover deformation. Nezhad, *et al.* [2011] and Das, *et al.* [2014]

observed that the effective horizontal stiffness of both B-FREI and U- FREIs decrease with the increase in horizontal displacements, although the rate of decrease in U-FREI is faster than that of corresponding B-FREI due to rollover deformation. The reduction of shear area due to rollover deformation was considered by Nezhad [2014] for calculation of effective horizontal stiffness of U- FREI as

$$K_{ub} = \frac{GA_{eff}}{t_r} \tag{5.8}$$

where, A_{eff} is the effective plan area in contact with the support surfaces of the U-FREI and is calculated as

$$A_{eff} = a\left(a - d\right) \tag{5.9}$$

d is the projected length of the curved part of the rollover region along the horizontal plane (see in Fig. 5.1).

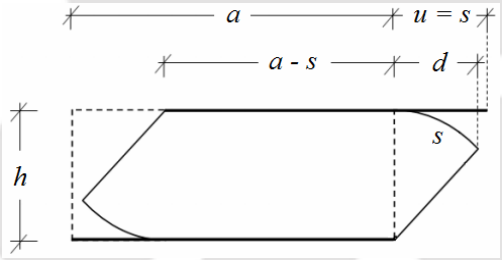

Fig. 5.1 Deformed configuration of U-FREI

According to Nezhad [2014], d is evaluated as

$$d = \frac{25}{16}\alpha h \tag{5.10}$$

where, h is the total height of the isolator, α is geometrical parameter which relates d and curved length, s, at a given horizontal displacement, u. The relation between u, s and α as proposed by Nezhad [2014] is expressed as

$$u = \frac{25}{64}h\left[2\alpha\sqrt{1+4\alpha^2} + \ln\left(2\alpha + \sqrt{1+4\alpha^2}\right)\right] \tag{5.11}$$

Thus, for a known value of u and h, α is found from Eq. (5.11), which is used for calculation of A_{eff} using Eq. (5.9).

However, as discussed, the decrease in secant horizontal stiffness of U-FREI with the increase in horizontal displacements is dependent not only on the effective plan area of isolator due to rollover deformation, but also on the effective shear modulus of isolator. Thus, in the present study, an analytical relationship is proposed for predicting the horizontal response of U- FREI, including the influence of both effective shear modulus, G_{eff}, and effective plan area, A_{eff}, as

$$K_{ub} = \frac{G_{eff} A_{eff}}{t_r} \tag{5.12}$$

$$or \quad K_{ub} = \left(\frac{A_{eff}}{A} \right) K_b \tag{5.13}$$

Thus, Eqs. (5.2) and (5.12) can serve as a basic analytical tool for estimating the variation of horizontal stiffness with applied shear displacement for B-FREI and U-FREI respectively. The observations from numerical and experimental studies of both B-FREI and U-FREI types *A1*, *B1* and *B2* presented in Chapter 3 and 4 are used for the performance evaluation of the proposed analytical methods.

5.3. Performance Evaluation of Proposed Analytical Approach for Predicting K_{eff}^{h} of FREI

A rational approach is proposed for predicting the effective horizontal stiffness of both B-FREIs and U-FREIs. With the increasing horizontal displacements, the FREIs undergo nonlinear displacement and the resulting horizontal stiffness from proposed analytical approaches are compared with experimental as well as numerical results and also with results of few previous studies to evaluate the acceptability of these proposed analytical approaches.

As proposed in Section 5.2, the secant horizontal stiffness of B-FREI is determined using Eq. (5.2), while the same for U-FREI is computed using Eq. (5.12). Effective shear modulus for both B-FREI and U-FREI are computed using Eq. (5.7). However, the value of G_{eff} is observed to decrease with the increase in horizontal displacements. Strauss, *et al.* [2014] also observed through experimental investigation that the rate of decrease in G_{eff} is not constant with displacement. In the present study, from FE results shown in Tables 4.1-4.3 in Chapter 4, it is observed that the effective horizontal stiffness of B-FREIs decrease faster at horizontal displacement range from zero to $1.00t_r$ and at much slower rate for horizontal displacement beyond $1.00t_r$. Therefore, in this section, two analytical methods are proposed for predicting the effective horizontal stiffness of FREI, as proposed method 1 and 2. The proposed method 1 simply takes the effective shear modulus of FREIs using Eq. (5.7) for the entire displacement range from zero to $1.50t_r$. However, in the proposed method 2, the effective shear modulus of FREI is evaluated by Eq. (5.7) for applied displacements up to $1.00t_r$ and the same is kept constant for displacements beyond $1.00t_r$. Thus, effective shear modulus in method 2 can be evaluated from Eq. (5.14).

$$\left.\begin{aligned} G_{eff} &= G\left[1-\left(\frac{p_z}{p_{crit,0}\left(1-\left(\frac{u}{a}\right)^2\right)}\right)^2\right]\left(1-\frac{u}{a}\right) \qquad \text{for} \quad 0 \le u \le 1.0t_r \\ G_{eff} &= G\left[1-\left(\frac{p_z}{p_{crit,0}\left(1-\left(\frac{1.0t_r}{a}\right)^2\right)}\right)^2\right]\left(1-\frac{1.0t_r}{a}\right) \qquad \text{for} \quad 1.0t_r < u \le 1.5t_r \end{aligned}\right\} \tag{5.14}$$

In both the proposed methods, the effective horizontal stiffness of B-FREIs and U-FREIs are calculated using Eqs. (5.2) and (5.12) respectively. In the evaluation of effective horizontal stiffness for U-FREI, additional consideration of effective contact area is considered, in which the effective contact area is calculated by Eq. (5.9).

Comparison of effective horizontal stiffness of U-FREIs obtained from two proposed analytical methods, FE analysis, experimental results and two methods suggested by Gerhaher, *et al.* [2011] using Eq. (5.6) and Nezhad [2014] using Eq. (5.8) with increasing horizontal displacements are shown in Fig. 5.2. As may be seen from Fig. 5.2, proposed methods 1 and 2 have shown very good agreement with experimental and numerical results up to $1.00t_r$. However, in the range from $1.00t_r$ to $1.50t_r$, proposed method 2 has agreed better for isolators A1 and B1, while proposed method 1 is relatively better than proposed method 2 for isolator B2. As mentioned earlier, experimental investigations are conducted up to $0.89t_r$ from the view point of safety of test set up and hence finite element results are compared with experimental results up to that range only. The evaluated values of effective horizontal stiffness for all the three un-bonded isolators using FE analysis have shown excellent agreement with those from experimental investigations and thus the values of effective horizontal stiffness using FE method for the extended range up to $1.50t_r$ are considered as the basis for comparison. It may however be observed that the values of K_{eff} based on Gerhaher, *et al.* [2011] and Nezhad [2014] are having significant deviation from the values of K_{eff} as obtained from experiment up to $0.89t_r$ and FE analysis for the entire considered range.

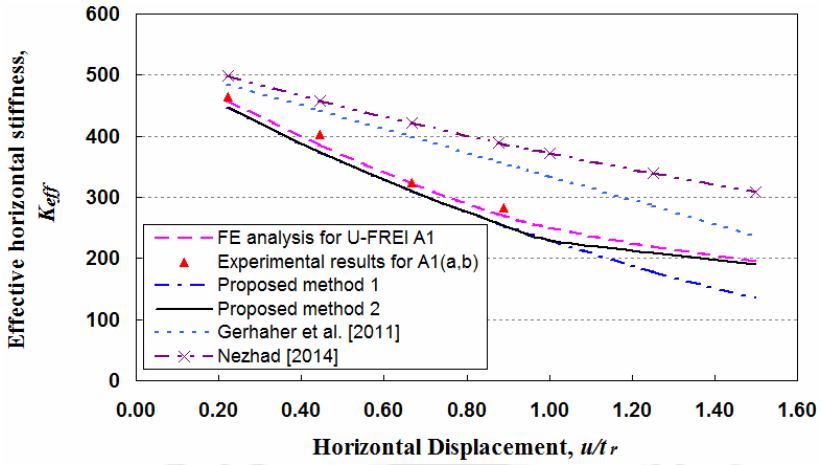

(a) Isolator A1

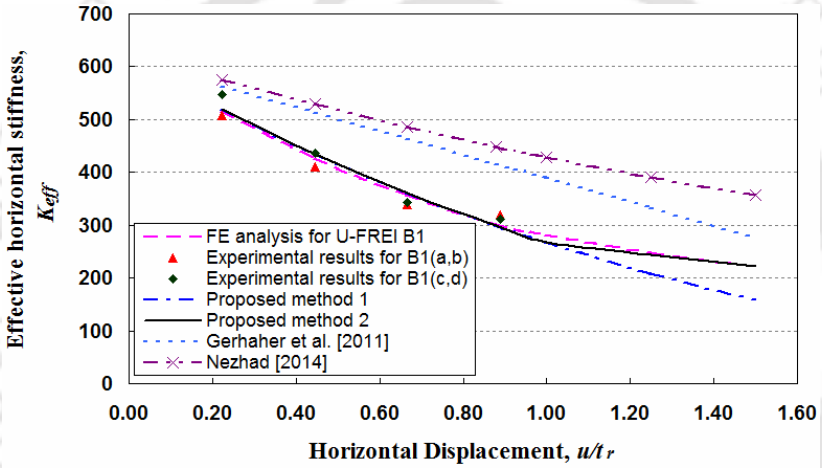

(b) Isolator B1

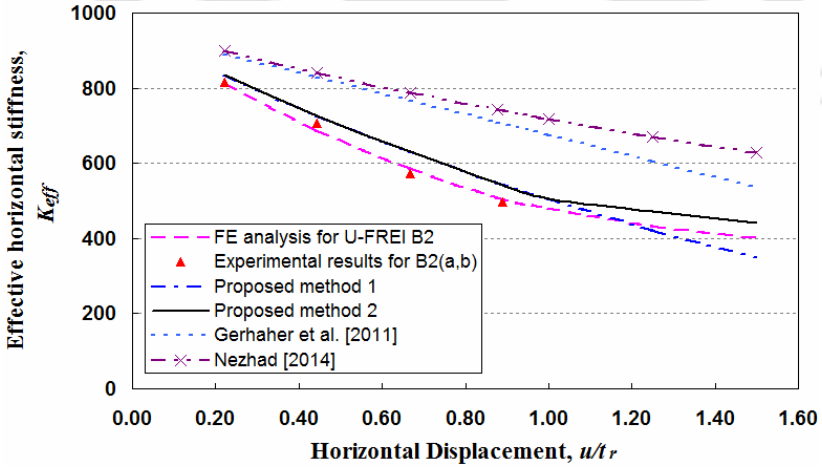

(c) Isolator B2

Fig. 5.2 Effective horizontal stiffness versus displacement of types A1, B1, B2 U-FREIs obtained from experiments, FE analysis and analytical methods

Comparison of effective horizontal stiffness of B-FREI specimen types A1, B1, B2 as obtained from two proposed methods, FE analysis and few methods suggested by Gerhaher [2010] using Eq. (5.3), and Naeim and Kelly [1999] using Eq. (5.1) with increasing horizontal displacement up to $1.50t_r$ are shown in Fig. 5.3. As may be seen from Fig. 5.3, the effective horizontal stiffness of B-FREI obtained from FE analysis decreases with the increasing horizontal displacement. However, the rates of the decrease in effective horizontal stiffness obtained from Gerhaher [2010] and Naeim and Kelly [1999] are almost constant and show significant deviation from those obtained from FE analysis. Strauss, *et al.* [2014] however observed from experimental investigations that the estimation of K_{eff} is better if G_{eff} is evaluated using Eq. (5.7), which was suggested by Gerhaher, *et al.* [2011] for U-FREI than with Eq. (5.5) proposed by Gerhaher [2010] for B-FREI.

It can be seen from Fig. 5.3 that the effective horizontal stiffness of B-FREI as obtained from FE analysis decreases with the increase in the horizontal displacements. However, rate of decrease up to displacement range of $1.00t_r$ is significantly higher than that in the displacement range of $1.00t_r$ to $1.50t_r$. These rates up to $1.00t_r$ and for $1.00t_r$ - $1.50t_r$ are found from FE analysis as 33.1% and 7.9% for isolator A1, 33.6% and 8.6% for isolator B1, 32.8% and 7.8% for isolator B2. The varying magnitudes of effective horizontal stiffness with increase in imposed horizontal displacements are calculated as per two proposed methods. These calculated values for all the three considered isolators A1, B1, B2 are plotted in Fig. 5.3. It is observed that both the proposed methods have matched very well with finite element based results for all the three bonded isolators up to $1.0t_r$. However, in the range of $1.0t_r$ - $1.5t_r$, the proposed method 2 has agreed better for isolators A1 and B1, while the proposed method 1 is relatively better than the proposed method 2 for isolator B2. However, it should be noted that the values of K_{eff} based on

Gerhaher [2010] and Naeim and Kelly [1999] are significant deviation from the values of K_{eff} as obtained from FE analysis.

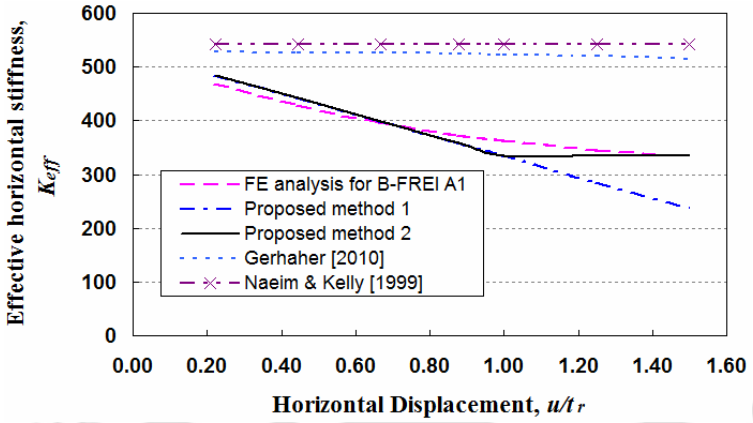

(a) Isolator A1

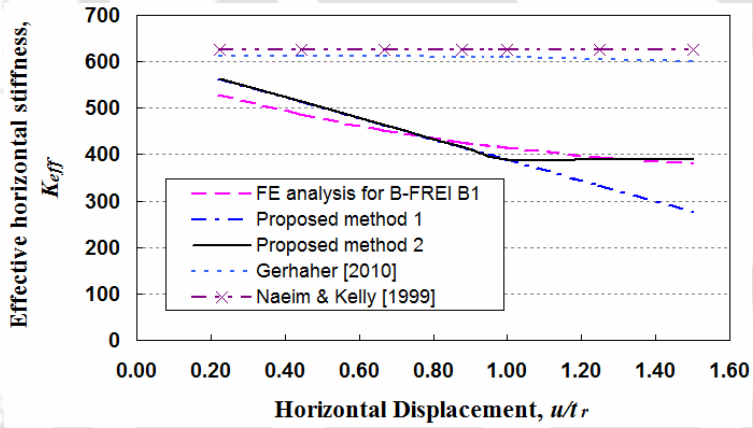

(b) Isolator B1

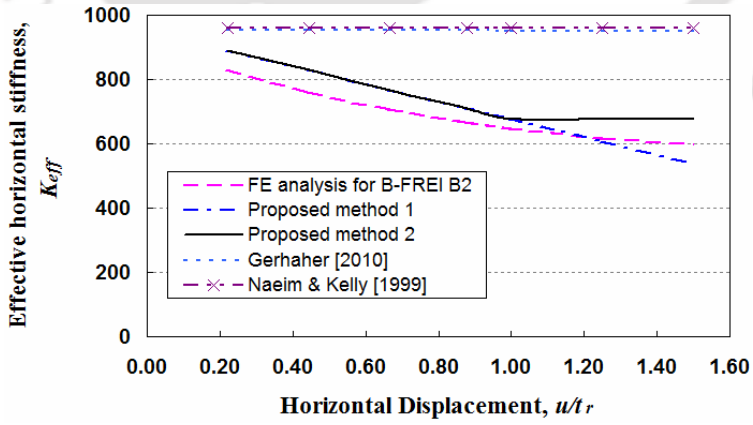

(c) Isolator B2

Fig. 5.3 Effective horizontal stiffness versus displacement of types A1, B1, B2 B-FREIs obtained from FE analysis and analytical methods

Thus, based on the observations from Figs. (5.2) and (5.3), it can very well be assumed that Eqs. (5.2) and (5.12) may be considered as a basic analytical tool for predicting the effective horizontal stiffness of B-FREI and U-FREI respectively. The effective horizontal stiffness of B-FREI is influenced by the reduction of effective shear modulus with displacement, while that of U-FREI is affected by the reduction of shear modulus as well as reduction in contact area of isolator undergoing rollover deformation. Further, it is observed to have good agreement with experimental and numerical results, when the evaluation of reduction in shear modulus is done using Eq. (5.7) for both B-FREI and U-FREI. However, the rate of decrease in G_{eff} is actually not constant with displacement. In one of the proposed analytical methods, it is suggested that the magnitude of G_{eff} may be kept constant beyond the displacement of $1.00t_r$ and is observed to be a little sensitive to shape factor. Thus, further studies should be carried out involving experimental investigations of isolators having different shape factors, with different vertical pressures and subjected to large displacements.

Further, it may be noted that experimental observations are obtained up to principal stretch of about 1.3. Expectedly, Mullin's effect is not really observed as this becomes more significant at higher values of stretch. The numerical analysis, however, could not capture such effect even though the stretch values are a little higher (up to 1.54) as the material is modelled as hyper-elastic only.

5.4. Concluding Remarks

In this chapter, an analytical approach is proposed as a basic tool for predicting the secant horizontal stiffness of both B-FREI and U-FREI. Decrease in the horizontal stiffness of B-FREI with increasing horizontal displacement is due to decrease in effective shear modulus, while that of U-FREI is due to decrease in both effective shear

modulus as well as the contact area of the isolator due to rollover deformation. The evaluated values of K_{eff} using the analytical approach show reasonably good agreement with experimental and FE based results. Thus, these analytical tools can be very useful in arriving at quick and reliable estimation of initial configurations of isolators while designing FREI supported isolated buildings.

Chapter 6

Stability Analysis of a Prototype U-FREI

6.1. Introduction

From the literature review, it is observed that most of the suggested models for predicting stability of elastomeric isolators were used for conventional isolators in bonded application. There are very few studies for ascertaining the stability of FREIs in an un-bonded application. Moreover, scaled sizes of elastomeric isolators were considered in these studies with low shape factors. Therefore, it is necessary to carry out the studies for predicting the stability of a prototype U-FREI with high shape factor.

Determination of the stability limit of a prototype isolator by experimental tests is relatively accurate, but it is difficult to investigate in laboratory due to constraints of experimental facility. In view of this, stability analysis of a prototype U-FREI is presented in this chapter, where detailed results from FE analysis are used. A prototype FREI, type B1 is investigated under the action of varying vertical load and cyclic horizontal displacement to determine the critical load carrying capacity. Further, the horizontal response of the U-FREI is also evaluated under the design vertical load and increasing horizontal displacement up to $2.00t_r$ (180 mm) to observe the rollout instability of the isolator.

6.2. Procedure for Determination the Critical Load Carrying Capacity of U-FREI

As observed from literature, stability of an elastomeric isolator is evaluated based on the relation of shear force with horizontal displacement. The critical load capacity of the

elastomeric isolator is defined as the vertical load for which the horizontal stiffness is reduced to zero. When the elastomeric isolator is subjected to simultaneously the vertical load, P, and increasing horizontal displacement, u, shear force may pass through a maximum value, as illustrated in Fig. 6.1. The point of maximum shear force is considered the stability limit defined by the critical horizontal displacement, u_{cr}, and corresponding vertical load referred to herein as the critical load, P_{cr}.

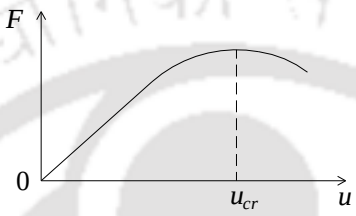

Fig. 6.1 Shear force versus horizontal displacement

From theoretical analysis:

$$K_h = \frac{\partial F}{\partial u} = 0 \tag{6.1}$$

Using chain rule,

$$K_h = \frac{\partial F}{\partial u} = \frac{\partial F}{\partial P} \times \frac{\partial P}{\partial u} = 0 \tag{6.2}$$

where F, u, P are shear force, horizontal displacement and vertical load, respectively.

There is no requirement that $\partial F/\partial P$ must be equal to zero. Therefore,

$$\frac{\partial P}{\partial u} = 0 \tag{6.3}$$

where $\partial P/\partial u$ = derivative of the vertical load with respect to the horizontal displacement.

For a conventional elastomeric isolator in bonded application, the prediction of critical load capacity is often conducted by two quasi-static methods (Sanchez, *et al.*, 2013). In the first method, the isolator is subjected to a constant vertical load, P, and a

monotonically increasing horizontal displacement, u, until the isolator reaches its stability limit ($K_h = 0$). The point of equilibrium is determined directly from shear force-horizontal displacement response as the point where the slope equals zero. The second method includes shearing the isolator to a constant horizontal displacement, u, and applying monotonically increasing vertical load, P, while monitoring a reduction in shear force F. Repeating this procedure for different horizontal displacement levels provides unique equilibrium trajectories (F vs P) from which the point of neutral equilibrium, thus critical point (u_{cr}, P_{cr}) can be indirectly obtained.

However, for a FREI in un-bonded application subjected simultaneously to vertical load and horizontal dynamic displacements, the evaluation of critical load needs to be appropriately considered. Particularly for performance-based design, it is important to extend the theoretical understanding on the stability of the isolator based on static/quasi-static methods to dynamic behavior and enhance the ability to predict the response when subjected to extreme earthquake loading. Thus, it should use a dynamic method under cyclic loading to evaluate the critical load capacity of the U-FREI.

In dynamic method, the U-FREI undergoes simultaneously a variation of the vertical load and cyclic horizontal displacement. Two important parameters such as the effective horizontal stiffness and equivalent viscous damping (or damping factor) are obtained from the hysteresis loops using Eqs. (3.1) and (3.2) in Chapter 3. The horizontal stiffness of a U-FREI includes two components termed as horizontal secant stiffness and the tangential stiffness. In order to calculate the critical buckling load of the isolator obtained from the dynamic method, a curve is fitted to shear force-displacement hysteresis loop. According to the previous studies by Nezhad *et al.* [2008] and Raaf *et al.* [2011], a method of fitting a polynomial to shear force-displacement hysteresis data is developed. The fitted curve, denoted as backbone curve, represents an idealized

evaluate of horizontal response of isolator with the damping forces removed as shown in Fig. 6.2.

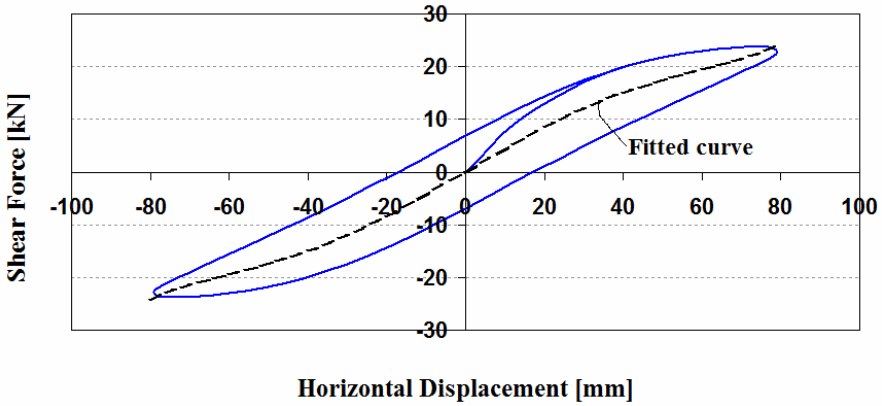

Fig. 6.2 Illustration of a fitted backbone curve in a hysteresis loop

The total horizontal load, $f_{b,i}$, experienced by the i^{th} isolator is described as:

$$f_{b,i}(t) = f_{sb,i}(t) + f_{db,i}(t) \tag{6.4}$$

where, $f_{sb,i}$ is stiffness force and $f_{db,i}$ is the corresponding force due to damping.

In a simple approach, the stiffness force can be modelled as a polynomial of order 5 given by:

$$f_{sb,i}(t) = k_{b,i}(v_b(t)) \times v_b(t) = b_0 v_b(t) + b_1 v_b^2(t) + b_2 v_b^3(t) + b_3 v_b^4(t) + b_4 v_b^5(t) \tag{6.5}$$

where, $v_b(t)$ is the horizontal displacement and $k_{b,i}(v_b(t))$ is the horizontal secant stiffness as a function of horizontal displacement:

$$k_{b,i}(v_b(t)) = b_0 + b_1 v_b(t) + b_2 v_b^2(t) + b_3 v_b^3(t) + b_4 v_b^4(t) \tag{6.6}$$

The five parameters b_0 to b_4 are determined by applying a least squares fit to shear force-displacement hysteresis data.

The corresponding force due to damping, $f_{db,i}$, represents an idealized Rayleigh damping:

$$f_{db,i}(t) = c_{b,i}(t) \times \dot{v}_b(t) \tag{6.7}$$

where $c_{b,i}(t)$ is the damping coefficient dependent on a equivalent viscous damping ratio ξ, tributary mass of structure on each isolator (m_i) and the horizontal secant stiffness $k_{b,i}(v_b(t))$:

$$c_{b,i}(t) = 2\xi\sqrt{k_{b,i}(v_b(t))m_i} \tag{6.8}$$

The tangential stiffness of the i^{th} isolator, $k_{tb,i}(v_b(t))$, as a function of horizontal displacement is

$$k_{tb,i}(v_b(t)) = \frac{df_{sb,i}(t)}{dv_b(t)} = b_0 + 2b_1v_b(t) + 3b_2v_b^2(t) + 4b_3v_b^3(t) + 5b_4v_b^4(t) \tag{6.9}$$

where the parameter b_0 is the tangential stiffness of the i^{th} isolator at $v_b(t) = 0$.

According to the remark of the previous study by Stanton *et al.* [1990], the tangential stiffness at zero horizontal displacement in a shear force-displacement hysteresis loop is referred to as the transverse stiffness (K_t) of the isolator. The transverse stiffness is not necessarily the minimum tangential stiffness in every fully reserved hysteresis loop under constant vertical load. However, the transverse stiffness represents the tangential stiffness at which zero horizontal stiffness first occurs under increasing vertical load. The vertical load corresponding to a transverse stiffness of zero ($K_t = 0$) is defined as the critical buckling load of a U-FREI under cyclic loading.

6.3. Details of Input Loads

In this chapter, a U-FREI, type B1 is used to study the stability of the isolator. Similar to Chapter 4, FE simulation of the isolator is done using ANSYS v.14.0.

The isolator is subjected to a variation of the vertical load to determine the predicting stability of the U-FREI under cyclic horizontal displacement and the effect of vertical load on the dynamic properties. First, the isolator is loaded simultaneously to a design vertical load of 350 kN and two fully sinusoidal cycles of horizontal displacement of

amplitude 80 mm ($0.89t_r$), as shown in Fig. 6.3, applied at the top rigid plate. The magnitude of the design vertical load corresponds to factored column load and the value is obtained from the analysis of the actual building. Next, amplitude of horizontal displacement is increased up to 135 mm ($1.50t_r$). The vertical load is subsequently increased and the process is repeated starting at the displacement amplitude of 80 mm. The complete simulation is considered for three displacement amplitudes of 80, 112.5 and 135 mm ($0.89t_r$, $1.25t_r$ and $1.50t_r$) and four vertical loads of 350, 550, 700 and 850 kN.

On the other hands, the horizontal response of the U-FREI is also subjected under the design vertical load of 350 kN and increasing horizontal displacement up to $2.00t_r$ (180 mm) to investigate the rollout instability of the isolator.

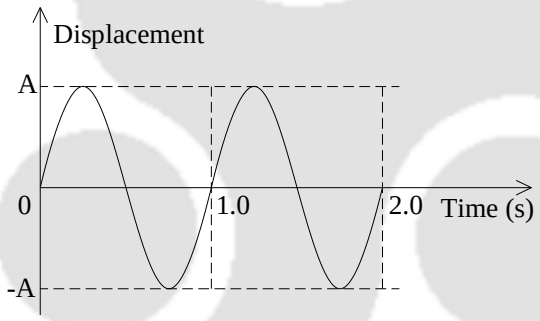

Fig. 6.3 Imposed horizontal displacement history

6.4. FE Analysis Results and Discussion

Force-displacement relationship and other associated parameters from the adopted FE model of U-FREI are found to agree very well with those from experimental investigations and the detailed validation of the FE model is shown in Chapter 4. Thus, the accuracy of adopted FE model is established. In view of this, the FE model is considered for analysis up to very large displacement, wherein analysis is done for varying vertical loads as well as cyclic horizontal displacement. Evaluation of the

critical buckling load carrying capacity, rollout instability and effect of vertical load on dynamic properties of the U-FREI, type B1 are presented in this section.

6.4.1. Critical Buckling Load Carrying Capacity

The objective of the dynamic stability analysis is to determine the critical buckling load at which the isolator would no longer be able to maintain positive incremental force resisting capacity. As discussed above, the isolator is subjected to a variation of the vertical loads under cyclic horizontal displacement. According to the fitting method, the fitted backbone curves and corresponding hysteresis loops of the U-FREI for each vertical load and displacement amplitude of 80 mm as obtained from FE analysis are shown in Fig. 6.4. The fitted backbone curve is obtained from the average value of shear forces at any given horizontal displacement in the corresponding hysteresis loop and is described by a polynomial. It can be seen from Fig. 6.4, each cycle of FE analysis result maintains both symmetric and comparable hysteresis loops for all vertical loads investigated. Similarly, considering other displacement amplitudes ($1.25t_r$ and $1.50t_r$), the fitted backbone curves of the isolator under different vertical loads (350, 550, 700 and 850 kN) are shown in Fig. 6.5.

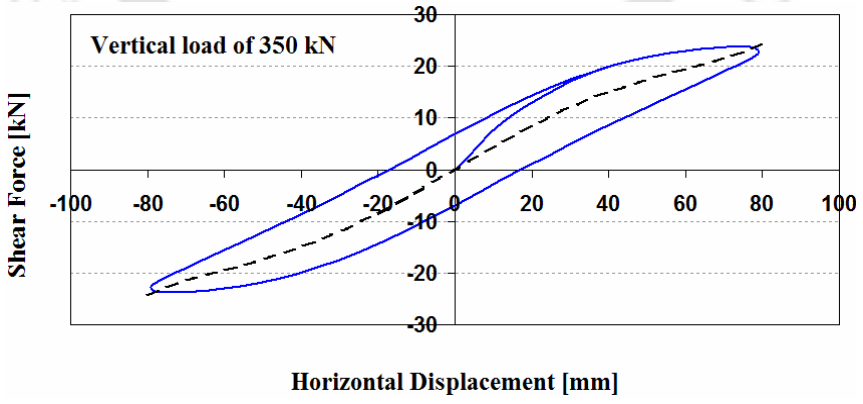

(a) Vertical load of 350 kN

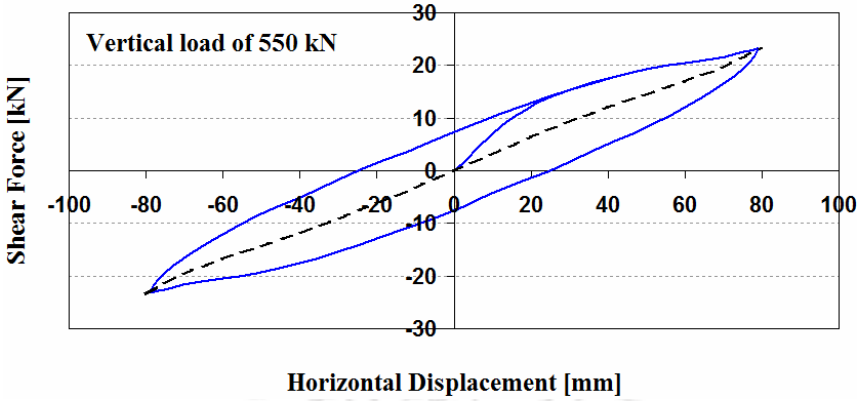

(b) Vertical load of 550 kN

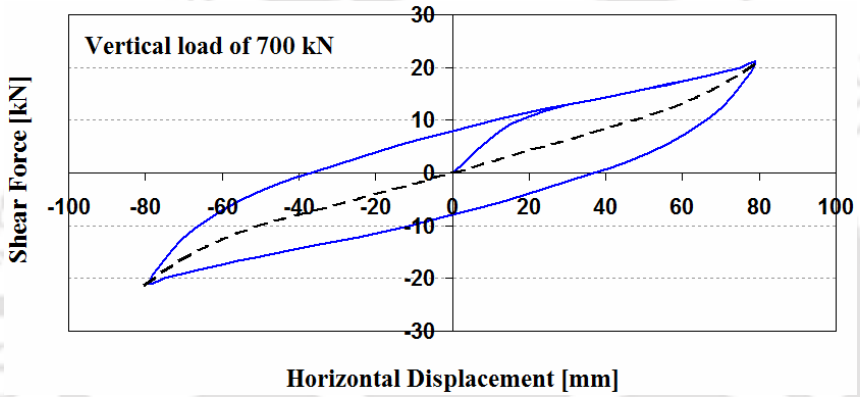

(c) Vertical load of 700 kN

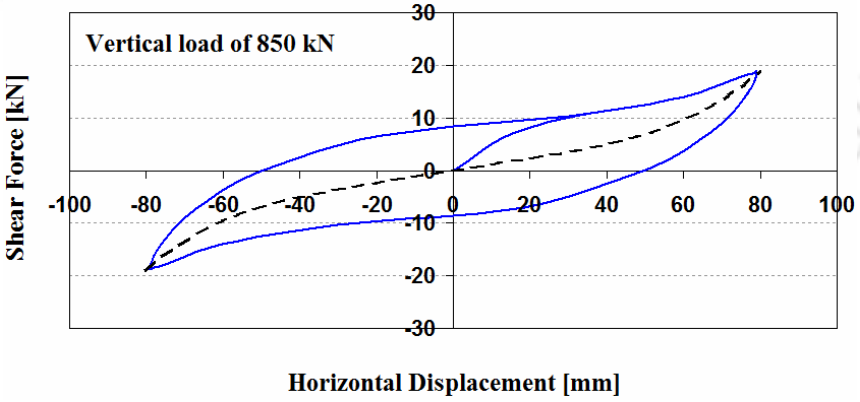

(d) Vertical load of 850 kN

Fig. 6.4 Hysteresis loops and fitted backbone curves of U-FREI under different vertical loads at displacement amplitude of 80 mm

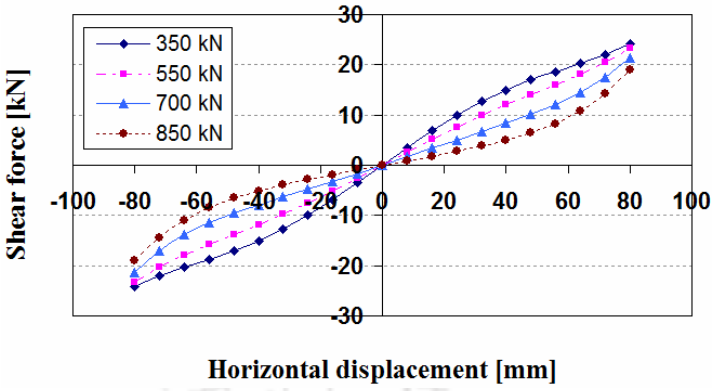

(a) Displacement amplitude of 0.89t_r (80 mm)

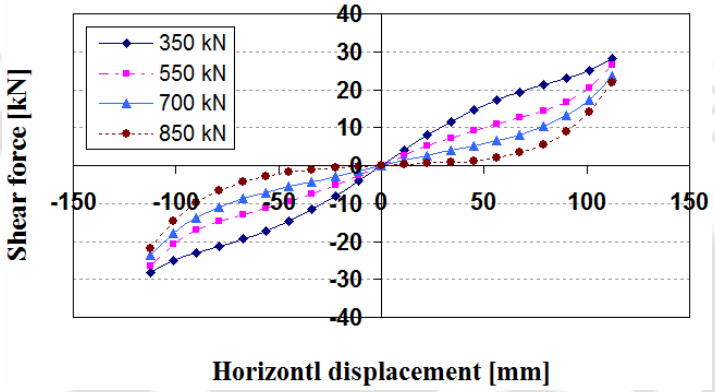

(b) Displacement amplitude of 1.25t_r (112.5 mm)

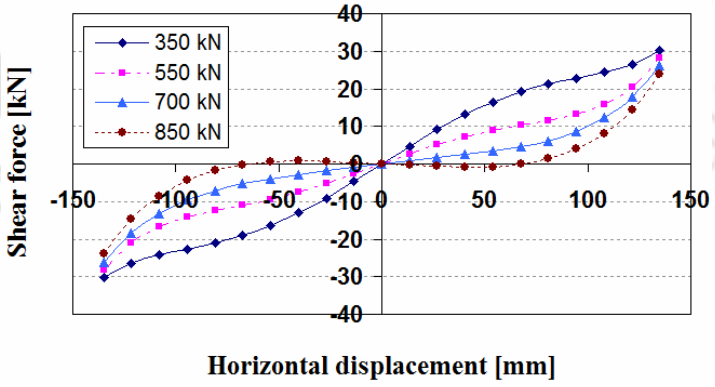

(c) Displacement amplitude of 1.50t_r (135 mm)

Fig. 6.5 Fitted backbone curves of U-FREI under variation of vertical loads and horizontal displacement amplitudes

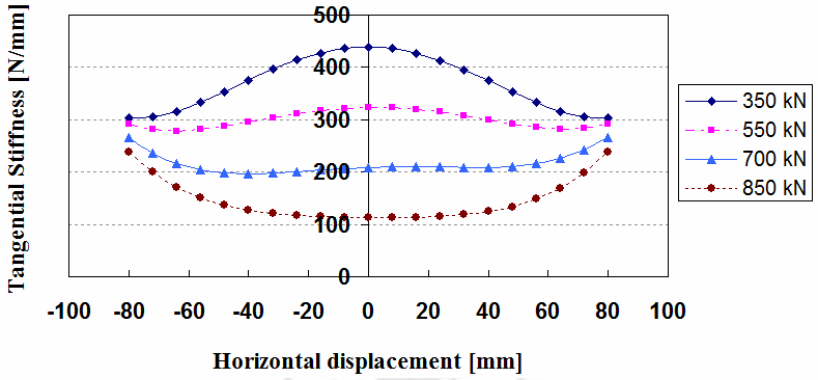

(a) Displacement amplitude of 0.89t_r (80 mm)

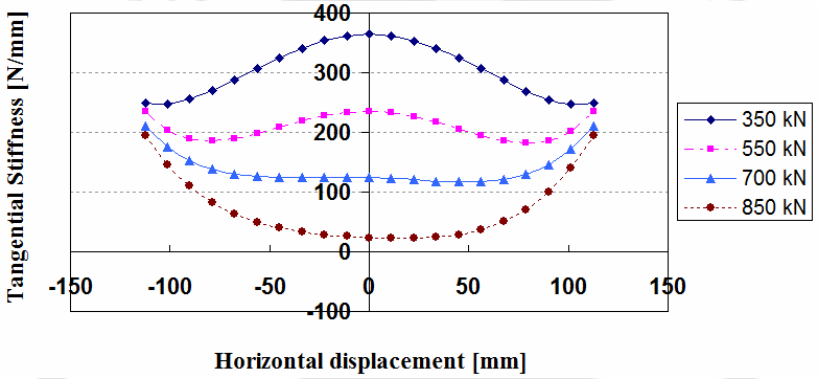

(b) Displacement amplitude of 1.25t_r (112.5 mm)

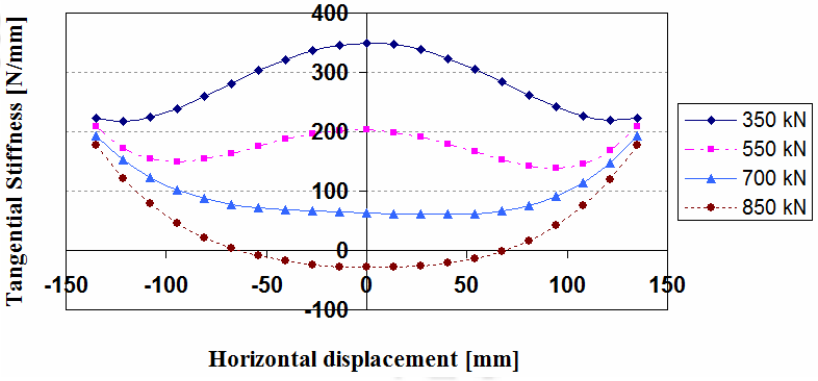

(c) Displacement amplitude of 1.50t_r (135 mm)

Fig. 6.6 Tangential stiffness obtained from the first derivative of the fitted backbone curve at different displacement amplitudes

The tangential stiffness results of the isolator under variation of vertical loads and displacement amplitudes are evaluated from Eq. (6.9) and are presented in Fig. 6.6. It can be seen from Fig. 6.6 that the tangential stiffness at zero horizontal displacement does not represent the minimum effective stiffness in a fully sinusoidal cycle of horizontal displacement under low vertical loads of 350 and 550 kN. As the vertical load increases, the minimum slope of the backbone curve (tangential stiffness) occurs at zero horizontal displacement. It should be noted that the tangential stiffness at zero horizontal displacement is referred to as the transverse stiffness (K_t) of the isolator (Stanton *et al.*, 1990). According to Fig. 6.6, the transverse stiffness may acquire a negative value at large horizontal displacement and under large vertical loads (Fig. 6.6(c)). Consequently, the vertical load corresponding to zero transverse stiffness is predicted by introducing a best fit linear interpolation.

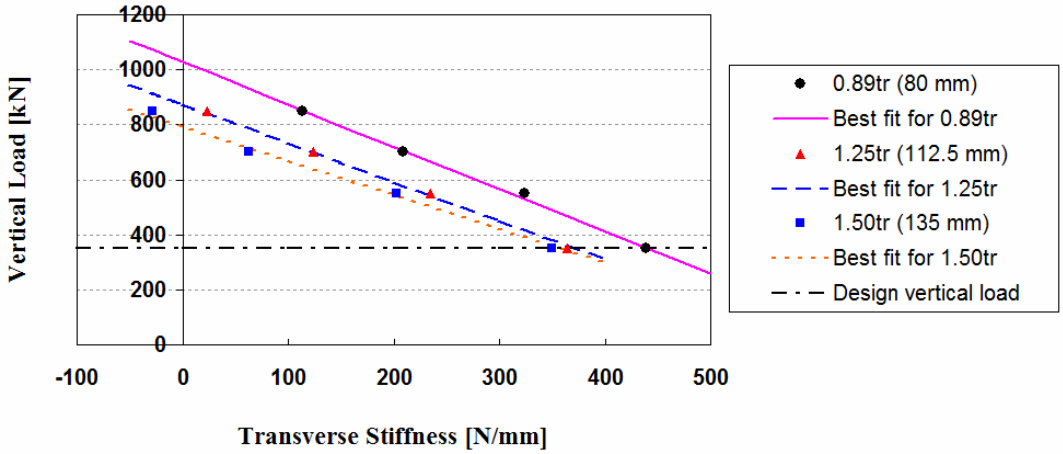

Fig. 6.7 Vertical load - Transverse stiffness relations of the U-FREI

Vertical load-transverse stiffness relations of the U-FREI at different amplitudes of horizontal displacement are shown in Fig. 6.7. It can be observed from Fig. 6.7 that the transverse stiffness of the isolator decreases with the increase in vertical load. The

decrease in transverse stiffness is observed to be nearly linear corresponding to each of the considered amplitude of horizontal displacement.

As discussed above, the vertical load corresponding to zero transverse stiffness is defined as the critical buckling load for a U-FREI. As expected, the transverse stiffness decreases with the increase in vertical load. The points corresponding to zero transverse stiffness of the isolator for different amplitudes of horizontal displacements are obtained by introducing a best fit linear interpolation (Fig. 6.7). The critical buckling loads are obtained from the points which have zero transverse stiffness. The relation of the critical buckling loads versus horizontal displacement amplitude is shown in Fig. 6.8.

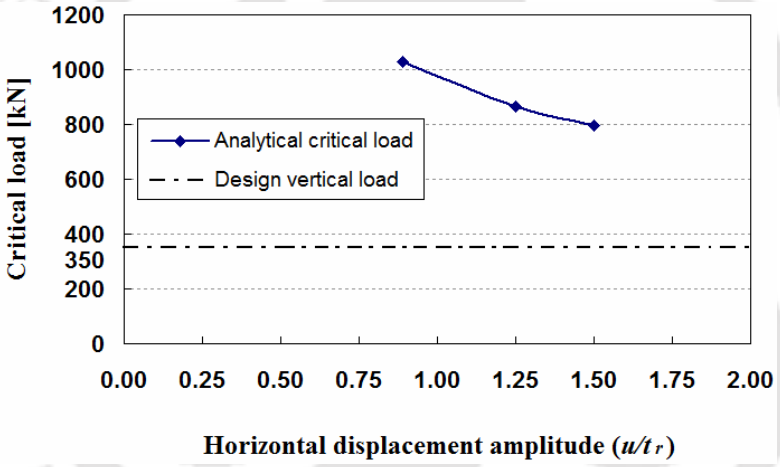

Fig. 6.8 Critical buckling load capacity of the U-FREI

It can be seen from the Fig. 6.8 that the critical buckling load decreases with the increase in horizontal displacement amplitude, and it is relatively great at low displacement amplitude. The critical load carrying capacity as obtained from FE analysis is significantly higher than the design vertical load, as example, the critical loads are found to be 2.9, 2.5 and 2.3 times higher than the design vertical load at displacement amplitude of $u = 0.89t_r$, $1.25t_r$ and $1.50t_r$ respectively. It is similar to the observation made by Raaf *et al.* [2011] based on the experimental critical load carrying

capacity of a scaled model of U-FREI. From these results, it is thus realized that the prototype un-bonded specimen in experimental tests (in Chapter 3) did not obviously show any sign of damage and susceptibility to buckling under the design vertical load.

6.4.2. Effect of Vertical Load on Dynamic Properties of the U-FREI

During the course of evaluation of critical load carrying capacity of the U-FREI, the effect of the vertical load on the mechanical properties of the isolator under cyclic horizontal displacement is also investigated. The effective horizontal stiffness and equivalent viscous damping of the isolator under variation of vertical loads and displacement amplitudes obtained from Eqs. (3.1) and (3.2) in Chapter 3 are provided in Table 5.1 and are plotted in Figs. 6.9 and 6.10.

Table 6.1 Mechanical properties of the U-FREI under different vertical loads

Vertical load (kN)	Amplitude of horizontal displacement					
	80 mm		112.5 mm		135 mm	
	K_{eff}^{h} (kN/m)	β (%)	K_{eff}^{h} (kN/m)	β (%)	K_{eff}^{h} (kN/m)	β (%)
350	301.67	13.46	247.09	14.58	222.03	15.42
550	288.09	15.61	233.67	16.92	209.04	17.87
700	267.53	18.19	218.00	19.90	189.40	21.04
850	238.72	21.69	194.13	24.45	165.19	27.00

It can be seen from Figs. 6.9 and 6.10 that the effective horizontal stiffness of the U-FREI decreases, while the equivalent viscous damping increases with the increase in the vertical load at any given amplitude of horizontal displacement. The decreases in effective stiffness are found to be 20.9%, 21.4% and 25.6% under the vertical load ranging from 350 kN to 850 kN at the displacement amplitude of $0.89t_r$, $1.25t_r$ and $1.50t_r$, respectively. At a given vertical load, the effective horizontal stiffness decreases, while the damping factor increases with increasing horizontal displacement amplitude.

It is presented in more detail later. Despite the reduction in the effective horizontal stiffness at high vertical loads, the U-FREI could maintain symmetric force-displacement hysteresis under cyclic loading.

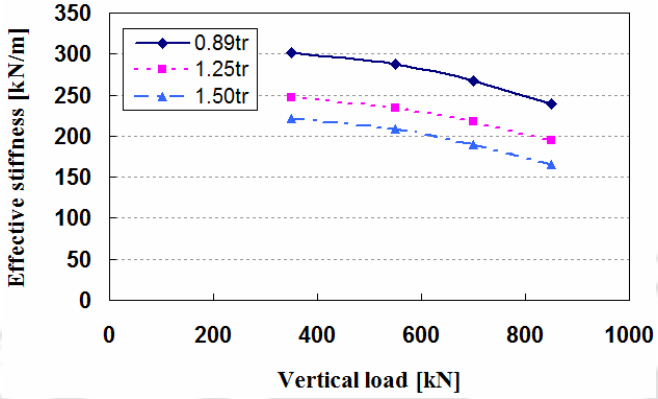

Fig. 6.9 Effective horizontal stiffness versus vertical load

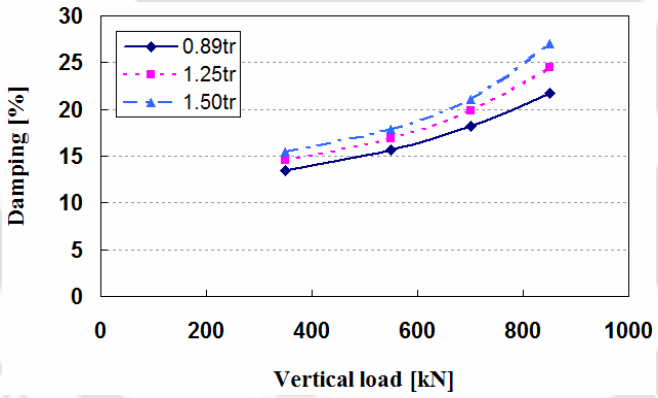

Fig. 6.10 Equivalent viscous damping versus vertical load

6.4.3. Rollout Instability of the U-FREI under Design Vertical Load

As observed, the U-FREI is not susceptible to buckling under the design vertical load at the amplitude of displacement less than $1.50t_r$. In this case, it is necessary to investigate the horizontal response of the isolator under design vertical load of 350 kN and increasing horizontal displacement such that the original vertical faces of isolator establish full contact with the support surfaces, herein up to $2.00t_r$ (180 mm). At the

large horizontal displacement, rollover deformation of the U-FREI occurs and the rollout instability may be observed. Rollout is defined as the instability of a recessed isolator under large shear displacement. The objective is to determine the horizontal displacement at which the horizontal stiffness will be zero under design vertical load.

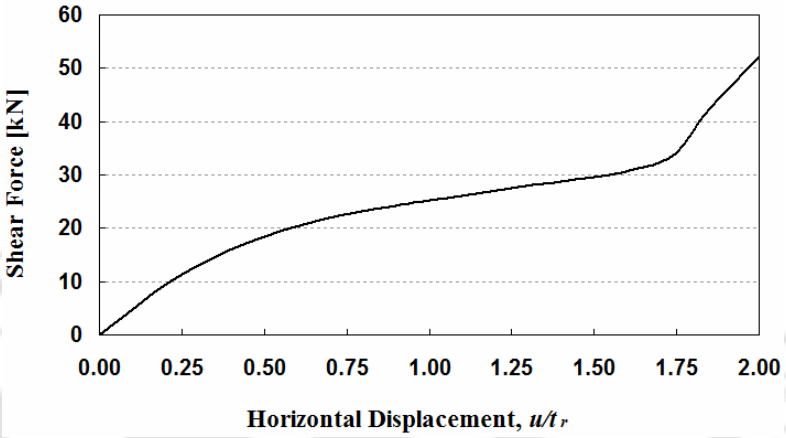

Fig. 6.11 Horizontal load-displacement curve of the U-FREI

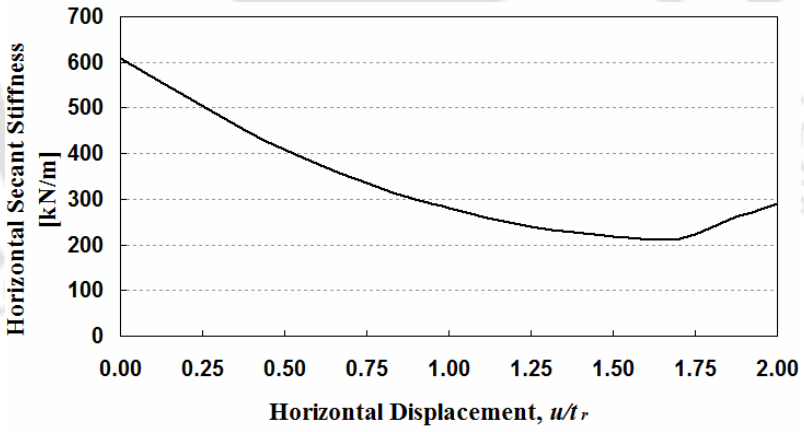

Fig. 6.12 Horizontal secant stiffness versus displacement

The shear force-displacement curve and horizontal secant stiffness-displacement relationship of the U-FREI under design vertical load and increasing horizontal displacement up to $2.00t_r$ are shown in Figs. 6.11 and 6.12. It can be seen from these figures that positive force resisting capacity is observed throughout the displacement

range from zero to $2.00t_r$, and hence the isolator remains stable. Thus, the rollout instability of the U-FREI is not observed.

6.5. Concluding Remarks

This chapter presents the prediction of stability of the prototype U-FREI type B1 in Chapters 3 and 4 based on dynamic response computed from FE analysis. The isolator is subjected to a various levels of vertical loads under cyclic horizontal displacement to determine the effect of vertical load on the dynamic properties and the predicting stability of the U-FREI. Further, the horizontal response of the isolator is also gradually increased to investigate the rollout instability under design vertical load. The concluding remarks are as follows.

- Critical buckling load of a U-FREI as obtained by dynamic stability analysis corresponds to the point in which horizontal stiffness is reduced to zero. The critical buckling load of the isolator decreases with the increase in horizontal displacement amplitude.
- Critical load carrying capacity of the prototype U-FREI as obtained from FE analysis is significantly higher than the design vertical load. This further explains why all the isolators even after repeated use in experimental investigations under the action of design vertical load and cyclic horizontal displacements (Chapter 3) are observed to have no sign of damage and susceptibility to buckling.
- Effective horizontal stiffness of the U-FREI decreases, while the damping factor increases with the increase in the vertical load at any given amplitude of horizontal displacement.
- Prototype U-FREI is observed to remain stable under the action of design vertical load and increasing horizontal displacement up to $2.00t_r$.

Chapter 7

Vulnerability Assessment of a Prototype Low-rise Masonry Building Supported on U-FREIs

7.1. Introduction

Low-rise masonry building can sustain gravity loads very easily due to high compressive strength of masonry, but are highly susceptible to ground shaking due to their low tensile as well as shear strength making them often susceptible to damage. Discussion in Chapter 1 clearly revealed that assessment of seismic vulnerability of low-rise masonry buildings located in seismic prone regions, like in the north-eastern part of India, is an essential step in risk mitigation of these buildings.

Fragility curve is a powerful solution tool for vulnerability assessment of such structures. Few studies on the seismic fragility analyses of masonry buildings have been performed in recent time. Base isolation is an effective methodology to reduce the seismic vulnerability of a structure. A few researches evaluated the efficiency of base isolation by analytical fragility curves. Most of these studies reported the analytical fragility curves for reinforced concrete buildings and highway bridges with conventional SREIs. U-FREI is an improved device for seismic mitigation of low-rise buildings. However, no studies are found in the literature on the vulnerability assessment of low-rise masonry buildings supported on U-FREIs. Thus, there is a need for quantification of reduction in seismic vulnerability of a base-isolated low-rise masonry building supported on U-FREIs as compared to the fixed-base building.

Seismic vulnerability of a two-storey stone masonry building supported on U-FREI is evaluated in this chapter. The prototype building is located at Tawang, India and is the

first such U-FREIs supported prototype low-rise masonry building constructed anywhere in the world. Reduction in seismic vulnerability of the base-isolated building as compared to that of the fixed-base building is evaluated by analytical fragility curves. Significant reduction in probability of exceedance at all the considered damage states of base-isolated building is observed as compared to that of fixed-base building.

7.2. Description of base-isolated masonry building

A two-storey base-isolated stone masonry building is constructed at Tawang, India supported on U-FREIs for seismic isolation. Low-rise masonry building is considered, since similar structures are built as common dwelling units in the South East Asia even in the highest seismic zone. This is the first U-FREI supported prototype low-rise masonry building constructed anywhere in the world. Building materials like stone and brick masonry are generally used in the construction available in these regions.

The building is comprising of two main components, namely, stone masonry walls and reinforced concrete floors. The roof is covered by galvanized iron sheets supported on truss structures. A view of the prototype building supported on U-FREIs is shown in Fig. 7.1. A typical floor plan of the building is shown in Fig. 7.2(a). Reinforced concrete basement beams (A & B) are provided at two different levels as indicated in Fig. 7.1. U-FREIs are placed between the two beams without any connections at fourteen numbers of locations shown in Fig. 7.2(b). Masonry walls that are nearly perpendicular to the seismic loading direction are referred to as "out-of-plane" walls, while masonry walls that are oriented parallel to the seismic loading direction are referred to as "in-plane" walls.

This prototype building represents a class of similar low-rise masonry buildings in parts of north-eastern part of India. The material characteristics and construction practice are

generally similar. The detailed material properties of the masonry building are discussed in the next section.

Base isolation using U-FREIs for the two-storey masonry building is designed to resist strong ground motion due to earthquakes. Fourteen FREIs are used, which comprises of nine isolators of type B1 and remaining five isolators of type B2 as detailed in Chapter 3. Horizontal load-displacement relationships (backbone curves) and effective horizontal stiffness of typical U-FREIs, types B1 and B2 with increasing displacement as obtained from experimental investigations in Chapter 3 are used to represent the properties of isolator.

Fig. 7.1 Prototype base-isolated masonry building located at Tawang, India

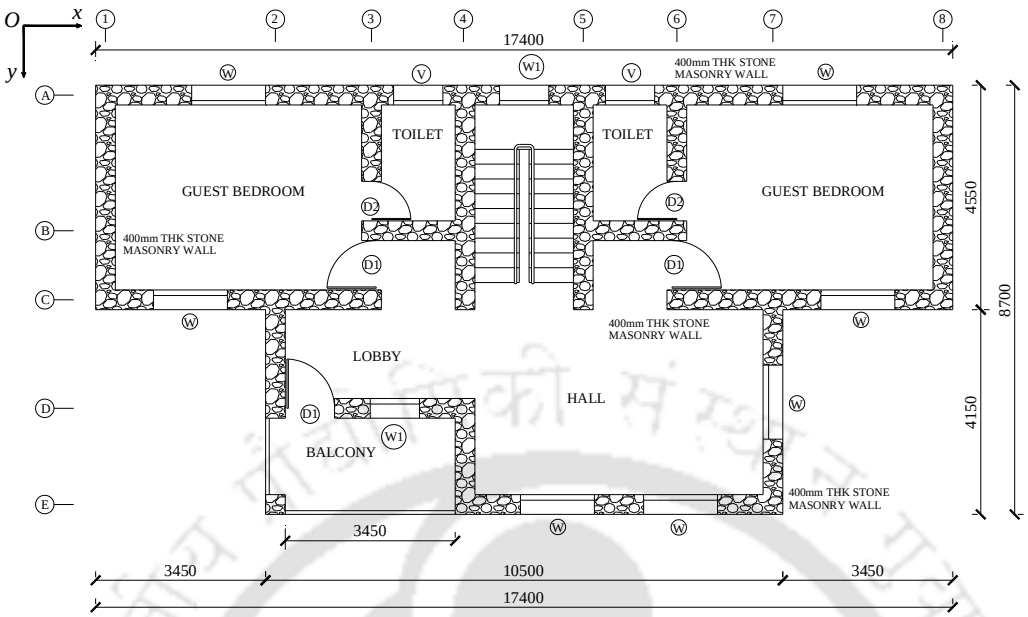

(a) Typical Floor Plan

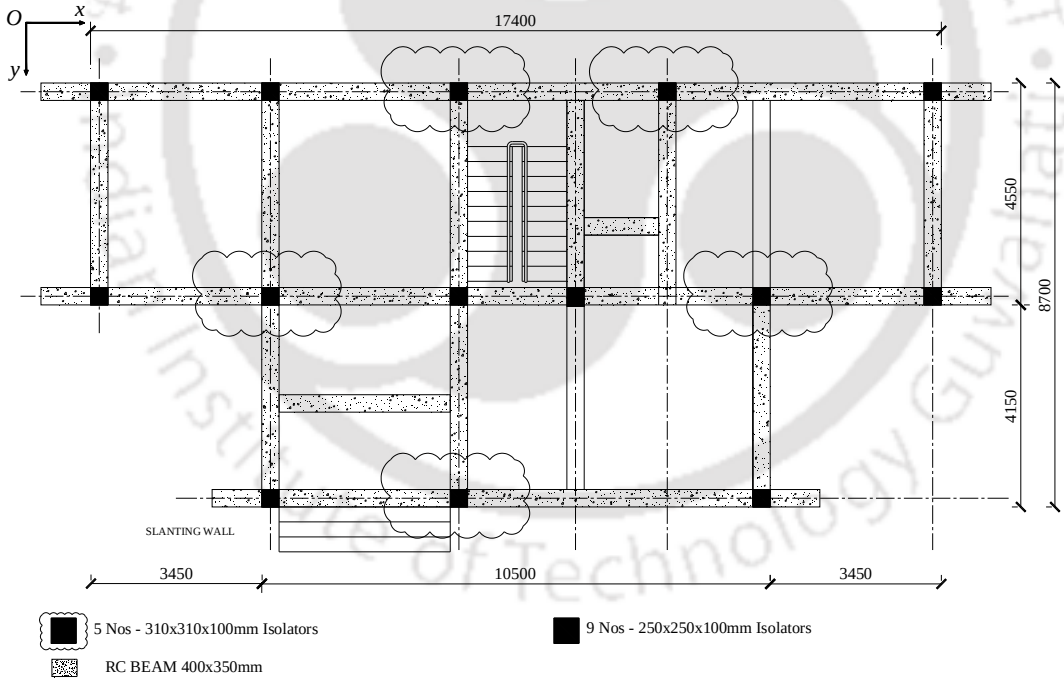

(b) Plan showing locations of base isolators

Fig. 7.2 Plan views of base-isolated masonry building

7.3. Numerical modelling of masonry building

Three-dimensional FE model of base-isolated masonry building as shown in Fig. 7.3 is simulated in SAP2000 nonlinear. Isolators are modelled by rubber isolator element defined under link type of elements. Backbone curves obtained from experimental force-displacement hysteresis loops of typical U-FREIs in Chapter 3 under horizontal cyclic loading are used to represent the properties of isolator along *X* and *Y*-axis. A bilinear hysteric model is used to define the property of isolator. The fixed-base condition is simulated by providing fixity at the basement beam level A. In the present study, masonry walls are modelled as nonlinear layered shell elements. Mohr-Coulomb failure criterion with associated flow rule is used, which reflects main characteristics of stone masonry, like frictional behaviour and limited tensile strength (Milani, *et al.*, 2006, 2007). The anisotropic behaviour of masonry is modelled by stress-strain curves for compression, tension and shear behaviour.

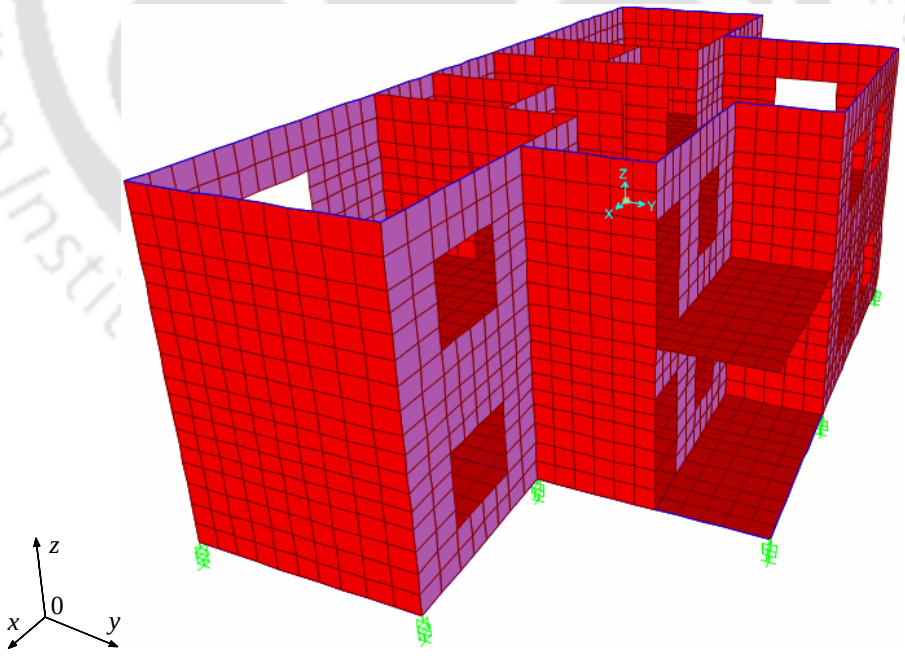

Fig. 7.3 FE model of the base-isolated masonry building in SAP2000

Stone masonry building is considered since similar structures are prevalent in the north-eastern zone of India. Thus, material properties are selected to represent the masonry material used in almost all masonry buildings of the zone. In the present study, stone masonry with a compressive strength f_b = 7.5 MPa and mortar with a compressive strength f_j = 2.5 MPa are considered. Both pushover and dynamic analyses are carried out to evaluate the seismic vulnerability of the masonry building.

7.3.1. Uniaxial compressive and tensile behaviour of masonry prism

Uniaxial compressive and tensile behaviour of masonry prism is defined using the relationship suggested from a number of laboratory tests carried out by Kaushik, *et al.* [2007], Akhaveissy and Milani [2013]. Properties of materials used in the building are given in Table 7.1 and the uniaxial compressive as well as tensile behaviour of masonry prism are shown in Fig. 7.4.

Table 7.1 Material properties of stone masonry

Young's modulus E_m (MPa)	Shear modulus G_m (MPa)	Compressive strength f'_m (MPa)	Tensile strength f_t (MPa)
1247	499	2.27	0.1

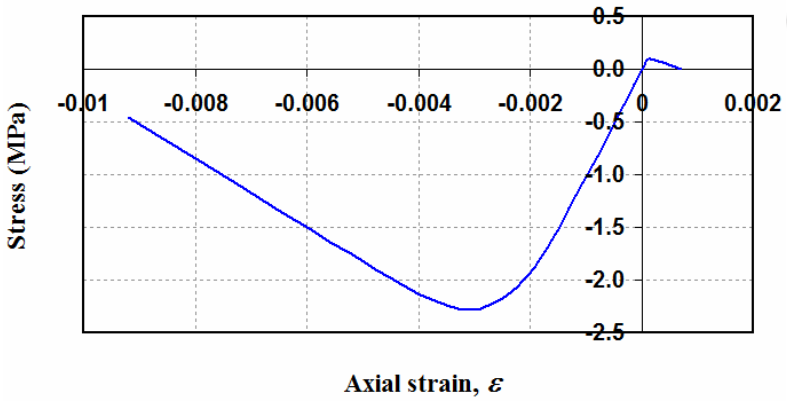

Fig. 7.4 Compressive and tensile behaviour of masonry prism used in the numerical simulation

7.3.2. Stress-strain behaviour of masonry prism in shear

Shear resistance is represented by cohesion and friction between stone (or brick) and mortar, which can be expressed with Mohr-Coulomb friction as

$$\tau = c + \sigma \times \tan\varphi \tag{7.1}$$

where σ is compressive stress and $\tan\varphi$ represents friction between stone and mortar. Numerical analysis is carried out using SAP2000 nonlinear considering a Mohr-Coulomb failure criterion with a cohesion value of 0.1 MPa and ignoring friction. The stress-strain behaviour of masonry prism in shear is shown in Fig. 7.5.

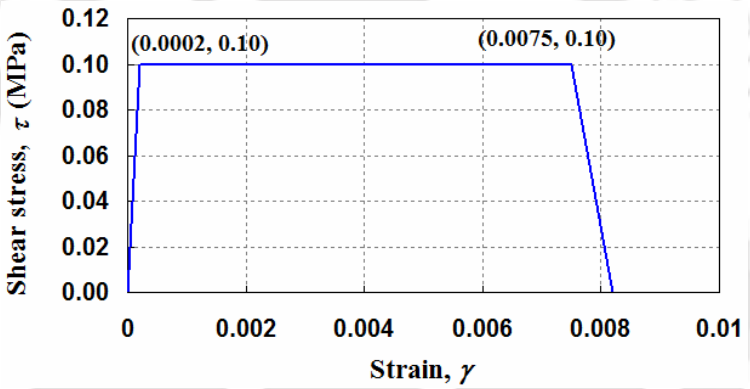

Fig. 7.5 Stress-strain plot for shear of masonry prism

7.3.3. Loads and boundary conditions

The prototype masonry building is analysed for gravity load, and horizontal load from earthquake induced ground motion. The gravity load includes the weight of building and superimposed dead load put on floors. In order to evaluate the effectiveness of base isolation, simulation of the building is performed for fixed-base and base-isolated conditions. For fixed-base (FB) building, all nodes at ground level are fixed in all the directions. However, for base-isolated (BI) building, fourteen isolators are placed at locations as per Fig. 7.2(b). These isolators modelled using rubber isolator element in

SAP2000 nonlinear utilizes the parameters obtained from experimental force-displacement hysteresis loops of U-FREIs under horizontal cyclic displacement.

For simulation of un-bonded isolators, the nonlinear horizontal force-deformation behaviour as obtained from experimental investigations is modelled through the bilinear hysteresis loop characterized by three parameters namely (i) The effective stiffness, K_{eff}, (ii) Initial stiffness K_1 and the post yield to pre-yield stiffness ratio, n (= K_2/K_1), where K_2 is post yield stiffness, and (iii) Yield strength F_y. A bilinear hysteresis loop of typical rubber isolator is illustrated in Fig. 7.6.

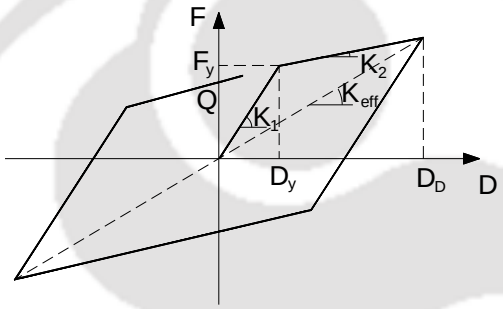

Fig. 7.6 Idealised bilinear hysteresis loop of rubber isolator

Vertical stiffness (K_V) of a laminated elastomeric isolator is given by (Naeim & Kelly, 1999)

$$K_V = \frac{E_c A}{t_r} \tag{7.2}$$

where E_c is the compression modulus.

According to Kelly and Konstantinidis [2011], the compression modulus, E_c, for a rectangular isolator having the width of $2b$ and length l, can be expressed in terms of the shape factor, S, and the aspect ratio of isolator, $\rho = 2b/l$, as

$$E_c = \frac{384}{\pi^4} GS^2 (1+\rho)^2 \sum_{m=1,3,5,\ldots}^{\infty} \frac{1}{m^4}\left(1 - \frac{2\rho}{m\pi}\tanh\left(\frac{m\pi}{2\rho}\right)\right) \tag{7.3}$$

In particular, the compression modulus for a square isolator is $E_c = 6.748GS^2$.

Vertical stiffness of these isolators supported on the building are furnished in Table 7.2.

Table 7.2 Vertical stiffness of U-FREIs

Description	250x250x100	310x310x100
Compression modulus, E_c, (MPa)	948.94	1459.09
Vertical stiffness, K_V, (kN/m)	658984.4	1557979.9

Thus, with the values of stiffness as detailed in Table 7.2, the designed isolators are observed to have experienced insignificant vertical deformation under the maximum possible vertical load as computed considering all possible load combinations as per IS: 1893 (Part 1), 2002.

7.3.4. Verification of 3D nonlinear model

In order to assess the appropriateness of the adopted 3D FE model of the masonry building in SAP2000 nonlinear, results of pushover analysis for the FB building obtained from SAP2000 and ABAQUS are compared. The response of a masonry building using 8-noded solid elements and concrete damage-plasticity (CDP) model for brick masonry in ABAQUS was compared with experimental results by Choudhury, *et al.* [2015] and the simulated results were observed to be in very good agreement with experimental results. In this study, pushover analysis of the sample FB masonry building is also conducted by ABAQUS using 8-noded solid elements and CDP material model for masonry (Fig. 7.7). Pushover curves of the FB building obtained from 3D nonlinear models using SAP2000 and ABAQUS are compared in Fig. 7.8.

A comparison of pushover curves as obtained from SAP2000 and ABAQUS shows that the discrepancy is insignificant. All the subsequent analysis of the building is carried out using nonlinear layered shell elements in SAP2000 nonlinear as it is observed to be computationally less demanding.

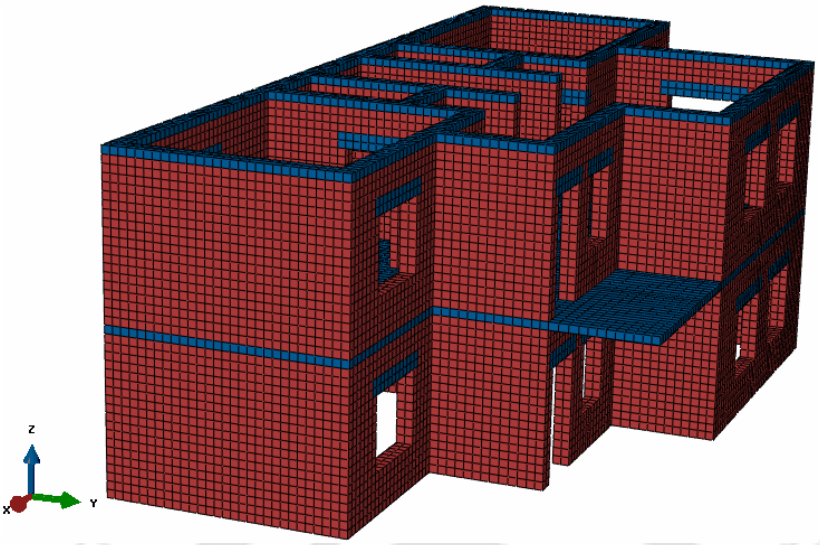

Fig. 7.7 FE model of FB masonry building in ABAQUS

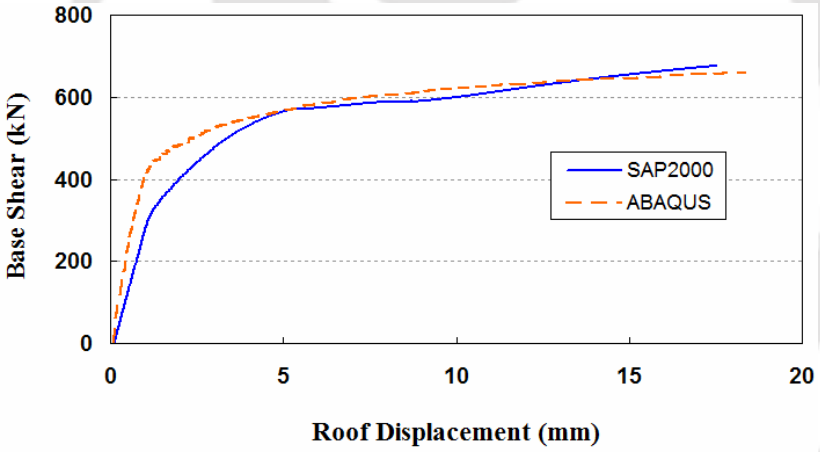

Fig. 7.8 Pushover curves of FB building

7.4. Identification of damage states

In order to assess the vulnerability of a masonry building, it is necessary to define damage states (DS) of the building under seismic loads. The damage states may be directly obtained from pushover analysis. Some approaches in literature proposed limits of damage classifications for masonry buildings, but the deformation thresholds may be the best indicators of identifying the damage state limits for the buildings. Calvi [1999]

introduced the inter-storey drifts to define different damage states for masonry building. Lagomarsino and Giovinazzi [2006] proposed different thresholds of the spectral displacement to obtain the damage states of a structure. In this study, thresholds based on the inter-storey drifts from Calvi [1999] are employed to define damage states for the masonry building.

Calvi [1999] proposed four damage states for masonry structures, such as no damage and slight damage, moderate damage, extensive damage and collapse damage, in which inter-storey drifts were used to describe the damage state limits. Different damage states for FB masonry building as obtained from Calvi [1999] can be observed in Fig. 7.9. Following the outlined criteria as shown in Table 7.3, the thresholds of the inter-storey drifts are obtained for damage state limits of FB masonry building. As observed by Calvi [1999], masonry buildings do not show a clear elastic limit, since cracking starts at early stages and tends to extend progressively. Thus, it is reasonable to condense the two first damage states (no damage and slight damage) into a single one.

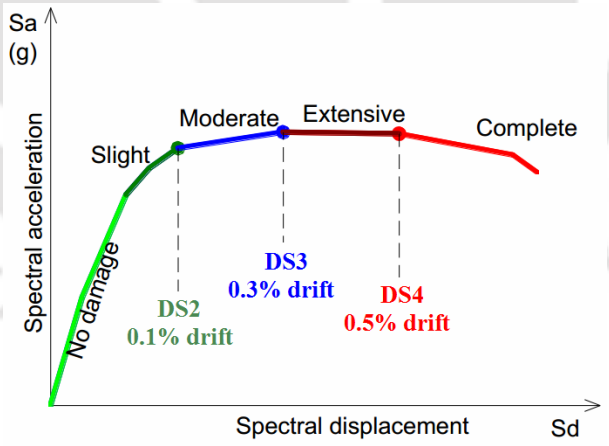

Fig. 7.9 Performance levels on pushover curve (Calvi, 1999)

For BI masonry building, the damage state limits are also evaluated similar to the FB building using inter-storey drifts given in Table 7.3. Further, a damage state DS5 is added to include any possible damage/instability of U-FREIs system. The damage state

DS5 is defined in terms of magnitude of displacement of U-FREI corresponding to the instant of commencement of hardening behaviour, which is u_h = 155 mm (i.e. 1.70t_r). The isolators are observed to have reduction in stiffness till 1.70t_r with increasing displacement and subsequently exhibit increase in stiffness. Further, ASCE/SEI 7-10 also specifies the performance evaluation of isolators up to a maximum of 1.50t_r. Keeping all these in view, the limiting displacement value for DS5 is taken as 1.70t_r without considering hardening behaviour of the isolator.

Table 7.3 Damage state thresholds and criteria for FB masonry building provided by Calvi [1999]

Damage state	Performance criteria
DS1	- No damage and slight damage.
DS2 (*Moderate damage)*	- Structure can be utilized after the earthquake, without any need for significant strengthening and repair to structural elements. - The suggested inter-storey drift limit is 0.1%.
DS3 *(Extensive damage)*	- The building cannot be used after the earthquake without significant repair. Still, repair and strengthening is feasible. - The suggested inter-storey drift limit is 0.3%.
DS4 *(Collapse)*	- Repairing the building is neither possible nor economically reasonable. The structure will have to be demolished after the earthquake. Beyond this DS global collapse with danger for human life has to be expected. - The suggested inter-storey drift limit is 0.5%.

7.5. Vulnerability assessment of masonry building

In this section, the vulnerability assessment is done by carrying out nonlinear analysis using pushover method. Analytical fragility curves for different damage states of both FB and BI masonry buildings are developed. Reduction in seismic vulnerability of the

BI building is assessed by comparing analytical fragility curves corresponding to different damage states of these buildings.

7.5.1. Pushover analysis

Pushover curve corresponds to the first mode of vibration of the masonry building, based on the assumption that the fundamental mode of vibration contains the predominant response of the building. In the case of the analyzed building, a force distribution is established corresponding to the first mode shape oriented along the weaker axis, i.e. *Y*-axis. Thus, in all analyses presented in this paper, only the *Y*-direction of seismic loading is considered. Static pushover curve of the building describes the relationship between base shear and roof displacement.

Capacity evaluation of the masonry building is performed considering damage state limits suggested by Calvi [1999]. Pushover analysis data and criteria as presented in Table 7.3 are used to determine inter-storey drifts of the building in *Y*-direction. According to geometrical dimensions of the actual building, the height of each floor is 3.0 m, and the inter-storey drifts corresponding to different damage states are obtained from Table 7.3. It may be noted that the horizontal displacement limit of the damage of U-FREIs in BI building (DS5) is 155 mm. Identification of damage states and its representation on pushover curves for both FB and BI buildings are shown in Figs. 7.10 & 7.11.

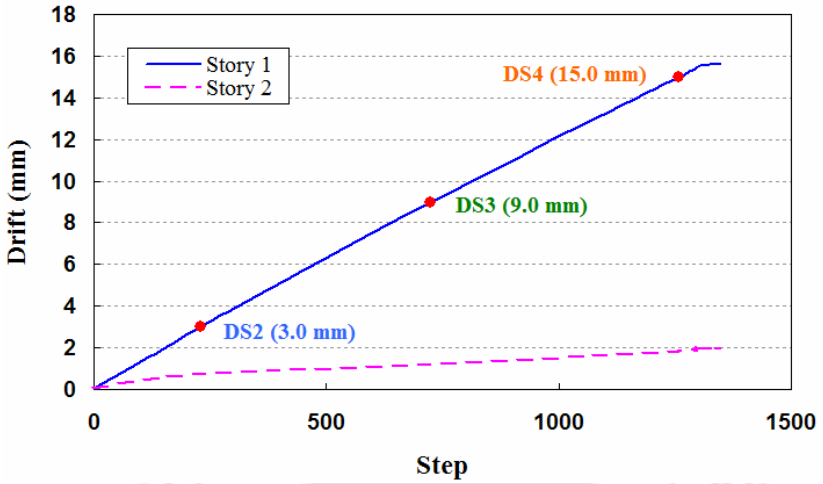

(a) Inter-storey drifts

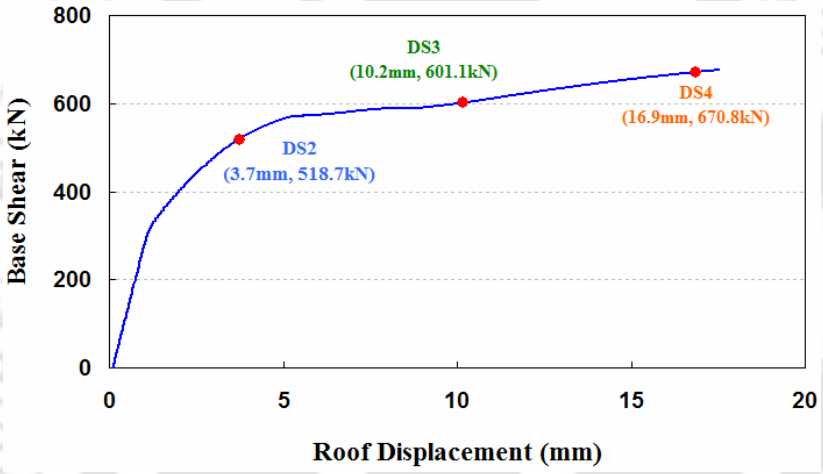

(b) Pushover curve

Fig. 7.10 Inter-storey drifts and pushover curve in *Y*-direction of FB building

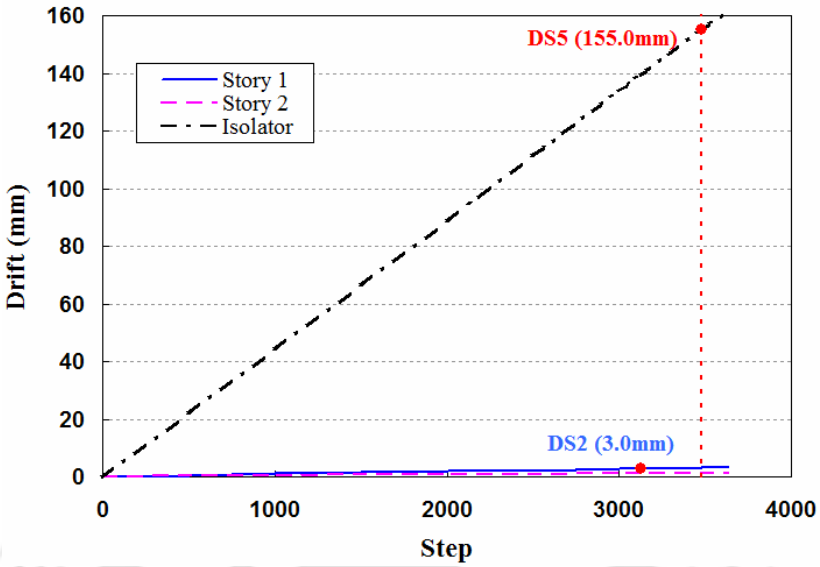

(a) Inter-storey drifts

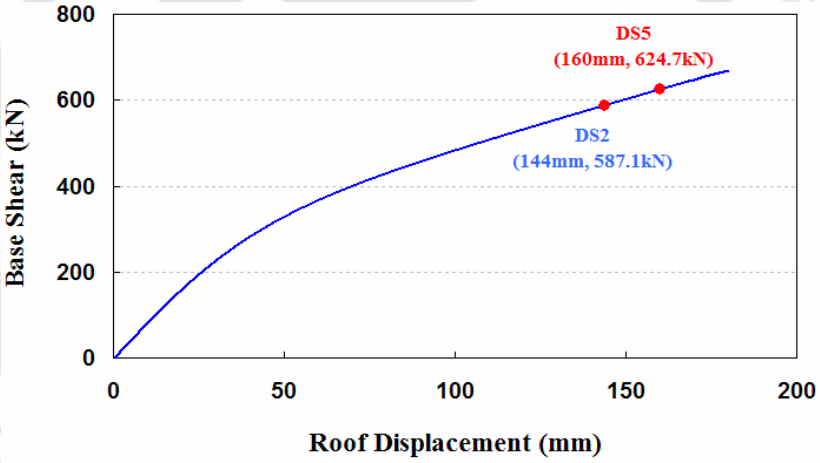

(b) Pushover curve

Fig. 7.11 Inter-storey drifts and pushover curve in *Y*-direction of BI building

Comparison of pushover curves of FB building and BI building is shown in Fig. 7.12. In this figure, the base shear force has been plotted with respect to the relative roof displacement of the BI building. The effect of introduction of base isolation system may be observed from Figs. 7.10 & 7.11, where the absolute displacement of BI building is far larger than that of FB building. This difference is due to low horizontal stiffness of isolation system. On comparison of the relative displacement of the BI building with the

absolute displacement of the FB building as shown in Fig. 7.12, it can be observed that the pushover curves of the structure have similar shapes. Further, at any particular damage state (e.g. DS2) having same value of inter-storey drift, base shear of BI building is observed to be higher than that of FB building. Thus, higher magnitude of imposed force is necessary in BI building to cause a specific level of inter-storey drift than that in the same building with bases fixed.

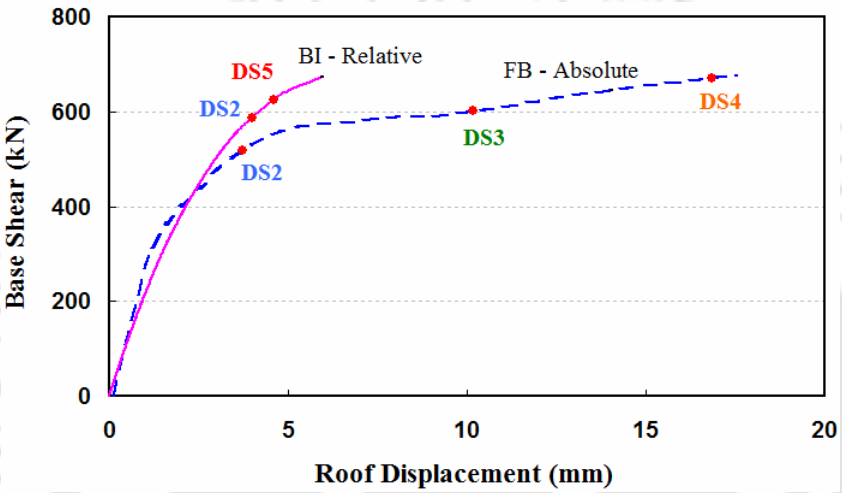

Fig. 7.12 Comparison of pushover curves of FB building for absolute displacement and BI building for relative displacement with different damage states

SAP2000 nonlinear automatically converts pushover curve to spectral acceleration-spectral displacement curve. Thus, spectral acceleration-spectral displacement curves for both FB and BI buildings with different damage states are shown in Fig. 7.13.

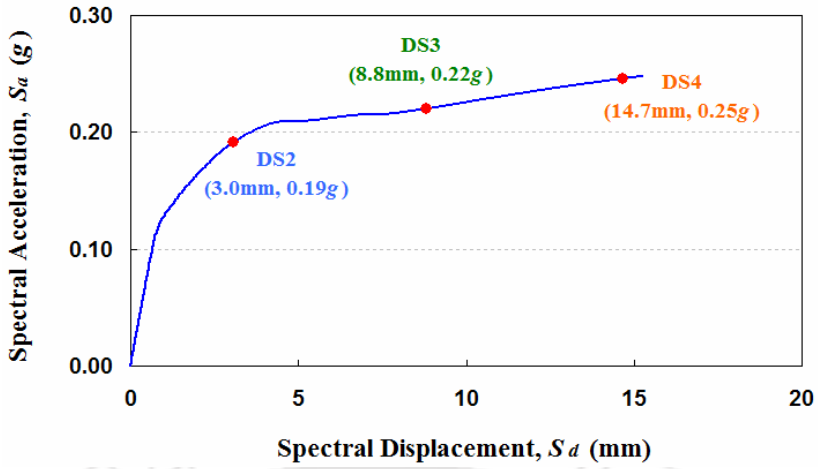

(a) FB building

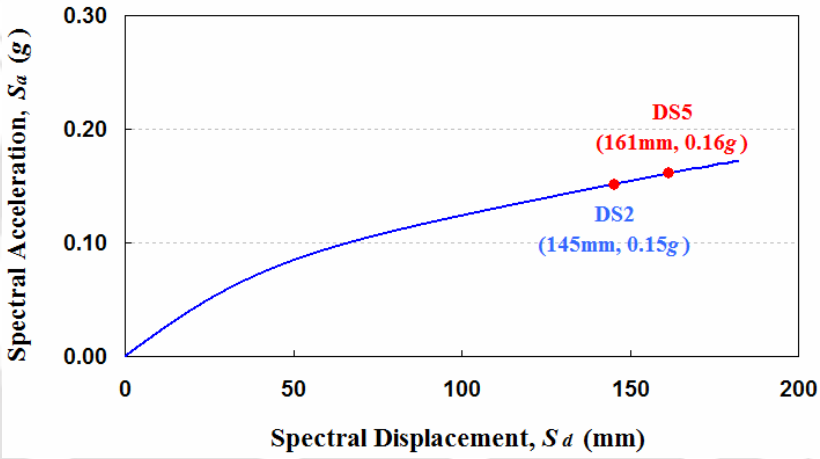

(b) BI building

Fig. 7.13 Acceleration-displacement response spectra of the building

It can be seen from Figs. 7.10-7.13 that the damage phases of FB masonry building occur sequentially from no damage to complete collapse. Further, all the damages are mainly concentrated in ground of FB building, while storey 2 shows damage close to DS2 only. However, unlike the FB building, the collapse damage of BI building is occurred due to the collapse of U-FREIs, while the superstructure is observed to experience only moderate damage, DS2. Further, comparison of acceleration-displacement response spectra of both FB and BI buildings shows that spectral

displacement of BI building at a damage state is far larger than that of FB building. It means that the BI building is capable of resisting a larger seismic intensity induced displacement as compared to FB building, while maintaining much lower damage level.

7.5.2. Analytical fragility assessment

Fragility curves are usually represented in the form of lognormal cumulative distribution of the probability of reaching or exceeding a given damage state for a given intensity measure. According to HAZUS (FEMA, 2003), the conditional probability of being in, or exceeding, a particular damage state, DS, given the spectral displacement, S_d, is defined by:

$$P[DS|S_d] = \Phi\left(\frac{1}{\beta_{DS}}\ln\left(\frac{S_d}{S_{d,DS}}\right)\right) \tag{7.4}$$

where, $\Phi[.]$ is the standard normal cumulative distribution function; $S_{d,DS}$ is the median value of spectral displacement at which the building reaches the threshold of a damage state, DS; β_{DS} is the standard deviation of the natural logarithm of spectral displacement for damage state, DS.

In order to calculate the probabilities starting from the distribution function $\Phi[.]$, it is necessary to define $S_{d,DS}$ and β_{DS} for each damage state. The values of $S_{d,DS}$ are obtained from Fig. 7.13. The parameter β_{DS} is obtained from HAZUS (FEMA, 2003) for low-rise masonry building, and here the β_{DS} is taken as 0.65 for all damage states.

Fragility curves of different damage states for both FB and BI buildings are shown in Fig. 7.14. Comparison of these fragility curves for both FB and BI buildings shows significant reduction in seismic vulnerability of BI building. Specifically, the values of probability of exceeding a given damage state (e.g. collapse state) of BI building is very much lesser than that of FB building. Thus, the BI building using U-FREIs as isolators

is much safer than the FB building under same intensity of earthquakes induced vibration.

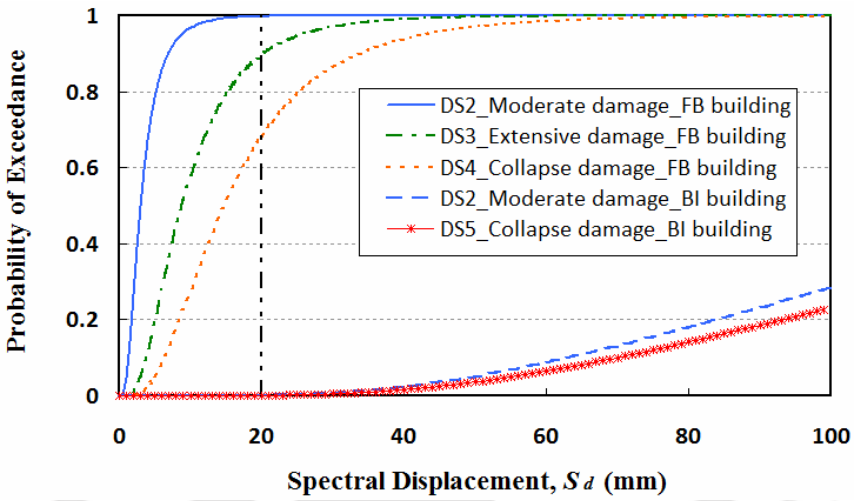

Fig. 7.14 Comparison of fragility curves of FB and BI building

Reduction in the probability of exceeding a given damage state of BI building as compared to that of FB building is clearly evident from comparison of the damage probabilities at any given spectral displacement demand (S_d). Damage probability matrices at spectral displacement S_d = 20 mm of both FB and BI buildings are shown in Fig. 7.15. As seen from this figure, while the damage probabilities in complete collapse states is very high followed by extensive and moderate damages of FB building, the damage probabilities of BI building are predominantly at no damage and slight damage states. Thus, seismic vulnerability of BI building is significantly reduced as compared to FB building.

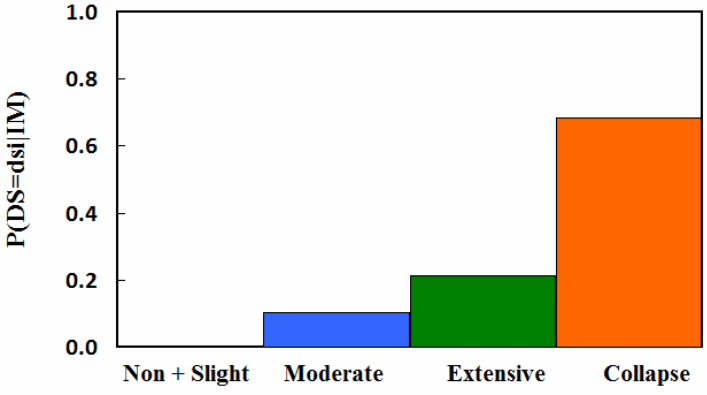

(a) FB building

(b) BI building

Fig. 7.15 Damage probability matrices for FB and BI buildings at S_d = 20 (mm)

7.6. Dynamic response of masonry building under ground motion

In order to evaluate the effectiveness of base isolation system, the dynamic responses of both FB and BI buildings under the action of various recorded real earthquakes are investigated. In the present study, two ground motions from as El-Centro (N-S Comp), US, 1940 and Koyna (Longitudinal Comp), India, 1967, as shown in Fig. 7.16, are selected.

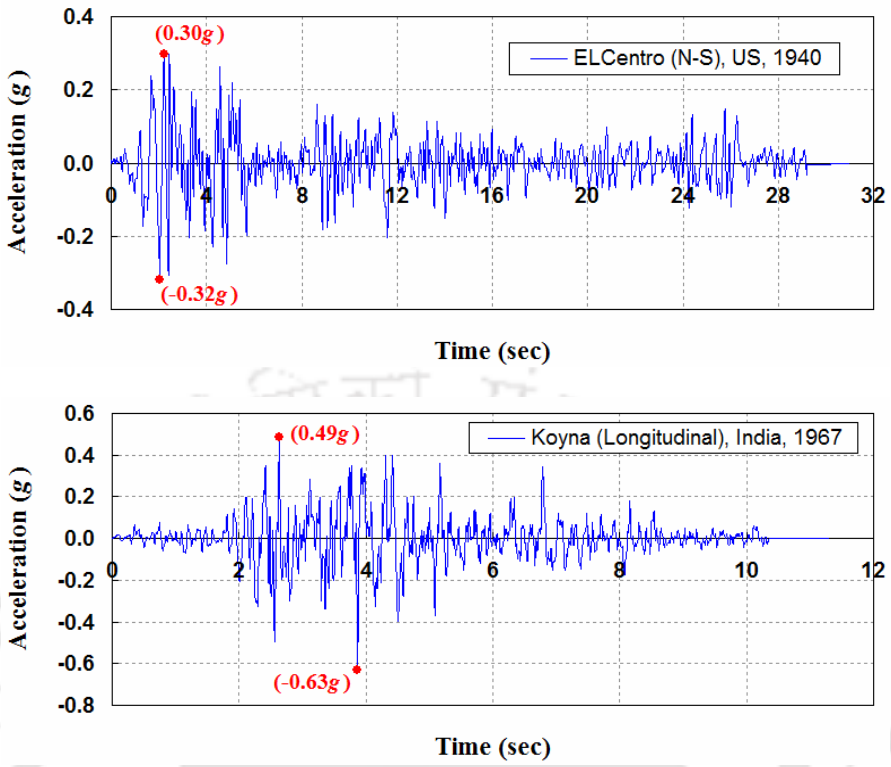

Fig. 7.16 Real time-history record of selected earthquake motions

From results of FE analysis, it is found that the seismic responses (acceleration, inter-storey drift) of BI building are significantly lower than those of FB building. Peak absolute values of floor accelerations and inter-storey drifts of both buildings under various earthquakes are presented in Table 7.4.

Table 7.4 Peak values of floor accelerations and inter-storey drifts under various earthquakes

Parameter	FB building		BI building	
	El-Centro	Koyna	El-Centro	Koyna
Peak acceleration at 1st floor level (m/s^2)	0.65*g*	1.34*g*	0.09*g*	0.08*g*
Peak acceleration at roof level (m/s^2)	1.05*g*	1.57*g*	0.10*g*	0.09*g*
Peak drift at 1st storey (mm)	5.0	8.6	0.7	0.7
Peak drift at 2nd storey (mm)	3.0	4.8	0.4	0.4

It may be seen from Table 7.4 that significant reduction in magnitude of peak floor accelerations of BI building has taken place as compared to FB building for the sample excitations. Specifically, reduction of peak floor acceleration between FB building and BI building under El-Centro earthquake is found from 0.65*g* to 0.09*g* at 1st floor level and 1.05*g* to 0.10*g* at roof level. Further, the magnitudes of peak acceleration at different floor levels of BI building are almost same under each excitation, which indicates the absence of any noticeable acceleration amplification along the height of the BI building model. Unlike the BI building, the magnitude of peak acceleration of FB building at roof level is significantly higher than that at the 1st floor level as expected. Similar to the acceleration, magnitudes of peak inter-storey drifts of BI building are significantly lesser than that of FB building, thus clearly indicating the lesser possibility of any damage in the superstructure of the BI building. The detailed time history of floor acceleration and the inter-storey drift of both FB and BI buildings under each earthquake excitations are shown in Figs. 7.17 & 7.18.

Horizontal displacement responses of U-FREIs of the base isolation system under different earthquakes are shown in Fig. 7.19. It can be seen from the figure that the peak values of horizontal displacement of U-FREIs under the action of El-Centro and Koyna accelerograms are found to be 66 and 58 mm respectively. As mentioned earlier, the designed U-FREIs are able to maintain stability up to maximum horizontal displacement of 155 mm, and hence the adopted base isolation system is capable of ensuring overall safety and stability of the structure under the considered earthquakes induced vibration.

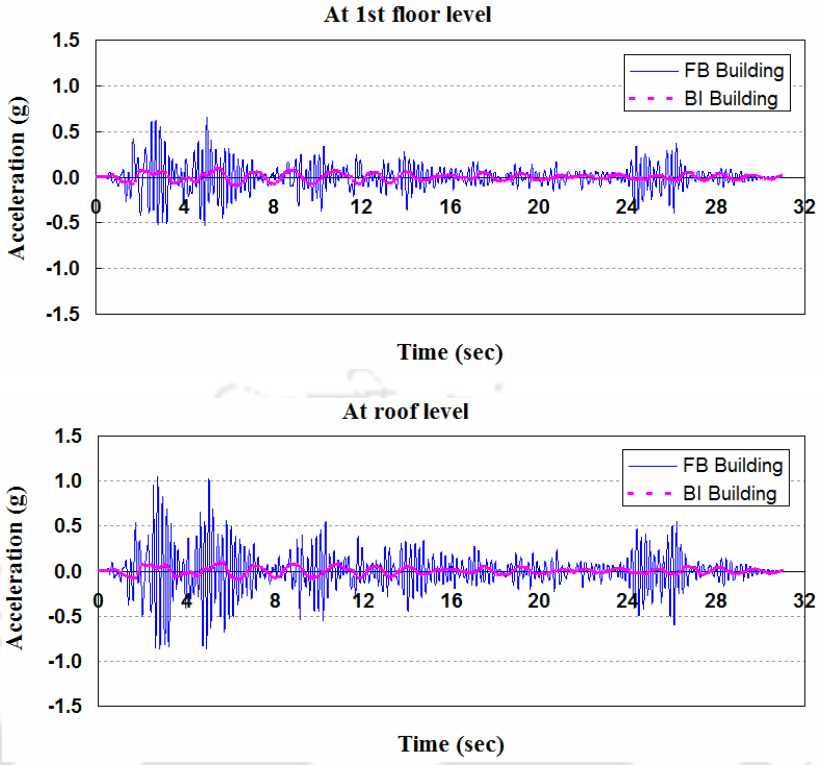

(a) El-Centro, US, 1940

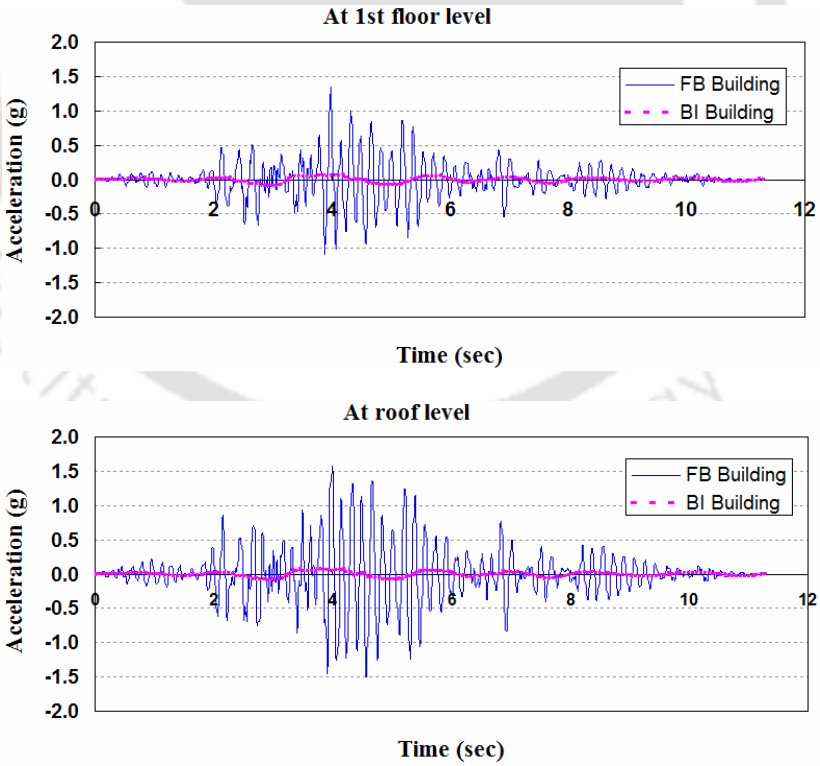

(b) Koyna, India, 1967

Fig. 7.17 Floor acceleration responses of the building under different earthquakes

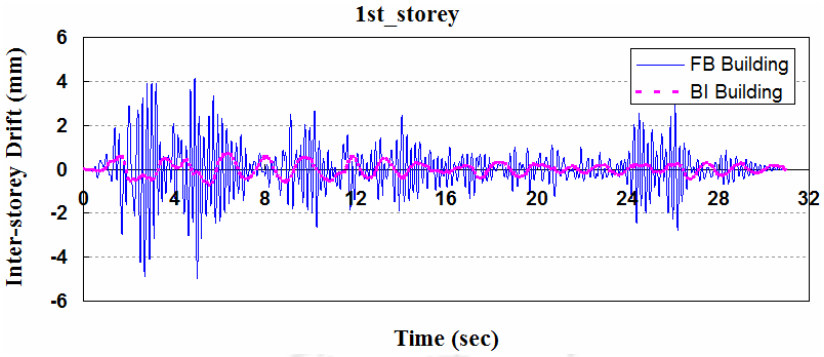

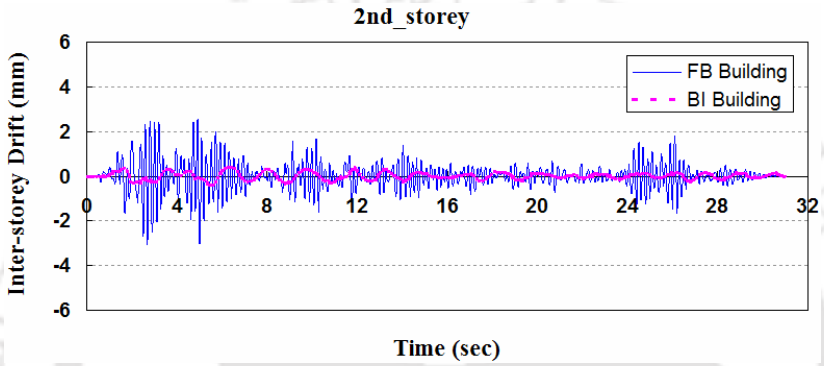

(a) El-Centro, US, 1940

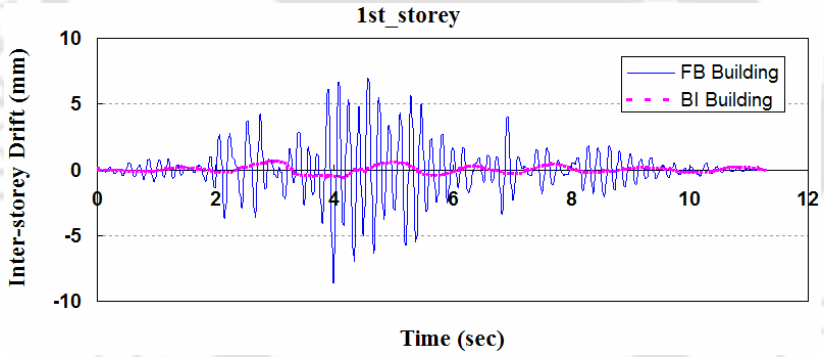

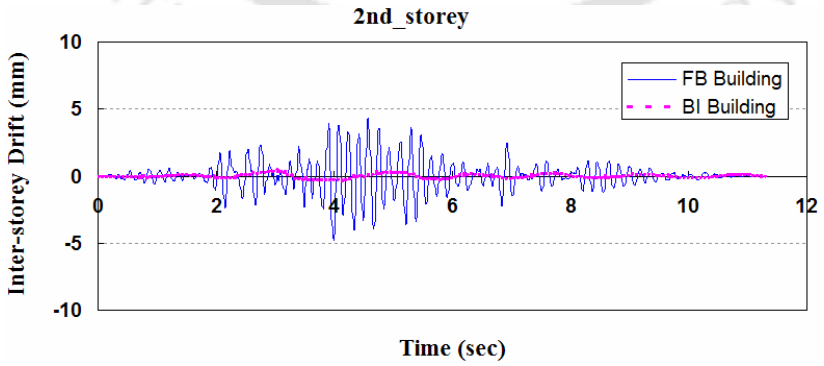

(b) Koyna, India, 1967

Fig. 7.18 Time history of inter-storey drift of the building under various earthquakes

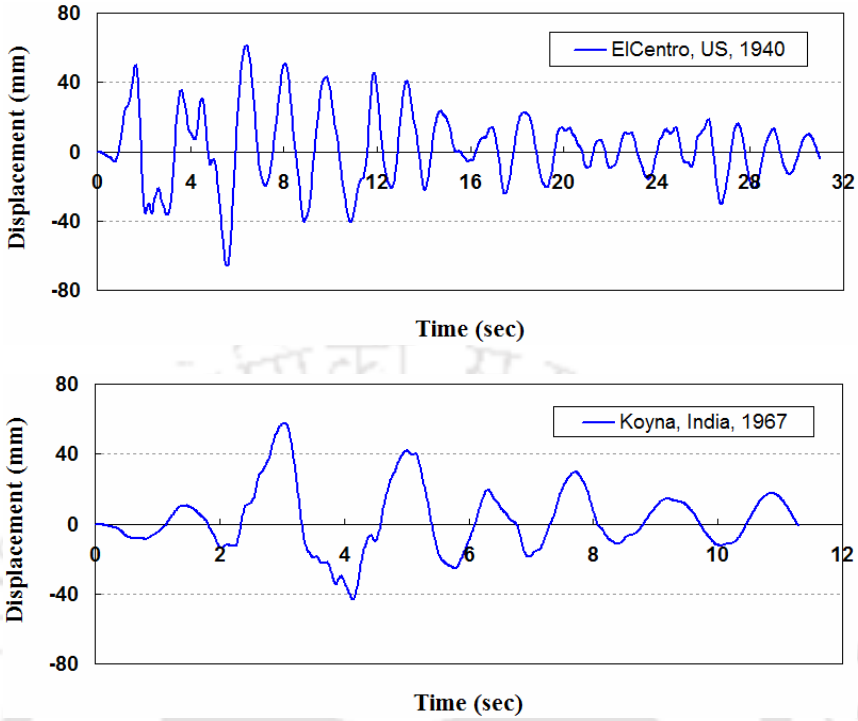

Fig. 7.19 Horizontal displacement responses of U-FREIs under different earthquakes

7.7. Concluding Remarks

This chapter establishes effectiveness of U-FREIs in controlling seismic response of low-rise masonry building under seismic excitation. A two-storey masonry building supported on fourteen U-FREIs located at Tawang, representative of a common building typology in many parts of north-eastern zone of India is selected to evaluate the seismic vulnerability under ground motions. 3D nonlinear models are simulated for both FB and BI buildings. Significant reduction in seismic vulnerability of BI building as compared to that of FB building is observed from comparison of the analytical fragility curves. Further, comparison of floor acceleration and inter-storey drift responses of both FB and BI buildings under various ground motions are also investigated. The concluding remarks are as follows:

- Fragility curves corresponding to different damage states clearly indicate a significant reduction in seismic vulnerability of BI building supported on U-FREIs as compared to that of FB building.
- Floor acceleration and inter-storey drift responses of BI building under excitations from earthquakes are significantly lesser than those of FB building.
- Effectiveness of U-FREIs in base isolation system increases with the increase in horizontal displacement.
- U-FREIs maintain a stable rollover configuration within the estimated displacement limit.
- Finally, U-FREI is found to be very effective in reduction of seismic vulnerability of low-rise masonry buildings. Introduction of U-FREIs at the interface of substructure and superstructure of a masonry building would be simple and hassle free because of its light weight and un-bonded boundary condition. This will enable implementation of this technology in the less developed countries witnessing high seismic activity.

Chapter 8

Step-by-step Design Procedure for U-FREIs

8.1. Introduction

The design of new seismically isolated buildings in different parts of the world is mostly carried out as per provision of either of the two codes: American Society of Civil Engineers 2013 (ASCE/SEI 7-10) and Uniform Building Code 1997 (UBC-97). The provisions in these codes related to the design requirements for base-isolated buildings are similar. However, UBC-97 is a bit more complicated and conservative as far as seismic isolation design is concerned as documented by Naeim and Kelly [1999]. Thus, this chapter limits the design requirements for base-isolated buildings as per provisions of ASCE/SEI 7-10.

Primarily intended to be used in the design of new buildings, the ASCE/SEI 7-10 does not really cover the retrofit of existing buildings using isolation, although most retrofit projects do follow either the ASCE or UBC regulations closely. ASCE/SEI 7-10 regulations are written in such a way that these provisions are not specific to any particular isolation systems. These regulations require that any isolation system should be stable for the imposed displacement and gravity load demand.

The underlying philosophy is that an isolated building designed using ASCE/SEI 7-10 regulations will be expected to outperform fixed-base construction under the action of moderate to large earthquakes. It is not the intent of the code to reduce the construction cost but to minimize damage in isolated structures and their contents by taking advantage of the fact that seismic isolation permits an elastic response in the structures and low floor accelerations for even large earthquake input.

U-FREI is relatively new seismic base isolator and the design procedure for this type of un-bonded isolator is not found in literature. Naeim and Kelly [1999] presented the basis for design of isolation system like high-damping rubber bearings (HDRB), natural rubber bearings (NRB), lead rubber bearings (LRB), and friction pendulum bearings (FPB). However, no documents are currently available giving detailed step-by-step design procedure for U-FREIs.

In this chapter, step-by-step design procedure of U-FREIs is introduced following the design provisions of ASCE/SEI 7-10. Detailed design calculations are also shown for the prototype isolators considered in the present research. The primary purpose of presenting the step-by-step design procedure is to assist design engineer with a readily available document, which will be useful in arriving at the preliminary sizes of U-FREIs to be adopted in a base isolated building project.

8.2. Mechanical Properties of U-FREIs

8.2.1. Shape Factor

One of the most important parameters in design of laminated elastomeric isolator is shape factor, *S*, defined as the ratio of the loaded area to load free area of a rubber layer. For a rectangular isolator with the width, *2b*, and length, *l*, in plan dimensions and a single rubber layer thickness of t_e, the shape factor is computed by

$$S = \frac{bl}{(l+2b)t_e} \tag{8.1}$$

For a square isolator with the width of *a* and a single rubber layer thickness of t_e:

$$S = \frac{a}{4t_e} \tag{8.2}$$

Generally, for better seismic performance, the prototype isolators should have the value of shape factor more than 10 (Naeim and Kelly, 2009).

8.2.2. Horizontal Stiffness

- The horizontal stiffness of a conventional bonded SREI is given by

$$K_H = \frac{GA}{t_r} \tag{8.3}$$

- As demonstrated in Chapter 5, the horizontal stiffness of a B-FREI is calculated as

$$K_H^b = \frac{G_{eff} A}{t_r} \tag{8.4}$$

For a square isolator with the width of a, the effective shear modulus G_{eff} is given as

$$G_{eff} = G\left[1-\left(\frac{p_z}{p_{crit,0}\left(1-\left(\frac{u}{a}\right)^2\right)}\right)^2\right]\left(1-\frac{u}{a}\right) \tag{8.5}$$

$p_{crit,0}$ is the critical stress state according to Kelly [2003] and is given by

$$p_{crit,0} = \frac{P_{crit}}{a^2} \text{ with } P_{crit} = \frac{\sqrt{2}\pi GASr}{t_r} \text{ and } r = \frac{a}{2\sqrt{3}} \tag{8.6}$$

u is the horizontal displacement and r is the radius of gyration.

- The horizontal stiffness of an U-FREI is computed by

$$K_H^{ub} = \frac{G_{eff} A_{eff}}{t_r} \text{ or } K_H^{ub} = \left(\frac{A_{eff}}{A}\right) K_H^b \tag{8.7}$$

where, A_{eff} is the effective plan area that in contact with the support surfaces of the U-FREI at the horizontal displacement, u.

According to Nezhad [2014], the effective plan area, A_{eff}, of a square isolator is determined by two approximation methods. In the method 1 the contribution of 25% of the rollover region, in addition to the central region of the isolator is taken into account in calculating the effective plan area as follows

$$A_{eff} = a\left(a - \frac{3}{4}u\right) \tag{8.8}$$

In the second method, the effective plan area is calculated as

$$A_{eff} = a(a-d) \tag{8.9}$$

where, d is the projected length of the curved part of the rollover region along the horizontal plane as shown in Fig. 5.1 Chapter 5, and is given as

$$d = \frac{25}{16}\alpha h \tag{8.10}$$

where, h is the total height of the isolator, α is a geometrical parameter which relates d and curved length, s, at a given horizontal displacement, u. The relation between u, s and α as proposed by Nezhad [2014] is expressed as

$$u = s = \frac{25}{64}h\left[2\alpha\sqrt{1+4\alpha^2} + \ln\left(2\alpha + \sqrt{1+4\alpha^2}\right)\right] \tag{8.11}$$

Thus, for a known value of u and h, α is found from Eq. (8.11), which is used for the evaluation of A_{eff} using Eq. (8.9).

8.2.3. Vertical stiffness

The vertical stiffness of a laminated elastomeric isolator is given by

$$K_V = \frac{E_c A}{t_r} \tag{8.12}$$

where E_c is the instantaneous compression modulus of the rubber-steel composite under the specified level of vertical load.

According to Kelly and Konstantinidis [2011], for a rectangular isolator with the width and length of $2b$ and l respectively, the compression modulus can be expressed in terms of the shape factor, S, and the aspect ratio of the pad, $\rho = {2b}/{l}$, as

$$E_c = \frac{384}{\pi^4}GS^2(1+\rho)^2\sum_{m=1,3,5...}^{\infty}\frac{1}{m^4}\left(1-\frac{2\rho}{m\pi}\tanh\left(\frac{m\pi}{2\rho}\right)\right) \tag{8.13}$$

From Eq. (8.13), for a square isolator $E_c = 6.748GS^2$, while for an infinite strip $E_c = 4GS^2$.

8.3. Step-by-Step Procedure for the Design of U-FREIs as per ASCE/SEI 7-10

Step 1: Evaluate the mapped spectral response acceleration parameter at a period of 1 second, S_1 ($S_1 \leq 0.60$g).

Step 2: Select site soil profile category. Determine site coefficient F_v from Table 11.4-2.

Step 3: Determine seismic coefficients S_{M1} and S_{D1}:

$$S_{M1} = F_v S_1 \tag{8.14}$$

$$S_{D1} = \frac{2}{3} S_{M1} \tag{8.15}$$

Step 4: Select type of isolation bearings and the damping coefficient B_D (Table 17.5-1).

Step 5: Select a desired period of the isolated structure at the design displacement, T_D.

$$T_D \geq 3T_{fixed-base}^{elastic} \tag{8.16}$$

Step 6: Estimate the effective horizontal stiffness of isolator K_{eff}^{h}:

$$T_D = 2\pi\sqrt{\frac{W}{K_{D,\min} g}} \quad \rightarrow \quad K_{eff}^{h} = \frac{W}{g}\left(\frac{2\pi}{T_D}\right)^2 \tag{8.17}$$

Step 7: Estimate the design horizontal displacement D_D:

$$D_D = \left(\frac{g}{4\pi^2}\right)\frac{S_{D1} T_D}{B_D} \tag{8.18}$$

Step 8: Estimate the total rubber thickness required t_r:

$$\gamma = \frac{D}{t_r} \quad \rightarrow \quad t_r = \frac{D}{\gamma} \tag{8.19}$$

Step 9: Determine the plan dimensions of U-FREI

$$A > \frac{K_{eff}^{h} t_r}{G} \tag{8.20}$$

Step 10: Find the number of rubber layers, n_e and total thickness of isolator, h for a chosen thickness of a rubber and fibre layer, t_e and t_f, respectively.

Consider shape factor, S, for prototype isolators as more than 10.

Step 11: Re-calculate the actual values of effective horizontal stiffness of the U-FREIs, K_{eff}^{ub}, using Eq. (8.7).

Step 12: Experimental tests for the evaluation of actual values of K_{eff}^{ub} and K_v of the U-FREI.

8.4. Design Example

Design of U-FREIs for seismic isolation of two-storey masonry building as shown in Fig. 7.1 is presented in this section. The total weight of the structure is estimated at 481.1 tons. U-FREIs of two sizes: namely B1 (9 numbers) and B2 (5 numbers) are used for seismic isolation of the building. Design vertical load on an isolator B1 and B2 is 350 kN and 550 kN respectively. The fixed-base period of the building is estimated to be about 0.28 seconds (from simulated model in SAP 2000). The project site is located at Tawang in northeastern part of India (zone V) on a site with soil Class B.

Step-by-step design procedure of U-FREIs are as follows:

Step 1. For seismic zone V of IS: 1893 (Part 1), 2002, spectral acceleration is 0.50g corresponding to time period of 1 second for medium soil.

Step 2. Soil type is class B.

The value of F_v = 1.0 is obtained from ASCE/SEI 7-10 Table 11.4-2 for site Class B and S_1 = 0.50.

Step 3. The spectral coefficients needed for calculation of minimum displacements are obtained from Eqs. (8.14) and (8.15):

$$S_{M1} = F_v S_1 = 1.0 \times 0.50g = 0.50g$$

$$S_{D1} = \frac{2}{3} S_{M1} = \frac{2}{3} \times 0.50g = 0.33g$$

Step 4. For preliminary design, 10% damping is assumed. From Table 17.5-1 of ASCE/SEI 7-10, $B_D = 1.20$.

Step 5. The effective period of the isolated structure at the design displacement:

$$T_D \geq 3T_{fixed\,base} = 3 \times 0.28 = 0.84(\sec)$$

The value of T_D is however chosen as 1.60 (sec) for preliminary design as per the guidelines of ASCE/SEI 7-10.

Step 6. The effective horizontal stiffness of isolator is obtained from Eq. (8.17) as

$$K_{eff}^{B1} = \frac{W_1}{g}\left(\frac{2\pi}{T_D}\right)^2 = \frac{350}{9.81} \times \left(\frac{2\pi}{1.60}\right)^2 = 550.2\,(kN/m)$$

$$K_{eff}^{B2} = \frac{W_2}{g}\left(\frac{2\pi}{T_D}\right)^2 = \frac{550}{9.81} \times \left(\frac{2\pi}{1.60}\right)^2 = 864.6\,(kN/m)$$

Step 7. The design displacement is obtained from Eq. (8.18) as

$$D_D = \left(\frac{g}{4\pi^2}\right)\frac{S_{D1}T_D}{B_D} = \left(\frac{9.81}{4\pi^2}\right)\frac{0.33 \times 1.60}{1.20} = 0.11(m)$$

Step 8: Considering $\gamma = 125\%$. From Eq. (8.19):

$$\gamma = \frac{D}{t_r} = 1.25 \rightarrow t_r = \frac{D}{\gamma} = \frac{0.11}{1.25} = 0.088\,(m) = 88\,(mm);$$

Step 9: Prototype elastomer with $G = 0.90$ MPa, Eq. (8.20) will provide

$$A_{eff\,1} > \frac{K_{eff}^{B1} t_r}{G} = \frac{550.2 \times 0.088}{0.9 \times 10^3} = 0.054\left(m^2\right) \rightarrow a_1 > \sqrt{A_{eff\,1}} = 0.232\,(m)$$

$$A_{eff\,2} > \frac{K_{eff}^{B2} t_r}{G} = \frac{864.6 \times 0.088}{0.9 \times 10^3} = 0.085\left(m^2\right) \rightarrow a_2 > \sqrt{A_{eff\,2}} = 0.292\,(m)$$

Actually, the horizontal stiffness of a U-FREI should be calculated using Eq. (8.7) to address the reduction in shear modulus with increasing displacement as well as the change in area of contact with support surfaces. Thus, values of the width of square U-FREIs are to be chosen higher than the values evaluated from Eq. (8.20).

Chosen a_1 = 0.25 (m) = 250 (mm) and a_2 = 0.31 (m) = 310 (mm).

Therefore, $A_1 = a_1^2 = 0.25^2 = 0.0625\left(m^2\right); A_2 = a_2^2 = 0.31^2 = 0.0961\left(m^2\right)$.

Step 10: Selection of other geometric details of isolators:

Consider a shape factor of S_1 = 12 for isolator B1 and S_2 = 15 for isolator B2.

From Eq. (8.2), the thickness of a individual elastomer layer, t_e, is calculated as

$$\begin{cases} t_e^{B1} = \dfrac{a_1}{4S_1} = \dfrac{250}{4\times 12} = 5.21(mm) \\ t_e^{B2} = \dfrac{a_2}{4S_2} = \dfrac{310}{4\times 15} = 5.17(mm) \end{cases}$$

Consider t_e = 5 (mm), number of elastomer layers, n_e = 88/5 = 17.6

Choose n_e = 18 for both isolators B1 and B2.

Thus, $t_r = n_e \times t_e = 18\times 5 = 90(mm)$;

Using t_f = 0.55 (mm) as thickness of a carbon fibre reinforcement layer, the total height of the isolator = 90 + 0.55 x (18 - 1) = 100 (mm).

Finally, sizes of isolators B1, B2 are 250 mm x 250 mm x 100 mm and 310mm x 310 mm x 100 mm respectively.

8.5. Conclusion

This chapter presents step-by-step procedure for the design of U-FREIs for seismic isolation of buildings. Detailed design calculations are also shown for the prototype isolators considered in the present research.

Chapter 9

Summary and Conclusions

9.1. Summary

The present work is an effort towards the development of prototype U-FREIs to be used for reducing seismic vulnerability of low-rise masonry building. The study is a combination of experimental, numerical and analytical exercises. The main components of this study are (i) development of light weight, less expensive prototype U-FREIs for seismic response control of low-rise stone masonry building in seismic zones, (ii) experimental investigations on prototype U-FREIs under simultaneous action of constant vertical load and cyclic horizontal displacement for the evaluation of their mechanical properties, (iii) FE analysis of both B-FREI and U-FREI for evaluation of their behaviour, stiffness, damping and stress-strain profile, (iv) validation of FE model of U-FREIs by comparing the results obtained from FE analysis with those from experiments, (v) evaluation of the effect of shear modulus, shape factor and loading direction on the horizontal behaviour of prototype U-FREIs, (vi) suggestion of an analytical method for predicting the horizontal stiffness of FREIs, (vii) numerical study for predicting stability of a prototype U-FREI, (viii) vulnerability assessment of a base-isolated masonry building supported on U-FREIs using analytical fragility curves. This is the first U-FREIs supported prototype low-rise masonry building constructed anywhere in the world and (ix) suggestion of a step-by-step procedure for design of prototype U-FREIs for seismic isolation of low-rise buildings.

In order to understand the horizontal behaviour of prototype U-FREIs and effect of shear modulus and different directions of horizontal loading on it, experimental investigations are carried out. Testing of isolators with different dimensions in plan and

different values of shear modulus is carried out under the simultaneous action of design vertical load and cyclic horizontal displacement. Horizontal load-displacement hysteresis loops are plotted to determine the effective horizontal stiffness and damping of the isolators. Since the angle of incidence of earthquake to a structure may be from any directions, experimental evaluation for the effect of different loading directions (0^o, 15^o, 30^o and 45^o) on horizontal response of prototype square U-FREI is also carried out.

Analysis of FREIs using numerical technique like FE method is carried out to encompass both bonded and un-bonded FREIs and for a displacement range much beyond the limitations encountered during experimental study. These force-displacement hysteresis loops of U-FREIs obtained from the FE analysis are compared with those obtained from testing to validate the FE model of U-FREIs. The deformed shapes of U-FREIs under different amplitudes of horizontal displacement are monitored and compared with those obtained from experimental investigation. Comparison of horizontal stiffness, damping, stress and strain at different levels of bonded and un-bonded FREIs are presented. Effect of shear modulus and shape factor on horizontal response of the isolator is evaluated. Influence of loading direction on horizontal load-displacement behaviour of square B-FREI and U-FREI is also studied.

An analytical method for the evaluation of secant horizontal stiffness of B-FREI and U-FREI is presented. The method incorporating the effect of both nonlinearity of shear modulus and effective shear area with increase in displacement is proposed as a basic analysis tool for predicting the secant horizontal stiffness of U-FREIs.

Stability analysis of a prototype U-FREI is also presented, where detailed results obtained from FE analysis are used. A prototype U-FREI is investigated under the action of varying vertical load and cyclic horizontal displacement to determine the

critical load carrying capacity. Effect of vertical load on the horizontal response of the U-FREI is also evaluated.

Seismic vulnerability of a two-storey stone masonry building supported on U-FREIs is evaluated by analytical fragility curves. Significant reduction in probability of exceedance of all the considered damage states of the base-isolated building is observed as compared to that of fixed-base building.

Finally, step-by-step design procedure of U-FREIs is introduced following the design provisions of ASCE/SEI 7-10. Detailed design calculations are also shown for the prototype isolators considered in the present research.

9.2. Major Findings

Major findings from the present study may be summarized as below:

1) Effective horizontal stiffness of U-FREI decreases and equivalent viscous damping increases with increase in horizontal displacement due to rollover deformation.
2) Good agreement is observed between the findings from experimental and FE analysis. FE analysis for FREI can be considered to be an effective tool for computation of response of U-FREI, particularly for very large applied displacement, which may be otherwise difficult in experimental study. FE analysis using the adopted FE model can also be regarded as very important for initial design as multiple possibilities can be reliably explored before actual manufacturing of isolators, followed by laboratory tests.
3) Horizontal stiffness of U-FREI is significantly lesser than that of B-FREI at higher displacement and hence possesses higher seismic isolation efficiency.

4) A comparison of stress pattern at large displacement between B-FREI and U-FREI shows a considerably lower compressive stress demand in elastomer layers as well as significantly lower peeling stress demand on the bond between elastomer and fibre reinforcement layers in U-FREI.

5) Decrease in horizontal stiffness of B-FREI with increasing horizontal displacement is due to decrease in effective shear modulus, while that of U-FREI is due to both decrease in effective shear modulus as well as the contact area of the isolator due to rollover deformation. An analytical approach is proposed as a basic tool for predicting the secant horizontal stiffness of both B-FREI and U-FREI. Horizontal stiffness evaluated by proposed analytical models are in good agreement with that obtained from numerical analysis and experiment.

6) Peak values of compressive stress in elastomer layers and tensile stress in fibre reinforcement layers of U-FREI with smaller shape factor are higher than those of U-FREI with larger shape factor, while the peak values of shear strain in elastomer layers of these U-FREIs are quite comparable at any given applied displacement.

7) Generally, as the loading direction changes from 0^o to 45^o, the effective horizontal stiffness of square U-FREI increases at any given displacement amplitude ($u < 1.70t_r$).

8) Effective horizontal stiffness of U-FREI starts to increase at large horizontal displacement in the range $1.70t_r$ to $2.00t_r$. Hardening behaviour in load-displacement relationship of square U-FREI becomes more pronounced when the loading direction changes from 0^o to 45^o.

9) Maximum design displacement should be assessed based on stiffness corresponding to applied horizontal load along the fibre direction, while the seismic efficacy should be assessed based on stiffness for load along 45^o to any of

the fibre directions. Structures supported on U-FREIs may consider them as limiting values for seismic applications.

10) Critical buckling load of a U-FREI as obtained by dynamic stability analysis corresponds to the point in which horizontal stiffness is reduced to zero. The critical buckling load of the isolator decreases with the increase in horizontal displacement amplitude.

11) Critical load carrying capacity of the prototype U-FREI as obtained from FE analysis is significantly higher than the design vertical load as per codal requirement.

12) Significant reduction in probability of exceedance of any damage states of base-isolated masonry building supported on prototype U-FREIs is observed as compared to that of fixed-base building.

13) Floor acceleration and inter-storey drift of base-isolated building under excitations from earthquakes are significantly lesser than those of fixed-base building.

14) U-FREIs can be a very popular choice for seismic isolation of low-rise building as they are light weight and less expensive.

9.3. Recommendations for Future Work

Areas in which this work can be extended through additional research include the following:

- To monitor the response of the base-isolated masonry building supported on U-FREIs located at Tawang, India under ground motion of actual earthquakes likely to occur in near future.
- Effect of near-field motion on response of U-FREIs can be evaluated.

- Experimental study on horizontal load-displacement behaviour of prototype U-FREIs under different values of vertical pressure and larger displacement amplitudes.
- To study the horizontal load-displacement behaviour of prototype U-FREIs under a range of vertical loads and rotational deformations.
- To study the horizontal load-displacement behaviour of a partially bonded FREI.

REFERENCES

Abo-El-Ezz A., Nollet M.J and Nastev M. (2013), "Seismic fragility assessment of low-rise stone masonry buildings", *Earthquake Engineering and Engineering Vibration*, Vol. 12(1), pp. 87-97, DOI: 10.1007/s11803-013-0154-4.

Akhaveissy A.H. and Milani G. (2013), "Pushover analysis of large scale un-reinforced masonry structures by means of a fully 2D non-linear model", *Construction and Building Materials*, Vol. 41, pp. 276-295.

Al-Anany Y.M. and Tait M.J. (2015), "A numerical study on the compressive and rotational behavior of fiber reinforced elastomeric isolators (FREI)", *Composite Structures*, Vol. 133, pp. 1249-1266.

ANSYS®, Release 14.0, Help System, Analysis Guide, ANSYS, Inc, USA.

Ashkezari G.D., Aghakouchak A.A. and Kokabi M. (2008), "Design, manufacturing and evaluation of the performance of steel like fiber reinforced elastomeric seismic isolators", *Journal of Material Processing Technology*, Vol. 197, pp. 140-150.

ASCE/SEI 7-10 (2013), "Minimum Design Load for Buildings and Other Structure", *American Society of Civil Engineers: Virginia, United States of America*.

ATC40 (1996), "Seismic evaluation and retrofit of concrete buildings", Vol. 1, Applied Technology Council (ATC).

Bakhshi A. and Karimi K. (2008), "Performance evaluation of masonry building using a probabilistic approach", *SCIENTIA INRANICA*, Vol. 15(3), pp. 295-307.

Barbat A.H., Pujades L.G. and Lantada N. (2008), "Seismic damage evaluation in urban areas using the capacity spectrum method: Application to Barcelona", *Soil Dynamics and Earthquake Engineering*, Vol. 28, pp. 851-865.

Bilgin H. and Korini O. (2012), "Seismic capacity evaluation of un-reinforced masonry residential buildings in Albania", *Natural Hazards and Earth System Sciences*, Vol. 12, pp. 3753-3764, DOI: 10.5194/nhess-12-3753-2012.

Buckle I., Nagarajaiah S. and Ferrell K. (2002), "Stability of Elastomeric Isolation Bearings: Experimental study", *Journal of Structural Engineering, ASCE*, Vol. 128(1), pp. 3-11.

Buckle I.G. and Kelly J.M. (1986), "Properties of Slender Elastomeric Isolation Bearings During Shake Table Studies of a Large-Scale Model Bridge Deck", *Joint Sealing and bearing systems for concrete structures, ACI*, Detroit, Mich., Vol. 1, pp. 247–269.

Buckle I.G. and Liu H. (1993), "Stability of elastomeric seismic isolation systems", *Proc. Sem. Seismic Isolation, Passive Energy Dissipation and Active Control, Applied Technology Council*, Report ATC17-1, pp. 293-305.

Buckle I.G. and Liu H. (1994), "Experimental Determination of Critical Loads of Elastomeric Isolators at High Shear Strain", *NCEER Bulletin*, Vol. 8(3), pp. 1-5.

Calvi G.M (1999), "A displacement-based approach for vulnerability evaluation of classes of buildings", *Journal of Earthquake Engineering*, Vol. 3(3), pp. 411-438, DOI: 10.1080/13632469909350353.

Chalhoub M.S. and Kelly J.M. (1991), "Analysis of Infinite-Strip-Shaped Base Isolator with Elastomer Bulk Compression", *Journal of Engineering Mechanics, ASCE*, Vol. 117(8), pp. 1791-1805.

Chang H. (1988), "Nonlinear Elastomer Analysis - Survey of Computer Codes and Case Study for Caliper Seal", *Computers & Structures*, Vol. 30(5), pp. 1165-1173.

Chopra A.K. (2007), "Dynamics of Structures: Theory and Applications to Earthquake Engineering" (Third Edition). *Prentice Hall: Upper Saddle River, New Jersey*.

Choudhury T, Milani G. and Kaushik H. B. (2015), "Comprehensive numerical approaches for the design and safety assessment of masonry buildings retrofitted with steel bands in developing countries: The case of India", *Construction and Building Materials*, Vol. 85, pp. 227-246.

Das A., Dutta A. and Deb S.K. (2014), "Performance of fiber-reinforced elastomeric base isolators under cyclic excitation", *Structural Control and Health Monitoring*, DOI: 10.1002/stc.1668.

Das A. (2015), "Seismic response control of low-rise buildings using fiber-reinforced elastomeric isolator", *PhD-Thesis*, IIT Guwahati.

Das A., Deb S.K. and Dutta A. (2016a), "Shake table testing of un-reinforced brick masonry building test model isolated by U-FREI", *Earthquake Engineering and Structural Dynamics*, Vol. 45, pp. 253-272, DOI: 10.1002/eqe.2626.

Das A., Deb S.K. and Dutta A. (2016b), "Comparison of numerical and experimental seismic responses of FREI supported on un-reinforced brick masonry model building", *Journal of Earthquake Engineering*, DOI: 10.1080/13632469.2016.1140098.

Datta T.K. (2003), "A state-of-the-art review on active control of structures", *ISET Journal of Earthquake Technology*, Vol. 40(1), pp. 1-17.

Dezfuli F.H. and Alam M.S. (2014), "Performance of carbon fiber-reinforced elastomeric isolators manufactured in a simplified process: experimental investigations", *Structural Control and Health Monitoring*, Vol. 21, pp. 1347-1359.

Dorfmann A. and Ogden R.W. (2004), "A constitutive model for the Mullins effect with permanent set in particle-reinforced rubber", *International Journal of Solids and Structures*, Vol. 41, pp.1855-1878.

EN 1337-3 (2005), "Structural bearings, Part 3: Elastomeric bearings", *European Committee for Standardization, CEN/TC250*, Brussels.

Engelen N.C.V., Osgooei P.M., Tait M.J. and Konstantinidis D. (2014), "Experimental and finite element study on the compression properties of Modified Rectangular Fiber-Reinforced Elastomeric Isolators (MR-FREIs)", *Engineering Structures*, Vol. 74, pp. 52-64.

Engelen N.C.V., Osgooei P.M., Tait M.J. and Konstantinidis D. (2015a), "Partially bonded fiber-reinforced elastomeric isolators (PB-FREIs)", *Structural Control and Health Monitoring*, Vol. 22, pp. 417-432, DOI:10.1002/stc.1682.

Engelen N.C.V., Tait M.J. and Konstantinidis D. (2015b), "Model of the shear behavior of unbonded fiber-reinforced elastomeric isolators", *Journal of Structural Engineering, ASCE*, Vol. 141(7): 04014169-1-11.

Engelen N.C.V., Konstantinidis D. and Tait M.J. (2016), "Structural and nonstructural performance of a seismically isolated building using stable unbonded fiber-reinforced elastomeric isolators", *Earthquake Engineering and Structural Dynamics*, Vol. 45, pp. 421-439, DOI: 10.1002/eqe.2665.

Gerhaher U (2010), "Faserverstärkte Elastomerlager - Konzeption und Bemessung", *PhD-Thesis*, BOKU University [in German].

Gerhaher U., Strauss A. and Bergmeister K. (2011), "Verbesserte Bemessungsrichtlinien für Bewehrte Elastomerlager", Bautechnik, Vol. 88(7), [in German].

Han X., Kelleher C.A., Warn G.P. and Wagener T. (2013), "Identification of the Controlling Mechanism for Predicting Critical Loads in Elastomeric Bearings", *Journal of Structural Engineering, ASCE*, Vol. 139(12), 04013016-1-12.

Haringx J.A. (1948), "One highly compressible helical springs and rubber rods and their application for vibration-free mountings. I.", *Philips Res. Rep.*, Vol. 3, pp. 401-449.

Haringx J.A. (1949a), "One highly compressible helical springs and rubber rods and their application for vibration-free mountings. II.", *Philips Res. Rep.*, Vol. 4, pp. 49-80.

Haringx J.A. (1949b), "One highly compressible helical springs and rubber rods and their application for vibration-free mountings. III.", *Philips Res. Rep.*, Vol. 4, pp. 206-220.

HAZUS-MH Document (2003), *Federal Emergency Management Agency (FEMA) Distribution Center*.

Herrmann L.R., Ramaswamy A. and Hamidi R. (1989), "Analytical Parameter Study for Class of Elastomeric Bearings", *Journal of Structural Engineering, ASCE*, Vol. 115(10), pp. 2415-2434.

Holzapfel G.A. (1996), "On Large Strain Visco-elasticity: Continuum Formulation and Finite Element applications to Elastomeric Structures", *International Journal for Numerical methods in Engineering*, Vol. 39(22), pp. 3903-3926.

Hwang H., Jernigan J.B. and Lin Y.W. (2000), "Evaluation of seismic damage to Memphis bridges and highway systems", *Journal of Bridge Engineering, ASCE*, Vol. 5(4), pp. 322-330.

Ibrahim R.A. (2008), "Review Recent advances in nonlinear passive vibration isolators", *Journal of Sound and Vibration*, Vol. 314, pp. 371-452.

Iizuka M. (2000), "A marcoscopic model for predicting large-deformation behaviors of laminated rubber bearings", *Engineering Structures*, Vol. 22(4), pp. 323-334.

Imbimbo M. and Kelly J.M. (1998), "Influence of Material Stiffening on Stability of Elastomeric Bearings at large Displacements", *Journal of Engineering Mechanics, ASCE*, Vol. 124(9), pp. 1045-1049.

IS: 1893 Part 1 (2002), "Criteria for Earthquake Resistant Design of Structures", *Bureau of Indian Standard: New Delhi*.

Jara J.M., Madrigal E., Jara M. and Olmos B.A. (2013), "Seismic source effects on the vulnerability of an irregular isolated bridge", *Engineering Structures*, Vol. 56, pp. 105-115.

Jerrams S., Sanders K. and Goo K.B. (2001), "Realistic Modelling of Earthquake-Isolation Bearings", *Journal of Material Processing Technology*, Vol. 118, pp. 158-164.

Kang B.S., Kang G.J. and Moon B.Y. (2003), "Hole and Lead Plug Effect on Fiber Reinforcement Elastomeric Isolator for Seismic Isolation", *Journal of Material Processing Technology*, Vol. 140, pp. 592-597.

Karim K.R. and Yamazaki F. (2001), "Effect of earthquake ground motions on fragility curves of highway bridge piers based on numerical simulation", *Earthquake Engineering and Structural Dynamics*, Vol. 30, pp. 1839-1856.

Kaushik H.B., Rai D.C. and Jain S.K. (2007), "Stress-Strain characteristics of clay brick masonry under uniaxial compression", *Journal of Materials in Civil Engineering, ASCE*, Vol. 19(9), pp. 728-739.

Kelly J.M. (1986), "A Seismic Base Isolation: Review and Bibliography", Computational Mechanics Publications, *Soil Dynamics and earthquake Engineering*, Vol. 5(3), pp. 202-216.

Kelly J.M. (1999), "Analysis of Fiber-Reinforced Elastomeric Isolators", *Earthquake Engineering Research Center, University of California, Berkeley, USA, JSEE*, Vol. 2(1), pp. 19-34.

Kelly J.M. and Takhirov S.M. (2001), "Analytical and Experimental Study of Fiber-Reinforced Elastomeric Isolator", *PEER Report*, 2001/11, Pacific Earthquake Engineering Research Center, University of California, Berkeley, USA.

Kelly J.M. and Takhirov S.M. (2002), "Analytical and Experimental Study of Fiber-Reinforced Strip Isolators", *PEER Report*, 2002/11, Pacific Earthquake Engineering Research Center, University of California, Berkeley, USA.

Kelly J.M. (2003), "Tension Buckling in Multilayer Elastomeric Bearings", *Journal of Engineering Mechanics, ASCE*, Vol. 129(12), pp. 1363-1368.

Kelly J.M. (2009), "Base isolation: Origins and development", *National Information Service for Earthquake Engineering*, University of California, Berkeley, USA, pp. 1-6.

Kelly J.M. and Konstantinidis D.A. (2011), "Mechanics of Rubber Bearings for Seismic and Vibration Isolation", *John Wiley & Sons, Ltd*, Publication.

Kelly J.M. and Calabrese A. (2012), "Mechanics of Fiber Reinforced Bearings", *PEER Report*, 2012/101, Pacific Earthquake Engineering Research Center, University of California, Berkeley, USA.

Kim S.H. and Feng M.Q. (2003), "Fragility analysis of bridges under ground motion with spatial variation", *International journal of Non-Linear mechanics, PERGAMON*, Vol. 38, pp. 705-721.

Koh C.G. and Kelly J.M. (1988), "A simple mechanical model for elastomeric bearings used in base isolation", *Int. J. Mech. Sci.*, Vol. 30(12), pp. 933-943.

Koh C.G. and Kelly J.M. (1989), "Viscoelastic Stability Model for Elastomeric Isolation Bearings", *Journal of Structural Engineering, ASCE*, Vol. 115(2), pp. 285-302.

Koh C.G. and Lim H.L. (2001), "Analytical Solution for Compression Stiffness of Bonded Rectangular Layers", *International Journal of Solids and Structures*, Vol. 38, pp. 445-455.

Kulak R.F. and Wang C.Y. (1991), "Design and Analysis of Seismically Isolated Structures", *Nuclear Engineering and Design*, Vol. 127(3), pp. 419-432.

Kumar M., Whittaker A.S. and Constantinou M.C. (2015), "Experimental investigation of cavitation in elastomeric seismic isolation bearings", *Engineering Structures*, Vol. 101, pp. 290-305.

Lagomarsino S. and Giovinazzi S. (2006), "Marcoseismic and mechanical models for the vulnerability and damage assessment of current buildings", *Bull Earthquake Eng, Springer*, Vol. 4, pp. 415-443, DOI: 10.1007/s10518-006-9024-z.

Milani G., Lourenco P.B. and Tralli A. (2006), "Homogenised limit analysis of masonry walls, Part I: Failure surfaces", *Computers and Structures*, Vol. 84, pp. 166-180, DOI: 10.1016/j.compstruc.2005.09.005.

Milani G., Lourenco P.B. and Tralli A. (2007), "3D homogenized limit analysis of masonry buildings under horizontal loads", *Engineering Structures*, Vol. 29, pp. 3134-3148, DOI: 10.1016/j.engstruct.2007.03.003.

Moon B.Y., Kang G.J., Kang B.S. and Kelly J.M. (2002), "Design and manufacturing of fiber reinforced elastomeric isolation", *Journal of Material Processing Technology*, Vol. 130-131, pp. 145-150.

Moon B.Y., Kang G.J., Kang B.S. and Cho D.S. (2004), "Design of Elastomeric Bearing System and Analysis of its Mechanical Properties", *KSME International Journal*, Vol. 18(1), pp. 20-29.

Mordini A. and Strauss A. (2008), "An Innovative Earthquake Isolation System using Fiber Reinforced Rubber Bearings", *Engineering Structures*, Vol. 30(10), pp. 2739-2751.

Mullins L. (1969), "Softening of rubber by deformation", *Rubber Chemistry and Technology*, Vol. 42(1), pp. 339-362.

Naeim F. and Kelly J.M. (1999), "Design of Seismic Isolated Structures: From Theory to Practice", *John Wiley & Sons*, INC.

Nagarajaiah S., Reinhorn A.M. and Constantinou M.C. (1991), "Nonlinear Dynamic Analysis of 3D Base-Isolated Structures", *Journal of Structural Engineering, ASCE*, Vol. 117(7), pp. 2035-2054.

Nagarajaiah S. and Ferrell K. (1999), "Stability of Elastomeric Seismic Isolation Bearings", *Journal of Structural Engineering, ASCE*, Vol. 125(9), pp. 946-954.

Naghshineh A.K., Akyuz U. and Caner A. (2014), "Comparison of Fundamental Properties of New Types of Fiber-mesh-reinforced Seismic Isolators with Conventional Isolators", *Earthquake Engineering and Structural Dynamics*, Vol. 43(2), pp. 301-316.

Nezhad H.T., Tait M.J. and Drysdale R.G. (2008a), "Testing and Modeling of Square Carbon Fiber-reinforced Elastomeric Seismic Isolators", *Structural Control and Health Monitoring*, Vol. 15, pp. 876-900.

Nezhad H.T., Tait M.J. and Drysdale R.G. (2008b), "Lateral Response Evaluation of Fiber-Reinforced Neoprene Seismic Isolator Utilized in an Unbonded Application", *Journal of Structural Engineering, ASCE*, Vol. 134(10), pp. 1627-1637.

Nezhad H.T., Drysdale R.G. and Tait M.J. (2009a), "Parametric Study on the Response of Stable Unbonded-Fiber Reinforced Elastomeric Isolator (SU-FREIs)", *Journal of Composite Materials, SAGE*, Vol. 43(15), pp. 1569-1587.

Nezhad H.T., Tait M.J. and Drysdale R.G. (2009b), "Shake Table Study on an Ordinary Low-Rise Building Seismically Isolated with SU-FREIs (Stable Unbonded-Fiber Reinforced Elastomeric Isolators)", *Earthquake Engineering and Structural Dynamics*, Vol. 38, pp. 1335-1357.

Nezhad H.T., Tait M.J. and Drysdale R.G. (2009c), "Simplified Analysis of a Low-rise Building Seismically Isolated with Stable Un-bonded Fiber Reinforced Elastomeric Isolators", *Canadian Journal of Civil Engineering*, Vol. 36(7), pp. 1182-1194.

Nezhad H.T., Tait M.J. and Drysdale R.G. (2011), "Bonded versus Unbonded Strip Fiber Reinforced Elastomeric Isolators: Finite Element Analysis", *Composite structures*, Vol. 93, pp. 850-859.

Nezhad H.T. (2014), "Horizontal stiffness solutions for unbonded fiber reinforced elastomeric bearings", *Structural Engineering and Mechanics*, Vol. 49 (3), pp. 395-410.

Nielson B.G. and DesRoches R. (2007), "Analytical seismic fragility curves for typical bridges in the Central and Southeastern United States", *Earthquake spectra, Earthquake Engineering Research Institute*, Vol. 23(3), pp. 615-633, DOI: 10.1193/1.2756815.

Ogden R.W. (1972), "Large deformation isotropic elasticity - on the correlation of theory and experiment for incompressible rubber-like solids", *Proc. R. Soc. Lond. A.*, Vol. 326, pp. 565-584.

Osgooei P.M., Tait M.J. and Konstantinidis D. (2014a), "Three-dimensional finite element analysis of circular fiber-reinforced elastomeric bearings under compression", *Composite Structures*, Vol. 108, pp. 191-204.

Osgooei P.M., Tait M.J. and Konstantinidis D. (2014b), "Finite element analysis of unbonded square fiber-reinforced elastomeric isolators (FREIs) under lateral loading in different directions", *Composite Structures*, Vol. 113, pp. 164-173.

Osgooei P.M., Tait M.J. and Konstantinidis D. (2016a), "Seismic isolation of a shear wall structure using rectangular fiber-reinforced elastomeric isolators", *Journal of Structural Engineering, ASCE*, Vol. 142(2): 04015116-1-10.

Osgooei P.M., Konstantinidis D. and Tait M.J. (2016b), "Variation of the vertical stiffness of strip-shaped fiber-reinforced elastomeric isolators under lateral loading", *Composite Structures*, Vol. 144, pp. 177-184.

Padgett J.E. and DesRoches R. (2008), "Methodology for the development of analytical fragility curves for retrofitted bridges", *Earthquake Engineering and Structural Dynamics*, Vol. 37, pp. 1157-1174.

Padgett J.E. and DesRoches R. (2009), "Retrofitted Bridge Fragility Analysis for Typical Classes of Multispan Bridges", *Earthquake Spectra*, Vol. 25(1), pp. 117-141.

Park J., Towashiraporn P., Craig J.I. and Goodno B.J. (2009), "Seismic fragility analysis of low-rise un-reinforced masonry structures", *Engineering Structures*, Vol. 31, pp. 125-137.

Pauletta M., Cortesia A. and Russo G. (2015), "Roll-out instability of small size fiber-reinforced elastomeric isolators in unbonded applications", *Engineering Structures*, Vol. 102, pp. 358-368.

Peng S.H. and Chang W.V. (1997), "A Compressible Approach in Finite Element Analysis of Rubber- Elastic Materials", *Computers & Structures*, Vol. 62(3), pp. 573-593.

Petrovcic S. and Kilar V. (2015), "Modelling and analysis of seismic base-isolated masonry heritage structures", *SECED-2015 Conference: Earthquake risk and Engineering towards a resilient world*, July 9-10th, Cambridge, UK.

Raaf M.G.P.D, Tait M.J. and Nezhad H.T. (2011), "Stability of Fiber-reinforced Bearings in an Un-bonded Application", *Journal of Composite Materials, SAGE*, Vol. 45(18), pp. 1873-1884.

Roeder C.W. and Stanton J.F. (1983), "Elastomeric bearings: State of the Art", *Journal of Structural Engineering, ASCE*, Vol. 109(12), pp. 2853-2871.

Rota M., Penna A. and Magenes G. (2010), "A methodology for deriving analytical fragility curves for masonry buildings based on stochastic nonlinear analyses", *Engineering Structures*, Vol. 32, pp. 1312-1323.

Russo G. and Pauletta M. (2013a), "Sliding Instability of Fiber-reinforced Elastomeric Isolators in Un-bonded Applications", *Engineering Structures*, Vol. 48, pp. 70-80.

Russo G., Pauletta M. and Cortesia A. (2013b), "A Study on Experimental Shear Behavior of Fiber-reinforced Elastomeric Isolators with Various Fiber Layouts, Elastomers and Aging Conditions", *Engineering Structures*, Vol. 52, pp. 422-433.

Sanchez J., Masroor A., Mosqueda G. and Ryan K. (2013), "Static and Dynamic Stability of Elastomeric Bearings for Seismic Protection of Structures", *Journal of Structural Engineering, ASCE*, Vol. 139(7), pp. 1149-1159.

SAP2000 v.15 (2014), Computers and Structures Inc., *CSI Analysis Reference Manual*, Berkeley, California, USA.

Sasso M., Palmieri G., Chiappini G. and Amodio D. (2008), "Characterization of Hyperelastic Rubber-Like Materials by Biaxial and Uniaxial Stretching Tests Based on Optical Methods", *Polimer Testing*, Vol. 27(8), pp. 995-1004.

Siqueira G.H., Sanda A.S., Paultre P. and Padgett J.E. (2014), "Fragility curves for isolated bridges in eastern Canada using experimental results", *Engineering Structures*, Vol. 74, pp. 311-324.

Spizzuoco M., Calabrese A. and Serino G. (2014), "Innovative low-cost recycled rubber-fiber reinforced isolator: Experimental test and Finite Element Analyses", *Engineering Structures*, Vol. 76, pp. 99-111.

Stanton J.F., Scroggins G., Taylor A.W. and Roeder C.W. (1990), "Stability of Laminated Elastomeric Bearings", *Journal of Engineering Mechanics, ASCE*, Vol. 116(6), pp. 1351-1371.

Strauss A., Apostolidi E., Zimmermann T., Gerhaher U. and Dritsos S. (2014), "Experimental investigations of fiber and steel reinforced elastomeric bearings: Shear modulus and damping coefficient", *Engineering Structures*, Vol. 75, pp. 402-413.

Sussman T. and Bathe K.J. (1987), "A Finite Element Formulation for Nonlinear Incompressible Elastic and Inelastic Analysis", *Computers & Structures*, Vol. 26(1/2), pp. 357-409.

Symans M.D. (2003), "Seismic protective systems: Seismic isolation", *NEHRP Recommended Provisions: Instructional and Training Materials, FEMA 451B*, Topic 15-7: Seismic isolation.

Tavares D.H., Padgett J.E. and Paultre P. (2012), "Fragility curves of typical as-built highway bridges in eastern Canada", *Engineering Structures*, Vol. 40, pp. 107-118.

Tsai H.C. and Lee C.C. (1998), "Compression Stiffness of Elastic Layers Bonded Between Rigid Plates", *International Journal of Solids Structures*, Vol. 35(23), pp. 3053-3069.

Tsai H.C. and Kelly J.M. (2001), "Stiffness Analysis of Fiber-Reinforced Elastomeric Isolator", *PEER Report*, 2001/05, Pacific Earthquake Engineering Research Center, University of California, Berkeley.

Tsai H.C. and Kelly J.M. (2002a), "Stiffness Analysis of Fiber-Reinforced Rectangular Seismic Isolator", *Journal of Engineering Mechanics, ASCE*, Vol. 128(4), pp. 462-470.

Tsai H.C. and Kelly J.M. (2002b), "Bending Stiffness of Fiber-Reinforced Circular Seismic Isolator", *Journal of Engineering Mechanics, ASCE*, Vol. 128(11), pp. 1150-1157.

Tsai H.C. (2003), "Flexure Analysis of Circular Elastic Layers Bonded Between Rigid Plates", *International Journal of Solids and Structures*, Vol. 40, pp. 2975-2987.

Tsai H.C. (2004), "Compression Stiffness of Infinite-strip Bearings of Laminated Elastic Material Interleaving with Flexible Reinforcements", *Journal of Material Processing Technology*, Vol. 41, pp. 6647-6660.

Tsai H.C. (2005), "Compression Analysis of Rectangular Elastic Layers Bonded Between Rigid Plates", *International Journal of Solids and Structures*, Vol. 42, pp. 3395-3410.

Tsai H.C. and Kelly J.M. (2005a), "Buckling of Short Beams with Warping Effect Included", *International Journal of Solids and Structures*, Vol. 42, pp. 239-253.

Tsai H.C. and Kelly J.M. (2005b), "Buckling Load of Seismic Isolator Affected by Flexibility of Reinforcement", *International Journal of Solids and Structures*, Vol. 42, pp. 255-269.

Tsai H.C. (2006), "Compression Stiffness of Circular Bearings of Laminated Elastic Materials Interleaving with Flexible Reinforcements", *International Journal of Solids and Structures*, Vol. 43, pp. 3484-3497.

Tsai H.C. (2008), "Deformation Analysis of Infinite-Strip Bearings of Laminated Elastic Materials Interleaving with Tension-Only Reinforcements", *International Journal of Solids and Structures*, Vol. 45, pp. 2836-2849.

Vemuru V.S., Nagarajaiah S., Masroor A. and Mosqueda G. (2014), "Dynamic Lateral Stability of Elastomeric Seismic Isolation Bearings", *Journal of Structural Engineering, ASCE*, Vol. 140(14), A4014014-1-14.

Warn G.P., Whittaker A.S. and Constantinou M.C. (2007), "Vertical Stiffness of Elastomeric and Lead-Rubber Seismic Isolation Bearings", *Journal of Structural Engineering, ASCE*, Vol. 133(9), pp. 1227-1236.

Weisman J. and Warn G.P. (2012), "Stability of Elastomeric and Lead-Rubber Seismic Isolation Bearings", *Journal of Structural Engineering, ASCE*, Vol. 138(2), pp. 215-223.

Zhang J. and Huo Y. (2009), "Evaluating effectiveness and optimum design of isolation devices for highway bridges using the fragility function method", *Engineering Structures*, Vol. 31, pp. 1648-1660.

Publications from this Thesis Work

(A) International Journals:

[1] Ngo V.T., Dutta A. and Deb S.K. [2017], "Evaluation of horizontal stiffness of fibre reinforced elastomeric isolators", **Earthquake Engineering and Structural Dynamics**, DOI: 10.1002/eqe.2879.

[2] Ngo V.T., Dutta A. and Deb S.K. [2016], "Predicting stability of a prototype un-bonded fibre reinforced elastomeric isolator by finite element analysis", under review in International Journal of Computational Methods, ISSN: 0219-8762.

[3] Ngo V.T., Deb S.K. and Dutta A. [2016], "Effect of horizontal loading direction on performance of prototype square unbonded fibre reinforced elastomeric isolator", under review in Structural Control and Health Monitoring.

[4] Ngo V.T., Deb S.K. and Dutta A. [2017], "Vulnerability assessment of a prototype low-rise masonry building supported on un-bonded fibre reinforced elastomeric isolators", under review in Journal of Performance of Constructed Facilities, *ASCE*.

(B) International Conferences:

[1] Ngo V.T., Dutta A. and Deb S.K. "Predicting stability of a prototype un-bonded fibre reinforced elastomeric isolator by finite element analysis", Proceedings of the International Conference on Computational Methods, 7th ICCM2016, 1st-4th August, 2016, Berkeley, CA, USA, Vol. 3, pp. 500-518.

[2] Ngo V.T., Deb S.K., Dutta A., Ray N. and Mitra A.J. "Performance evaluation of fiber reinforced elastomeric isolators under cyclic load", Proceedings of the 8th World Congress on Joints, Bearing and Seismic Systems for Concrete Structures, 25-29th September, 2016, Atlanta, Georgia, USA, paper 8-51.

[3] Ngo V.T., Deb S.K. and Dutta A. "Innovative base isolation technique for reduction of seismic vulnerability of buildings", Seminar on Modern Technology and Materials, Public Works Dept.: Buildings & NH, Govt. of Assam, India, 23-25th September, 2016, pp. 39-44.